UNIVERSITÀ DEGLI STUDI DI PADOVA
Facoltà di Scienze MM.FF.NN.
Dipartimento di Fisica Galileo Galilei

TESI

Investigation of the magnetic topology of helical RFP plasmas

Relatore: Dott. Emilio Martines

Relatore: Prof. Piero Martin

dottoranda: Barbara Momo

Anno Accademico 2007-2008

Contents

Prefazione

Questa tesi si inserisce nel contesto della ricerca sulla fusione termonucleare controllata come possibile fonte alternativa di energia. La fusione è il processo che alimenta il sole e tutte le altre stelle attive, il progetto è quello di riprodurre questo processo in macchine da laboratorio: il progetto, affascinante ma di non facile realizzazione, si scontra soprattutto con la difficoltà di confinare alte temperature e densità di plasma, stato ionizzato della materia (il cosiddetto *quarto stato della materia*).
La ricerca civile in questo campo è quasi interamente dedicata allo studio del confinamento dei plasmi da fusione con campi magnetici. Le configurazioni di campo magnetico più studiate sono quelle dette Tokamak, Stellarator e Reversed–Field–Pinch (RFP), che confinano i plasmi in macchine toroidali. Tokamak e Stellarator sono le configurazioni che storicamente hanno dato i migliori risultati in termini di confinamento di particelle ed energia: vanno ricordati rispettivamente i due progetti per la futura generazione delle macchine da fusione, ITER (progetto di collaborazione internazionale oggi in costruzione a Cadarache, Francia) e Wendelstein–7X (progetto in costruzione a Greifswald, Germania).
Per quanto riguarda il RFP, il più grande esperimento oggi attivo è l'esperimento RFX (oggi RFX–mod), in funzione a Padova dal 1990, dove si è svolto questo lavoro di tesi. Nei RFP il plasma è riscaldato per effetto ohmico da un'alta corrente che fluisce nel plasma, ma la presenza di molte instabilità, considerate intrinseche alla configurazione, ha storicamente condotto a bassi tempi di confinamento e quindi a poca fiducia nel RFP come possibile configurazione per un reattore. La ricerca su questo tipo di macchine è oggi rivalutata da nuovi risultati, che dimostrano come all'aumentare della corrente il plasma spontaneamente si porti in uno stato meno caotico con proprietà di confinamento migliorate. Questi stati sono chiamati SHAx (Single Helical Axis) perché caratterizzati da superfici magnetiche elicoidali.

Obiettivo di questa tesi è lo studio e la caratterizzazione della topologia magnetica degli equilibri SHAx (in RFX–mod ottenuti per correnti di plasma superiori a 1.5 MA), sia nella regione centrale del plasma (*plasma core*) che nella zona di bordo dove dominano gli effetti dell'interazione plasma–parete (*plasma edge*).

Il primo passo per caratterizzare i nuovi equilibri elicoidali è stato la ricerca di buone coordinate elicoidali. Si è fatto uso per questo di coordinate curvilinee (per descrivere la geometria toroidale del sistema) e della meccanica hamiltoniana applicata ai campi magnetici in un toro (il che permette di usare le coordinate azione–angolo del sistema).
Il risultato di questo studio è un codice (SHEq, Single Helical Equilibria) che usa le metriche elicoidali per la ricostruzione delle quantità di plasma (componenti del campo o dei flussi magnetici e della densità di corrente) durante gli stati SHAx, ed è quindi per esempio utile per interpretare i dati sperimentali delle varie diagnostiche.
Parte di questa tesi si è svolta in collaborazione con il gruppo di Teoria di TJ–II (Ciemat, Madrid) per l'evoluzione temporale degli equilibri elicoidali di SHEq in accordo con la legge di Ohm (che non è iniziale vincolo).
La parte più sperimentale di questa tesi riguarda lo studio della zona di bordo dove un'interazione regolare del plasma con la parete riflette la deformazione elicoidale della colonna di plasma. Una parte del tempo nella campagna sperimentale 2011 di RFX–mod è stata dedicata allo studio di particolari condizioni al contorno per favorire e controllare la regolarità dell'interazione plasma–parete.

I risultati principali di questa tesi sono stati pubblicati in:
- B. Momo et. al *Plasma Phys. Control. Fus* (2011) [1];
- E. Martines, R. Lorenzini, B. Momo et al. *Plasma Phys. Control. Fus* (2011) [2];
- E. Martines, R. Lorenzini, B. Momo et al., *Nucl. Fusion* (2010) [3].

Il lavoro ì così organizzato:

Introduzione

- *Capitolo 1: Cos'è un Reversed Field Pinch?*
  Questo capitolo introduce brevemente la fisica del confinamento magnetico del plasma in macchine toroidali da fusione e si concentra sulla descrizione del RFP e delle sue caratteristiche prncipali. Particolare attenzione è dedicata agli stati elicoidali SHAx.

Riferimenti teorici

- *Capitolo 2: Meccanica hamiltoniana applicata ai campi magnetici*
  Questo capitolo fornisce le basi per usare la meccanica hamiltoniana applicata ai campi magnetici in macchine toroidali da fusione. Chiarifica il significato della forma canonica del campo magnetico attraverso l'uso del potenziale vettore e del teorema di Stokes. Riunisce le formu-

lazioni e considerazioni dei principali testi e articoli sull'argomento.

- *Capitolo 3: Ricostruzione delle autofunzioni della perturbazione magnetica*
  Questo capitolo è dedicato a specificare come utilizzare i risultati teorici del capitolo 2 per dati reali. Viene ripreso l'articolo di P. Zanca and D. Terranova, *Reconstruction of magnetic perturbation in a toroidal reversed field pinch*, Plasma Phys. Control. Fusion 46 (2004) in cui si spiega come ricostruire le autofunzioni delle perturbazioni (decomposte secondo Fourier) al campo magnetico di equilibrio assial–simmetrico. Particolare attenzione è dedicata all'*accoppiamento toroidale* tra i modi che nasce da metriche curvilinee.

Il lavoro di tesi

- *Capitolo 4: Coordinate elicoidali in sistemi toroidali*
  Vengono qui definiti alcuni sistemi di coordinate elicoidali che descrivono un'elica in un toro. Gli stati SHAx sono aprossimati a pure eliche (toroidalmente chiuse) descritte dalla sovrapposizione di un unico modo della perturbazione al campo magnetico di equilibrio assial–simmetrico. Punto di partenza è quindi la ricostruzione delle armoniche della perturbazione spiegata nel capitolo 3. Vengono discussi limiti e vantaggi dei vari sistemi di coordinate trovati. Viene introdotto il codice SHEq.

- *Capitolo 5: Componenti covarianti e controvarianti del campo magnetico*
  L'uso di coordinate curvilinee impone attenzione sia rispetto alla differenza tra componenti covarianti e controvarianti dei vettori che all'accoppiamento toroidale tra i modi che ne consegue. Viene mostrato l'effetto dell'accoppiamento toroidale tra i modi sia nelle componenti covarianti che in quelle controvarianti del campo magnetico.

- *Capitolo 6: Applicazioni*
  Si discutono alcune applicazioni del codice SHEq, in particolare: la ricostruzione delle superfici magnetiche; le medie sulle superfici di flusso che restitiuscono i profili radiali (mediati) delle quantità di plasma; il *safety factor profile* (fattore di sicurezza) per definire gli equilibri elicoidali.

- *Capitolo 7: Evoluzione dell'equilibrio: il vincolo ohmico*
  Date le alte correnti di plasma, qualsiasi equilibrio deve soddisfare la legge di Ohm (o il cosiddetto *vincolo ohmico* in condizioni stazionarie). In questo capitolo prima la dinamo laminare (legata alla deformazione elicoidale della colonna di plasma) è discussa come effetto elettrostatico. Poi si dimostra che gli equilibri di SHEq sono non stazionari, e si presenta il lavoro svolto a TJ–II (Ciemat, Madrid) per evolvere gli equilibri elicoidali in accordo alla legge di Ohm.

- *Capitolo 8: Plasma di bordo in stati SHAx*
  Si discute l'interazione regolare del plasma con la parete durante gli stati SHAx. Vengono presentate alcune recenti scariche della campagna sperimentale 2011 di RFX–mod per il controllo della zona di bordo plasma attraverso l'imposizione di condizioni al contorno elicoidali.

Dettagli di calcolo

- *Capitolo 9: Dettagli di calcolo...*
  Si raccolgono qui i dettagli dei conti svolti in questa tesi. In particolare quelli relativi alle derivate delle armoniche complesse delle perturbazioni di flusso magnetico e quelli relativi alle metriche delle geometrie elicoidail–toroidali.

Appendici

- *Appendici A1–A3:*
  Si trovano qui brevi riassunti di tematiche utili per seguire meglio il testo della tesi. In particolare sono raccolte le equazioni MHD e le coordinate toroidali usate come punto di partenza per la costruzione delle coordinate elicoidali–toroidali introdotte nel capitolo 4.

Abstract

The work carried out during these three years is part of the research activity on controlled thermonuclear fusion as a (future) energy source that would meet the requirements of a clean, renewable and abundant resource. Fusion reactions are well known to physicists since 1930 and the ambitious idea is to reproduce in laboratory the process that powers the Sun and all the stars. Its reproduction on Earth in a fusion reactor is limited by the inability of confining high density and temperature plasmas, necessary to overcome the Coulomb repulsion between nuclei and bring the reactants within the range of their strong interaction.
Civil research is mainly devoted to the study of magnetic plasma confinements. Presently Tokamak, Stellarator and Reversed Field Pinch (RFP) configurations are the most explored magnetic configurations, the first two being the most promising for a fusion reactor (the ITER Tokamak in Cadarache, France, and the Wendelstein–7X Stellarator in Greifswald, Germany, are now under construction as the next step in fusion research).
The study of the reversed field pinch configuration is getting new momentum from recent results, and this thesis has been carried out in the largest RFP device in the world, which is in operation in Padova, Italy, since 1990: the RFX–mod device (previously called RFX). RFPs are Ohmically heated devices, with high currents flowing in the plasma. In the past, their performance has been limited by the intrinsic presence of many instabilities that degrade the confinement. At present, new high–plasma–current (higher than 1.5 MA in RFX–mod) states have been discovered, which show that as the plasma becomes hotter it spontaneously undergoes a transition to a state with improved confinement properties due to the emergence of an ordered spontaneous magnetic structure in the otherwise chaotic core. These states (named SHAx, Single Helical Axis) are characterized by magnetic surfaces winding around a helical axis and are therefore considered as the helical RFP states.

The aim of this thesis is to investigate and model the magnetic topology related to helical SHAx state equilibria, taking into account both the core region and the edge.
As a first step, new helical coordinates to well describe the helical shape of

Abstract

SHAx states on a torus has been defined. This has been carried out making use of the curvilinear metrics theory (to well consider the toroidicity of the helical system) and Hamiltonian mechanics tools applied to magnetic field (to make use of action–angle as a smart choice of coordinates).
The practical outcome of this thesis is the code named SHEq (Single Helical Equilibria), which uses the complete definition of the helical metrics to compute all the (helical) equilibrium plasma quantities and can be therefore useful to interpret the data from different diagnostics.
Furthermore, this should allow to verify if the equilibrium satisfies the Ohmic constraint, *a posteriori* since the Ohm's law is not an initial constraint for SHEq's equilibrium reconstruction. This highlights that SHEq's equilibria are not steady state, and a part of this thesis has been carried out in collaboration with the Theory Group of TJ-II (Ciemat, Madrid), where I worked for about three months, in order to evolve in time helical equilibria accordingly to Ohm's law too.
Finally, a more experimental part of the thesis concerns the edge region. From the point of view of plasma–wall interaction SHAx states appears with a regular helical pattern and a part of this thesis is also devoted to the study of some discharges (done during the 2011 RFX–mod experimental campaign) where particular boundary conditions were applied in order to favor and sustain both the helical deformation in the core and a more regular helical pattern in the plasma–wall interaction.

The main results of this work have been published in:
- *B. Momo et. al* Plasma Phys. Control. Fus *(2011) [1];*
- *E. Martines, R. Lorenzini, B. Momo et al.* Plasma Phys. Control. Fus *(2011) [2];*
- *E. Martines, R. Lorenzini, B. Momo et al.,* Nucl. Fusion *(2010) [3].*

The thesis is organized as follows:

Introduction

- *Chapter 1: What is a Reversed Field Pinch?*
  Briefly introduces the concepts of magnetic confinement in fusion devices with particular attention to the Reversed Field Pinch (RFP) axi–symmetric configuration. Special emphasis is given to the difference between low and high plasma current discharges and to SHAx features, where one or more modes break the axi–symmetry. The necessity of the dynamo process is discussed, together with its electrostatic explanation that overtakes Taylor's theory for the RFP.

Theoretical basis

- *Chapter 2: Hamiltonian mechanics for magnetic field lines*
  This chapter gives an overview of the Hamiltonian mechanics applied to magnetic fields in a toroidal device. The derivation of the canonical representation of the magnetic field $\mathbf{B}$ is proposed, and its physical meaning is clarified using the vector potential $\mathbf{A}$ ($\mathbf{B} = \nabla \times \mathbf{A}$) and Stoke's theorem. We follow and collect the considerations of famous papers on the Hamiltonian mechanics of magnetic fields.

- *Chapter 3: Mode eigenfunction reconstruction*
  This chapter is devoted to specify how to apply the theoretical results of chapter 2 to real data, and which measurements are necessary for the reconstruction of the (Fourier decomposed) harmonics of the perturbation (to the axi–symmetric magnetic field). Special attention is given to the toroidal coupling that arises between modes due to curvilinear metrics. The chapter follows the paper by P. Zanca and D. Terranova, *Reconstruction of magnetic perturbation in a toroidal reversed field pinch*, Plasma Phys. Control. Fusion 46 (2004).

Thesis original work

- *Chapter 4: Helical coordinates in toroidal systems*
  It is the first chapter regarding the original work of this thesis. *Good* helical coordinate systems are defined in order to describe SHAx states, that are modeled as pure Single Helicity (SH) states (which are the superposition of a single mode of the perturbation to the axi–symmetric configuration). The advantages and disadvantages are discussed for all the coordinate systems. The starting point is the reconstruction of the helical magnetic surfaces, using the magnetic flux eigenfunction inside the plasma volume introduced in chapter 3. The SHEq–code can always choose between all coordinate systems when computing helical equilibria.

- *Chapter 5: Covariant and contravariant magnetic field components*
  The use of curvilinear metrics (as the helical coordinate systems in a torus) imposes to consider the difference between covariant and contravariant components of any vector, and the toroidal coupling between modes introduced in chapter 3. In this chapter is shown how the effect of the toroidal coupling on the harmonics of the magnetic fluxes can be seen in both the covariant and contravariant magnetic field components.

- *Chapter 6: Applications*
  This chapter discusses some applications of the SHEq code. For example magnetic flux reconstructions, the calculation of flux surface averages of any plasma quantity, and the helical safety factor profile.

- *Chapter 7: Equilibrium evolution: the Ohmic constraint*
  Due to high currents flowing in the plasma, any equilibrium must satisfy Ohm's law (or the Ohmic constraint that arises for steady state condition). In this chapter, first the laminar dynamo (which origins from a helical deformation of the plasma column) is discussed as an electrostatic effect. Then it is shown that SHEq's equilibria are not steady state (do not satisfy the Ohmic constraint) and the work done in collaboration with the Theory Group of TJ-II (Ciemat, Madrid) in order to evolve in time the helical equilibria according to Ohm's law is presented.

- *Chapter 8: Plasma boundary in SHAx states*
  This is the most experimental chapter, which presents the work done for the analysis of the plasma–wall interaction during SHAx states: a crucial point for RFX–mod operation not yet well understood. Special attention is devoted to a set of recent discharge (2011 experimental RFX–mod campain), where the ambitious objective was the control of the plasma–wall interaction using different (helical) boundary condition.

Detailed calculations

- *Chapter 9: Detailed calculations*
  Here are collected the detailed calculation done for this thesis, in particular those regarding the radial derivative of the complex harmonics of the fluxes and the helical–toroidal coordinates.

Appendixes

- *Appendixes A1–A3:*
  In the appendixes one can find some brief summary of arguments related to this thesis but not originally developed during the work. In particular one can find a brief summary of MHD equations and details regarding the toroidal coordinate system (and the curvilinear metrics) introduced in chapter 3.

Chapter 1

What is a Reversed Field Pinch?

1.1 About magnetic confinement of fusion plasmas

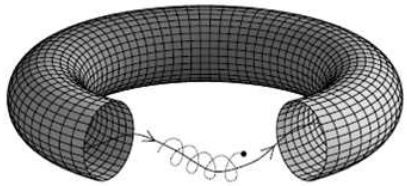

Figure 1.1: A picture showing the principle of toroidal confinement. It seems easy, but it is not...

The first picture in this section shows the principle of magnetic confinement in toroidal devices: a charged particle gyrates (dotted line) around a magnetic field line (continuous line) and it is confined within the vacuum vessel.

Historically, the plasma magnetic confinement developed starting from the first experiments about the *pinch effect*, in which a current channel contracts through the self–magnetic field of the current, investigated by Bennet in 1934 [4]. One can think to an applied toroidal magnetic field and to a toroidal current induced in the plasma by a transformer. The pinch effect due to the toroidal current adds to the toroidal magnetic field a poloidal component: the magnetic field lines are helix that wrap around the torus. The averaged poloidal angle $\Delta\theta$ traversed by a field line after one toroidal transit ($\Delta\varphi = 2\pi$) is called the rotational transformation angle ι, [5][1]. A

[1]The number of turns of a magnetic field line in the poloidal direction every toroidal

non–null rotational transform arises from the helical winding of the magnetic field lines, and it is necessary to balance the shift due to the curvature and the spatial gradient of the toroidal magnetic field.
Tokamak and RFP (Reversed Field Pinch) devices are the main toroidal pinch devices for fusion studies. The main concept of the Tokamak was proposed in 1952 by two Soviet physicists, Tamm and Sacharov, and then realized for the first time by another Russian physicist, L.A. Artsimovich, [6]. Whereas, the RFP configuration was first observed in the ZETA experiment (a pinch device) at Harwell in the mid 1960s, as a spontaneous self–generation of the toroidal magnetic field.
A non–null rotational transform can also be created without a pinch effect, by helically shaped magnetic field coils outside the plasma, as in is the case of the Stellarator devices.

In this thesis we will focus on the RFP configuration.

1.2 The Reversed Field Pinch

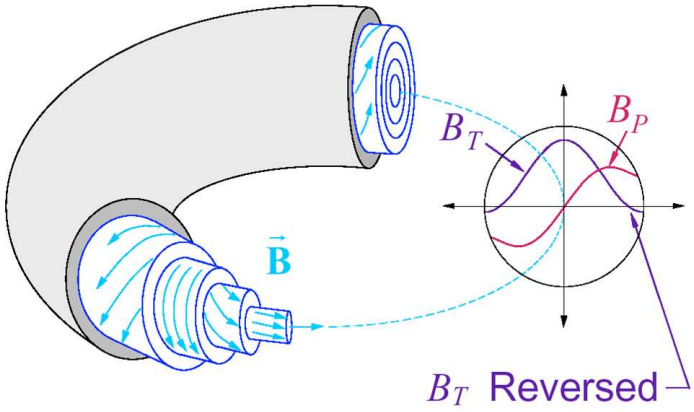

Figure 1.2: RFP axi–symmetric magnetic field configuration.

In fig. 1.2 the poloidal and toroidal component of the (toroidal) Reversed Field Pinch configuration are drawn. The RFP configuration can be described by an axi–symmetric magnetic field, with the peculiarity of comparable toroidal and poloidal component amplitude, and the reversal of the toroidal one at the edge (whence the name to the configuration). In the past,

turn are usually indicated by the symbol ι. Rigorously $\iota = \iota/(2\pi)$, but in this thesis we will use the symbol ι instead of ι.

RFP's performance has been limited by the intrinsic presence of many instabilities, such as tearing modes, that degrade the confinement, but were also considered to be necessary for the sustaining of the magnetic field reversal through the dynamo effect [7]. Actually, the reversal can be sustained also in a non–chaotic magnetic configuration [8, 9, 10], as the so–called Single Helical AXis (SHAx) states, recently discovered in RFX–mod experiment (and the main subject of this thesis).

1.2.1 Start up of the configuration

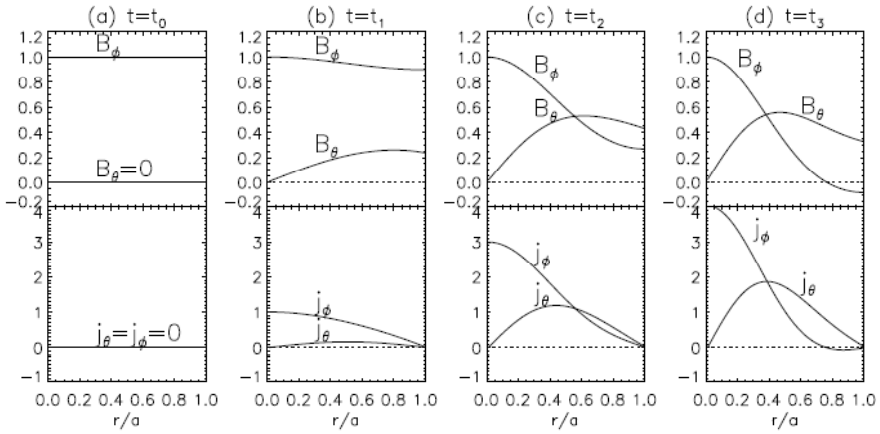

Figure 1.3: Reproduced from H. Ji, S.C. Prager, [7]. *Qualitative illustration of time evolution of the normalized magnetic field and current density profiles in a pinch plasma when the electric field is increased in sequence: (a) initial state, where only a toroidal field exist; (b) a small electric field to drive mainly toroidal current in Tokamaks; (c) a modest electric field to significantly drive both toroidal and poloidal current components; (d) and, finally, an RFP configuration is realized when the toroidal magnetic field reverses its direction.*

The toroidally symmetric vacuum vessel is surrounded by a set of toroidal field coils which produce the initially toroidal magnetic field. A central solenoid provides then the loop voltage necessary to trigger the discharge, and to drive the toroidal plasma current inside the vessel that produces the poloidal magnetic field component. In fig.1.3 one can see the time evolution of the magnetic field and current density components, as the applied electric field increases.
Most of the magnetic field is produced by currents flowing in the plasma. The poloidal field is produced by the induced toroidal current, while the toroidal magnetic field, much stronger in the core than at the edge (where it assumes

just a small value with a reversed sign), must be generated by poloidal currents inside the plasma. These poloidal currents can not be driven by the toroidal loop voltage alone: a dynamo is acting in the plasma, with continuous generation of a toroidal flux to provide and sustain the configuration. Therefore, the toroidal winding provides only a small toroidal field. It can act as a flux conserver, in this case the coils react to the existence of the poloidal currents in order to keep the total flux constant: in the outer region the toroidal field is thereby reduced and even reversed. But, in RFP experiments, aided reversal is generally preferred to self–reversal, and the toroidal winding provides a small (chosen) negative toroidal field.
The resulting equilibrium configuration is the one in fig.1.2.

1.2.2 Shifted magnetic flux surfaces

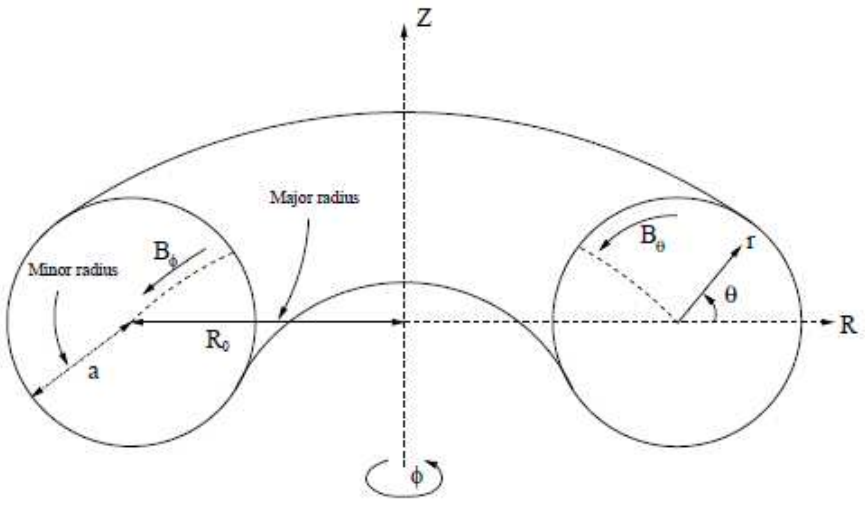

Figure 1.4: The cylindrical (R, Z, φ) and machine (r, θ, φ) coordinate systems, applied to a torus.

The magnetic equilibrium in fig.1.2 is related to magnetic flux surfaces where the magnetic field lines lie by definition. We refer to magnetic flux surfaces with circular poloidal cross section[2], even if other shape could in principle be investigated. In cylindrical approximation one can think to nested circular magnetic flux surfaces, whereas a shift (and therefore non concentric

[2]The edge radial magnetic field due to perturbations breaks the perfect circularity of the magnetic flux surfaces, and must be controlled either by a thick shell or by a feedback active control. This in RFX–mod is done by a number of saddle coils.

magnetic flux surfaces) characterizes the real toroidal system [11][3].

On the circular flux surfaces are defined the toroidal coordinate systems used in RFX–mod, all collected in appendix B.2 [4]. All of these coordinate systems are defined by a radial variable to label the magnetic flux surface, and by two angles: a poloidal angle θ and a toroidal angle φ (that one can see in fig. 1.4 for the easier of these coordinate systems, the machine one).

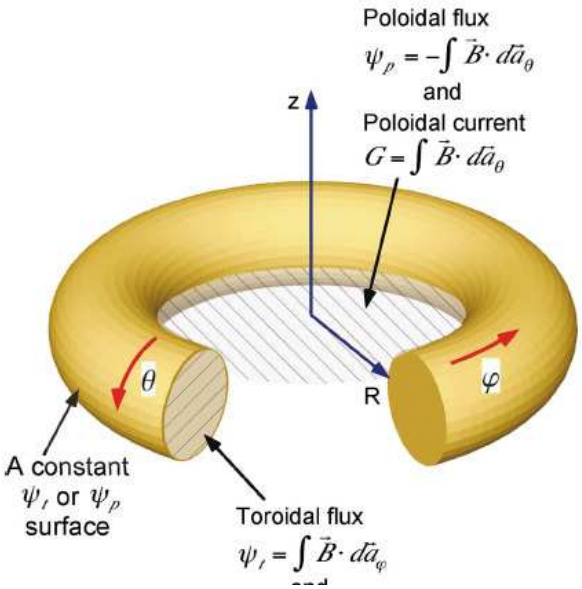

Figure 1.5: Reproduced from [12]. *Magnetic fluxes and currents defined using the cross–sectional area for the toroidal flux ψ_t and the current I and using the central hole of the torus for the poloidal flux ψ_p and the current G. The poloidal angle is θ and the toroidal angle is φ. (R, Z, φ) are ordinary cylindrical coordinates.*

Magnetic flux surfaces can be labeled with every quantity which is constant on them: by definition it must be any function f for which its gradient is perpendicular to the magnetic field $\mathbf{B}$:

$$\mathbf{B} \cdot \nabla f = 0\,. \tag{1.1}$$

From the equilibrium force balance equation, that needs to balance the pres-

[3] Shifted magnetic flux surfaces are not a peculiar feature of RFP configurations, but it is common to all the toroidal devices.

[4] The only coordinate system that takes into account the toroidicity is the (r, ϑ, φ) coordinate system, defined also in chapter 3. The complexity of taking into account the toroidal geometry, through the shift term, is related to curvilinear metrics (see appendix B).

sure gradient with the Lorentz force, one obtains the relation

$$\mathbf{J} \times \mathbf{B} = \nabla p \,. \tag{1.2}$$

Both the current density $\mathbf{J}$ and the pressure gradient ∇p are orthogonal to the magnetic field $\mathbf{B}$: the kinetic pressure is constant on the magnetic flux surfaces, where also the plasma current flows.
Some other example of label for magnetic flux surfaces are the magnetic fluxes, or the safety factor q defined as the ratio between their differentials:

$$\psi_t(r) = \int \mathbf{B} \cdot d\mathbf{\Sigma}_{tor} \tag{1.3}$$

$$\psi_p(r) = \int \mathbf{B} \cdot d\mathbf{\Sigma}_{pol} \tag{1.4}$$

$$q(r) = \frac{d\psi_t}{d\psi_p} \tag{1.5}$$

ψ_t is the toroidal flux through $\mathbf{\Sigma}_{tor}$, the surfaces defined by the constancy of the radius r at the toroidal angle $\varphi = const$; and ψ_p is the poloidal flux, i.e. the flux through $\mathbf{\Sigma}_{pol}$, the $r = const$ surface at the poloidal angle $\theta = const$. A qualitative picture of the two fluxes is in fig.1.5 and fig.2.4.

It is worth noting that the magnitude B of the magnetic field is not constant on the magnetic flux surfaces $r = const$. Due to the toroidicity of the geometry, the magnitude of the magnetic field depends both on the radius r and on the poloidal angle. One can think to the High or Low Field Side typical in Tokamaks.

1.2.3 Internal resonances: MH vs QSH and SHAx states

The safety factor profile

A distinctive feature of the RFP configuration is the safety factor profile, defined in eq.(1.5) and plotted in fig. 1.6. The safety factor profile related to the axi–symmetric equilibrium is monotonically decreasing and it reverses its sign at the edge, due to the reversal of the toroidal magnetic field.

The safety factor profile can be defined also as the inverse of the rotational transform ι, whose geometrical meaning is the number of turns of a magnetic field line in the poloidal direction, after a complete turn in the toroidal one[5].
The small edge value of q, related to the weak reversal of the toroidal magnetic field, means that (in contrast to Tokamaks) magnetic field lines at the

[5]We remind that we use the symbol ι instead of $\imath$.

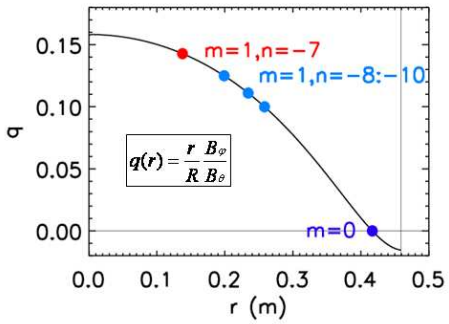

Figure 1.6: The axi–symmetric safety factor profile in the cylindrical approximation.

edge are almost poloidal. For $q = 0$ the magnetic field is only poloidal, i.e. on the reversal surface where the toroidal magnetic field vanishes.
As one can see in fig. 1.6, a lot of magnetic flux surfaces where q assumes a rational value with low mode numbers are present in the plasma, which means:

$$q(r) \quad = \quad \frac{m}{n}\,. \tag{1.6}$$

These values of q are said *rational* or *resonant*, as the corresponding flux surfaces, where magnetic filed lines close on themself after m poloidal and n toroidal turns. The term *resonant* arises from the fact that, around these surfaces, tearing modes with the same m poloidal mode number and n toroidal mode number are destabilized.
Tearing modes are resistive, non–linear modes with saturated amplitudes, and are responsible for the origin of the magnetic islands. Magnetic islands are a change in the magnetic topology that arises where the resonant condition

$$\mathbf{k} \cdot \mathbf{B} = 0 \tag{1.7}$$

between the wave vector $\mathbf{k}$ of the perturbation[6] and the magnetic field is satisfied. Equation (1.7) is verified exactly on the resonant flux surfaces[7], and in fig. 1.7 is given a picture of the magnetic island of a $m = 1$ mode in the poloidal plane and of a $n = 2 - 3$ mode in the toroidal one. On the reversal surfaces, where $q = 0$ by definition, all the modes of the $m = 0$ spectrum are resonant, and one speaks of the $m = 0$ island chain.

[6] In the cylindrical approximation, $k_\theta = m/r$ and $k_\varphi = n/R$, where r and R are the minus and major radius respectively.
[7] See [13, 11] for a treatment of magnetic island theory.

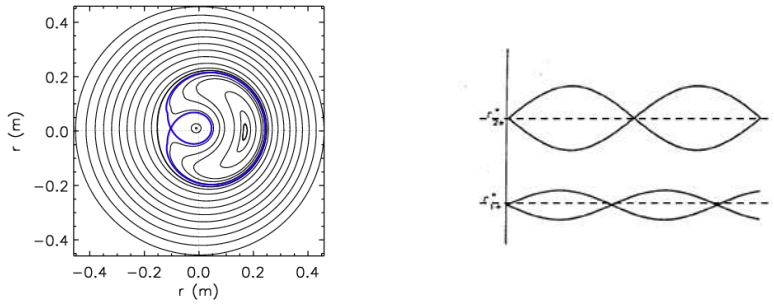

Figure 1.7: Left: A $m = 1$ magnetic island on the poloidal plane. Right: An example of magnetic island around the reversal surfaces on the toroidal plane. This figure is intended as a qualitative picture of magnetic islands on the poloidal and toroidal plane. The reconstruction of the magnetic configuration related to experimental data is better explained later (see chapters 6–8).

MHD spectra

At low plasma current (below 800 kA in RFX–mod), a wide spectrum of tearing modes is present in the so–called Multiple Helicity (MH) regime. Typically, the largest tearing modes are mostly in the $m = 1$ and $m = 0$ MHD spectra, and many modes with different toroidal mode number n and comparable amplitudes are simultaneously destabilized in the plasma. The consequence of the superposition of magnetic islands associated to resonant tearing modes is a stochastic plasma core [14], that entails flat density and temperature profiles. This is in agreement with images of the plasma core from soft X–ray (SXR) tomography (fig.1.8 bottom left) which display a poloidally symmetric emissivity.
At higher plasma currents, transient states where just one (m, n) mode dominates the spectra are observed in all the large RFP devices. These states are called Quasi Single Helicity (QSH) states due to the presence of secondary modes with small but finite amplitude. QSH regimes are associated to a reduced level of chaos and improved confinement properties. This is due to the presence of partially conserved magnetic flux surfaces in the plasma core, that turn out to be the magnetic island related to the dominant mode. From the measurements, this can be seen in the bean–like hot structure evident from the SXR tomography (fig.1.8 bottom right) and shows up also in the electron temperature profiles measurements that exhibit a strong Internal Transport Barrier (ITB) in correspondence of the magnetic island edges [15, 16].
Increasing the plasma current, an increase in the amplitude of the dominant mode, together with a decrease in the amplitude of the secondary modes, can be observed (fig.1.9 left). For high plasma currents (usually above 1.5 MA in RFX–mod), and in correspondence to a threshold value of the dominant

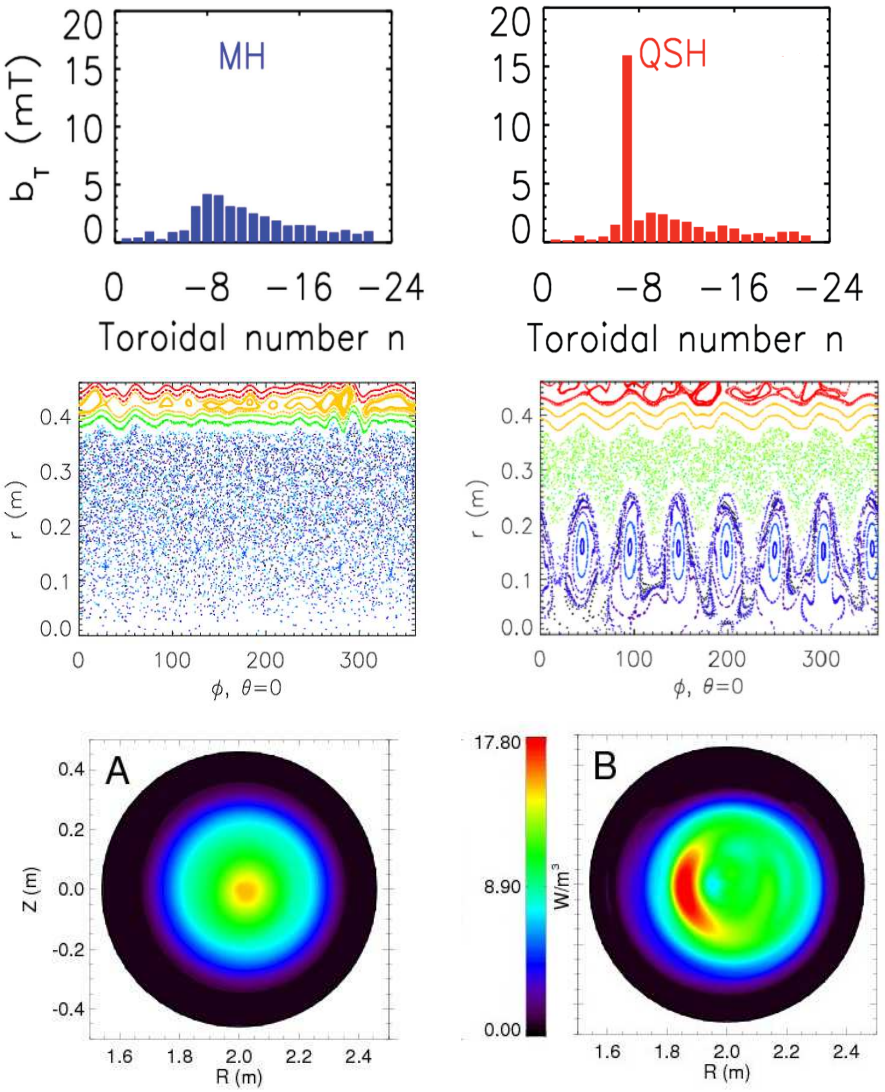

Figure 1.8: *Left.* MH features: MHD spectrum where many modes have comparable amplitudes; Poincaré plot with the typical chaotic core; SXR tomography on the poloidal plane, which displays a poloidally symmetric emissivity. MH are the typical state for low plasma current discharges, and only transient states in high plasma discharges. *Right.* QSH features: MHD spectrum where just one mode dominates the spectra; Poincaré plot where the coherent structure in the plasma core, related to the dominant mode, is evident; SXR tomography on the poloidal plane, which displays the bean–like hot structure. QSH are the typical state for high plasma current discharges, and only transient states in low plasma discharges. This figure is intended to be a qualitative picture to summarize MH and QSH features.

amplitude (experimentally of about the 4% of the total magnetic field at the edge), the plasma self–organizes into a helical state, named Single Helical Axis (SHAx), [17, 18, 19].

In fig.1.9 (right) the time evolution of the dominant and the secondary modes in both a low and high plasma current discharges is also plotted. One can see that the MH phases at high plasma current are just transient phases, whereas are the typical state for low current discharges. On the contrary, at high plasma current, helical states are reached but in a non–stationary way, their persistence increasing with plasma current.

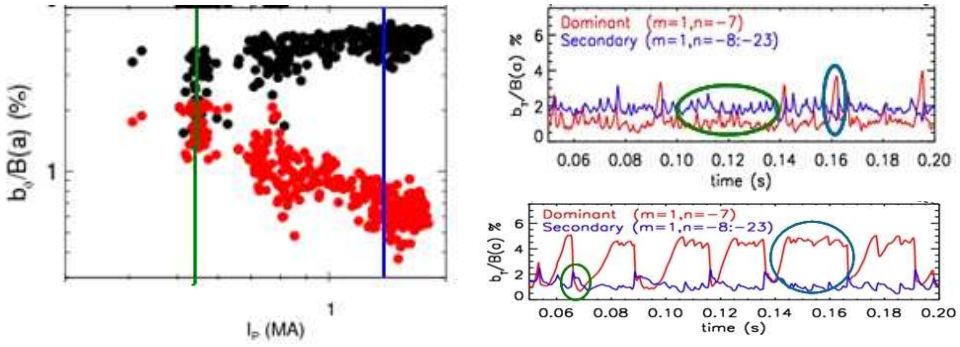

Figure 1.9: *Left:* The amplitude of the dominant mode (black) and of the secondary modes (red) are plotted against the value of the plasma current. *Right:* The time evolution of the dominant mode (red) and of the secondary modes (blue) in a low (up) and high (down) plasma discharges.

DAx and SHAx states

SHAx states are improved confinement RFP states, characterized by nested magnetic flux surfaces winding around a single helical axis, but enclosed in an almost axi–symmetric boundary. This state is the result of two successive bifurcations, occurring when the current progressively increases. The first one is of MHD type, and brings the plasma from the MH to the QSH regime. At lower currents (and below the threshold value of the dominant amplitude), the QSH regime includes a magnetic island and two axes are therefore present in the magnetic system: the unperturbed axi–symmetric axis and the one related to the island O–point. As one can see in fig. 1.10, in such states (named Double AXis, DAx) a helical thermal structure is observed together with an electron transport barrier (ITB) where the maximum of the electron temperature in strongly correlated with the position of the magnetic island. The second bifurcation changes the topology of the magnetic field: when the dominant mode exceeds the threshold amplitude, the X–point of its magnetic island is expelled and the original axi–symmetric

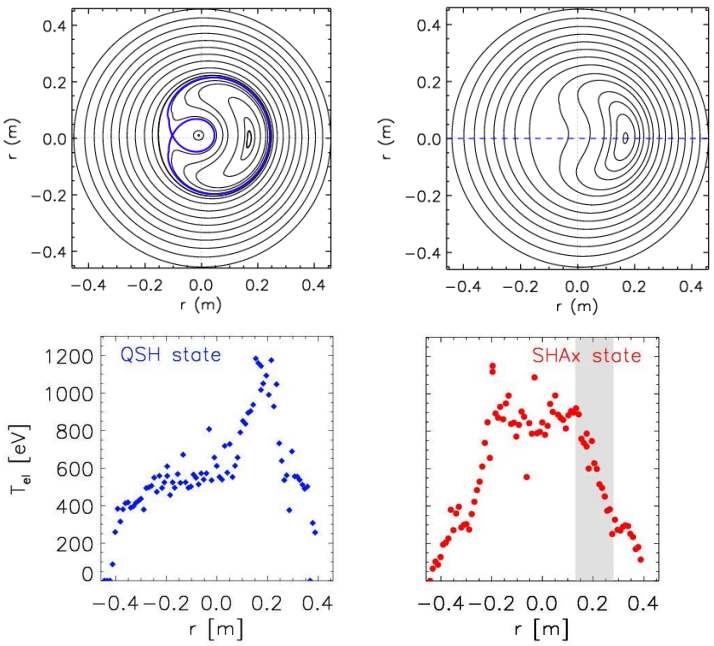

Figure 1.10: *Left.* DAx state topology on the poloidal plane where the island related to the dominant $m = 1$ can be seen. And the relative temperature profile from Thomson scattering data, where the internal transport barrier (ITB) can be seen. *Right.* SHAx state topology on the poloidal plane where the bean–shaped flux surfaces can be seen. And the relative temperature profile from Thomson scattering data where the internal transport barrier (ITB) and the internal flat profile can be seen.

axis is replaced by a helical magnetic axis, which coincides with the previous island O–point and that becomes the only magnetic axis (which motivates the term SHAx) of the system.
During SHAx states, the region inside the ITB spans a larger volume than in DAx states, and it is related to a flat temperature profile (fig. 1.10). The maximum electron temperature gradients at the ITB are similar between DAx and SHAx states. The safety factor profile changes its shape during the transition to a SHAx state, going through a maximum located in the vicinity of the former separatrix and therefore in correspondence of the steep temperature gradient (see chapter 6). The region of shear reversal[8] seems to be more resilient to chaos, and a QSH state without separatrix (SHAx state) can be therefore considered an improved confinement state with respect to the DAx state[9].

[8]The shear profile is defined as the radial derivative of the safety factor profile. A shear reversal therefore indicates a maximum or a minimum in the safety factor profile.
[9]This can be understood also using the Hamiltonian mechanics theory.

The transition from a chaotic MH regime to a stationary SH (Single Helicity) regime where chaos is suppressed was theoretically predicted to occur when the visco–resistive dissipation grows, therefore in correspondence of the high dissipation limit of the system. Numerical simulations show a continuous transition from MH to SH when the plasma dissipation increases, with an intermediate phase where the system displays a temporal intermittency between MH and QSH[10].
The first theoretical proof of the existence of SH states was their discovery in 1990 in 3D numerical simulations. The numerical scenario is qualitative similar to the experimental one: an increase of the dissipation parameters (as the Hartmann number[11]) in the former seems to have the same role of an increase of the plasma current in the latter (and viceversa). Experimentally, a pure SH regime is not reached, but it can be observed the transition between QSH and MH regimes (and viceversa). However, the relation between the high dissipation regime and high plasma discharges is still not understood, and the reason why high current is beneficial for real discharges is still awaiting a theoretical explanation.

Plasma properties, such as electron temperature and SXR emissivity, have been found constant on helical magnetic flux surfaces, indicating that SHAx states can be described by MHD equilibrium with almost invariant flux surfaces. In contrast, stationary low current MH states do not exist due to the temporal fluctuation of all the modes of the perturbation.
In this thesis we look for the magnetic reconstruction of the helical SHAx state equilibria, and to their evolution in time in chapter 7.
3D visco–resistive MHD simulations in toroidal geometry (and not in the simplified cylindrical one) show that the toroidal coupling between modes[12] prevents the system to reach a pure Single Helicity state. The toroidal chaos stays limited during the Quasi Single Helicity SHAx states, and in the following we model them as pure SH states, even in a toroidal geometry.
SHAx states are related to the dominant mode of the $m = 1$ spectrum, and they are studied in chapters 4–7. The contribution of the correspondent dominant mode in the $m = 0$ spectrum, important at the edge and in the plasma–wall interaction, is analyzed in chapter 8. The plasma deformation due to $m = 1$ and $m = 0$ modes can be seen in fig.1.11.
As yet the SHAx regimes are usually obtained at low densities ($n/n_G < 0.2$,

[10] In [20] the transition between MH and SH phases is described as a second order phase transition, where the control parameter is the Hartmann number.

[11] The Hartmann number H is defined as the dimensionless number $(\eta_0\nu_0)^{-1/2}$, where η_0 is the central resistivity and ν_0 the central plasma viscosity, therefore the increase of the dissipation parameters corresponds to a decrease of H and viceversa. It is found to be the right control parameter for the dynamics in numerical simulations [20].

[12] See chapter 3: the toroidal coupling acts between modes with same toroidal mode number n and different poloidal mode number m.

where n_G is the Greenwald density limit, [11]), and the understanding of the plasma-wall interaction is of crucial importance specially in RFX–mod, where no divertors protect the wall.

The magnetic topology of a SHAx state (3D shape in fig. 1.12) is like that of a non resonant saturated kink. This helical deformation makes the helical RFP plasmas similar to Stellarator's one. But in a Stellarator the helical magnetic field is almost completely defined by external coils, while in RFPs SHAx states is mainly produced by internal currents.
In chapter 6.3 we however compare the helical rotational transform during a SHAx state and the one typical of TJ-II Stellarator, in Ciemat (Madrid).

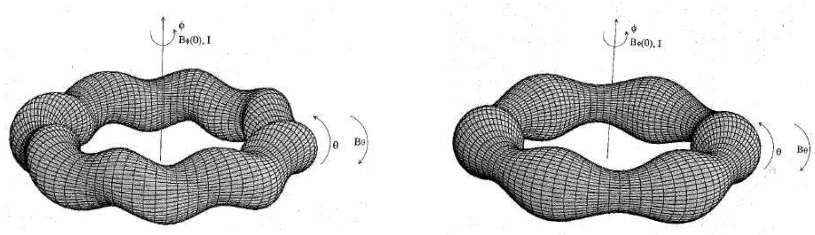

Figure 1.11: The plasma deformation due to $m = 1$ (*left*) and $m = 0$ (*right*) modes.

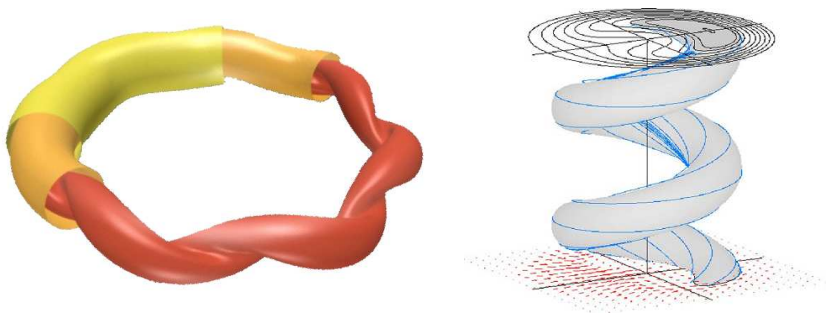

Figure 1.12: *Left:* 3D shape of a SHAx state. *Right:* Reproduced from [21]. The intersection of the helix with the poloidal plane, and the typical bean–like structure that characterize a SHAx state on the poloidal plane.

1.2.4 The reversal of the toroidal magnetic field and the dynamo

A dynamo process is necessary to sustain the Reversed Field Pinch configuration, for time longer that the resistive ones[13]. Without any mechanism that continuously produces toroidal magnetic flux, after a short time the toroidal magnetic field profile would be constant and equal to its edge value (see the diffusive equation (A.12) and fig.1.13).

The dynamo is therefore a process acting against the resistive diffusion, and

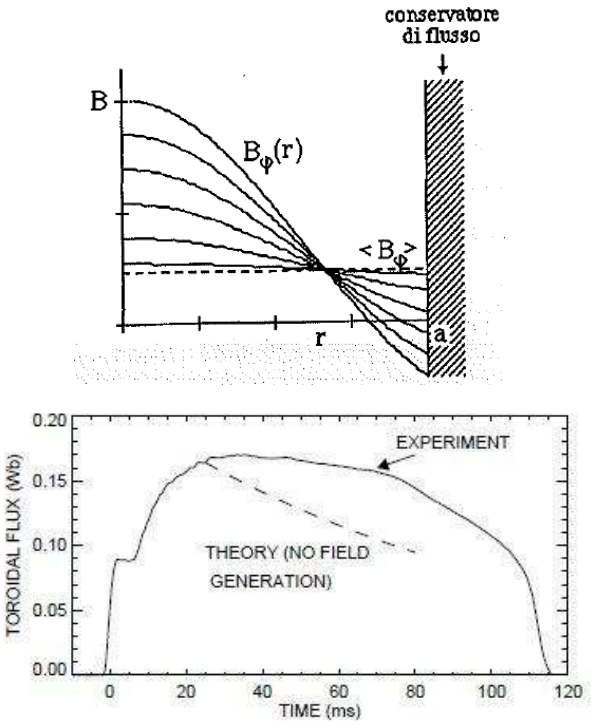

Figure 1.13: *Top:* The resistive diffusion of the toroidal magnetic field without the dynamo action. *Bottom:* The toroidal flux as function of time during a typical RFX–mod discharge. The dashed line represents the theoretical diffusive exponential decay without field regeneration.

it has been proved to be necessary for the stability of the configuration [22]. Other examples show the necessity of a dynamo, in particular to provide the reversal of the toroidal magnetic field. Let us use the Ampère's law, in

[13]The time for the resistive diffusion of the magnetic field is defined in appendix A.1 (comment to eq.(A.12)), as the characteristic time $\tau_R = \mu_0 a^2/\eta$ with a the radius of the vacuum chamber.

stationary condition and in cylindrical approximation for simplicity[14]:

$$J_\theta = -\frac{1}{\mu_0}\frac{\partial B_\varphi}{\partial r} \tag{1.8}$$

On the reversal surface, if the poloidal current density vanishes (as it should be with magnetic field lines only poloidal), the toroidal magnetic field is minimum, due to the vanishing of its radial derivative. But the minimum of the toroidal magnetic field contradicts its reversal assumption (as one can see comparing the two B_φ profiles in fig. 1.14): this highlights the necessity of a poloidal current density component, that can not be driven by the applied toroidal loop voltage[15].

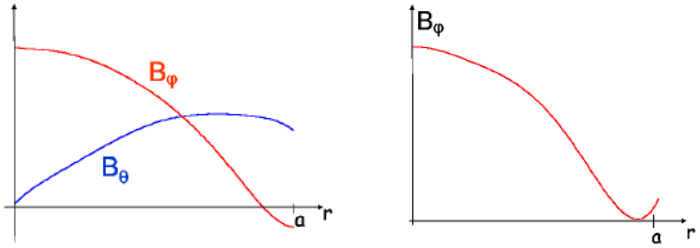

Figure 1.14: *Left:* The axi–symmetric RFP magnetic field components. *Right:* The toroidal magnetic field profile without a dynamo process.

The same can be proved looking at the parallel Ohm's law: on the reversal flux surface, where $\mathbf{B} = B_\theta$,

$$\mathbf{E}_\parallel = \eta_\parallel \mathbf{J}_\parallel \iff E_\theta = \eta_\parallel J_\theta \,. \tag{1.9}$$

The two sides of equation (1.9) are plotted in fig. 1.15. Again it is evident the necessity of a poloidal current at the reversal surface, that cannot be driven neither by the applied toroidal loop voltage neither by a $(\mathbf{v}\times\mathbf{B})$ term in the poloidal direction being $\mathbf{B} = B_\theta$.

Usually the dynamo process is understood as a $(\mathbf{v}\times\mathbf{B})$ term in the poloidal direction due to the non linear coupling between the velocity and the magnetic perturbation fields. Only one mode of the perturbation could be enough to sustain the dynamo: in this case the necessity of a dynamo is understood as the necessity of an helical deformation of the plasma column,

[14] Therefore exchanging the role of the axial B_z magnetic field and of the B_φ toroidal one.

[15] The pinch of the magnetic field lines due to the applied electric field is what produces just poloidal magnetic field lines at the reversal.

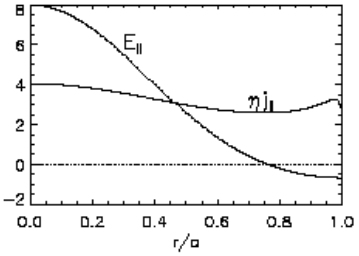

Figure 1.15: Mismatch between the applied electric field $E_\parallel$ and the resistive counterpart. It is noted that $E_\parallel > \eta j_\parallel$ at the center (necessity of anti–dynamo) while $E_\parallel < \eta j_\parallel$ at the edge (necessity of a dynamo process).

and the RFP is seen as a helically distorted paramagnetic pinch. One speaks of the *laminar RFP dynamo*, see section 7.1.
In any case, the field reversal is a consequence of the loss of the axi–symmetry of the system. This is known as the Cowling's theorem [23], for which no dynamo can sustain an axi–symmetric RFP.

1.2.5 Standard and laminar dynamo explanations. From Taylor to the *wire model*

Taylor relaxation theory

Taylor relaxation theory was the first explanation of the reversed configuration in fig. 1.2. It came in 1974 [24], when computers were not able to run a MHD simulation, and considers a plasma with null pressure and velocity in a cylindrical flux conserver. The plasma is considered as an isolated system, therefore it should reach the minimum energy state consistent with the constraints given by the global magnetic invariants.
The energy to be minimized is the total magnetic energy W, neglecting the internal energy due to the vanishing pressure:

$$W = \int_V \frac{B^2}{2\mu_0}\, dV \tag{1.10}$$

and Taylor proposes to consider as a constraint to the system the constancy of the magnetic helicity[16] K defined as

$$K = \int_V \mathbf{A} \cdot \mathbf{B}\, dV \tag{1.11}$$

[16]Magnetic helicity K defined in equation (1.11) to be distinguished from the geometric helicity of a magnetic perturbation. When speaking of the helicity of a mode in this thesis we are referring to the geometrical one, if not differently specified.

where $\mathbf{A}$ is the vector potential ($\mathbf{B} = \nabla \times \mathbf{A}$) and V the plasma volume enclosed by a given magnetic flux surface (Taylor considers the constancy of the total magnetic helicity inside the last closed magnetic flux surface).
The magnetic helicity K is constant for non resistive plasmas, but it can be considered approximately constant if the variation of K is much slower than the energy variation. This is experimentally verified and Taylor's picture is consistent even for low resistivity plasmas[17].
Woltjer's theorem states that a system constrained to constant magnetic helicity minimizes its energy reaching a (linear) force free configuration: $\mathbf{J} = \sigma\,\mathbf{B}$ with a constant σ profile. In cylindrical geometry the solutions are the Bessel functions (J_0 and J_1), for which $\nabla \times \mathbf{B} = \sigma\,\mathbf{B}$ and:

$$\begin{cases} B_r(r) = 0 \\ B_\theta(r) = B_0 J_1(\sigma r) \\ B_z(r) = B_0 J_0(\sigma r) \end{cases}$$

These solutions are called Bessel Function Model (BFM) and are plotted in fig. 1.16. One can see that these are not far from the experimental magnetic fields, and that the solution for B_z accounts for the reversal.
For a complete description of the BFM solution it is useful to introduce two

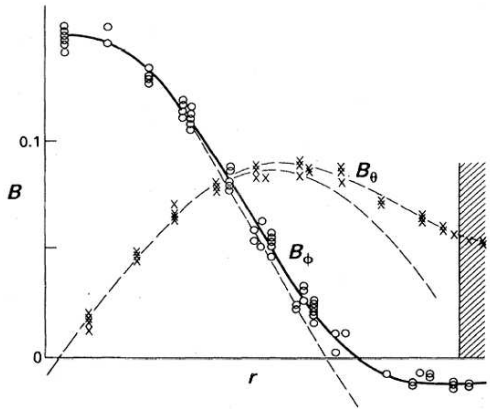

Figure 1.16: BFM solutions and experimental magnetic field profiles. Reproduced from H.A.B. Bodin, [26].

parameters, the *reversal parameter* F and the *pinch parameter* Θ, defined as

$$\Theta = \frac{B_\theta(a)}{\langle B_\varphi \rangle} \quad F = \frac{B_\varphi(a)}{\langle B_\varphi \rangle} \tag{1.12}$$

[17] Taylor's picture can be considered consistent with resistive plasma also if one can assume that the relaxation process is due to small scale fluctuation. In this case the energy decays faster than the magnetic helicity. But the dynamo process that must act to account for the reversal is due to large scale fluctuations, as tearing or kink modes [25].

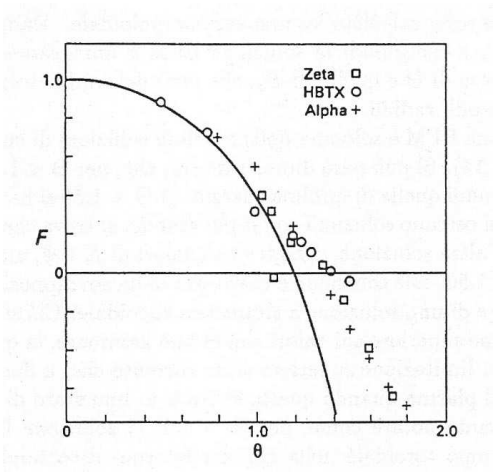

Figure 1.17: Schematic $F - \Theta$ diagram, as predicted by the BFM model (continuous line) and experimental values found in different devices.

where $\langle B_\varphi \rangle$ is the average of the toroidal magnetic field over the poloidal cross section and a the minor radius of the vacuum chamber. In general, since the toroidal field reverses for $r < a$, in the RFP F is always negative and the value Θ is always high. On the contrary, the Tokamak could be characterized with low Θ values and F positive everywhere. A common way to display the BFM model prediction is the $F - \Theta$ diagram (fig.1.17), in which the RFP states (the configurations with a reversed toroidal field) are supposed to exist for $\Theta > 1.2$. The experimental points overplotted in the same figure show a qualitatively reasonable agreement just in the central region. In the same plot, one could follow the start up of the discharge (from (a) to (d) in fig.1.3).

The BFM solutions correspond to the axi–symmetric reversed equilibrium states predicted by Taylor's theory[18]. This is in contrast with the already cited Cowling's theorem [23], for which a reversed axi–symmetric equilibrium can not exist. This is only one of the experimental and theoretical results that disagree with Taylor's relaxation theory.
Taylor gives an explanation for the final relaxed state, but does not specify the nature of the relaxation. A dynamo process must act against the magnetic field diffusion, and this breaks the axi–symmetry of the equilibrium system in agreement with Cowling's theorem. Moreover, the experimental σ profile is not constant over the whole plasma radius, in particularly it

[18]Taylor's theory can predict also a helical minimum energy state, corresponding to a mode resonating outside the reversal radius. But the geometrical helicity of this mode is opposite to the one of the experimental helical SHAx states, that correspond to a mode resonating inside the reversal surface. This is one of the criticism to Taylor's theory.

strongly varies outside the reversal radius[19]. RFP's plasmas are essentially ohmic, but a high plasma resistivity is out of Taylor's assumption[20]. Moreover, the plasma is not an isolated system[21]. In [25] one can find a more accurate elucidation of the Taylor's theory criticisms, and a new paradigm for the RFP that accounts for these. Its explanation in the next section can be found in D.F.Escande, *What is a RFP?*, to be published.

The wire model

In the new model, the RFP is described as a self–organized magnetic system that results from the nonlinear saturation of a resistive kink mode[22].
The intuitive toy model that explains the self–reversal of the axial magnetic field in a cylindrical system is called *wire model*, [29, 30].

A finite, but small, axial magnetic field is present inside the cylinder. This means a poloidal current is flowing in external coils on the cylinder (Fig. 1.18 (a)). The wire is in unstable equilibrium, and a small perturbation triggers a kink. The unstable kink is the one with a pitch whose sign is such that the poloidal part of the current flowing in the wire has the same orientation as the one in the cylinder, which brings a mutual attractive force (Fig. 1.18 (b)). Such a pitch brings also a solenoidal effect which increases the magnetic field and flux inside the kinked wire. The flux conserver imposes accordingly a decrease of the magnetic field and flux outside. As long as the current in the cylinder keeps its sign, the instability cannot quench. The continuing growth of the magnetic field and flux inside the kinked wire forces the outer magnetic field and the current in the cylinder to reverse.

This model exhibits a self–organized magnetic system where it is essential the loss of axi–symmetry to provide the reversal. Differently from Taylor's theory, this model explains the reversal without considering a closed system, accounting for the plasma resistivity, and predicting a helical magnetic equilibrium configuration in agreement with experiments[23] and the Cowling's

[19] The σ profile is constant in the chaotic radial domain: as shown by Rusbridge [27], σ must be constant along magnetic field lines in force free and stationary condition (because $\mathbf{J} = \sigma \mathbf{B}$ and $\nabla \cdot \mathbf{J} = 0$, then $\mathbf{B} \cdot \nabla \sigma = 0$). This explains why σ is constant in the chaotic core of MH states, even without the necessity of Taylor's theory.

[20] See footnote 17.

[21] Considering instead the plasma as an open ohmic system with fixed currents one can use an electrotechnics result, which states that such a system maximizes its magnetic energy (instead of relaxing toward a minimum energy state). See [25] and reference [45] therein: P. Lorrain and D.R. Corson, *Electromagnetic Fields and Waves*, New York: Freeman (1987).

[22] This model is a variant of the Kadomtsev one, that proposes a model for the saturation of a resistive kink for Tokamaks, in order to find the reversal of the axial magnetic field component. See Kadomtsev [28], and [25, 29].

[23] But in RFP experiments usually aided reversal is preferred to the self–reversal of this

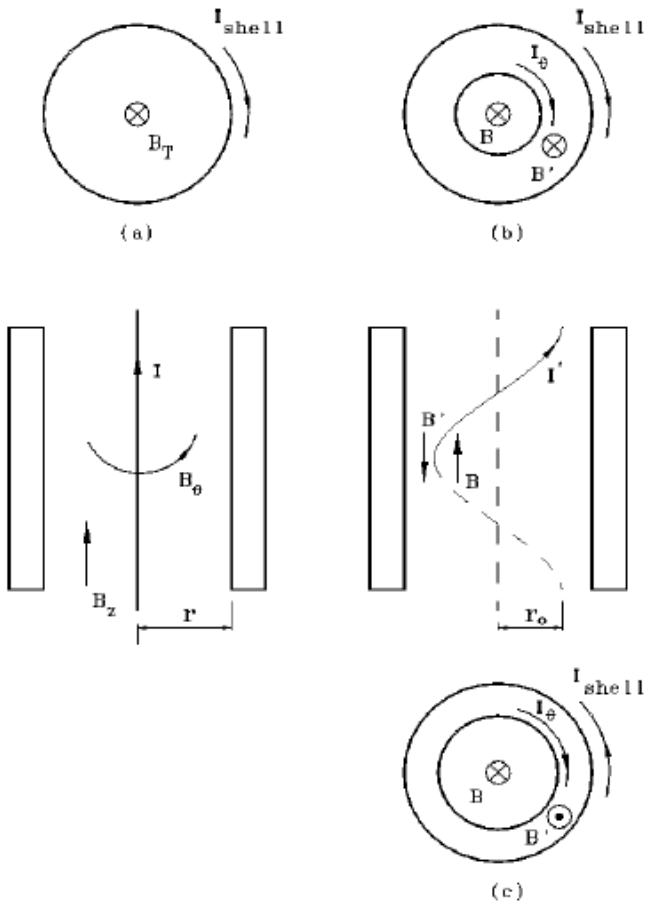

Figure 1.18: The *wire model*. (a): current-carrying wire in a flux conserver. The wire carries a current I_z, parallel to a magnetic field B_z whose flux is conserved by the conducting shell; (b): growth of the instability of I_θ; (c): a stable equilibrium with reversed field is reached. Reproduced from [30].

theorem. Differently from Taylor's theory, the origin of the dynamo velocity field is explained: as a consequence of the helical deformation of magnetic flux surfaces, a helical electrostatic potential generates the dynamo velocity as an electrostatic drift. This is called *laminar dynamo*, and better explained in section 7.1.

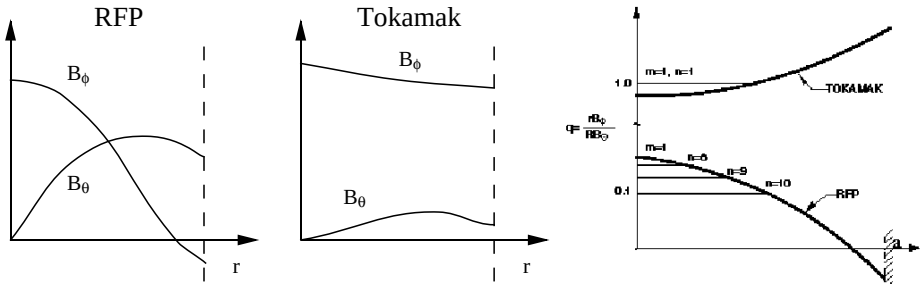

Figure 1.19: *Left, Middle:* The axi–symmetric RFP and Tokamak magnetic field components. *Right:* The RFP and Tokamak safety factor profile.

1.2.6 Main differences with Tokamak configurations

In a RFP most of the magnetic field is produced by the currents flowing in the plasma. For the same axial applied toroidal field, the plasma current is one order of magnitude larger in a RFP than in a Tokamak.
As a consequence, for the same plasma resistivity (and the same axial toroidal field), the ohmic heating (proportional to the squared plasma current) is two orders of magnitude larger in RFPs than in Tokamaks. Therefore, no additional heating is required for high plasma temperatures in RFP devices, and no superconducting magnets are required for strong magnetic field (the maximum magnetic field being bounded by the ability of driving high plasma currents and not by the maximum value imposed by the superconducting technology).
Another result of the high plasma current in a RFP is that the equilibrium magnetic field has poloidal and toroidal components of comparable amplitudes. As one can see in fig. 1.19, the similar amplitude of the two components of the equilibrium magnetic field pushes the value of the safety factor profile always below 1 in the RFP configuration. The $q = 1$ is known as the Kruskal–Shafranov limit[24]: below this limit the toroidal configuration should be stable (as Tokamak case), above helical MHD instabilities with $m = 1$ are triggered in the plasma (m is the poloidal mode number of the perturbation, and $m = 1$ are the kink instabilities of the type in fig.1.11 left). The self–organized magnetic system that results from the nonlinear saturation of a resistive kink mode corresponds to a full MHD relaxation that involves the toroidal field reversal and it turns out to be resilient to disruption.

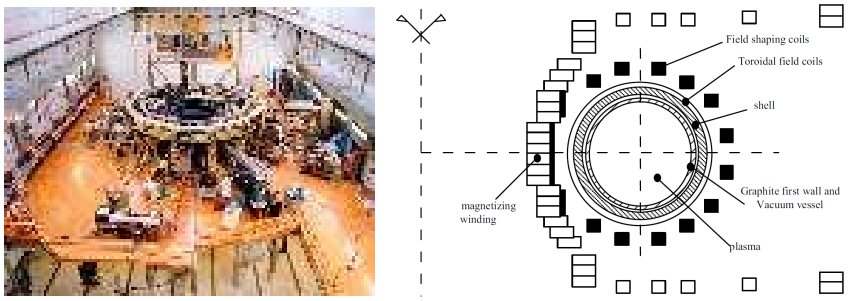

Figure 1.20: *Left:* The RFX–mod experiment. *Right:* Scheme of the poloidal section of RFX–mod experiment.

Major radius	$= 2\ m$
Minor radius	$= 0.459\ m$
Plasma current	$\leq 2\ MA$
Discharge duration	$\leq 0.5\ s$
Plasma density range	$\approx 1 \div 10 \times 10^{19}\ m^{-3}$
Plasma volume	$\approx 10\ m^3$
Working gas	H, He

Table 1.1: Main parameters of RFX-mod device.

1.3 RFX–mod experiment

The **R**eversed **F**ield E**X**periment *modified* (RFX-mod) [31], the upgraded version of the previous RFX [32], is a toroidal device for the study of the magnetically confined plasma in the RFP configuration. Located at the Istituto Gas Ionizzati (IGI) [33] of the National Research Council (CNR) [34] of Padova, it is operational since 2004 under the management of the Consorzio RFX, a research organization promoted by CNR, ENEA (the Italian National agency for new technologies, Energy and sustainable economic development) [35], University of Padova [36], Acciaierie Venete S.p.A. (a private partner) [37] and INFN (the Italian National Institute of Nuclear Physics) [38], within the framework of the Euratom - ENEA Association.

The main parameters of the RFX-mod device (the largest RFP in operation) are shown in the tab.1.1. As in all RFPs, plasma heating is purely ohmic. Despite a toroidal magnetic field ten times smaller (the whole magnetic system is shown in fig.1.20), this device allows exploring current regimes

model.

[24] See [11] for a treatment of the Kruskal–Shafranov limit.

(up to 2 MA) comparable to those of the large tokamaks.

First wall

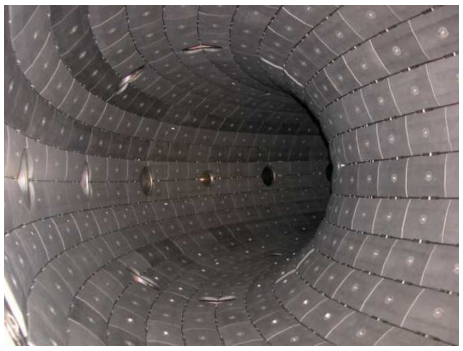

Figure 1.21: First wall, graphite tiles.

The RFX–mod first wall is composed by 2016 graphite tiles, covering completely the inner part of the vacuum vessel. In the new machine the tiles have been redesigned to achieve a more uniform power deposition on the plasma facing surface, to minimize the emissivity due to plasma wall-interaction and finally to give housing to a large number of in-vessel probes. These design requirements led to a substantial reduction of the tile thickness with respect to the original design [39].

The active feedback control system

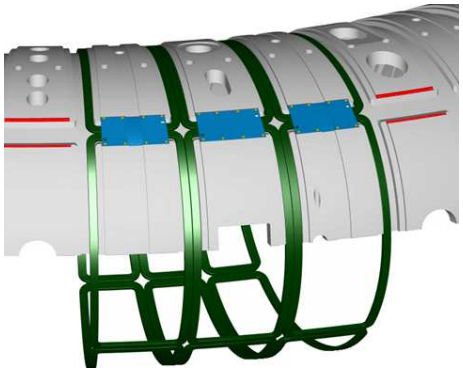

Figure 1.22: Saddle coils

With respect to the original RFX design, the present machine underwent some crucial modifications that allowed significant performance improvements.
The original RFX thick stabilizing shell (which had a magnetic field penetration time constant $\tau_{shell} = 500$ ms) was replaced with a thinner one, whose time constant for penetration of vertical magnetic field (≈ 50 ms) is ≈ 10 times shorter than pulse duration. Moreover, RFX-mod has been equipped with one of the most advanced system for feedback control of MHD stability with active coils among fusion devices. The system is based on 192 active saddle coils, which cover the whole plasma boundary (fig. 1.22). The coils are arranged in 48 toroidal locations; in each toroidal location there are 4 poloidal coils, according to the low m/high n structure of MHD modes in the RFP (where m and n are the poloidal and toroidal mode numbers, respectively). Each coil is independently driven by individual power supplies and can produce a radial magnetic field up to 50 mT DC and 3.5 mT at 100 Hz [31, 40, 41, 42]. Different algorithms for real-time tearing modes control have been developed to exploit the full capability of the feedback system, the most important being the Virtual Shell (VS) scheme [41] and the Clean Mode Control (CMC) [43]. The latter, in particular, has drastically changed the performance of the device, reducing the amplitude of the dynamo modes at the plasma boundary, mitigating their phase and wall locking and finally removing the aliasing of the sidebands that limits the VS control scheme [44].

The plasma current increase (the 2 MA have been achieved in 2010) is only the most evident one among a turn of outstanding achievements that considerably enhanced the interest about the RFX-mod developments and enriched the RFP physics, [45].

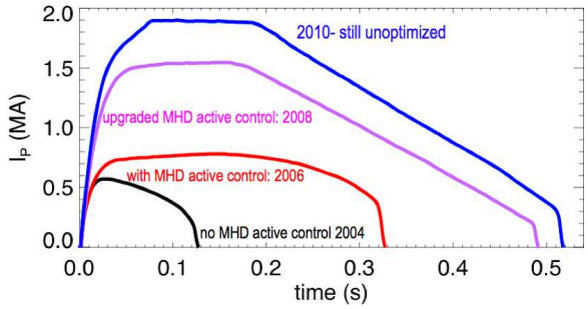

Figure 1.23: Plasma current waveforms obtained in RFX-mod since its restart in December 2004

As said, the plasma current increase (higher than 1.5 MA) has been accompanied by the observation of the helical SHAx states.

Chapter 2

Hamiltonian mechanics for magnetic field lines

This chapter gives an overview of the Hamiltonian mechanics applied to magnetic fields in a toroidal device.
Any divergence free field (as the magnetic field, for which $\nabla \cdot \mathbf{B} = 0$) in a torus can be written in its *canonical* form. For the magnetic field:

$$\mathbf{B} = \nabla\psi_t \times \nabla\theta - \nabla\psi_p \times \nabla\varphi \tag{2.1}$$

where in general $\psi_t \equiv \psi_t(r,\theta,\varphi)$ and $\psi_p \equiv \psi_p(r,\theta,\varphi)$ are the poloidal and toroidal fluxes[1] and (r,θ,φ) general toroidal coordinates. Using this relation one can see that magnetic field lines follow Hamiltonian trajectories for one–degree–of–freedom Hamiltonians:

$$\begin{cases} \frac{d\theta}{d\varphi} = \frac{B^\theta}{B^\varphi} = \frac{\partial\psi_p}{\partial\psi_t} \\ \\ \frac{d\psi_t}{d\varphi} = \frac{B^\rho}{B^\varphi} = -\frac{\partial\psi_p}{\partial\theta} \end{cases} \tag{2.2}$$

can be identified with the canonical equation of motion

$$\begin{cases} \frac{dq}{dt} = \frac{\partial H}{\partial p} \\ \\ \frac{dp}{dt} = -\frac{\partial H}{\partial q} \end{cases} \tag{2.3}$$

if

$$\text{canonical time } t \quad \leftrightarrow \quad \varphi \tag{2.4}$$
$$\text{Hamiltonian } H \quad \leftrightarrow \quad \psi_p \tag{2.5}$$
$$\text{position coord. } q \quad \leftrightarrow \quad \theta \tag{2.6}$$
$$\text{momentum } p \quad \leftrightarrow \quad \psi_t \tag{2.7}$$

[1] The fluxes are intended normalized to (2π). See section 2.7 for further details or the geometrical interpretation of these fluxes.

This is usually the starting point to relate Hamiltonian mechanics and magnetic field theory, with the general form:

$$\mathbf{A} = \nabla g + \psi_t \nabla\theta - \psi_p \nabla\varphi \tag{2.8}$$

for the vector potential $\mathbf{A}$ ($\mathbf{B} = \nabla \times \mathbf{A}$), [12].

In this chapter we propose the derivation of the canonical representation of the magnetic field, eq.(2.1), which clarifies the interpretation. We follow and collect the considerations of famous papers on the Hamiltonian mechanics of the magnetic fields, as [46, 47, 48, 5, 49, 50].
In *section 2.1* we introduce a variational principle for magnetic field lines in an heuristic but physically intuitive way; in *section 2.2* the same variational principle for the vector potential $\mathbf{A}$, from which the magnetic field line equations (in physical space) follow, is presented in a mathematically rigorous way; in *section 2.3* we prove the equivalence between this variational priciple and the one of Hamiltonian mechanics from which the canonical equations of motion (in phase space) derive. From this equivalence one can deduce the association between canonical and magnetic variables, for which it is natural to use the covariant components of the vector potential A_i; in *section 2.4* we show the equivalence between canonical transformation (related to the choice of the canonical variables) and gauge transformation (related to the choice of the vector potential $\mathbf{A}$); in *section 2.5* we introduce a usefull statement of Noether's theorem to be applied in any Hamiltonian context, and in particular to the symmetries of magnetic fields in fusion devices; in *section 2.6* Action–Angle coordinates are defined, that are nothing but straight–field–line coordinates on magnetic flux surfaces; in *section 2.7* the physical interpretation of the covariant component A_i clarifies the theoretical steps of the preceding sections: using Stokes theorem we prove the equivalence between A_i and the magnetic fluxes, and one can finally understand identifications (2.4)–(2.7); in *section 2.8* the main results of the chapter are shown following the more common (but less rigorous) way followed for example by A. Boozer [12] and W.D. D'Haeseleer [51]; in *section 2.9* a resumptive example is presented, for a system where a helical symmetry is supposed; in *section 2.10* a final simple example is proposed, to the study of an axi–symmetric magnetic field.
The example in section 2.9 is particularly important for the study of SHAx states, and will be used in chapter 4 to model them.

2.1 Variational principle for magnetic field lines. Intuitive physical approach

The Euler–Lagrange proof for the stationary action principle for magnetic field lines can be done in a rigorous way (as we do in section 2.2), and similar to what is done in Hamiltonian mechanics. Magnetic fields exhibits naturally also the geometrical elements of the differential geometry approach which uses symplectic manifolds (see the book of V.I. Arnold [46]) and we choose this intuitive approach to introduce the Hamiltonian theory for magnetic field lines.

We need to introduce in advance the definition of the Action for magnetic systems, equation (2.10):

$$S(\mathbf{x}) \quad = \quad \int_{\mathbf{x}_0}^{\mathbf{x}_1} A_i(\mathbf{x})\, dx^i \tag{2.9}$$

for the general $x^i = (x^1, x^2, x^3)$ coordinates and using the Einstein convention to sum over repeated indices.
$\mathbf{A}$ is the vector potential, and the variation of the Action in equation (2.12) implies the circulation of the vector potential along a closed circuit C. Using Stokes theorem, the variation of the Action δS is nothing but the flux of the magnetic field through any surface having this circuit as a boundary.

In fig.2.1 one finds two examples for the circuit C, both constructed as the sum of two segments L (light blue in the picture) and L' (green in the picture): in fig.2.1 a) the segment L is chosen along a magnetic field line, whereas in fig.2.1 b) L is not everywhere tangent to $\mathbf{B}$. In both cases L is weakly distorted into L' to compute δS along the circuit C.
Let us study more in details the example a), where L lies along a magnetic field line. We define a flux tube T_ϵ about L with a small radius ϵ and we suppose the small distortion L' confined into T_ϵ. The flux of the magnetic field B across the circuit C cannot therefore be larger than the flux across T_ϵ, that is of order ϵ^2. Because the variation of the curve L is just of order ϵ, the variation of the Action δS is second order in the variation of L. Therefore the Action S is stationary along a magnetic field line.
Let us study more in details the example b) where L does not lie on a magnetic field line. We choose a point P that belongs both to a magnetic field line (that we call M) and to the segment L; and a point Q that belongs to the line perpendicular both to M and L and going through P; we choose the point Q to be close to the point P, in order to have PQ of order ϵ. We then choose a segment $[r_3, r_4]$ of order 1 of L that includes the point P, and slightly distort L into a line L' coincident with L out of $[r_3, r_4]$: L' is the sum of the two segments joining r_3 and r_4 to Q. In this way we have defined the circuit C if fig.2.1 b) and we need to calculate the magnetic flux through

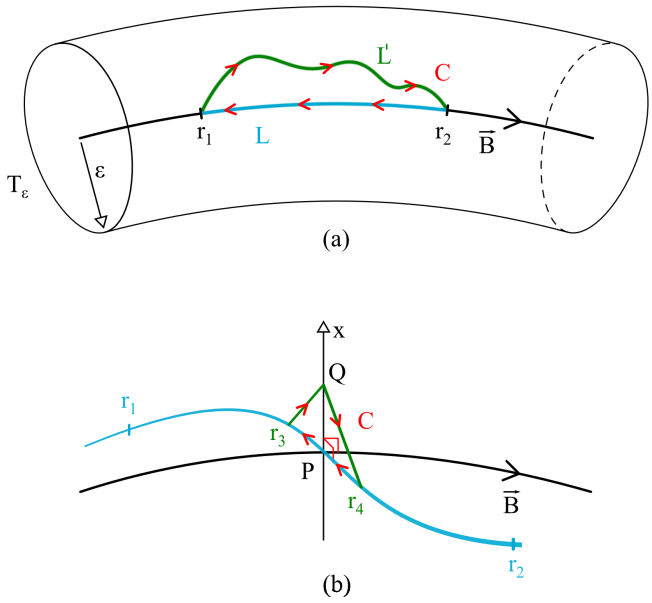

Figure 2.1: A physical intuitive approach to the variational principle for magnetic field lines.

it. Because L is not tangent to the magnetic field line (M), this flux is of order ϵ. Since the flux is of same the order as the variation of L, the Action S is not stationary along a curve L that is not tangent to a magnetic field line.

Therefore the Action S of a magnetic system is stationary on a curve L if and only if L is a segment of a magnetic field line, which proves principle (2.9).
In the next section we prove this in an algebraic way.

2.2 Variational principle for magnetic field lines

As was shown by Cary and Littlejohn [48] and already implicitly present in I. Morozov and L. S. Solovèv, Rev. Plasma Phys. 2, 229 (1966) [5], it is possible to obtain the magnetic field line equations from a variational principle, in the same way as we can find the canonical equations of motion in phase space from a variational principle that makes the action integral extremum in the Hamiltonian context. We define the action along a segment of magnetic field

line, between $\mathbf{x}_0$ and $\mathbf{x}_1$, as

$$S(\mathbf{x}) = \int_{\mathbf{x}_0}^{\mathbf{x}_1} \mathbf{A}(\mathbf{x}) \cdot d\mathbf{x} \tag{2.10}$$

$$= \int_{\lambda_0}^{\lambda_1} \Big(\mathbf{A}(\mathbf{x}(\lambda)) \cdot \frac{d\mathbf{x}}{d\lambda}\Big) d\lambda \tag{2.11}$$

where $\mathbf{A}$ is the vector potential that describes the magnetic field $\mathbf{B}$, and $\mathbf{x}(\lambda)$ is a parametrization of the magnetic field line with the curve parameter λ. The stationary action principle for field line flow can then be written as

$$\delta S = \delta \int_{\mathbf{x}_0}^{\mathbf{x}_1} \mathbf{A}(\mathbf{x}) \cdot d\mathbf{x} = 0 \tag{2.12}$$

$$= \delta \int_{\lambda_0}^{\lambda_1} \Big(\mathbf{A}(\mathbf{x}(\lambda)) \cdot \frac{d\mathbf{x}}{d\lambda}\Big)\, d\lambda = 0 \tag{2.13}$$

with the usual requirement that the arbitrary variation $\delta\mathbf{x}(\lambda)$ vanishes at the end points $\mathbf{x}_0 = \mathbf{x}(\lambda_0)$ and $\mathbf{x}_1 = \mathbf{x}(\lambda_1)$. Following Elsasser [50] we now prove in a formal way that equation (2.13) is true if and only if

$$\Big(\nabla \times \mathbf{A}\Big) \times \frac{d\mathbf{x}(\lambda)}{d\lambda} = 0 \tag{2.14}$$

which means that $\dot{\mathbf{x}} \equiv d\mathbf{x}/d\lambda$ is parallel to $\mathbf{B} = \nabla \times \mathbf{A}$, as required for magnetic field lines. In the following, the fields $\mathbf{A}(\mathbf{x})$ and $\mathbf{B}(\mathbf{x})$ are always taken at $\mathbf{x} = \mathbf{x}(\lambda)$ even when this is not explicitly stated.

$$0 = \delta \int_{\lambda_0}^{\lambda_1} d\lambda \,\Big[\mathbf{A}(\mathbf{x}) \cdot \dot{\mathbf{x}}\Big] \tag{2.15}$$

$$= \int_{\lambda_0}^{\lambda_1} d\lambda \,\delta\Big[\mathbf{A} \cdot \dot{\mathbf{x}}\Big] \tag{2.16}$$

$$= \int_{\lambda_0}^{\lambda_1} d\lambda \,\Big[\delta\mathbf{A} \cdot \dot{\mathbf{x}} + \mathbf{A} \cdot \delta\dot{\mathbf{x}}\Big] \tag{2.17}$$

$$= \int_{\lambda_0}^{\lambda_1} d\lambda \,\Big[\Big(\nabla \cdot \delta\mathbf{x}\Big)\Big(\mathbf{A} \cdot \dot{\mathbf{x}}\Big) + \Big(\mathbf{A} \cdot \delta\dot{\mathbf{x}}\Big)\Big] \tag{2.18}$$

$$= \int_{\lambda_0}^{\lambda_1} d\lambda \,\Big[\Big(\nabla \cdot \delta\mathbf{x}\Big)\Big(\mathbf{A} \cdot \dot{\mathbf{x}}\Big)\Big] - \int_{\lambda_0}^{\lambda_1} d\lambda \,\Big[\Big(\nabla \cdot \dot{\mathbf{x}}\Big)\mathbf{A} \cdot \delta\mathbf{x}\Big] \tag{2.19}$$

$$= \int_{\lambda_0}^{\lambda_1} d\lambda \,\Big[\nabla(\mathbf{A} \cdot \dot{\mathbf{x}}) - (\nabla \cdot \dot{\mathbf{x}})\mathbf{A}\Big] \cdot \delta\mathbf{x} \tag{2.20}$$

Therefore

$$0 = \Big[\nabla(\mathbf{A} \cdot \dot{\mathbf{x}}) - (\nabla \cdot \dot{\mathbf{x}})\mathbf{A}\Big] \tag{2.21}$$

$$= \dot{\mathbf{x}} \times \Big[\nabla \times \mathbf{A}\Big]_{\mathbf{x}\equiv\mathbf{x}(\lambda)} \tag{2.22}$$

equivalent to (2.14) as requested. This ends the proof, but let us make more precise some of its steps. Between (2.17) and (2.18) we use the general relation

$$\delta\mathbf{A}(\mathbf{x}) = \frac{\partial \mathbf{A}}{\partial \mathbf{x}}\,\delta\mathbf{x} = (\nabla\cdot\delta\mathbf{x})\,\mathbf{A} \quad . \tag{2.23}$$

Between (2.18) and (2.19) we simply integrate by parts, remembering that

$$\delta\dot{\mathbf{x}} \equiv \delta(\frac{\partial \mathbf{x}}{\partial \lambda}) = \frac{\partial}{\partial \lambda}(\delta\mathbf{x}) \tag{2.24}$$

and between (2.19) and (2.20) we highlight $\delta\mathbf{x}$ in the equation. Between (2.21) and (2.22) we use the classical formula for the gradient of a scalar product between two general vectors, and the fact that $\mathbf{x}(\lambda)$ is independent of space:

$$\nabla(\mathbf{A}\cdot\dot{\mathbf{x}}) = \mathbf{A}\times(\nabla\times\dot{\mathbf{x}}) + \dot{\mathbf{x}}\times(\nabla\times\mathbf{A}) + (\mathbf{A}\cdot\nabla)\dot{\mathbf{x}} + (\dot{\mathbf{x}}\cdot\nabla)\mathbf{A} \tag{2.25}$$

2.3 Hamiltonian description of magnetic field lines

In this section we show the equivalence between the variational principle for magnetic field lines in physical space (introduced in section 2.2) and the one for Hamiltonian dynamics in phase space, in order to highlight the link between the two fields of knowledge and to derive in a straightforward way the Hamiltonian description of field lines.
Following E. Piña & T. Ortiz, J. Phys. A 21, 1292 (1988) [49], we prove this equivalence for an arbitrary coordinate system $x^\mu = (x^1, x^2, x^3)$.
In such a system, the variational principle (2.13) becomes

$$0 = \delta\int_{\lambda_0}^{\lambda_1} d\lambda\; A_\mu(\mathbf{x})\,\frac{dx^\mu}{d\lambda} \equiv \delta\int A_\mu dx^\mu \quad . \tag{2.26}$$

where we used the classical covariant expression of the dot product. We now recall that the canonical equations of a N degree of freedom mechanical system can be derived from the variational principle

$$0 = \delta\int_{t_0}^{t_1} dt\,\left[\mathbf{p}\cdot\frac{d\mathbf{q}}{dt} - H(\mathbf{p},\mathbf{q},t)\right] \tag{2.27}$$

$$= \delta\int_{t_0}^{t_1} \left[\mathbf{p}\,d\mathbf{q} - H(\mathbf{p},\mathbf{q},t)\,dt\right] \tag{2.28}$$

where $(\mathbf{p},\mathbf{q})$ are the canonical variables (N-vectors) and $H(\mathbf{p},\mathbf{q},t)$ the Hamiltonian of the system[2].

[2] The $\mathbf{p}\cdot\frac{d\mathbf{q}}{dt} - H(\mathbf{p},\mathbf{q},t)$ term is therefore the Lagrangian of the system.

In section 2.2 we saw that magnetic field lines can be derived from a stationary action principle: magnetic field lines in physical space are analogous to the flow of a dynamical system with one degree of freedom ($N = 1$)[3].
We can therefore compare the so–called Poincaré–Cartan invariant form, typical of dynamical systems and written in canonical coordinates,

$$p dq - H\, dt = \left[p \frac{dq}{dt} - H(p, q, t) \right] dt \tag{2.29}$$

with the equivalent form valid for magnetic systems in physical spaces, written in the general coordinates $x^\mu = (x^1, x^2, x^3)$

$$A_\mu dx^\mu = A_1\, dx^1 + A_2\, dx^2 + A_3\, dx^3 \quad for \quad \mu = 1, 2, 3 \quad . \tag{2.30}$$

In general it is $A_i \equiv A_i(x^1, x^2, x^3)$. Identifying the two forms, apparently there are three elements in the sum (2.30) for magnetic field lines, and just two in eq.(2.29) for the $N = 1$ dynamics. The covariant components of the vector potential, A_i, are defined up to gauge transformations[4]: one of the component in the sum can be killed using the choice of an axial gauge, $A_i = 0$ for one of the indexes. The identification become trivial, and it is the way to obtain the identification with canonical variables (p, q, H, t) in the physical space.

As an example, we choose the axial gauge $A_2 = 0$ (following [49]):

$$A_1\, dx^1 + A_3\, dx^3 = p\, dq - H\, dt \tag{2.31}$$

that means that we can identify

$$\begin{aligned} p &= A_1(x^1, x^2, t) && (2.32)\\ q &= x^1 && (2.33)\\ H &= -A_3(q, p, t) && (2.34)\\ t &= x^3 && (2.35) \end{aligned}$$

where we invert (possibly only locally) the relation $p = A_1(x^1, x^2, t)$ in order to write $x^2 = x^2(x^1, p, t)$ and therefore the Hamiltonian as a function of the canonical variables, $H = H(p, q, t)$.

A mere change of the numbers of the coordinates enables to deal with the gauge $A_1 = 0$ or $A_3 = 0$. Different choices of the gauge correspond to different sets of canonical variables.
Let us write explicitly the set of variables for the choice $A_1 = 0$:

$$A_2\, dx^2 + A_3\, dx^3 = p\, dq - H\, dt \tag{2.36}$$

[3] We will prove this in a rigorous way also in section 2.5.1
[4] Any gauge transformation can be written as $A_i \mapsto A_i + \partial F / \partial u^i$.

that, as before, means

$$p = A_2(x^1, x^2, t) \tag{2.37}$$
$$q = x^2 \tag{2.38}$$
$$H = -A_3(q, p, t) \tag{2.39}$$
$$t = x^3 \tag{2.40}$$

where we again invert the relation for the canonical momentum p in order to write the Hamiltonian H as a function of the canonical coordinates.

By exchanging the order of $p\,dq$ and $-H\,dt$ in eq.(2.31) we note that the role of the canonical momentum (e.g. $p = A_2(x^1, x^2, t)$ in the gauge $A_1 = 0$) can always be exchanged with minus the Hamiltonian variable ($H = -A_3(p, q, t)$), which shows the huge freedom in the definition of a Hamiltonian for magnetic field lines. However an arbitrary choice of *time* does not guarantee magnetic field lines to be fully parametrized by a time running from $-\infty$ to $+\infty$. Section 2.5.2 shows that the choice of *time* can guided by the existence of a symmetry.

2.4 Gauge or canonical transformation?

In section 2.3 we see that different choices of gauge correspond to different sets of canonical variables, and we need to choose an axial gauge in order to make the identification between the magnetic and the Hamiltonian system. In this section we prove that gauge transformations are nothing but canonical transformations, using the language of Hamiltonian mechanics.
From Hamiltonian flow theory we know that the equations of motion (and therefore the magnetic field line equations) are independent under canonical transformations. It is easy to prove[5] that the Hamiltonian flows are independent from both canonical and gauge transformations. This is true because

[5]Lagrangian, Action, and equation of motion are independent from both gauge and canonical transformation. Let us define gauge transformations. Under a gauge transformation, the vector potential transforms as

$$\mathbf{A} \mapsto \mathbf{A} + \nabla S \tag{2.41}$$
$$A_\mu \mapsto A_\mu + \frac{\partial S}{\partial x^\mu} \tag{2.42}$$

where the function $S(\mathbf{x})$ is a scalar, and ∇S its gradient. The correspondent Poincarè–Cartan (P–C) form and the Lagrangian transform respectively as:

$$A_\mu\, dx^\mu \mapsto A_\mu\, dx^\mu + dS \tag{2.43}$$
$$A_\mu \frac{dx^\mu}{d\lambda} \mapsto A_\mu \frac{dx^\mu}{d\lambda} + \frac{dS}{d\lambda} \tag{2.44}$$

so a gauge transformation add to the P–C form the total differential of the scalar S, and to the Lagrangian the total derivative ($d/d\lambda$) of the same function S. The Action transforms

both can be identified, as we now show.

Any canonical transformation[6] $(p,q) \mapsto (P,Q)$ can be described as:

$$p\,dq - H\,dt = P\,dQ - K\,dt + dF \tag{2.47}$$

where $F(q,Q,t)$ is a generating function. By definition,

$$dF(q,Q,t) = p\,dq - P\,dQ + (K-H)dt \tag{2.48}$$

$$p = \frac{\partial F}{\partial q}\ ,\ P = \frac{\partial F}{\partial Q}\ ,\ K = H + \frac{\partial F}{\partial t} \quad . \tag{2.49}$$

Under a gauge transformation[7], the corresponding Poincaré–Cartan (P–C) form $p\,dq - H\,dt = A_\mu dx^\mu$ transforms as:

$$A_\mu\,dx^\mu \quad \mapsto \quad A_\mu\,dx^\mu + dS \tag{2.55}$$

so any gauge transformation adds to the P–C form the total differential of some scalar $S(\mathbf{x})$.

---

as

$$\int L\,d\lambda = \int A_\mu \frac{dx^\mu}{d\lambda} d\lambda \mapsto \int L\,d\lambda + S \quad . \tag{2.45}$$

The variational principle give magnetic field line equations due to the minimization of the Action:

$$0 = \delta \int L\,d\lambda \mapsto \delta \int L\,d\lambda + \delta S = 0 \tag{2.46}$$

where $\delta S = 0$ due to the vanishing variation of the position at the boundaries. It is therefore evident that the magnetic *field line flow* does not change under gauge transformations. And this is obviously true also for the Hamiltonian form $\gamma_\mu dz^\mu = p\,dq - H\,dt$ of a mechanical system, proving that *Hamiltonian flows* are independent, not just of canonical transformations, but also of gauge transformations. The notation $\gamma_\mu dz^\mu = p\,dq - H\,dt$, similar to $A_\mu dx^\mu$, is defined for mechanical systems in section 2.5.1

[6] For a definition of canonical transformations and their generating functions see [46].

[7] By definition,

$$A_\mu\,dx^\mu \quad \mapsto \quad A_\mu\,dx^\mu + dS \tag{2.50}$$

Using the gauge $A_1 = 0$ and the identifications (2.36)–(2.40), under a gauge transformation:

$$p \quad \mapsto \quad p' = p + \frac{\partial S}{\partial q} \tag{2.51}$$

$$H \quad \mapsto \quad H' = H - \frac{\partial S}{\partial t} \tag{2.52}$$

remembering that $x^2 = q$, $x^3 = t$ and

$$A_2 \quad = \quad p \quad ,\ A_2' = p' \tag{2.53}$$

$$-A_3 \quad = \quad H \quad ,\ -A_3' = H' \tag{2.54}$$

The generating function S of the gauge transformation must be $S(\mathbf{x}) = S(x_1,q,t)$. Inverting the relation $p = A_2(x_1,q,t)$ one can think to $S \equiv S(p,q,t)$.

Let us apply the same gauge transformation defined by the function $S(x, y, t)$ of the two variables (x, y) parametrized by t, before and after the canonical transformation (2.47). This means performing the gauge transformation in the (p, q) coordinate with $S(p, q, t)$ and the gauge transformation in the (P, Q) coordinate with $S(P, Q, t)$:

$$p\,dq - H\,dt + dS = P\,dQ - K\,dt + dF + dS \tag{2.56}$$

where $F \equiv F(q, Q, t)$.
Now assume that the canonical transformation and the subsequent gauge transformation are connected by condition [50]

$$F(q, Q, t) + S[P(q, Q, t), Q, t] = 0 \tag{2.57}$$

where $P(q, Q, t)$ is defined by equation 2.49. Then we find

$$p\,dq - H\,dt + dS = P\,dQ - K\,dt \quad . \tag{2.58}$$

This means that $S[P(q, Q, t), Q, t]$ is the generating function of the reciprocal canonical transformation

$$(P, Q) \;\mapsto\; (p, q) \tag{2.59}$$

$$K \;\mapsto\; H \tag{2.60}$$

By equation (2.57) we can therefore read any gauge transformation as a canonical one, and vice versa.

There are many gauges for the vector potential $\mathbf{A}$, but magnetic filed lines are intrinsic objects in the physical space, that do not depend on the coordinate system. In the same way, there are many choices of canonical variables $(\mathbf{p}, \mathbf{q})$ and correspondingly of Hamiltonian $H(\mathbf{p}, \mathbf{q}, t)$, but the Hamiltonian flow is an intrinsic object in phase space. This is due to the way the Poincaré-Cartan integral invariant accommodates gauge or canonical transformations.

2.5 Symmetries and Noether theorem

2.5.1 Equivalence between the variational principles for magnetic field lines and for Hamiltonian mechanics

In order to be able to write also the variational principle for the dynamics in phase space in general coordinates, we need to go through some changes in the notation. This will allow to use a formally identical statement of Noether theorem for magnetic field lines systems in physical space and for dynamical systems in phase space. We follow Cary and Littlejohn [48].

Let z^i and γ^i be collections of $2N$ coordinates, defined in a $2N-$dimensional space as:

$$z^i \equiv (q_1, ..., q_N, p_1, ..., p_N) \equiv (q_j, p_j)\,,\ i = 1, ..., 2N\ \ (j = 1, ..., N) \tag{2.61}$$

$$\gamma_i \equiv (p_1, ..., p_N, \underbrace{0, ..., 0}_{j+N}) \equiv (p_j, 0)\,,\ i = 1, ..., 2N\ \ (j = 1, ..., N) \tag{2.62}$$

In a similar way we define the $(2N+1)$ components z^μ and γ^μ of vectors in the $(2N+1)$ dimensional 'extended phase space':

$$z^\mu \equiv (t, q_1, ..., q_N, p_1, ..., p_N) \equiv (t, q_j, p_j)\,,\ \mu = 0, ..., 2N\ \ (j = 1, ..., N) \tag{2.63}$$

$$\gamma_\mu \equiv (-H, p_1, ..., p_N, \underbrace{0, ..., 0}_{j+N}) \equiv (-h, p_j, 0)\,,\ \mu = 0, ..., 2N\ \ (j = 1, ..., N) \tag{2.64}$$

Note that z^i and z^μ are the definitions of the canonical coordinates in the $2N$ dimensional phase space and in the $2N+1$ dimensional extended phase space respectively. The Hamiltonian $H(\mathbf{p}, \mathbf{q}, t)$ is nothing but $-\gamma_0$.
We are now able to re–write the stationary action principle (2.28) in general coordinates, remembering that $H \equiv H(\mathbf{p}, \mathbf{q}, t)$:

$$0 = \delta \int_{t_0}^{t_1} dt \left[\mathbf{p} \cdot \frac{d\mathbf{q}}{dt} - H(\mathbf{p}, \mathbf{q}, t)\right] \tag{2.65}$$

$$= \delta \int_{t_0}^{t_1} dt \left[\gamma_i \frac{dz^i}{dt} - H\right] \tag{2.66}$$

$$= \delta \int_{t_0}^{t_1} dt\, \gamma_\mu \frac{dz^\mu}{dt} \tag{2.67}$$

Equation (2.66) is the variational principle written in the (z^i, γ^i) canonical variables and true in the $2N-$dimensional phase space; equation (2.67) is the variational principle written in the (z^μ, γ^μ) canonical variables and true in the $(2N+1)-$dimensional extended phase space.
Moreover, the $\gamma_\mu dz^\mu$ term is a scalar[8], and it must be $\gamma_\mu dz^\mu = \Gamma_\mu dZ^\mu$ for any change of coordinates[9] $z^\mu \mapsto Z^\mu$. It allows to write

$$0 = \delta \int_{t_0}^{t_1} dt \left(\gamma_\mu \frac{dz^\mu}{dt}\right) = \delta \int_{t_0}^{t_1} dt \left(\Gamma_\mu \frac{dZ^\mu}{dt}\right) \equiv \delta \int \Gamma_\mu\, dZ^\mu \tag{2.68}$$

This is the variational principle valid in the extended phase space for any kind of coordinates Z^μ, and we can therefore see that the variational principle (2.67) derived for canonical variables has the same form in any coordinate

[8] We remind the Einstein convention to sum over repeated indices.
[9] Under the change of coordinates $z^\mu \mapsto Z^\mu$, γ^μ transforms with the general rules for the component of covariant vectors: $\gamma_\mu \mapsto \gamma_\nu\, \partial z^\nu / \partial Z^\mu$

system.
This is what we were looking for, as we can see comparing the variational principles for magnetic field lines and Hamiltonian flow: equation (2.68) and (2.26) are now formally identical.
This shows that magnetic field lines in physical space are analogous to the flow of a dynamical system in the extended phase space $(2N+1)-$dimensional. This means that the problem of finding magnetic filed lines in $3-$dimensional physical spaces is equivalent to solve the dynamical problem for a system with $N = 1$ degree of freedom. From now on we can use the Hamiltonian formalism also for magnetic problems without confusion.

2.5.2 A common statement for Noether theorem

There are many statements of the Noether theorem, that essentially associates any symmetry of a system with a constant of the motion[10]. We use here, and we don't prove it, the Noether theorem for the Poincarè–Cartan form $\gamma \equiv \gamma_\mu\, dx^\mu$ or $A_\mu\, dx^\mu$, following [48] and using the result of section 2.5.1. *If the components γ_μ (A_μ) of the Poincaré–Cartan form are independent of one of the coordinates, say z^α (x^α), then the quantity γ_α (A_α) is an invariant of the flow $\partial z^\mu/\partial t$ ($\partial x^\mu/\partial\lambda$).*[11] The coordinate z^α (x^α) is said *ignorable coordinate*, and we can always find an appropriate frame of reference (gauge) that reveals the symmetry of the system.

Let us write this in an explicit way, in the general coordinates $x^\mu = (x^1, x^2, x^3)$, choosing the third coordinate x^3 as an ignorable coordinate. This means the components of the form $A_\mu\, dx^\mu$ are independent of x^3: $A_i \equiv A_i(x^1, x^2)$ for every $i = 1, 2, 3$:

$$A_\mu\, dx^\mu = A_1(x^1, x^2)\, dx^1 + A_2(x^1, x^2)\, dx^2 + A_3(x^1, x^2)\, dx^3 \quad . \qquad (2.70)$$

Noether theorem states that the quantity $A_3(x^1, x^2)$ is a constant of the motion, conserved by the flow.
Choosing for the ignorable coordinate the coordinate $z^0 = t$ ($\alpha = 0$), from the previous statement, the conservation of the Hamiltonian $H = -\gamma_0$ for

[10] Considering the phase space Lagrangian $L(\mathbf{q}, \dot{\mathbf{q}}, t)$ (instead of the Hamiltonian $H(\mathbf{p}, \mathbf{q}, t)$) one can prove Noether theorem using Euler–Lagrange equations:

$$\frac{\partial L}{\partial q_i} - \frac{d}{dt}\frac{\partial L}{\partial \dot{q}_i} = 0 \qquad (2.69)$$

When an ignorable coordinate exists for the Lagrangian (let us say the coordinate q_i, $\partial L/\partial q_i = 0$), then the symmetry corresponds to a translation in q ($\partial L/\partial \dot{q}_i = const$) and (Noether theorem) there exists a constant of the motion ($(d/dt)(\partial L/\partial \dot{q}_i) = 0$). By definition $p_i \equiv \partial L/\partial \dot{q}_i$, and Noether thorem is true also in phase space using $H(\mathbf{p}, \mathbf{q}, t)$ and forgetting about the Lagrangian L.

[11] One can find this statement of Noether theorem in [48].

time independent systems follows. One can always think of the Hamiltonian flow itself as a time independent canonical transformation: going back to the previous example, we can then think of x^3 as the canonical time t and of $A_3(x^1, x^2)$ as the conserved Hamiltonian (for the Hamiltonian system associated to $\mathbf{A}$):

$$H = -A_3(x^1, x^2) \equiv \psi(x^1, x^2) = const \quad . \tag{2.71}$$

In the context of Hamiltonian mechanics, $H(p, q) \equiv E = const$ defines the constant energy surfaces in phase space, and a periodic motion when the $E-$contours are closed curves. The surfaces defined by $H = -A_3 = \psi(x^1, x^2) = const$ are the flux surfaces of the integrable magnetic system associated to $\mathbf{A}$, where the field line flow lies.
Let us note that in the context of fusion machines this implies a confined field line flow when the $\psi-$contours are closed in some region of interest. A typical example are the nested toroidal flux surfaces in the Tokamak due to the toroidal symmetry of the machine (in our notation, $x^3 \equiv \varphi$ is used as the canonical time in this case).

We saw from the examples in section 2.3 that some freedom can arise in the choice of the canonical momentum and of the Hamiltonian when we look for the canonical variables in a magnetic system: the canonical momentum and the Hamiltonian can always exchange their role if the chosen coordinates do not reveal any symmetry. We saw in this section that the Hamiltonian of a system with one degree of freedom is univocally determined if a symmetry is evident, which eliminates the freedom also in the choice of the canonical momentum. The ignorable coordinate is therefore interpreted as the canonical time[12].
We go back to the examples of section 2.3 because we can now re–write them without any freedom in the identification of the canonical variables. We keep on using the general coordinates $x^\mu = (x^1, x^2, x^3)$, keeping in mind that one can for example use (x^1, x^2, x^3) as the cylindrical (R, z, φ) or toroidal (r, θ, φ) coordinates. We choose x^3 as canonical time t (the ignorable coordinate) and start from (2.70) and (2.71), with $A_i = A_i(x^1, x^2)$:

$$\begin{aligned} A_\mu \, dx^\mu &= A_1(x^1, x^2)\, dx^1 + A_2(x^1, x^2)\, dx^2 + A_3(x^1, x^2)\, dx^3 & (2.72) \\ &= p\, dq - H\, dt & (2.73) \end{aligned}$$

$$\begin{aligned} t &= x^3 & (2.74) \\ H &= -A_3(x^1, x^2) & (2.75) \end{aligned}$$

[12] We will see that not all the symmetries define good canonical time, because the symmetry do not guarantee any magnetic field line to be fully parametrized by a time running from $-\infty$ to $+\infty$. An example of that is the toroidal angle in RFP devices,that reverses at the edge. We will find some solution for this in chapter 4.

In order to identify also the canonical variable (p, q) we need now to choose the axial gauge. Choosing the gauge $A_1 = 0$, (2.72) simply reduces to:

$$A_\mu \, dx^\mu = A_2(x^1, x^2) \, dx^2 + A_3(x^1, x^2) \, dx^3 \tag{2.76}$$
$$= p \, dq - H \, dt \tag{2.77}$$

and therefore

$$q = x^2 \tag{2.78}$$
$$p = A_2(x^1, x^2) \tag{2.79}$$

The Hamiltonian must be function of the canonical variables, and not of the general coordinates x^μ. This is done inverting (at least locally) relation (2.79).
As we can see, we can divide the example in two parts: first we must find the ignorable coordinate to choose the canonical time and the Hamiltonian of the system, and then we must impose an axial gauge to identify the canonical variable (p, q).
To conclude, let us note also that inverting relation (2.71) one can write the first coordinate $x^1 = x^1(H, x^2)$, which means that one can always choose the Hamiltonian as the first coordinate by inverting this relation. In the case of magnetic flux surfaces the Hamiltonian can be used to label them. Then H will be called *radial* coordinate. In general, any function of the Hamiltonian only can be used to label magnetic flux surfaces, and we will use the general symbol ρ to indicate any of these *radial* functions[13].

2.6 Action–Angle variables

Hamiltonian systems with one degree of freedom and a time independent Hamiltonian ($H \equiv H(p, q)$) are always integrable and $H(p, q) = E = const$ defines the constant energy surfaces in phase space. In magnetic systems we can say this in an equivalent way: the field line flow lies on magnetic flux surfaces.
When this is true, one can always find a canonical transformation $(p, q) \mapsto (P, Q)$ such that the new Hamiltonian is a function only of the new momenta, $H = H(P)$: the position variable Q is a ignorable coordinate in this frame of reference, and the momentum P is a constant of the motion because of Noether theorem.
In the case of bounded energy surfaces in phase space (or closed magnetic flux surfaces[14]) the motion is periodic in time and the new $(P, Q) \equiv (I, \zeta)$ canonical variables are called *Action–Angle* coordinates. By definition

[13] We use the same symbol ρ for every surface, even if in a rigorous way one should distinguish between different topological orbits in the case of magnetic island.

[14] We will always use the word *closed* in its physical meaning, as magnetic flux surfaces closing on themselves, and not in its topological definition.

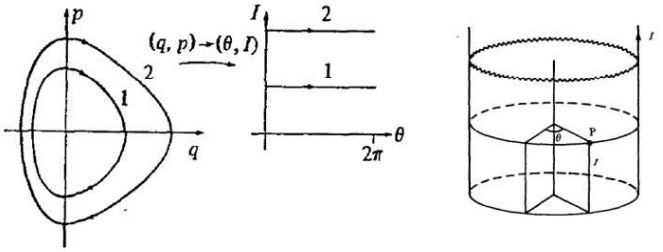

Figure 2.2: The Action–Angle canonical transformation for one degree of freedom periodic system in phase space. Reproduced from Hervieux lessons on internet. In this figure Angle θ corresponds to Angle ζ in the text.

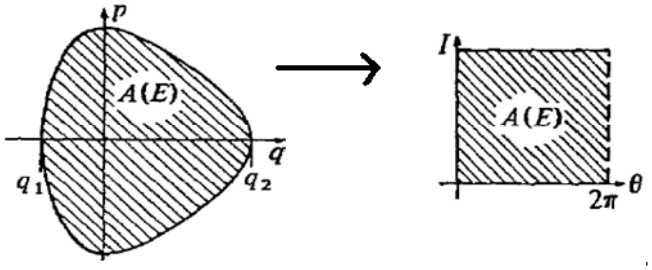

Figure 2.3: The Action–Angle canonical transformation of the area of a bounded energy surfaces for one degree of freedom periodic system in phase space. Reproduced from Hervieux lessons on internet. In this figure Angle θ corresponds to Angle ζ in the text.

Action–Angle coordinates are therefore defined by $I(E) = const$ and by an angle ζ that varies by 2π along any orbit of constant energy E. Areas are preserved by canonical transformations, and we can use this to find a simple definition for the Action I. Say $A(E)$ the area inside the orbit with constant energy E [15],

$$A(E) = \oint p(q,E)\,dq = \oint I(E)\,d\zeta \equiv \int_0^{2\pi} I(E)\,d\zeta = 2\pi\, I(E) \qquad (2.81)$$

from which[16]

$$I(E) = \frac{A(E)}{2\pi} = \frac{1}{2\pi}\oint p(q,E)\,dq \qquad (2.82)$$

[15] Because of Stokes theorem written for differential forms,

$$A(E) = \iint dp\,dq = \oint p\,dq \quad . \qquad (2.80)$$

[16] Again, $p \equiv p(q,H)$ inverting the relation $H = H(p,q)$, $H = const$.

In order to define the Angle we go back to the idea of (time independent) canonical transformation

$$p\,dq \;-\; H\,dt \mapsto I\,d\zeta \;-\; H(I)\,dt \tag{2.83}$$

and we use the generating function of type $F_2 \equiv F_2(q, I)$:

$$F_2(q, I) = \int p(q, I)\,dq \tag{2.84}$$

The transformation rules are

$$p(q, I) = \frac{\partial F_2}{\partial q} = \int_{q_0}^{q} \frac{\partial p}{\partial q}(q, I)\,dq \tag{2.85}$$

$$\zeta(q, I) = \frac{\partial F_2}{\partial I} = \int_{q_0}^{q} \frac{\partial p}{\partial I}(q, I)\,dq \qquad . \tag{2.86}$$

Equation of motion are now very simple:

$$\frac{dI}{dt} = -\frac{\partial H}{\partial \zeta} = 0 \tag{2.87}$$

$$\frac{d\zeta}{dt} = \frac{\partial H}{\partial I} = \omega(I) = const \quad . \tag{2.88}$$

The Action is constant along any orbit of constant energy E. The Angle ζ evolves linearly in time with a *frequency* $\omega(I)$ and varies by 2π along any orbit of constant energy E: over one period

$$\Delta F_2 \qquad = \oint dq\,\frac{\partial F_2}{\partial q} = \oint p\,dq = 2\pi\,I \tag{2.89}$$

$$\Longrightarrow \Delta\zeta = \frac{\Delta F_2}{\Delta I} = 2\pi \tag{2.90}$$

2.6.1 Action–Angle coordinates for magnetic systems

We can use all the results of Hamiltonian mechanics for magnetic field line systems: we simply re–write the previous results in an explicit way for these systems, where the analogues of bounded constant energy surfaces in phase space are the closed magnetic flux surfaces.
We use the symmetry of the system to find out the canonical time and the Hamiltonian, and the choice of an axial gauge to identify also the canonical variables (p, q): using again the general coordinates $x^\mu = (x^1, x^2, x^3)$ and the frame of reference where a symmetry with respect to the ignorable coordinate x^3 is manifest, together with the choice $A_1 = 0$, we have already found

equations (2.71), (2.74), (2.78), (2.79):[17]

$$t = x^3 \tag{2.91}$$
$$q = x^2 \tag{2.92}$$
$$p = A_2(x^1, x^2) \tag{2.93}$$
$$H = -A_3(x^1, x^2) = \psi(x^1, x^2) = const \tag{2.94}$$

From here we can easily apply eq.(2.82), (2.84), (2.86) to define the Action–Angle coordinate on $\psi = const$ surfaces[18]:

$$I(\psi) = \frac{1}{2\pi} \oint p(\psi, q)\, dq \equiv \frac{1}{2\pi} \oint A_2(\psi, x^2)\, dx^2 \tag{2.95}$$

$$F_2(x^2, I) = \int_{q_0}^{q} p(I, q)\, dq \equiv \int_{x_0^2}^{x^2} A_2(I, x^2)\, dx^2 \tag{2.96}$$

$$\zeta(x^2, I) = \frac{\partial F_2}{\partial I} \equiv \int_{x_0^2}^{x^2} \frac{\partial A_2}{\partial I}(I, x^2)\, dx^2 \tag{2.97}$$

Equations (2.87)–(2.88) of the motion in the $(I, \zeta)-$plane are the equation for the magnetic field lines:

$$\frac{dI}{dx^3} = 0 \tag{2.98}$$
$$\frac{d\zeta}{dx^3} = \omega(I) = \frac{dH}{dI} = \frac{d\psi}{dI} \tag{2.99}$$

To compute Action–Angle coordinates we go through a canonical change of coordinates, as written in eq.(2.83). Let us see how the general $x^\mu = (x^1, x^2, x^3)$ coordinates and the identification with the canonical variables change accordingly to this. From the identifications (2.91)–(2.94) it is clear that, with the change $(p, q) \mapsto (P, Q)$ in eq.(2.83), we are changing just the second coordinate ($x^2 = q$), that must be now identified with the Angle ζ ($x^2 \mapsto \zeta$). As a consequence, the covariant component $A_2 = p$ of the vector potential changes, being identified with the new momentum, the Action I ($A_2 \mapsto I$). The *time* x^3 and the first coordinate x^1 (due to the gauge $A_1 = 0$) are unchanged, and so is true also for the Hamiltonian:

$$(x^1, x^2, x^3) \mapsto (x^1, \zeta, x^3)$$

The only thing more that we can do is to perform the inversion of the function $H = \psi(x^1, x^2)$ to be able to write $x^1 = x^1(\psi, x^2)$ and therefore to choose the Hamiltonian as the *radial* coordinate that labels the magnetic flux surfaces,

[17] In these equations we need to invert $p = A_2(x^1, x^2)$ to obtain $x^1 = x^1(p, x^2)$ and therefore $H = H(p, q)$.

[18] We need to invert also $H(x^1, x^2) = \psi(x^1, x^2)$ to obtain $A_2 = A_2(\psi, x^2)$, and the function $I = I(\psi)$ to obtain $A_2(I, x^2)$.

instead of x^1. Working with Action–Angle coordinates we can therefore use the *Action–Angle coordinate system*:[19]

$$(x^1, x^2, x^3) \mapsto (I, \zeta, x^3)$$

The identification with canonical variables $(P, Q) = (I, \zeta)$ therefore gives:

$$t = x^3 \tag{2.100}$$
$$Q = \zeta \tag{2.101}$$
$$P = A_\zeta = I(\psi) \tag{2.102}$$
$$H = -A_3(I) = \psi(I) = const \tag{2.103}$$

Going back to equation (2.99) we can see that magnetic field lines written in Action–Angle coordinates are straight lines in the $(\zeta, I)-$plane. In magnetic filed line context, the (constant) frequency is called the rotational transform and it is indicated with ι. Usually the Action–Angle coordinates are named *magnetic* or *flux* or *straight–field–line coordinates*. In the presence of an MHD equilibrium another canonical transformation can bring to Boozer or Hamada magnetic coordinates, [51].

2.7 Intuitive physical approach

It is possible to derive the whole Hamiltonian mechanics from the Stokes theorem, and from its generalization using differential p–forms when dealing with $N > 1$ systems [46]. For $N = 1$ degree of freedom the Stokes theorem states the equivalence between a circulation and a flux:

$$\oint_l \mathbf{A} \cdot d\mathbf{l} = \int_\Sigma (\nabla \times \mathbf{A}) \cdot d\mathbf{\Sigma} \tag{2.104}$$

where Σ is any surfaces having the oriented circuit l as a boundary. If $\mathbf{A}$ is the vector potential, the circulation of $\mathbf{A}$ along l immediately implies the flux of the magnetic field $\mathbf{B} = \nabla \times \mathbf{A}$ through Σ. Using this, one can find the relations between covariant components[20] of the vector potential and magnetic fluxes in fusion devices.

Thinking of toroidal fusion devices we prove the relation between the A_i components and the magnetic fluxes. We use general toroidal coordinates, where θ is the poloidal angle and φ the toroidal one. We are going to use a difference between r and ρ in our notation: the radial coordinate r is not

[19] Where $t = x^3$, and the function $\psi = \psi(I)$ that can be inverted to write $\rho = I(\psi)$

[20] We write the covariant components of $\mathbf{A}$ in several coordinate systems, where $H = \psi$ is the Hamiltonian, and $\rho = f(\psi)$ any radial function that labels magnetic flux surfaces (e.g. $\rho = I(\psi)$ or $\rho = \psi(I)$ for Action–Angle coordinates). By definition:

$$\mathbf{A} = A_i \, \nabla x^i$$

necessarily constant on magnetic flux surfaces, as is ρ using our definition (see the end of section 2.5).
To define a flux one needs to define the surface through which the flux is computed. Usually the poloidal and toroidal magnetic fluxes are thought as the fluxes of the magnetic field $\mathbf{B}$ through a magnetic flux surface ($\rho = const$) at the angles $\theta = const$ and $\varphi = const$ respectively. Let us now use a more general definition even of the poloidal and toroidal fluxes, using the symbols ψ_P and ψ_T (and also the names poloidal and toroidal) for the fluxes across some surface Σ (to be specified) at the angles $\theta = const$ and $\varphi = const$ respectively. This allows to associate the magnetic fluxes to the covariant components of the vector potential $\mathbf{A}$ (see section 2.7.1).
The physical interpretation of the fluxes depends therefore on the surface Σ. Let us tell in advanced that one goes back to the classical definition of ψ_P and ψ_T as fluxes across magnetic flux surfaces at $\theta = const$ and $\varphi = const$ respectively when $\Sigma = \Sigma(\rho)$, therefore using Action–Angle coordinates. But let us show the definitions of these fluxes for different choices of the surface Σ: when no symmetry is evident in the system and therefore no flux surfaces can be found[21], the functions $\psi_P(r, \theta, \varphi)$ and $\psi_T(r, \theta, \varphi)$ measure the poloidal and toroidal fluxes across the $\Sigma = \psi_P(r, \theta, \varphi) = const$ and $\Sigma = \psi_T(r, \theta, \varphi) = const$ surfaces respectively. And even in the presence of flux surfaces ($H = -A_\varphi(r, \theta) = \psi(r, \theta) = const$), working with non–Action–Angle coordinates, the functions $\psi_P(r, \theta)$ and $\psi_T(r, \theta)$ are not necessarily constant over flux surfaces, and they measure the poloidal and toroidal fluxes across the $\Sigma = \psi_P(r, \theta) = const$ and $\Sigma = \psi_T(r, \theta) = const$ surfaces respectively[22]. The fluxes have therefore a clear physical interpretation only whenever there are well defined flux surfaces and Action–Angle coordinates are used ($H(\rho) = -A_\varphi(\rho) = \psi(\rho) = const$): $\psi_P = \psi_P(\rho)$ and $\psi_T = \psi_T(\rho)$ are flux functions that measure the poloidal and toroidal fluxes enclosed by the flux surface $\Sigma(I) = \psi(I) = const$.

---

therefore:

$$A_i \nabla x^i = \begin{cases} A_1 \nabla x^1 + A_2 \nabla x^2 + A_3 \nabla x^3 & \text{with} \quad x^\mu = (x^1, x^2, x^3) \\ \text{any general coordinates} & \\ A_\rho \nabla \rho + A_\zeta \nabla \zeta + A_3 \nabla x^3 = & \text{with} \quad x^\mu = (\rho, \zeta, x^3) \\ = A_\rho \nabla \rho + I \nabla \zeta + A_3 \nabla x^3 & \\ \text{Action–Angle coordinates} & \\ A_r \nabla r + A_\theta \nabla \theta + A_\varphi \nabla \varphi & \text{with} \quad x^\mu = (r, \theta, \varphi) \\ \text{general toroidal coordinates} & \\ A_\rho \nabla \rho + A_\theta \nabla \theta + A_\varphi \nabla \varphi & \text{with} \quad x^\mu = (\rho, \theta, \varphi) \\ \text{general toroidal coordinates} & \\ \ldots & \end{cases}$$

[21] Equivalent to constant energy surfaces.
[22] Choosing a symmetry with respect to the toroidal angle $\varphi = x^3$

We always consider the poloidal and toroidal flux between the magnetic axis and the surface Σ. It is worth noting the difference betwee the poloidal flux in fig.2.4 b) and fig.2.4 c): we always refer to the case b) when not differently specified.
For fixed magnetic flux surfaces, the spatial changes of the poloidal flux satisfy the relation: $\nabla\psi_P^r = -\nabla\psi_P^d$ (we use the symbols ψ_P^r or simply ψ_P for the poloidal flux across S_{pol}^r and ψ_P^d for the poloidal flux across S_{pol}^d in fig.2.4), [51].

We now prove all this and more.

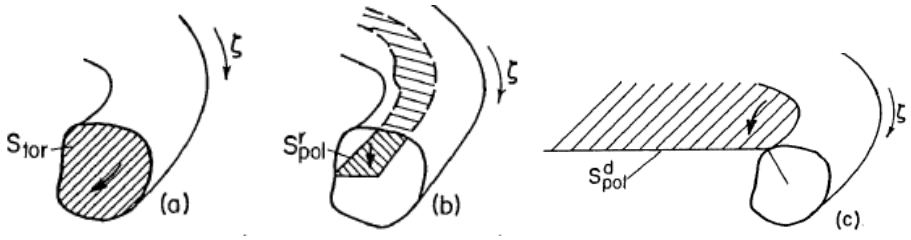

Figure 2.4: Reproduced from [51], pag.77. *Cross sections through which the magnetic fluxes characterizing a magnetic flux surface are defined. (a): The field lines intersecting S_{tor} determine the toroidal flux within a flux surface. (b): S_{pol}^r is a ribbon bounded by the magnetic axis and the flux surface. It 'contains' the poloidal (ribbon) flux which resides inside the flux surface. (c): S_{pol}^d is a disk touching the magnetic surface. It picks up the poloidal (disk) flux outside the flux surface.* The angle ζ in this figure is unfortunately what we call the toroidal angle φ in the text (not to be confused with the Angle ζ conjugated to the Action in the text).

2.7.1 The more general case

We first prove the more general case, for the general coordinates $x^\mu = (x^1, x^2, x^3)$ in the gauge $A_1 = 0$, which is that:

The component A_2 is a measure (up to 2π) of the flux across the surface defined by $A_2 = const$ at $x^3 = const$.

The component A_3 is a measure (up to 2π) of the flux across the surface defined by $A_3 = const$ at $x^2 = const$.

In a toroidal system, one can think of x^2 and x^3 as angle coordinates.

Let us prove it. Writing $\psi(i)$ the magnetic flux across a surface Σ at the angle $x^i = const$ (therefore with $i = 2, 3$), we can write

$$\begin{aligned}
\psi(i) &= \int_{\Sigma(i)} \mathbf{B} \cdot d\mathbf{\Sigma}(\mathbf{i}) = \int_{\Sigma(i)} (\nabla \times \mathbf{A}) \cdot d\mathbf{\Sigma}(i) = \oint_{\partial\Sigma(i)} \mathbf{A} \cdot d\mathbf{l} && (2.105)\\
&= \oint_{\partial\Sigma(i)} A_j \, dx^j = \oint_{\partial\Sigma(i)} A_j(x^1, x^2, x^3) \, dx^j && (2.106)\\
&= A_j(x^1, x^2, x^3) \oint_{\partial\Sigma(i)} dx^j && (2.107)\\
&= 2\pi \, A_j(x^1, x^2, x^3) && (2.108)
\end{aligned}$$

where, by definition, $d\mathbf{\Sigma}(i) = \sqrt{g} \, \nabla x^i \, dx^j \, dx^k$ is the infinitesimal element of a surface Σ at the angle $x^i = const$ and $d\mathbf{l}(i) = dx^i \, \mathbf{e}_i$. A line integral is performed along a curve, which means that one of the three coordinates is varied while two are held constant (Appendixes of [12, 52]).
We use the definition of the magnetic fluxes, the definition of the magnetic field through the vector potential and Stokes theorem in the first line (2.105). Because the x^i coordinate is constant (hypothesis) and of the chosen axial gauge $A_1 = 0$, $\mathbf{A} \cdot d\mathbf{l} = A_j \, dx^j$ in (2.106), without summation over j.
Thinking of x^j as an angle defined with respect to the magnetic axis of the system[23], its circulation in eq.(2.107) is equal to 2π.
But eq.(2.107) is true only if we are considering $A_j(x^1, x^2, x^3) = const$, and $\psi(i)$ turns out to be the flux across the surface $\Sigma = A_j(\mathbf{x})$ at $x^i = const$.
This ends the prof of the general case.

2.7.2 Two examples in toroidal geometry

Let us see some specific examples in toroidal geometry.

Using Action–Angle coordinates $x^\mu = (\rho, \zeta, \varphi)$.
$\psi(I) = const$ flux surfaces and φ ignorable coordinate.

$$\begin{aligned}
\psi_T &= \int_{\Sigma(\varphi)} \mathbf{B} \cdot d\mathbf{\Sigma}(\varphi) = \int_{\Sigma(\varphi)} (\nabla \times \mathbf{A}) \cdot d\mathbf{\Sigma} = \oint_{\partial\Sigma(\varphi)} \mathbf{A} \cdot d\mathbf{l} && (2.109)\\
&= \int_0^{2\pi} A_\zeta(I) \, d\zeta = \int_0^{2\pi} I(\psi) d\zeta && (2.110)\\
&= 2\pi \, A_\zeta = 2\pi \, I(\psi) && (2.111)\\
&\equiv \psi_T(I) \equiv \psi_T(\rho) && (2.112)
\end{aligned}$$

Here we used the definition of the toroidal flux, the definition of the magnetic field and Stokes theorem in the first line. The symbol $\Sigma(\varphi)$ defines the sur-

[23] When $x^i = x^2$ then $x^j = x^3$, and vice versa.

faces at $\varphi = const.$[24] Because of the constancy of the toroidal angle φ and of the choice $A_1 = A_\rho = 0$ for the axial gauge, we obtain the first relation of the second line, where we use also the identification of A_ζ with the momentum of the system in A–A coordinates, that is the Action I, eq.(2.102).

In the same way,

$$\begin{aligned}
\psi_P^d &= \int_{\Sigma(\zeta)} \mathbf{B}\cdot d\mathbf{\Sigma}(\zeta) = \int_{\Sigma(\zeta)} (\nabla\times\mathbf{A})\cdot d\mathbf{\Sigma} = \oint_{\partial\Sigma(\zeta)} \mathbf{A}\cdot d\mathbf{l} && (2.113)\\
&= \int_0^{2\pi} A_\varphi(I)\, d\varphi = -\int_0^{2\pi} \psi(I)\, d\varphi && (2.114)\\
&= 2\pi A_\varphi = -2\pi\,\psi(I) && (2.115)\\
&\equiv \psi_P^d(I) \equiv \psi_P^d(\rho) && (2.116)
\end{aligned}$$

Now the symbol $\Sigma(\zeta)$ defines the surfaces at $\zeta = const$[25] and we use the relation (2.103). This is called *poloidal* flux, imagine the Angle ζ in general as a straight poloidal–like angle.
Important is to note that the circulation in $d\varphi$, at the $\zeta = const$ angle, defines the surface named S^d_{pol} in fig.2.4), therefore this is the poloidal flux outside the flux surface (fig.2.4 c).

Summarizing , in A–A coordinates $x^\mu = (\rho, \zeta, \varphi)$:

$$\begin{aligned}
\psi_T(I) &= 2\pi\, I(\psi) = 2\pi\, A_\zeta(I) \equiv 2\pi A_2(I) && (2.117)\\
\psi_P^d(I) &= -2\pi\,\psi(I) = 2\pi A_\varphi(I) \equiv 2\pi A_3(I) && (2.118)
\end{aligned}$$

one can conclude that the Action I itself is a measure of the toroidal flux through magnetic surfaces, that corresponds also to the covariant component A_ζ associated to the Angle ζ (up to 2π). Also the poloidal flux is a flux through magnetic flux surfaces, for which a measure is given by the Hamiltonian ψ, corresponding to $-A_\varphi(I)$. Both the poloidal and the toroidal fluxes are flux functions (are constant on flux surfaces), and it is always possible to choose one of them as a label for magnetic flux surfaces: $\rho = \psi_P(\psi_T)$ or vice versa.

Using non-Action–Angle coordinates $x^\mu = (r, \theta, \varphi)$.

[24] Using general coordinates theory for the coordinates $x^\mu = (\psi, \zeta, \varphi)$, the definition of elementary surfaces elements is $d\Sigma(\varphi) = \sqrt{g}\,\nabla\varphi\, d\psi\, d\zeta$.
[25] $d\Sigma(\zeta) = \sqrt{g}\,\nabla\zeta\, d\psi\, d\varphi$ with $x^\mu = (\psi, \zeta, \varphi)$.

$\psi(r,\theta) = const$ flux surfaces and φ ignorable coordinate.

$$\begin{aligned}
\psi_T &= \int_{\Sigma(\varphi)} \mathbf{B}\cdot d\mathbf{\Sigma}(\varphi) = \int_{\Sigma(\varphi)} (\nabla\times\mathbf{A})\cdot d\mathbf{\Sigma} = \oint_{\partial\Sigma(\varphi)} \mathbf{A}\cdot d\mathbf{l} && (2.119)\\
&= \int_0^{2\pi} A_\theta(r,\theta)\, d\theta && (2.120)\\
&= 2\pi\, A_\theta(r,\theta) && (2.121)\\
&\equiv \psi_T(r,\theta) && (2.122)
\end{aligned}$$

Eq. (2.121) can be true if and only if in eq.(2.120) we consider the flux through the surface $A_\theta(r,\theta) = const$. Again the symbol $\Sigma(\varphi)$ defines the surfaces at $\varphi = const$ and we use the axial gauge $A_1 = A_r = 0$.

$$\begin{aligned}
\psi_P^d &= \int_{\Sigma(\theta)} \mathbf{B}\cdot d\mathbf{\Sigma}(\theta) = \int_{\Sigma(\theta)} (\nabla\times\mathbf{A})\cdot d\mathbf{\Sigma} = \oint_{\partial\Sigma(\theta)} \mathbf{A}\cdot d\mathbf{l} && (2.123)\\
&= \int_0^{2\pi} A_\varphi(r,\theta)\, d\varphi = -\int_0^{2\pi} \psi(r,\theta)\, d\varphi && (2.124)\\
&= 2\pi A_\varphi(r,\theta) = -2\pi\,\psi(r,\theta) && (2.125)\\
&\equiv \psi_P^d(r,\theta) && (2.126)
\end{aligned}$$

The symbol $\Sigma(\theta)$ defines the surfaces at $\theta = const$[26]. Remembering (2.71), we can write the equivalence in eq. (2.124). Again, (2.125) can be true if and only if in eq.(2.124) we consider the flux through the surface $A_\varphi(r,\theta) = const = -\psi(r,\theta)$: the Hamiltonian of the system is a measure of the poloidal flux across the magnetic surfaces even if we are not using Action–Angle coordinates.
Again, it is important to note that the circulation in $d\varphi$, at the $\theta = const$ angle, defines the surface named S^d_{pol} in fig.2.4), therefore this is the poloidal flux outside the flux surface (fig.2.4 c).

Summarizing, in the general (r,θ,φ) toroidal coordinates where the first coordinate r it is not necessarily a label of flux surfaces:

$$\begin{aligned}
\psi_T(r,\theta) &= 2\pi\, A_\theta(r,\theta) \equiv 2\pi A_2(r,\theta) && (2.127)\\
\psi_P^d(r,\theta) &= -2\pi\,\psi(r,\theta) = 2\pi A_\varphi(r,\theta) \equiv 2\pi A_3(r,\theta) && (2.128)
\end{aligned}$$

The Hamiltonian $\psi(r,\theta)$ is a measure of the poloidal flux across the $\psi(r,\theta) = const$ surfaces that correspond to the magnetic flux surfaces. The function $A_\theta(r,\theta)$ is a measure of the toroidal flux across the $A_\theta(r,\theta) = const$ surfaces, that in general do not correspond to the magnetic surfaces.

[26] $d\Sigma(\theta) = \sqrt{g}\,\nabla\theta\, dr\, d\varphi$ with $x^\mu = (r,\theta,\varphi)$.

In both cases[27], using general toroidal coordinates (r, θ, φ) and the axial gauge ($A_1 = A_r = 0$), we found that the toroidal flux (i. e. the flux at constant angle φ) is linked with the A_θ covariant component of the vector potential. And in the same way the poloidal flux (i. e. the flux at constant angle θ, but related to the flux outside the flux surface, see fig.2.4 c) is linked to A_φ:

$$\begin{aligned} A_i \nabla x^i &= \mathbf{A}(r,\theta,\varphi) = \psi_T(r,\theta)\,\nabla\theta/2\pi + \psi_P^d(r,\theta)\,\nabla\varphi/2\pi \quad (2.129) \\ &= \mathbf{A}(\rho,\zeta,\varphi) = \psi_T(\rho)\,\nabla\zeta/2\pi + \psi_P^d(\rho)\,\nabla\varphi/2\pi \quad (2.130) \end{aligned}$$

We conclude with some dimensional analysis, considering the magnetic fields $\mathbf{B}$ measured in Tesla $[T]$: the magnetic fluxes have the dimension of $[T\,m^2]$ by definition, and the magnetic potential $\mathbf{A}$ must have the dimensional of $[T\,m]$ because the circulation of $\mathbf{A}$ must be the flux of $\mathbf{B}$ (Stokes theorem).
Let us see that the covariant components of the vector potential have the dimension of the magnetic fluxes. To do this we must consider the properties of curvilinear coordinates (see appendix B), where one always consider the basis vectors not normalized and not dimensionless. In the case of covariant components the basis are the gradients of the coordinates, that have the dimension of $[m^{-1}]$ for adimensional angular coordinates (as θ and φ in toroidal coordinates). Using the definition $\mathbf{A} = A_i \nabla x^i$, the components A_i related to angular coordinates must have the dimension of $[T\,m^2]$ in order to obtain the correct dimension for $\mathbf{A}$: the correct dimension of the fluxes!

2.8 The magnetic field, $\mathbf{B} = \nabla \times \mathbf{A}$

2.8.1 The canonical representation of B

In the general coordinates $x^\mu = (x^1, x^2, x^3)$,

$$\begin{aligned} \mathbf{A} &= A_1 \nabla x^1 + A_2 \nabla x^2 + A_3 \nabla x^3 \quad (2.131) \\ \mathbf{B} &= \nabla A_1 \times \nabla x^1 + \nabla A_2 \times \nabla x^2 + \nabla A_3 \times \nabla x^3 \quad (2.132) \end{aligned}$$

with $A_i = A_i(x^1, x^2, x^3)$.
In the general toroidal coordinates $(x^1, x^2, x^3) = (r, \theta, \varphi)$, choosing the gauge

[27] (eq.(2.117)-(2.118) and (2.127)-(2.128))

($A_1 = A_r = 0$), one can write the following equivalent equations:

$$\begin{aligned} \mathbf{A} &= A_2 \nabla x^2 + A_3 \nabla x^3 && (2.133)\\ &= A_\theta \nabla\theta + A_\varphi \nabla\varphi && (2.134)\\ &= \psi_T \nabla\theta/2\pi + \psi_P^d \nabla\varphi/2\pi && (2.135) \end{aligned}$$

$$\begin{aligned} \mathbf{B} &= \nabla A_2 \times \nabla x^2 + \nabla A_3 \times \nabla x^3 && (2.136)\\ &= \nabla A_\theta \times \nabla\theta + \nabla A_\varphi \times \nabla\varphi && (2.137)\\ &= \nabla\psi_T \times \nabla\theta/2\pi - \nabla\psi_P \times \nabla\varphi/2\pi && (2.138) \end{aligned}$$

where $A_i = A_i(r, \theta, \varphi)$ with no symmetry in the system, $A_i = A_i(r, \theta)$ with symmetry in φ, or $A_i = A_i(\rho)$ using Action–Angle coordinates ($\theta \mapsto \zeta$) and the function ρ to label the flux surfaces. This is obviously true also for the fluxes ψ_P and ψ_T, remembering the identification between the fluxes and A_i.

The form (2.138) of the magnetic field is called the *canonical representation of* $\mathbf{B}$, obtained for the poloidal flux ψ_P between the magnetic axis and the surface Σ (for which $\nabla\psi_p^r = -\nabla\psi_p^d$, using ψ_p^r for the poloidal flux across S_{pol}^r and ψ_p^d for the poloidal flux across S_{pol}^d, see fig.2.4). Note therefore the minus sign in front of the Hamiltonian $\psi = \psi_P$. We call $\psi_P^r = \psi_P$.

Using the definition $\mathbf{B} = \nabla \times \mathbf{A}$ we can write also the contravariant[28] components of the magnetic field, using the definition of cross product in the general coordinates $x^\mu = (x^1, x^2, x^3)$, with the permutation (i, j, k) of the index $(1, 2, 3)$:

$$\sqrt{g}\, B^i = \frac{\partial A_j}{\partial x^k} - \frac{\partial A_k}{\partial x^j} \qquad (2.139)$$

Following this formula:

$$\begin{aligned} \sqrt{g}\, B^1 &= \frac{\partial A_2}{\partial x^3} - \frac{\partial A_3}{\partial x^2} \quad , \ (i,j,k) = (1,2,3) && (2.140)\\ \sqrt{g}\, B^2 &= \frac{\partial A_3}{\partial x^1} - \frac{\partial A_1}{\partial x^3} \quad , \ (i,j,k) = (2,3,1) && (2.141)\\ \sqrt{g}\, B^3 &= \frac{\partial A_1}{\partial x^2} - \frac{\partial A_2}{\partial x^1} \quad , \ (i,j,k) = (3,1,2) && (2.142) \end{aligned}$$

For the gauge $A_1 = 0$:

$$\begin{aligned} B^1 &= \frac{1}{\sqrt{g}} \Big(\frac{\partial A_2}{\partial x^3} - \frac{\partial A_3}{\partial x^2} \Big) && (2.143)\\ B^2 &= \frac{1}{\sqrt{g}} \frac{\partial A_3}{\partial x^1} && (2.144)\\ B^3 &= -\frac{1}{\sqrt{g}} \frac{\partial A_2}{\partial x^1} && (2.145) \end{aligned}$$

[28] Up index.

and for general toroidal coordinates (r, θ, φ), $(A_1 = A_r = 0)$:

$$B^r = \frac{1}{2\pi}\frac{1}{\sqrt{g}}\Big(\frac{\partial \psi_T}{\partial \varphi} - \frac{\partial \psi_P}{\partial \theta}\Big) \tag{2.146}$$

$$B^\theta = \frac{1}{2\pi}\frac{1}{\sqrt{g}}\frac{\partial \psi_P}{\partial r} \tag{2.147}$$

$$B^\varphi = -\frac{1}{2\pi}\frac{1}{\sqrt{g}}\frac{\partial \psi_T}{\partial r} \tag{2.148}$$

2.8.2 The covariant representation of B

The form (2.138) of the magnetic field is also called *covariant* representation of the magnetic field, when the fluxes are labels of the flux surfaces and therefore Action–Angle are used.
Let us now find some important results of this chapter using just the magnetic field **B** and forgetting about the vector potential **A**. This is a more common way to treat the magnetic field line problem, [12].

We say in section 2.5 that the surfaces defined by the constancy of the Hamiltonian (eq.(2.71) for the *time* x^3) are the flux surfaces of the magnetic system associated to **A**. Using the magnetic field instead of the vector potential, we now prove that necessary condition for the existence of flux surfaces is the existence of a function ρ for which

$$\mathbf{B} \cdot \nabla \rho = 0 \quad . \tag{2.149}$$

We can call any function that can label the flux surfaces with the symbol ρ, and we use it as the radial coordinate[29].
Necessary and sufficient condition (in any system of one degree of freedom) is still the existence of one ignorable coordinate (the canonical *time*). Let us therefore go back to eq.(2.71), but using toroidal coordinates:

$$H = -A_\varphi(r, \theta) = \psi(r, \theta) = const \tag{2.150}$$

and to eq.(2.128)

$$\psi_P(r, \theta) = -2\pi\psi(r, \theta) \tag{2.151}$$

in order to prove eq.(2.149): φ plays the role of the time, $\psi_T = \psi_T(r, \theta)$ and we use $\rho = H = \psi_P(r, \theta) = 2\pi A_\varphi(r, \theta)$. From the relation (2.138) for the canonical representation of the magnetic field,

$$\mathbf{B} \cdot \nabla \rho = (\nabla \psi_T \times \nabla \theta - \nabla \psi_P \times \nabla \varphi) \cdot \nabla \rho = \tag{2.152}$$

$$= (\nabla \psi_T \times \nabla \theta - \nabla \rho \times \nabla \varphi) \cdot \nabla \rho = \tag{2.153}$$

$$= \nabla \psi_T \times \nabla \theta \cdot \nabla \rho = \tag{2.154}$$

$$= 0 \tag{2.155}$$

[29] It is worth noting that in chaotic spaces, where magnetic flux surfaces are destroyed, relation 2.149 is still valid

where, for the last step, we used the dependence on (r, θ) of the fluxes, so

$$\nabla\psi_T = \frac{\partial\psi_T}{\partial r}\nabla r + \frac{\partial\psi_T}{\partial\theta}\nabla\theta \quad (2.156)$$

$$\nabla\rho = \frac{\partial\rho}{\partial r}\nabla r + \frac{\partial\rho}{\partial\theta}\nabla\theta \quad (2.157)$$

and, of course, the vanishing triple product between two parallel vectors.

At the end of section 2.6 we say that in the case of flux surfaces it is possible to look for Action–Angle variables (ρ, ζ, φ) on these surfaces (constant energy surfaces), and that these coincide with straight–field–line coordinates. In Action–Angle coordinate the canonical representation of the magnetic field is

$$\mathbf{B} = \nabla\psi_T(\rho) \times \nabla\zeta/2\pi - \nabla\psi_P(\rho) \times \nabla\varphi/2\pi \quad (2.158)$$

where the fluxes $\psi_P(\rho)$ and $\psi_T(\rho)$ are the flux functions that measure the poloidal and toroidal fluxes enclosed by the flux surface $\Sigma(\rho)$, respectively, and ψ the Hamiltonian. Straight–field–line coordinates can be found also without the Hamiltonian mechanics theory (e.g. the Action–Angle idea), but using a geometrical approach: eq. (2.158) is still valid, and is called the *covariant representation of the magnetic field*. Let us briefly follow W.D.D'haeseleer [51] to obtain this form.
The canonical form (2.138) of $\mathbf{B}$ written for the generic angular coordinates (θ, φ) on the flux surfaces $\rho = const$,

$$\mathbf{B} = \nabla\psi_T \times \nabla\theta/2\pi - \nabla\psi_P \times \nabla\varphi/2\pi \quad (2.159)$$

where the fluxes are function of all the coordinates (ρ, θ, φ), can also be written as

$$\mathbf{B} = \nabla\psi_T(\rho) \times \nabla\theta/2\pi - \nabla\psi_P(\rho) \times \nabla\varphi/2\pi + \nabla\rho \times \nabla\nu(\rho, \theta, \varphi) \quad ,(2.160)$$

where the fluxes are now function of the radial coordinate only, but now a new function[30] $\nu(\rho, \theta, \varphi)$ appears. To go back to a canonical form equivalent to the Action–Angle one (2.158) we need to perform a change of variables in order to eliminate ν: the change of variables is simple, once the function ν is known. It is sufficient to change one of the two angles (θ or φ, leaving the other unchanged) following these rules:

$$\theta \mapsto \theta_f = \theta + \frac{\widetilde{\nu}}{\dot{\psi}_T} = \theta + \lambda_T(\rho, \theta, \varphi) \quad \varphi_f = \varphi \quad (2.161)$$

or

$$\varphi \mapsto \varphi_f = \varphi - \frac{\widetilde{\nu}}{\dot{\psi}_P} = \varphi + \lambda_P(\rho, \theta, \varphi) \quad \theta_f = \theta \quad (2.162)$$

[30] Clebsch function, [51]

where $\widetilde{\nu}(\rho,\theta,\varphi)$ is the periodic part of the function ν and $\dot{\psi}$ the radial derivative of the fluxes. The unchanged angle can be considered the one that plays the role of *time*.
The new straight–field–line coordinates $(\rho,\theta_f,\varphi_f)$ are equivalent to the Action–Angle coordinates (ρ,ζ,φ). Action–Angle coordinates (where the Hamiltonian is a function of the momentum only) or straight–field–line coordinates (found by (2.161)–(2.162)) are not unique. One can always choose the more useful ones going to one another with a canonical transformation or following these rules:

$$\theta_f \mapsto \theta_F = \theta_f + \dot{\psi}_P\, G(\rho,\theta_f,\varphi_f) \tag{2.163}$$

$$\varphi_f \mapsto \varphi_F = \varphi_f + \dot{\psi}_T\, G(\rho,\theta_f,\varphi_f) \tag{2.164}$$

where G is an arbitrary periodic function of the straight angles θ_f and φ_f.[31]

Equations (2.146)-(2.148) for the contravariant components of $\mathbf{B}$ can be found in this approach, where just the magnetic field is considered together with the magnetic fluxes, using the definition of the contravariant components of a vector[32]:

$$B^i = \mathbf{B}\cdot\nabla x^i \tag{2.166}$$

What is missing in this approach, with respect to (2.139), is the equivalence between the fluxes and the covariant components of the vector potential, and therefore the intuitive physical interpretation of the Hamiltonian–magnetic systems.

2.8.3 Magnetic field line equations

Equation (2.14)

$$\frac{d\mathbf{x}}{d\lambda} = \mathbf{B}(\mathbf{x}) \tag{2.167}$$

is the definition for magnetic field lines, where λ is a parameter that varies along the magnetic lines. To see that the equations for magnetic field lines

[31] The function G can be derived from a magnetic differential equation when the Jacobian of the two straight field line systems are known:

$$2\pi\,\mathbf{B}\cdot\nabla G = \frac{1}{\sqrt{g_F}} - \frac{1}{\sqrt{g_f}} \tag{2.165}$$

[32] From the canonical form of the magnetic field alone, $\mathbf{B} = \nabla\psi_T\times\nabla\theta - \nabla\psi_P\times\nabla\varphi$ it easy to obtain equations (2.146)–(2.148). All the angular derivatives of the fluxes are suppressed by the dot product in the definition of contravariant components of a field, $B^i = \mathbf{B}\cdot\nabla x^i$, and only the terms $(\partial\psi/\partial r)\,\nabla r$ are of some interest in the expansion of the gradient of the fluxes. In the toroidal (r,θ,φ) coordinates, the whole gradient of a flux ψ is $\nabla\psi = (\partial\psi/\partial r)\,\nabla r + (\partial\psi/\partial\theta)\,\nabla\theta + (\partial\psi/\partial\varphi)\,\nabla\varphi$. To conclude one needs to use also the definition of the Jacobian of the same coordinate system, $(1/\sqrt{g}) = \nabla r\times\nabla\theta\cdot\nabla\varphi$.

are equivalent to the canonical equation of motion, we need first to choose one of the fluxes as the radial variable. In particular we need to choose the flux associated to the canonical momentum, in order to write the Hamiltonian as a function of (p, q, t): in the gauge $A_1 = 0$ for $t = x^3$ we know[33] that the canonical momentum is the toroidal flux, so $\rho = \psi_T$.
In terms of the $(\psi_T, \theta, \varphi)$ coordinates, the equation of a field line reads[34]:

$$\frac{d\psi_T}{B^\rho} = \frac{d\theta}{B^\theta} = \frac{d\varphi}{B^\varphi} \tag{2.172}$$

Therefore $d\theta/d\varphi = B^\theta/B^\varphi$ and it is easy to prove that this is exactly one of the canonical equations of motion:

$$\frac{d\theta}{d\varphi} = \frac{B^\theta}{B^\varphi} \Longleftrightarrow \frac{dq}{dt} = \frac{\partial H}{\partial p} \tag{2.173}$$

The equivalence is immediate remembering[35] eq.(2.146)–(2.148) that link the *up* components of the magnetic field to the derivative of the fluxes in the gauge $A_r = 0$, and the canonical identification valid in the same gauge once the toroidal angle $x^3 = \varphi$ has been chosen as the canonical time.
Analogously, for the second canonical equation one needs to prove that:

$$\frac{d\psi_T}{d\varphi} = \frac{B^\rho}{B^\varphi} \Longleftrightarrow \frac{dp}{dt} = -\frac{\partial H}{\partial q} \tag{2.174}$$

where $B^\rho = \mathbf{B} \cdot \nabla\psi_T$ and $B^\varphi = \mathbf{B} \cdot \nabla\varphi$. To prove this relation we follow an alternative way, as an example: to find $B^\varphi = \mathbf{B} \cdot \nabla\varphi$ we dot multiply the canonical equation (2.138) for $\mathbf{B}$ with $\nabla\varphi$; and to find B^ρ we dot multiply the same equation with $\nabla\psi_T$. The result is:

$$\frac{\mathbf{B} \cdot \nabla\psi_T}{\mathbf{B} \cdot \nabla\varphi} = \frac{-(\nabla\psi_P \times \nabla\varphi) \cdot \nabla\psi_T}{(\nabla\psi_T \times \nabla\theta) \cdot \nabla\varphi} \tag{2.175}$$

In the chosen $(\psi_T, \theta, \varphi)$ coordinates, the poloidal flux is $\psi_P = \psi_P(\psi_T, \theta, \varphi)$. Of its gradient, only the derivative of ψ_P with respect to the poloidal angle θ survives in the triple product of last equation, and this ends the proof with the identification $t = \varphi, q = \theta, p = \psi_T, H = \psi_P$:

$$\frac{d\psi_T}{d\varphi} = \frac{\mathbf{B} \cdot \nabla\psi_T}{\mathbf{B} \cdot \nabla\varphi} = -\frac{\partial\psi_P}{\partial\theta} \tag{2.176}$$

[33] In the gauge $A_1 = 0$ for $t = x^3$:

$$t = \varphi \tag{2.168}$$
$$q = \theta \tag{2.169}$$
$$p = A_\theta = \psi_T \tag{2.170}$$
$$H = -A_\varphi = -\psi_P \quad . \tag{2.171}$$

[34] Simply making the dot product of eq.(2.167) with the gradients of the coordinates.

[35] The same equations can be easily derived from the canonical form of the magnetic field alone, $\mathbf{B} = \nabla\psi_T \times \nabla\theta - \nabla\psi_P \times \nabla\varphi$, using the definition of contravariant components of a field, $B^i = \mathbf{B} \cdot \nabla x^i$.

2.9 A resumptive example: the helical symmetry

In this example we consider a plasma column with helical shape in a toroidal fusion device.
Starting from a toroidal system with coordinates (r, θ, φ), where θ is the poloidal angle and φ the toroidal one, the helical angle u is defined by

$$u = \theta - n\,\varphi \tag{2.177}$$

where n is the toroidal periodicity of the helix. Having a system with helical symmetry means that any flux quantity in the plasma depends only on the coordinate (r, u). We therefore have at least two chances to choose a frame of reference where the helical symmetry in the torus is manifest: (r, u, θ) and (r, u, φ). In the first one the ignorable coordinate that plays the role of time is the angle θ, whereas in the second one the canonical time is related to the toroidal angle φ[36].
Because of the reversal of the toroidal magnetic field at the edge of RFP devices, the canonical time φ in non monotonic, and therefore the more common choice for RFPs is to choose the poloidal angle θ as the time. As we will see in the case of the helical RFP states, the SHAx states, even the poloidal angle is not a good choice, and we prefer to use the toroidal one in the work of this thesis[37].

Let us choose the (r, u, φ) coordinate system to summarize the results of this chapter in the example of helical symmetry (canonical time related to the ignorable coordinate φ). We first find the identification between magnetic and canonical variables, using Noether theorem and the choice of the axial gauge $A_r = 0$ to identify the the Poincaré–Cartan form of the two systems:

$$A_\mu\, dx^\mu = \gamma_\mu\, dz^\mu = p\, dq \;-\; H\, dt \tag{2.178}$$

where A_i are the covariant component of the vector potential, $x^\mu = (r, u, \varphi)$ and γ_μ, z^μ are defined in eq.(2.64). We find Action–Angle variables as in eq.(2.95)–eq.(2.97). Then, we find the relations between $A_u(r, u)$ and the toroidal flux $\psi_T(r, u)$, between $A_\varphi(r, u)$ and the helical flux $\chi(r, u)$[38]; and

[36] In a torus a rigorous helical symmetry of magnetic flux surfaces does not exist. This is due to the toroidal coupling between modes with same toroidal mode number n and $\Delta m \pm 1$ in the poloidal mode number m: due to the toroidal geometry it is not possible to have a single (m, n) mode in the plasma, and therefore a it is not possible to find flux quantities that depend only on its helicity. More details are given in chapter 3–5. But in the work of this thesis I neglect the contribution of the $(m, n) = (0, n), (2, n)$ to the dominant one $(m, n) = (1, n)$: SHAx states are modelled as pure single helicity states, where the helical symmetry is taken as hypothesis, even in a toroidal geometry.

[37] Other toroidal–like angles without reversal have also been found, that can be used when the edge region must be taken into account in a more accurate way. See section 4.2.4

[38] defined at constant helical angle u

the same for Action–Angle coordinates: the relations between the Action $A_\zeta(\rho)$ and the toroidal flux $\psi_T(\rho)$, and between the Hamiltonian $A_\varphi(\rho)$ and the helical flux $\chi(\rho)$. Let us begin.
Given the ignorable coordinate $x^3 = \varphi$, one knows that (eq.(2.70))

$$A_\mu \, dx^\mu = A_r(r,u) \, dr + A_u(r,u) \, du + A_\varphi(r,u) \, d\varphi \tag{2.179}$$

is the Poincaré–Cartan form with $A_i(r,u)$. From Noether theorem (eq.(2.71)):

$$H \;\; = \;\; - A_\varphi(r,u) = \rho(r,u) = const \tag{2.180}$$

states the conservation of the Hamiltonian for time–independent systems, and (eq.(2.74)–(2.75))

$$t \;\; = \;\; \varphi \tag{2.181}$$
$$H \;\; = \;\; - A_\varphi(r,u) \quad . \tag{2.182}$$

Just when one chooses the axial gauge it is possible to make the identification also with the (p,q) canonical variables. Choosing $A_r = 0$, (eq.(2.78)–(2.79)):

$$q \;\; = \;\; u \tag{2.183}$$
$$p \;\; = \;\; A_u(r,u) \tag{2.184}$$

The Hamiltonian must be a function of the canonical variables, and not of the general coordinates (r,u). Once the identification $u = q$ has been found, one needs to invert at least locally the relation found for p to obtain $r(p,u)$ (and therefore $H(p,q)$). Constant energy surfaces in dynamical systems correspond to the magnetic surfaces, labelled by the Hamiltonian: inverting the relation (2.182) to write $r(H,u)$, one can use the Hamiltonian as the first coordinate to label the magnetic flux surfaces, eq.(2.180).
On conserved flux surfaces[39] ($\rho = const$) one can look for Action–Angle coordinates with a canonical change of coordinates $(p,q) \mapsto (P,Q) = (I,\zeta)$ in phase space, which correspond to a change of coordinate in the physical space of magnetic fields: $(\rho,u,\varphi) \mapsto (\rho,\zeta,\varphi)$[40]. Following eq.(2.95)–eq.(2.97), where equation (2.182) is inverted in order to obtain $A_u(\rho,u)$ and then the function $I(\rho)$ is inverted to obtain $\rho(I)$ and therefore $A_u(I,u)$, one obtains:

$$I(\rho) = \frac{1}{2\pi} \oint p \, dq \equiv \frac{1}{2\pi} \oint A_u(\rho,u) \, du \tag{2.185}$$

$$F_2(u,I) = \int_{q_0}^{q} p \, dq \equiv \int_{u_0}^{u} A_u(I,u) \, du \tag{2.186}$$

$$\zeta(u,I) = \frac{\partial F_2}{\partial I} \equiv \int_{u_0}^{u} \frac{\partial A_u}{\partial I}(I,u) \, du \tag{2.187}$$

[39] Equivalent to bounded constant energy surfaces in phase space.
[40] Instead of r we use the label of the magnetic flux surfaces ρ. As said one can always make this choice ones the conserved Hamiltonian of the system is known.

for the Action I, the generating function F_2 and the Angle ζ. The main property of Action–Angle coordinates is that the Hamiltonian is a function of the Action I only, $H = H(I)$, which means that the Action is a constant on flux surfaces. The angle ζ is found using the generating function $F_2(q, Q) = F_2(q, I)$ and evolves linearly in time with a constant frequency that correspond to the helical rotational transform.

We go back to the physical interpretation of the fluxes associated to the covariant components of the vector potential for any coordinate system as found in section 2.7.[41]. Here we can say that:
In the general (r, u, φ) coordinate system, with φ ignorable coordinate, for the gauge $A_r = 0$:
The component $A_u(r, u)$ is a measure (up to 2π) of the toroidal *flux across the surface defined by $A_u(r, u) = const$ at the toroidal angle $\varphi = const$.*
The component $A_\varphi(r, u)$ is a measure (up to 2π) of the helical *flux across the surface defined by $A_\varphi(r, u) = const$ at helical angle $u = const$:*

$$\psi_T(r, u) = 2\pi A_u(r, u) \tag{2.188}$$
$$\chi(r, u) = -2\pi A_\varphi(r, u) = -2\pi H \tag{2.189}$$

writing the symbol χ for the helical flux. $H = -A_\varphi(r, u) = const$ are the flux surfaces, but in general this is not true for $A_u(r, u) = const$. Both the fluxes are label of the magnetic flux surfaces just in Action–Angle coordinates (ρ, ζ, φ). In these coordinates, with φ ignorable coordinate, ρ label of the flux surfaces, for the gauge $A_\rho = 0$:
The component $A_\zeta(\rho) = I(\rho)$ is a measure (up to 2π) of the toroidal *flux across the surface defined by $A_\zeta(\rho) = I(\rho) = const$ at the toroidal angle $\varphi = const$.*
The component $A_\varphi(\rho)$ is a measure (up to 2π) of the helical *flux across the surface defined by $A_\varphi(\rho) = const$ at (straight) helical angle $\zeta = const$:*

$$\psi_T(\rho) = 2\pi I(\rho) = 2\pi A_\zeta \tag{2.190}$$
$$\chi(\rho) = -2\pi A_\varphi(\rho) = -2\pi H(\rho) \tag{2.191}$$

The Angle ζ is still a helical angle, and the Hamiltonian $H(\rho) = H(I)$ is the helical flux χ trough the flux surfaces, as well as $H(r, u)$.

[41] *From section 2.7.1. In the general coordinates $x^\mu = (x^1, x^2, x^3)$ and for the gauge $A_1 = 0$:*
The component A_2 is a measure (up to 2π) of the flux across the surface defined by $A_2 = const$ at $x^3 = const$.
The component A_3 is a measure (up to -2π) of the flux across the surface defined by $A_3 = const$ at $x^2 = const$.

Therefore we can write

$$\mathbf{A}(r,u,\varphi) = A_u\,\nabla u + A_\varphi\,\nabla\varphi = \psi_t(r,u)\,\nabla u - \chi(r,u)\,\nabla\varphi \quad (2.192)$$
$$\mathbf{A}(\rho,\zeta,\varphi) = A_\zeta\,\nabla\zeta + A_\varphi\,\nabla\varphi = \psi_T(\rho)\,\nabla\zeta - \chi(\rho)\,\nabla\varphi \quad (2.193)$$

We write $\psi_T(\rho)$ and $\psi_t(r,u)$ to emphasize the difference between the two *toroidal* fluxes: just the first one is a flux through magnetic flux surfaces. On the other hand, the helical flux is unchanged due to the (time–independent) canonical transformation that brings from (r,u,φ) to Action–Angle variables.
The corresponding contravariant representations of the magnetic field is:

$$\mathbf{B}(r,u,\varphi) = \nabla A_u \times \nabla u + \nabla A_\varphi \times \nabla\varphi \quad (2.194)$$
$$= \nabla\psi_t(r,u) \times \nabla u - \nabla\chi(r,u) \times \nabla\varphi \quad (2.195)$$
$$\mathbf{B}(\rho,\zeta,\varphi) = \nabla A_\zeta \times \nabla\zeta + \nabla A_\varphi \times \nabla\varphi \quad (2.196)$$
$$= \nabla\psi_T(\rho) \times \nabla\zeta - \nabla\chi(\rho) \times \nabla\varphi \quad (2.197)$$

The contravariant components of the magnetic field can be written following equations (2.143)–(2.144), or using the definition of contravariant indexes:

$$B^i = \mathbf{B}\cdot\nabla x^i$$

together with one of the (2.194)–(2.197). As useful example we write explicitly just the case corresponding to eq.(2.197), Action–Angle coordinates (ρ,ζ,φ) and the gauge $A_\rho = 0$:

$$B^\rho = 0 \quad (2.198)$$
$$B^\zeta = \frac{1}{\sqrt{g}}\frac{\partial\chi}{\partial\rho} \quad (2.199)$$
$$B^\varphi = \frac{1}{\sqrt{g}}\frac{\partial\psi_T}{\partial\rho} \quad (2.200)$$

$B^\rho = \mathbf{B}\cdot\nabla\rho = 0$ it is equivalent to (2.149), that defines ρ as label of magnetic flux surfaces, and can be prove here in the same way, but with $\rho(r,u)$.

To conclude we just want to emphasize that frequently we use the same symbols to indicate different quantities. As one must pay attention to the meaning of the fluxes in the different frame of reference (in the text we call them always in the same way, but for example $\psi_T(r,u,\varphi) \neq \psi_T(\rho)$), the same is true for example for the Jacobian of the coordinate system, that we

always call $\sqrt{g}$, but it is obviously different in different systems:[42]

$$\frac{1}{\sqrt{g}} = \nabla x^1 \cdot \nabla x^2 \times \nabla x^3 \text{ for } (x^1, x^2, x^3) \tag{2.205}$$

2.10 A short example: the axisymmetric field $\mathbf{B_0}$

In this short example we consider only the axisymmetric equilibrium magnetic field $\mathbf{B_0}$.
The (r, θ, φ) coordinate system introduced in section 3.1.1 are straight field line coordinates built on the circular flux surfaces of $\mathbf{B_0}$. In this coordinate system the fluxes depend on the radial coordinate only (as must be in every Action–Angle coordinate system). Both the poloidal and toroidal angle can be therefore used as the canonical time:

$$\mathbf{B_0}(r, \theta, \varphi) = \nabla\psi_T(r) \times \nabla\theta - \nabla\psi_P(r) \times \nabla\varphi \tag{2.206}$$

and the associated canonical variables can be

$$t = \varphi \tag{2.207}$$
$$H = -A_\varphi = \psi_P(r) \tag{2.208}$$
$$q = \theta \tag{2.209}$$
$$p = A_\theta = \psi_T(r) \tag{2.210}$$

or

$$t = \theta \tag{2.211}$$
$$H = -A_\theta = \psi_T(r) \tag{2.212}$$
$$q = \varphi \tag{2.213}$$
$$p = A_\varphi = \psi_P(r) \tag{2.214}$$

The canonical time θ is always increasing in the whole plasma volume and it is linked with a poloidal flux that is monotonic. It is a better choice for the canonical time in axisymmetric RFP equilibrium compared to the toroidal angle that changes its sign at the reversal. Due to the reversal of the toroidal component of the magnetic field, the toroidal flux $\psi_T(r)$ in a non monotonic

[42] Some examples:

$$\frac{1}{\sqrt{g}} = \nabla r \cdot \nabla\theta \times \nabla\varphi \text{ for } (r, \theta, \varphi) \tag{2.201}$$
$$= \nabla r \cdot \nabla u \times \nabla\varphi \text{ for } (r, u, \varphi) \tag{2.202}$$
$$= \nabla\rho \cdot \nabla\zeta \times \nabla\varphi \text{ for } (\rho, \zeta, \varphi) \tag{2.203}$$
$$= \nabla r \cdot \nabla u \times \nabla\theta \text{ for } (r, u, \theta) \tag{2.204}$$

function. The problem of a non monotonic Hamiltonian related to the time θ is not really a problem, because one can use any other flux function as radial coordinate, for example the poloidal flux $\psi_P(r)$.

Chapter 3

Mode eigenfunction reconstruction

The goal of this chapter is to underline what one needs in order to apply the theoretical results of chapter 2 to real data, and which measurements are necessary. In particular, following the paper of P. Zanca and D. Terranova [53], we define the toroidal coordinates (r, ϑ, φ) that are used to compute the toroidal and poloidal fluxes from magnetic measurements: going back to chapter 2 it is easy to see that the toroidal coordinates and the covariant components of the vector potential $\mathbf{A}$ (that are nothing but the fluxes) are the only quantities that one needs to know. This is true even in helical symmetry (section 2.9) where the helical angle $u = \theta - n\varphi$ and the helical flux χ (2.189) can be written as a composition of the poloidal and toroidal angles and fluxes.
The starting point in the work of my thesis is the reconstruction of poloidal and toroidal flux profiles, and their $\psi_P^{m,n}$ and $\psi_T^{m,n}$ harmonics. I do not need to solve eq.(3.36)–(3.37), because this is done by some common routines in RFX, written by the authors of [53] on the basis of their paper. I can therefore read the fluxes and their harmonics from the outputs of these routines. I refer often to the (r, ϑ, φ) coordinate system, built on the $\Sigma(r)$ flux surfaces of $\mathbf{B_0}$, because these are the coordinates on which the fluxes are computed (as explained in section 3.1.1, appendix B.2.3 and reference [53]).

Let us summarize the content of this chapter more in detail.
Due to the presence of tearing instabilities, which break the axi–symmetry of the magnetic field, we can think every quantity A inside the plasma (e.g. the magnetic field $\mathbf{B}$ and the magnetic fluxes) as composed by an axi–symmetric

part A_0 and a perturbation, usually Fourier decomposed as[1]:

$$A(r,\theta,\varphi) = A_0(r) + \sum_{m,n} a^{m,n}(r)\, e^{i(m\theta - n\varphi)} \tag{3.1}$$

$$= A_0(r) + \sum_{\substack{m \\ n>0}} a^{m,n}(r)\, e^{i(m\theta - n\varphi)} + c.c. \tag{3.2}$$

using the generic toroidal coordinates (r,θ,φ) where r is the radius of the circular–cross–section flux surfaces of the axi–symmetric part of the magnetic field, $\mathbf{B_0}$. A complete reconstruction of tearing mode eigenfunctions inside the whole plasma volume has been done in [53], where the magnetic perturbation is considered to be much smaller comparing to $\mathbf{B_0}$ in order to use a perturbative approach. The method solves a Newcomb–like equation, that arises from the force–free force–balance equation at the first order in the perturbation, in a non–orthogonal and curvilinear coordinate system that well describes the toroidal geometry of the problem. The solution of Newcomb's equation provides the harmonics $\psi_P^{m,n}$ and $\psi_T^{m,n}$ of the perturbation to the poloidal and toroidal flux respectively and we therefore need the relation that links the magnetic fluxes to the components of the magnetic field to provide a complete reconstruction of $\mathbf{B}$ in the plasma volume.

First the curvilinear straight–field–line coordinates (r,ϑ,φ) built on the circular flux surfaces of $\mathbf{B_0}$ are introduced. This is done in section 3.1.1, starting from the canonical representation of $\mathbf{B_0}$ (2.206) and following the method in section 2.8.2.
In par 3.1.2 the whole axisymmetric equilibrium is defined, which means that we write the equations for the differential shift $\Delta(r)$ of the flux surfaces $\Sigma(r)$ in toroidal symmetry, and for the fluxes $\psi_{P,0}$ and $\psi_{T,0}$ through $\Sigma(r)$.
The perturbation to $\mathbf{B_0}$, that deforms its circular flux surfaces $\Sigma(r)$, is introduced in section 3.2. Using the same coordinate system (r,ϑ,φ) built for $\mathbf{B_0}$ (now the field lines are not *straight* any more), one can write the first–order force–free force–balance equation, together to Ampère's law. This gives a system of Newcomb–like equations for each harmonic of the perturbation to the fluxes, $\psi_P^{m,n}$ and $\psi_T^{m,n}$. These are coupled equations, in which each mode (m,n) is coupled with the $(m\pm1,n)$ mode: we call this *toroidal coupling*. The equations that must be solved for $\psi_P^{m,n}$ and $\psi_T^{m,n}$ are ordinary differential equations (3.36)–(3.37), with boundary condition from magnetic measurements. We will find that the measure of the radial and toroidal magnetic field at the edge are enough to solve the system.

The toroidal coupling acts between modes with same n toroidal mode number and $\Delta m = \pm 1$ on the poloidal mode number, due to the curvilinear

[1] See appendix C.1 for a discussion on complex Fourier harmonics.
Here and in the following the convention of [53] on the sign of the resonant modes is used.

metrics.
The (r, ϑ, φ) are curvilinear coordinates, in order to take into account the toroidicity of the system. This arises from the shift term $\Delta(r)$, not neglected in the definition of the geometrical coordinates (eq.(3.4)), that defines the center of the non–concentric circular flux surfaces of $\mathbf{B_0}$. Due to this term the metric tensor is not diagonal[2], and the non–null non–diagonal terms ($g_{r\vartheta} \neq 0$) are what couples the modes with same n mode and $\Delta m = \pm 1$.
The toroidal coupling can not be therefore seen in the diagonal cylindrical coordinates[3], where the shift $\Delta(r)$ is neglected. Differently to these coordinates, working with curvilinear coordinates in general one must pay attention to covariant (*down*) and contravariant (*up*) vector components (see appendix B).

We said that the solution of Newcomb's equation provides the harmonics $\psi_P^{m,n}$ and $\psi_T^{m,n}$ of the perturbation to the poloidal and toroidal flux respectively, and we therefore need the relation that links the magnetic fluxes to the components of the magnetic field. We use the canonical representation of $\mathbf{B}$ in the general toroidal coordinate system (r, ϑ, φ)

$$\mathbf{B} = \nabla\psi_T \times \nabla\vartheta - \nabla\psi_P \times \nabla\varphi \tag{3.3}$$

and the formulas valid for both magnetic (when considering the axi–symmetric field $\mathbf{B_0}$) or non–magnetic coordinates (in the case of a perturbed magnetic field). $\psi_P(r, \vartheta, \varphi)$ and $\psi_T(r, \vartheta, \varphi)$ are the poloidal and toroidal fluxes respectively. In chapter 5 one can find the formulas for the covariant and contravariant components of the magnetic field, that involve the elements of the metric tensor. In particular one can find the formulas for the components of $\mathbf{B}$ in the case of SHAx states, that are modelled as pure Single Helicity (SH) states.

In the following sections one can find some details on how the Newcomb–like equations in toroidal geometry for the harmonics of the fluxes are obtained. But one must read [53] for the solution details.

3.1 Zero–th order equilibrium

3.1.1 The toroidal (r, ϑ, φ) coordinate system

Let us consider a zeroth-order axisymmetric toroidal plasma with circular cross-section, formed in a vacuum chamber with major radius R_0 and minor radius a. The flux surfaces are non-concentric circles, each having radius r,

[2] See then definition of the metrics in appendix B.2.
[3] See then definition of the cylindrical metrics in appendix B.2.1.

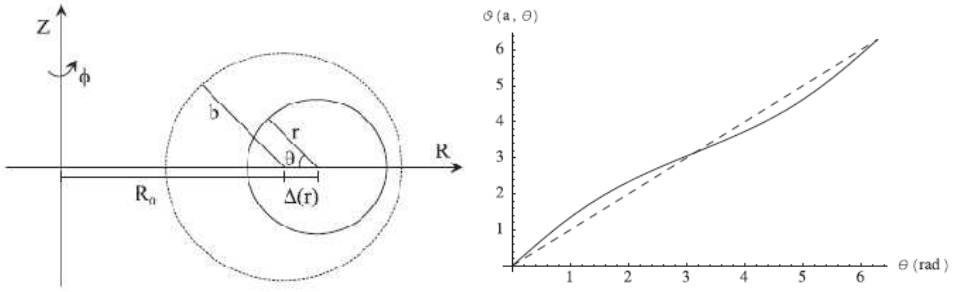

Figure 3.1: Reproduced from [53]. *Left: Geometrical co-ordinates. Right: Relation between the flux ϑ and geometrical θ poloidal angles at $r = a$. The deviation from the bisector (dashed line) is an increasing function of the radius.*

being horizontally shifted by a quantity $\Delta(r)$. The shift of the outermost flux surface is imposed as boundary condition (in the experiments this is obtained from external magnetic measurements). A point lying on one of these flux surfaces is identified by the radius r of the surface, by the poloidal angle θ measured with respect to the inboard mid plane, and by the toroidal angle φ. These coordinates, which we call geometric coordinates, u^i, are related to the standard cylindrical system (R, φ, Z) used to describe toroidal fusion devices by

$$R = R_0 - r\cos\theta + \Delta(r) \tag{3.4}$$

$$Z = r\sin\theta. \tag{3.5}$$

where R_0 is the torus major radius. The (r, θ, φ) coordinate system is curvilinear and non-orthogonal, in order to properly take into account the toroidal geometry. A complete knowledge of the metric tensor is essential (see appendix B for a brief reminder on curvilinear coordinates). The metric tensor and the Jacobian of the geometric coordinates are given in appendix B.2.2.

The contravariant representation of the zeroth-order magnetic field associated with the geometric coordinate system is

$$\mathbf{B}_0 = \nabla\psi_{T,0}(r) \times \nabla\theta - \nabla\psi_{P,0}(r) \times \nabla\varphi + \nabla r \times \nabla\nu(r,\theta) \tag{3.6}$$

where $\psi_{T,0}$ and $\psi_{P,0}$ are, respectively, the toroidal and poloidal flux divided by 2π. The equilibrium is fully defined once $\psi_{T,0}(r)$, $\psi_{P,0}(r)$, $\Delta(r)$ and $\nu(r,\theta)$ are known.
Following the standard procedure for introducing flux coordinates 2.8.2, one can define a new poloidal angle as

$$\vartheta = \theta + \lambda(r,\theta) \tag{3.7}$$

with $\lambda(r,\theta) = \nu(r,\theta)/\psi'_{T,0}(r)$. Here and in the following a prime designates derivative with respect to r of quantities which are functions of r only. In the $w^i = (r,\vartheta,\varphi)$ system, which we call flux coordinates, the magnetic field lines are straight and the magnetic field contravariant representation is simply

$$\mathbf{B}_0 = \nabla\psi_{T,0}(r) \times \nabla\vartheta - \nabla\psi_{P,0}(r) \times \nabla\varphi. \tag{3.8}$$

This provides simple formulas for the contravariant components B^i, given by

$$B_0^r = 0 \qquad B_0^\vartheta = \frac{1}{\sqrt{g_w}}\psi'_{P,0} \qquad B_0^\varphi = \frac{1}{\sqrt{g_w}}\psi'_{T,0} \tag{3.9}$$

where $\sqrt{g_w}$ is the Jacobian of the flux coordinate system:

$$\sqrt{g_w} = \left(\nabla r \cdot \nabla\vartheta \times \nabla\varphi\right)^{-1}. \tag{3.10}$$

The metric tensor and the Jacobian of the flux coordinates are also given in appendix B.2.3.
The determination of the parameter $\lambda(r,\theta)$ in (3.7) is possible for a large aspect ratio torus following a perturbative approach, as done first in [53]. Ampére's law allows to deduce the current density contravariant components J^i. From the force balance condition and $B_0^r = 0$ one gets $J_0^r = 0$. Using this information, and performing an expansion in the small aspect ratio parameter $\epsilon = a/R_0$, it is possible to compute the quantity relating θ and ϑ as

$$\lambda(r,\theta) = \lambda_1(r)\sin\theta + \lambda_2(r)\sin 2\theta + o(\epsilon^3). \tag{3.11}$$

where

$$\lambda_1(r) = \frac{r}{R_0} - \Delta'(r) \qquad \lambda_2(r) = \frac{r}{4R_0}\lambda_1(r). \tag{3.12}$$

The inverse of transformation (3.7) is then easily derived as

$$\theta = \vartheta - \lambda_1\sin\vartheta - \left(\lambda_2 - \frac{\lambda_1^2}{2}\right)\sin 2\vartheta + o(\epsilon^3). \tag{3.13}$$

Using equation (3.11) the relation between cylindrical (R,φ,Z) and flux coordinates w^i can also be found (up to a $o(\epsilon^3 b)$ approximation term):

$$R = R_0 - r\cos\vartheta + \Delta(r) - r\lambda_1(r)\sin^2\vartheta + \left(\frac{3}{2}r\lambda_1^2 - 2r\lambda_2\right)\sin^2\vartheta\cos\vartheta \tag{3.14}$$

$$Z = r\sin\vartheta - \frac{r}{2}\lambda_1(r)\sin 2\vartheta + \left(\frac{3}{2}r\lambda_1^2 - 2r\lambda_2\right)\sin\vartheta\cos^2\vartheta - \frac{r}{2}\lambda_1^2(r)\sin\vartheta$$

so $R \equiv R(r,\vartheta)$ and $Z \equiv Z(r,\vartheta)$.

The Jacobian of the flux coordinate system for a large aspect ratio torus is (B.2.3):

$$\sqrt{g_w} = \frac{R^2}{K(r)} \tag{3.15}$$

with

$$K(r) = \frac{R_0}{r}\left(1 + \frac{\Delta}{R_0} + \frac{r}{2R_0}\Delta' - \frac{r^2}{2R_0^2} + o(\epsilon^3)\right). \tag{3.16}$$

3.1.2 Equilibrium quantities: $\Delta(r)$, $\psi_{P,0}$ and $\psi_{T,0}$

It is possible to show that, for a force-free equilibrium, in flux coordinates the current density is proportional to the magnetic field through a coefficient which is a function of r only, that is

$$\mu_0 \mathbf{J}_0 = \sigma(r)\mathbf{B}_0. \tag{3.17}$$

It is convenient to define, for a generic field A, its hatted version as $\hat{A} = \sqrt{g_w}A$, which hides the Jacobian contribution. The zeroth-order hatted magnetic field and current density components, function of r only, are then:

$$\hat{B}_0^\vartheta = \psi'_{P,0} \qquad \hat{B}_0^\varphi = \psi'_{T,0} \qquad \mu_0\hat{J}_0^\vartheta = \sigma\psi'_{P,0} \qquad \mu_0\hat{J}_0^\varphi = \sigma\psi'_{T,0}. \tag{3.18}$$

Given the $\sigma(r)$ profile, which is an input to the algorithm, the zeroth-order force balance yields the following equations:

$$\frac{d}{dr}[K(r)\hat{B}_0^\varphi] = -\sigma(r)\hat{B}_0^\vartheta \tag{3.19}$$

$$\frac{\partial}{\partial r}\left[\frac{g^w_{\vartheta\vartheta}}{\sqrt{g_w}}\hat{B}_0^\vartheta\right] - \frac{\partial}{\partial\vartheta}\left(\frac{g^w_{r\vartheta}}{\sqrt{g_w}}\right)\hat{B}_0^\vartheta = \sigma(r)\hat{B}_0^\varphi. \tag{3.20}$$

The second equation contains metric coefficients which are function of r and ϑ. By using the expansion in harmonics described in appendix B.2.3, it can be split into two equations, one for $\hat{B}_0^\vartheta$ and one for Δ. Furthermore, because of the nonlinearity given by the fact that the metric coefficients depend on Δ, it is convenient to introduce a perturbative expansion:

$$\hat{B}_0^\vartheta = \hat{B}_1^\vartheta + \hat{B}_2^\vartheta + \ldots, \qquad \hat{B}_2^\vartheta = o(\epsilon^2)\hat{B}_1^\vartheta \tag{3.21}$$

$$\hat{B}_0^\varphi = \hat{B}_1^\varphi + \hat{B}_2^\varphi + \ldots, \qquad \hat{B}_2^\varphi = o(\epsilon^2)\hat{B}_1^\varphi. \tag{3.22}$$

The resulting equations for the lowest order contribution are

$$\frac{d}{dr}\left(\frac{R_0}{r}\hat{B}_1^\varphi\right) = -\sigma(r)\hat{B}_1^\vartheta \tag{3.23}$$

$$\frac{d}{dr}\left(\frac{r}{R_0}\hat{B}_1^\vartheta\right) = \sigma(r)\hat{B}_1^\varphi \tag{3.24}$$

which can be solved for $\hat{B}_1^\vartheta(r)$ and $\hat{B}_1^\varphi(r)$. The solution starts from the magnetic axis, where regularity imposes $\hat{B}_1^\vartheta \sim \sigma_0 R_0 r/2$ and $\hat{B}_1^\varphi \sim r$, and proceeds to the edge. The solutions are then rescaled so as to match a boundary condition, for example the edge poloidal field.
These solutions are then plugged into the equation for the shift

$$\Delta'' + \frac{\Delta'}{r}\left(1 + 2r\frac{d\hat{B}_1^\vartheta/dr}{\hat{B}_1^\vartheta}\right) + \frac{1}{R_0} = 0. \tag{3.25}$$

which is solved using the boundary conditions $\Delta'(0) = 0$ and an assigned value for $\Delta(b)$, b being the radius at which the magnetic measurements yielding the condition are located.
Having determined the shift $\Delta(r)$, the next order correction to the fields can be computed by

$$\begin{aligned}
&\frac{d}{dr}\left(\frac{R_0}{r}\hat{B}_2^\varphi\right) + \frac{d}{dr}\left[\frac{R_0}{r}\left(\frac{\Delta}{R_0} + \frac{r}{2R_0}\Delta' - \frac{r^2}{2R_0^2}\right)\hat{B}_1^\varphi\right] = -\sigma(r)\hat{B}_2^\vartheta \\
&\frac{d}{dr}\left(\frac{r}{R_0}\hat{B}_2^\vartheta\right) + \frac{d}{dr}\left[\frac{r}{R_0}\left(\frac{r^2}{2R_0^2} + \frac{\Delta'^2}{2} + \frac{r}{2R_0}\Delta' - \frac{\Delta}{R_0}\right)\hat{B}_1^\vartheta\right] = \sigma(r)\hat{B}_2^\varphi
\end{aligned} \tag{3.26}$$

Again, these equations are solved starting from the axis, where regularity requires $\hat{B}_2^\vartheta \sim 3r/(2\sigma_0 R_0)$ and $\hat{B}_2^\varphi \sim [3/(\sigma_0^2 R_0^2) - \Delta_0/R_0]r$, Δ_0 being the shift of the magnetic axis. In practice this correction turns out to be very small.

It is worth noting that this method of computing the zeroth-order axisymmetric equilibrium, if compared to the standard Grad-Shafranov equation, has the advantage of requiring simply the solution of five ordinary differential equations. This is obtained at the price of being restricted to deal with circular flux surfaces, which is however reasonable for present day RFP devices. While $\sigma(r)$ can in principle be any function, for the application described in the following the customary parametrization called α-Θ_0 model has been used, that is

$$\sigma = \frac{2\Theta_0}{a}\left[1 - \left(\frac{r}{a}\right)^\alpha\right]. \tag{3.27}$$

The two free parameters Θ_0 and α are adjusted so as to obtain given values of the two dimensionless parameters Θ and F, which are the well known pinch and reversal parameters used to describe RFP plasmas (see chapter 1.).

3.2 First–order contribution to the equilibrium

The next step is to add a non-axisymmetric perturbation to (3.8). In the gauge $A_r = 0$, where A_r is the covariant radial component of the vector

potential $\mathbf{A}$, the total magnetic field can be written as

$$\mathbf{B} = \nabla\psi_T \times \nabla\vartheta - \nabla\psi_P \times \nabla\varphi \tag{3.28}$$

where now ψ_T and ψ_P depend on all three coordinates. The $w^i = (r, \vartheta, \varphi)$ coordinates are not any more flux coordinates for the perturbed magnetic field, which means that magnetic field lines of $\mathbf{B}$ are not straight in this coordinate system, and the potentials ψ_T and ψ_P are not any more flux functions (see section 2.7). These potentials, related to the vector potential covariant components, can be Fourier expanded as

$$\psi_P(r,\vartheta,\varphi) = -A_\varphi(r,\vartheta,\varphi) = \psi_{P,0}(r) + \sum_{n\neq 0,m} \psi_P^{m,n}(r) e^{i(m\vartheta - n\varphi)} \tag{3.29}$$

$$\psi_T(r,\vartheta,\varphi) = A_\vartheta(r,\vartheta,\varphi) = \psi_{T,0}(r) + \sum_{n\neq 0,m} \psi_T^{m,n}(r) e^{i(m\vartheta - n\varphi)} \tag{3.30}$$

The perturbed quantities contain $n \neq 0$ terms only, and the harmonics amplitudes are complex (see appendix C.1 for a discussion on complex conjugation).

Given the representation (3.28) of the magnetic field, the total hatted contravariant magnetic field components are

$$\hat{B}^\vartheta = \frac{\partial\psi_P}{\partial r} \qquad \hat{B}^\varphi = \frac{\partial\psi_T}{\partial r} \qquad \hat{b}^r = -\frac{\partial\psi_T}{\partial\varphi} - \frac{\partial\psi_P}{\partial\vartheta}. \tag{3.31}$$

Computing the total current density components from Ampére's law and plugging them into the first-order force balance equation

$$\mathbf{j}\times\mathbf{B}_0 + \mathbf{J}_0\times\mathbf{b} = \frac{1}{\sqrt{g_w}}\epsilon^{ijk}(\hat{j}^i\hat{B}_0^j + \hat{J}_0^i\hat{b}^j)\nabla w^k = 0 \tag{3.32}$$

one obtains the proportionality between perturbed radial current and perturbed radial magnetic field

$$\mu_0\hat{j}^r = \sigma(r)\hat{b}^r \tag{3.33}$$

and

$$\left(\frac{\partial}{\partial\vartheta} + q\frac{\partial}{\partial\varphi}\right)(\mu_0\hat{j}^\vartheta - \sigma\hat{b}^\vartheta) + \hat{b}^r\frac{d\sigma}{dr} = 0 \tag{3.34}$$

$$\left(\frac{\partial}{\partial\vartheta} + q\frac{\partial}{\partial\varphi}\right)(\mu_0\hat{j}^\varphi - \sigma\hat{b}^\varphi) + \hat{b}^r q\frac{d\sigma}{dr} = 0. \tag{3.35}$$

By Fourier-transforming equations (3.33) and (3.35) (only two equations are needed, since for each mode there are two unknown functions $\psi_T^{m,n}$ and

$\psi_P^{m,n}$) and using Ampére's law the following equations are found:

$$
\begin{aligned}
& mK(r)\frac{d\psi_T^{m,n}}{dr} + n\left(\frac{g^w_{\vartheta\vartheta}}{\sqrt{g_w}}\right)^{0,0}\frac{d\psi_P^{m,n}}{dr} - \sigma(n\psi_T^{m,n} - m\psi_P^{m,n}) \\
& -in\left(\frac{g^w_{r\vartheta}}{\sqrt{g_w}}\right)^{1,0}[n\psi_T^{m+1,n} - n\psi_T^{m-1,n} - (m+1)\psi_P^{m+1,n} + (m-1)\psi_P^{m-1,n}] \\
& +n\left(\frac{g^w_{\vartheta\vartheta}}{\sqrt{g_w}}\right)^{1,0}\left[\frac{d\psi_P^{m+1,n}}{dr} + \frac{d\psi_P^{m-1,n}}{dr}\right] = 0
\end{aligned}
\tag{3.36}
$$

$$
\begin{aligned}
& \frac{d}{dr}\left(K(r)\frac{d\psi_T^{m,n}}{dr}\right) + \sigma\frac{d\psi_P^{m,n}}{dr} - n\left(\frac{g^w_{rr}}{\sqrt{g_w}}\right)^{0,0}[n\psi_T^{m,n} - m\psi_P^{m,n}] - \frac{n\psi_T^{m,n} - m\psi_P^{m,n}}{m - nq}\frac{d\sigma}{dr} \\
& -n\left(\frac{g^w_{rr}}{\sqrt{g_w}}\right)^{1,0}[n\psi_T^{m+1,n} + n\psi_T^{m-1,n} - (m+1)\psi_P^{m+1,n} - (m-1)\psi_P^{m-1,n}] \\
& -in\left(\frac{g^w_{r\vartheta}}{\sqrt{g_w}}\right)^{1,0}\left[\frac{d\psi_P^{m+1,n}}{dr} - \frac{d\psi_P^{m-1,n}}{dr}\right] = 0
\end{aligned}
\tag{3.37}
$$

In appendix B.2.3 one can find the metric tensor element combinations that appear in these equations.

The method used for the solution of these equations is described in detail in ref. [53]. The solution requires the knowledge of the corresponding harmonic amplitude for the radial component of the magnetic field at some surface outside the plasma, which represents the boundary condition. Furthermore, if the mode has a resonant surface inside the plasma, a discontinuity in the eigenfunction derivative should be allowed. The magnitude of this discontinuity is obtained by imposing a further boundary condition, that is the amplitude of the toroidal magnetic field component at the same surface where the radial one is determined (that is the surface where the sensors are located).

Chapter 4

Helical coordinates in toroidal systems

The goal in this chapter is to find *good* coordinate systems to describe SHAx states, modelled as pure SH states[1], beginning from the reconstruction of the magnetic flux surfaces, using the magnetic flux eigenfunctions inside the plasma volume introduced in the previous chapter.

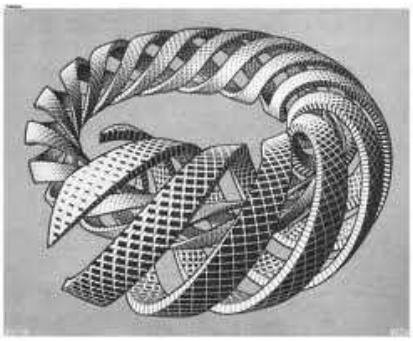

Figure 4.1: Escher, 1953

Let us introduce the problem.
In the perturbative approach to the magnetic field $\mathbf{B}$, introduced in the previous chapter, it is easy to find magnetic flux surfaces for the axi–symmetric part $\mathbf{B_0}$, and the function that can label them is the radius r of their circular cross-section[2]. Adding a generic perturbation, the circular flux surfaces that characterize $\mathbf{B_0}$ are deformed, and it is not clear a priori if other flux surfaces exist and which can be the function ρ to label them[3]: this is the general case

[1] Single Helicity states, where only the dominant mode of the SHAx states is considered.
[2] This is the equilibrium described in the introduction, for which $\mathbf{B} \cdot \nabla r = 0$.
[3] By definition flux surfaces exist if (necessary condition) there exist a function ρ for

of Multiple Helicity (MH) states, where no evidence of symmetries in the system is present. Considering instead SH states the perturbation has helical symmetry, which means that the fluxes ψ_P and ψ_T (and all the surface functions in the plasma) are functions only of the radius r and of the helical angle defined as $u = m\vartheta - n\varphi$ [4]:

$$\psi(r,u) = \psi_0(r) + \psi^{m,n}(r)\, e^{iu} + c.c. \tag{4.1}$$

This arises from (3.2) neglecting the sum over secondary modes (and considering the dominant mode with fixed (m,n), which is the $(1,7)$ mode in RFX–mod). In this case it has been shown (eq.(2.198) section 2.9) that flux surfaces exist ($\rho(r,u) = const$), and one can also look for Action–Angle coordinates on them, that correspond to straight–field–line coordinates. A good flux function is the helical flux (the Hamiltonian of the system), that will be called with the symbol χ from now on. The formal definition of χ will be given in section 4.1, and looking at its contour plot in fig.4.3 one can deduce that coordinate systems built on the circular–cross-section flux surfaces of $\mathbf{B_0}$ are not appropriate to describe helical flux surfaces. This is true especially in the inner bean–shaped surfaces which does not contain the magnetic axis of the axisymmetric equilibrium, due to the fact that one can identify two points that have the same value of the poloidal angle ϑ.
All the coordinate systems defined until now in RFX are based on the circular–cross-section flux surfaces of the axisymmetric equilibrium. Modelling SHAx states as pure SH states, the goal is to find coordinates based on the helical geometry, where the helical flux is used as the radial coordinate. The fundamental request for helical coordinates is then a non–orthogonal and curvilinear metric tensor, with angles defined with respect to the helical axis ($\nabla\rho = 0$), in order to well describe both the toroidal geometry of the problem and the new helical axis of the system. In section 4.2.1 an angle β with these features is defined using a geometrical approach, in sections 4.2.2-4.2.4 helical coordinates are found using the Hamiltonian form of the magnetic field and its properties defined in particular in section 2.9. This allows to find not just helical coordinates, but also to take advantage of the properties of helical *magnetic* coordinates looking for Action–Angle coordinates.

The practical outcome of this thesis is the code named SHEq (Single Helical Equilibria). It uses the helical coordinate systems, which in this

which $\mathbf{B}\cdot\nabla\rho = 0$ and are therefore defined by $\rho = const$. As said in chapter 2 this is the case only if a symmetry is manifest in the system, and ρ can be identified with the Hamiltonian H (due to Noether theorem) or any function $f(H)$. In section 2.8.2 we have already noticed that in chaotic spaces, where magnetic field line are destroyed, the relation $\rho = const$ is still valid. We refer here to conserved magnetic flux surfaces.

[4] ψ in the formula stays therefore for ψ_P, ψ_T or any flux function. See appendix C.1 for a discussion on the complex conjugated.

chapter[5] are defined in a mathematical way, in order to compute all the helical equilibrium plasma quantities. More than one helical–toroidal coordinate system are defined in this chapter, and all the metric tensor elements and the Jacobian of every coordinate system are usable in SHEq (metric tensor elements and Jacobians can be found in the detailed calculations of chapter 9).
Each plot in the following is computed by the SHEq–code. The abscissa ρ_h used in the plots is the square root of the normalized helical flux:

$$\rho_h = \sqrt{\frac{\chi - \chi_{min}}{\chi_{max} - \chi_{min}}}\,, \tag{4.2}$$

χ_{min} being the value of the helical flux on the helical axis and χ_{max} its value at the edge. Being a function of χ only, ρ_h is a label for helical flux surfaces that ranges between 0 on the helical axis and 1.
Bean–shaped surfaces which do not contain the magnetic axis of the axisymmetric equilibrium are called *internal* flux surfaces, the *external* flux surfaces are instead the surfaces which contain both the axisymmetric and the helical axis.

The main results of this chapter have been published in B. Momo et. al *Plasma Phys. Control. Fus* (2011) [1] and in E. Martines, R. Lorenzini, B. Momo et al. *Plasma Phys. Control. Fus* (2011) [2].
Some work has been performed by the RFX–mod team, to demonstrate that the helical flux here defined is a good flux function also from the experimental point of view. In particular, this work is presented in [54] (Nature, 2009). Here we just cite one of the tests of the helical equilibrium reconstruction, performed by considering an electron temperature (T_e) profile measured by a Thomson scattering system[6]. Due to the asymmetry of the helical flux with respect to the vacuum chamber, kinetic plasma quantities during SHAx states exhibit non symmetric profiles if plotted against the radius of the vaccum chamber r. This can be seen in fig.4.2(a) for T_e, where the two colors mark points that are on the two sides of the (helical) magnetic axis. The same function plotted as a function of the normalized helical flux ρ_h is shown in fig.4.2(b): it is immediately clear how the two half profiles collapse one onto the other. This is a proof that the helical flux evaluated with theoretical methods is indeed a flux function, in the hypothesis that the T_e profile is due to very fast parallel thermal transport and almost flat density profiles. Fig.4.2(c) is the reconstruction of the electron temperature map on the poloidal plane.

[5] Further details of the helical metrics can be found also in the detailed calculations of chapter 9.

[6] T_e profiles measured along a horizontal diameter of the chamber by a 84–point Thomson scattering system, [55].

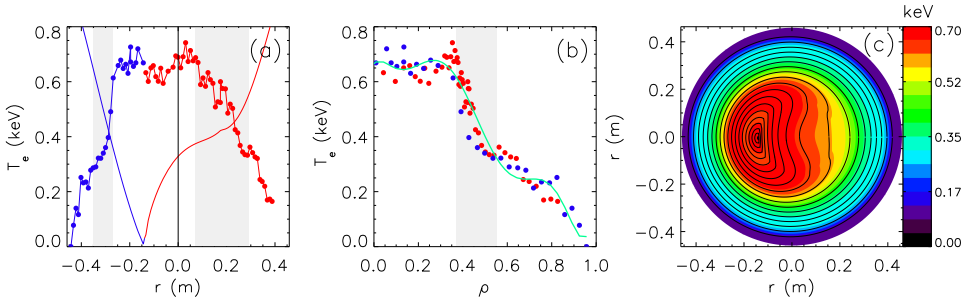

Figure 4.2: Reproduced from [2]. (a): Electron temperature profile from Thomson scattering data measured along a horizontal diameter, plotted as a function of the radius r of the vacuum chamber. The two colors mark the points that are on the two sides of the magnetic axis. The two continuous curve are the normalized helical flux ρ on the diameter. (b): Electron temperature profile, plotted as a function of the normalized helical flux ρ. (c): Temperature map on the poloidal plane. Data refer to shot 24599 at $t = 99ms$.

Let us remind the basic approximations used in this work: of considering SHAx states as pure SH states neglecting the contribution of the residual secondary modes; of the perturbative approach to reconstruct the harmonics of the perturbation, also for the dominant mode[7], solving a Newcomb–like equation in force free condition; and of assuming a $\alpha - \Theta_0$ model [56, 57] to fit experimental data for the zeroth–order parallel current density.

4.1 The radial coordinate χ

SHAx states are modelled as pure SH states, composed of the superposition of the zero–th order axisymmetric equilibrium and the dominant mode eigenfunction, that in RFX–mod is the $(m, n) = (1, 7)$. Any flux function has therefore helical symmetry during SHAx states, and one can go back to the helical example in section 2.9 to use Hamiltonian mechanics tools. We look in this section for the Hamiltonian of the system that is always a good radial coordinate and that can be used as label for flux surfaces.
In section 2.9 it has been found that

$$\mathbf{B} \cdot \nabla \chi = 0 \tag{4.3}$$

for the Hamiltonian $\chi(r, u)$ (or any function of χ only) and $u = m\vartheta - n\varphi$: u is the helical angle and χ is called helical flux. Its definition in terms of the

[7] We are confident on this approximation because the dominant mode is not more than some percent of the equilibrium part... even if this changes the topology so much!

poloidal and toroidal fluxes is

$$\chi = m\psi_P - n\psi_T \quad . \tag{4.4}$$

The poloidal and toroidal fluxes in SH can be written as (4.1)

$$\psi_P(r,u) = \psi_{P,0}(r) + \psi_P^{m,n}(r)\, e^{iu} + c.c. \tag{4.5}$$
$$\psi_T(r,u) = \psi_{T,0}(r) + \psi_T^{m,n}(r)\, e^{iu} + c.c. \tag{4.6}$$

and therefore

$$\chi = m\psi_P - n\psi_T \tag{4.7}$$
$$= [m\psi_{P,0} - n\psi_{T,0}](r) + [m\psi_P^{m,n} - n\psi_T^{m,n}](r)\, e^{iu} + c.c. \tag{4.8}$$
$$= \chi_0(r) + \chi^{m,n}(r)\, e^{iu} + c.c. \tag{4.9}$$
$$= \chi_0(r) + 2|\chi^{m,n}|(r)\, \cos(u + \phi_\chi) \tag{4.10}$$

with the same helical symmetry of any other flux function. Both the axisymmetric equilibrium part and its perturbation due to the single $(m,n) = (1,7)$ mode of the fluxes are computed as described in the preceding chapter. The amplitude $|\chi^{m,n}|(r)$ and phase $\phi_\chi(r)$ are defined in section 9.1 in terms of amplitude and phase of the poloidal and toroidal fluxes.

The helical flux is constant on the resulting flux surfaces of SHAx states, and a contour plot of χ is shown in fig.4.3. It can be seen that only the inner

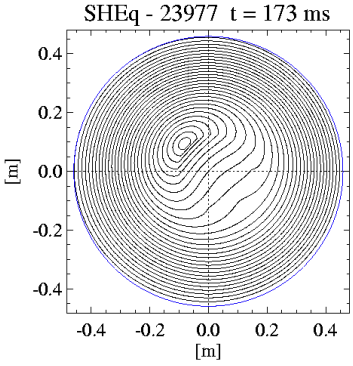

Figure 4.3: Contour plot of the helical flux χ.

surfaces are significantly distorted due to the inner resonant $(m = 1/n = 7)$ mode, and assume a bean–like shape. The outer ones retains a quasi–circular shape, with a shift due to perturbations.

In this section the helical flux $\chi(r,u)$ has been defined using the perturbative approach and choosing the SH due to the $(m,n) = (1,7)$ mode. As

said in section 2.9, the Hamiltonian does not change changing the angle coordinates if it is unchanged the periodicity $(m, n) = (1, 7)$ of the system. In fact $\chi(r, u) = \chi(I)$ if I is the Action of the system. This allows to compute the radial coordinate χ (that labels the helical flux surfaces) using the composition of two fluxes which are not flux functions for helical symmetries[8].

4.2 The angle coordinates

The radial variable is a label of the magnetic flux surfaces, and one can use the helical flux χ. Let us go back to the fundamental requests for the angular part of helical coordinates: a non–orthogonal and curvilinear metric tensor, with angles defined with respect to the helical axis ($\nabla\chi = 0$).
There are two ways to define the angular part of helical coordinate systems: the geometrical way described in section 4.2.1, or following the Hamiltonian theory of magnetic field lines, as described in section 4.2.2-4.2.4. The Hamiltonian way uses the helical symmetry of the system, which means that any plasma quantity depends on the r, u coordinates only, with $u = m\vartheta - n\varphi$. Due to the fact that plasma quantities do not depend explicitly on the angles ϑ or φ, one can choose two frames of reference where the helical symmetry is manifest, choosing either the poloidal or toroidal angle as ignorable coordinate (that corresponds to the canonical time of the magnetic–Hamiltonian system). In this chapter both options are described, for the (χ, u, φ) and (χ, u, ϑ) frame of reference[9]. However both choices are not *good* in RFP machines. The toroidal angle is not a good *time* because of its change in sign in correspondence of the reversal of the toroidal component of the magnetic field at the edge. Usually indeed the RFP community works with the poloidal angle as the canonical time, but in section 4.4 we prove that it is not a good choice during SHAx states. That's why in section 4.2.4 we introduce also the toroidal–like angle v that do not reverse, to be used as the canonical time. This a good choice especially to study the edge, but the physical meaning of the fluxes related with this *strange* angle it is not so clear any more.
The SHEq code can always choose between all these helical coordinates, with respect to the problem that must be solved.
All the metric tensor elements and the Jacobian of the coordinate systems have been calculated and can be found in the detailed calculation in section 9.2.

We refer to section 2.9 in all the result and calculations of the next sections.

[8] In other words, equation (4.4) can be used both with $\psi_{P,T}(r, u)$ and $\psi_{P,T}(\rho)$.
[9] Inverting the relation $\chi = \chi(r, u)$ the helical flux is used instead of r as first coordinate. This is what we always do in chapter 2 for the Hamiltonian of the system, chosen as radial coordinate of the system.

4.2.1 The geometrical angle β

We describe here the first new coordinate system that has been defined to well describe the helical equilibrium in SHAx states, using the helical flux χ as the 'radial' coordinate. Keeping φ as toroidal angle, a new poloidal–like angle β, which rotates around the helical axis ($\nabla\chi = 0$), must be defined. The coordinate system (χ, β, φ) is not a straight–field–line system, but it is easy defined in a geometrical way.

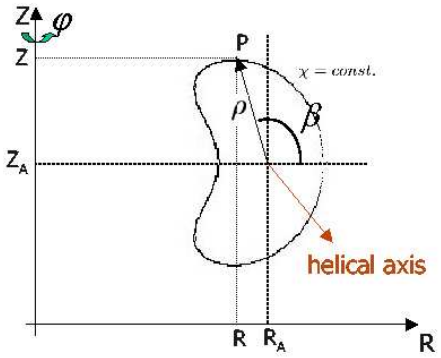

Figure 4.4: The geometrical approach to define the poloidal–like angle β on helical flux surfaces ($\chi = const$) and with respect to the helical axis ($\nabla\chi = 0$).

The definition of β, with respect to the cylindrical coordinates (R, φ, Z), is

$$\beta = \tan^{-1} \frac{Z - Z_a(\varphi)}{R - R_a(\varphi)} \tag{4.11}$$

where $R_a(\varphi)$ and $Z_a(\varphi)$ represent the cylindrical coordinates of the helical magnetic axis. Due to the dependence on the toroidal angle of the helical magnetic axis coordinates, also β depends on φ: $\beta = \beta(R, \varphi, Z)$. The definition (4.11) can be easily derived from fig.4.4:

$$\begin{cases} \rho \cos\beta = (R - R_a) \\ \rho \sin\beta = (Z - Z_a) \end{cases} \tag{4.12}$$

$$\Updownarrow$$

$$\tan\beta = \frac{Z - Z_a(\varphi)}{R - R_a(\varphi)} \quad . \tag{4.13}$$

We refer to section 9.2 for the derivation of the metric tensor and of the Jacobian of the new (χ, β, φ) coordinate system. Here we just mention that the metrics can be derived in a relatively easy way in terms of the metrics of the zero–th order flux coordinates (r, ϑ, φ) defined in chapter 3 and appendix B.2.3, using their relation with the cylindrical coordinates, equations (3.14).

4.2.2 The Hamiltonian time φ: (χ, u, φ) and (χ, u_h, φ)

Using the helical flux as radial coordinate, we start from the coordinate system (χ, u, φ) that emphasizes the helical symmetry with respect to u on the flux surfaces $\chi = const$. The presence of an ignorable coordinate allows to look for Action–Angle coordinates on the flux surface labelled by χ, following the resumptive example in section 2.9 and reaching the straight–field–line system (χ, u_h, φ) where u_h is the (new) Angle. The helical angle $u = m\vartheta - n\varphi$ is not defined with respect to the helical axis (the poloidal angle ϑ is not as well, being defined with respect to the axisymmetric axis of the system), whereas the Angle u_h (conjugated to the Action) is: by definition it increases by 2π over one turn around any helical flux surfaces, even the internal ones that do not enclose the axisymmetric axis, as seen in (2.90). That's why we am looking for A–A coordinates in this section, beginning from (χ, u, φ)[10].

Action–Angle coordinates are defined in section 2.6, and one needs the identification between canonical variables and magnetic quantities to apply formulas (2.95)–(2.97) for the Action, the generating function[11] and the Angle respectively. Due to the symmetry of the problem, the identifications are the ones of eq.(2.181)–(2.184) for the $A_1 = 0$ axial gauge

$$t = \varphi \tag{4.14}$$
$$H = -A_\varphi(r,u) = \chi(r,u) = const \tag{4.15}$$
$$q = u \tag{4.16}$$
$$p = A_u(r,u) = \psi_T(r,u) \tag{4.17}$$

and we need to apply eq.(2.185)–(2.187), as already found in section 2.9.

[10] Taking a back step, to define the toroidal helical systems one starts from the toroidal coordinate system (r, ϑ, φ) and defines the helical angle $u = m\vartheta - n\varphi$ to change frame of reference to (r, u, φ). In this coordinate system, remembering (4.1), the helical symmetry is manifest due to the ignorable coordinate φ that plays the role of the canonical time, and $\chi = \chi(r, u)$ as all the flux plasma quantities. Inverting this relation, one can use any flux function as radial coordinate instead of r.
In A–A coordinates, $\chi = \chi(I)$ if I is the Action: because $\chi(r, u)$ in (χ, u, φ) coordinates, one knows that this is not already an Action–Angle coordinate system.

[11] The generating function of the canonical transformation to Action–Angle coordinates. For the canonical transformation $(p, q) \mapsto (P, Q)$, $F_2 = F_2(q, P)$.

We can find the identification with canonical variables also beginning from the canonical representation of the magnetic field $\mathbf{B}$ valid for any divergence–free field in a toroidal device, introduced in eq.(2.138) for generic (r, ϑ, φ) toroidal coordinates. From this, equation (2.195)

$$\mathbf{B}(r, u, \varphi) = \nabla\psi_T(r, u) \times \nabla u - \nabla\chi(r, u) \times \nabla\varphi \tag{4.18}$$

can be derived simply substituting the poloidal angle ϑ and the poloidal flux $\psi_P(r, u)$ with the helical angle $u = \vartheta - n\varphi$ and the helical flux $\chi(r, u) = \psi_P - n\psi_T$ respectively. Using the identification of the magnetic fluxes to canonical variables (through the covariant components of the vector potential) as a mnemonic rule, one immediately knows that: φ plays the role of the time, $\psi_T(r, u)$ of the momentum conjugated to the helical angle u, and $\chi(r, u)$ the role of the Hamiltonian of the system.

In any case we go back to eq.(2.185)–(2.187), but using here a different notation: $\rho = \chi(r, u)$ for the radial variable, $I(\rho) \mapsto \psi_h(\chi)$ for the Action and $\zeta(I, u) \mapsto u_h(\chi, u)$ for the Angle.
Because $\psi_T(r, u)$ and $\chi(r, u)$, these functions may be locally inverted to yield the Hamiltonian as a function of the toroidal flux $\chi = \chi(\psi_T, u)$ or, vice versa, $\psi_T = \psi_T(\chi, u)$. The action is nothing but the curvilinear integral of the flux $\psi_T(\chi, u)$:

$$\psi_h(\chi) = \frac{1}{2\pi} \oint_{\Sigma(\chi)} \psi_T(\chi, u')\, du' \tag{4.19}$$

where $\Sigma(\chi)$ is the magnetic surface labelled by the helical flux χ. Inverting the relation $\psi_h(\chi)$ in the function $\chi(\psi_h)$, the flux $\psi_T(\chi, u)$ can be written as a function of (ψ_h, u), useful to provide the angle u_h conjugate to the Action through the definition of the generating function $F_2(\psi_h, u)$. For the canonical transformation from $(p, q) \equiv (\psi_T, u)$ to $(I, \zeta) \equiv (\psi_h, u_h)$:

$$F_2(\psi_h, u) = \int_{u_0}^{u} \psi_T(\psi_h, u')\, du' + f(\psi_h) \tag{4.20}$$

$$u_h(u, I) = \frac{\partial F_2}{\partial \psi_h} = \int_{u_0}^{u} \frac{\partial \psi_T}{\partial \psi_h}(\psi_h, u')\, du' \tag{4.21}$$

where $f(\psi_h)$ is an arbitrary function of the Action that can be set to zero, fixing the origin of the Angle u_h on the origin of the helical angle u.
Keeping fixed the canonical time and therefore the toroidal angle, and choosing the helical flux $\chi(\psi_h)$ as the radial coordinate, we end with the helical straight–field–line coordinates (χ, u_h, φ). In this coordinate system the canonical form of $\mathbf{B}$ can be written as:

$$\mathbf{B} = \nabla\psi_h(\chi) \times \nabla u_h - \nabla\chi \times \nabla\varphi \tag{4.22}$$

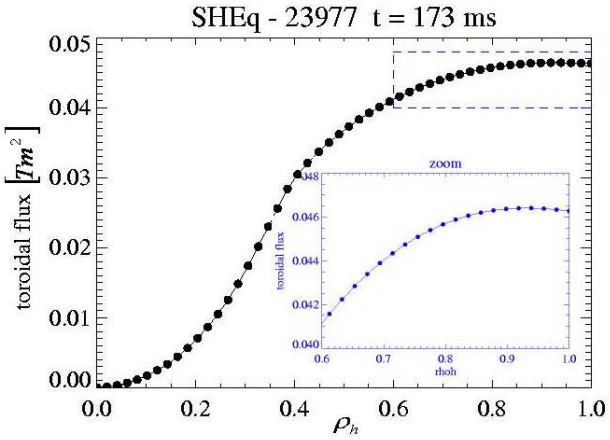

Figure 4.5: The toroidal flux $\psi_h(\chi)$.

with $\mathbf{B} \equiv \mathbf{B}(\chi, u_h, \varphi)$.

Let us see the main features of the new variables. As it must be, the Action $\psi_h(\chi)$ turns out to be the toroidal flux in Action–Angle coordinates. The proof can be done in the same way as done in section 2.7. What we want to emphasize is that the toroidal flux associated to the toroidal component of the magnetic field and to the toroidal angle φ in non monotonic, due to the reversal of the configuration at the edge. This can be seen in fig.4.5 for ψ_h.
The Angle u_h increases by 2π over one turn around any magnetic flux surface $\Sigma(\chi)$:

$$\Delta u_h = \oint_{\Sigma(\chi)} \frac{\partial \psi_T(\psi_h, u')}{\partial \psi_h} \, du' = \tag{4.23}$$

$$= \frac{\partial}{\partial \psi_h} \oint_{\Sigma(\chi)} \psi_T(\psi_h, u') \, du' = \tag{4.24}$$

$$= \frac{\partial (2\pi \psi_h)}{\partial \psi_h} = 2\pi \tag{4.25}$$

and this confirms that it is a good angle defined with respect to the helical axis.
In (4.20) the function $f(\psi_h)$ has been set to zero, fixing the origin of the Angle u_h on the origin of the helical angle u. This means that, like u, also u_h does not have its zero always on the horizontal plane, but it turns around with the toroidal angle φ. The example at $\vartheta = 0$, where $u = -n\varphi$, for some value of the toroidal angle can be found in fig.4.11. We will find this of some interest later.

Till here we went trough the mathematical expressions to be used. From an operative point of view[12] we just need to begin with eq.(4.5)–(4.6) to compute the helical flux (as in eq.(9.2)) and the toroidal flux $\psi_T(r,u)$. Integrals and derivatives of the fluxes are computed numerically, but further analytic calculation used to simplify numerical computation can be found in section 9.1.

To conclude, let us note that in the cylindrical limit, where the helical deformation vanishes, $\psi_h = \psi_T$ and $u_h = u$.

4.2.3 The Hamiltonian time ϑ: (χ, u, ϑ) and $(\chi, u_{\vartheta h}, \vartheta)$

The toroidal flux $\psi_h(\chi)$ defined in the previous section is a flux function (it is constant on flux surfaces), but it is not a good radial variable because it is not monotonic (as said, due to the reversal of the toroidal magnetic field in RFP machines). That's why usually the RFP community chooses the poloidal angle ϑ as the canonical time. We analyze this choice for the helical symmetry of SHAx states, ending up with an Action–Angle coordinate system that defines a poloidal flux ψ_{P2} (conjugated to the Angle $u_{\vartheta h}$). But, being related to the poloidal angle ϑ, that is not defined with respect to the helical axis, we will see that it is not a *good* poloidal flux during SHAx states. And that is why even this choice of the canonical time ϑ is not always good in RFPs[13].
In helical coordinates the choice of ϑ as canonical time brings to the (χ, u, ϑ) coordinate system. From the Hamiltonian point of view this is a problem similar to the one where the ignorable coordinate was the toroidal angle φ: the canonical time is now the poloidal angle ϑ but one can prove that it is an always increasing time along a field line, even in the *internal* bean–shaped flux surfaces[14]. From the physical point of view the poloidal flux

[12] SHEq's implementation

[13] As it is for the axisymmetric equilibrium.

[14] For instance, for orbits close to the helical axis, one could think that ϑ is not evolving monotonically, which would disqualify it to be used as a time. In the *internal* bean–shaped flux surfaces one can demonstrate that the time ϑ flows always in the same direction while evolves the time φ:

$$\frac{d\vartheta}{d\varphi} > 0$$

always inside the bean–shaped flux surfaces. Going back to the definition of the rotational transform as the frequency in Action–Angle context, one can write:

$$\frac{d\vartheta}{d\varphi} = n + \frac{du}{d\varphi} \tag{4.26}$$

$$= n + \frac{du}{du_h}\frac{du_h}{d\varphi} = n + \iota_h \frac{du}{du_h} \tag{4.27}$$

using the definition $\vartheta = u + n\varphi$ and remembering that we are moving on constant flux surfaces ($\chi = const$). ι_h is introduced in section 2.6.1, and is exactly the frequency on

does not reverse, and we do not crash with the problem of non monotonic fluxes (fig.4.6). In this section we look for Action–Angle coordinates beginning from the (χ, u, ϑ) coordinate system, ending with the straight–field–line coordinates $(\chi, u_{\vartheta h}, \vartheta)$, in exactly the same way as done for (χ, u_h, φ).

The canonical identification of the magnetic variables is already found, in the gauge $A_1 = 0$, for general (x^1, x^2, x^3) coordinates with x^3 as ignorable coordinate, in eq.(2.91)–(2.94). It is worth noting that in the example of this section (and differently from the previous examples) the third ignorable coordinate is $x^3 = \vartheta$. Therefore:

$$t = \vartheta \tag{4.28}$$
$$q = u \tag{4.29}$$
$$p = A_u(r,u) = \psi_P(r,u) \tag{4.30}$$
$$H = -A_\vartheta(r,u) = \chi(r,u) = const \tag{4.31}$$

We apply formulas (2.95)–(2.97) for the Action, the generating function and the Angle respectively, as done for the canonical time φ, but with the new canonical identifications. Because $\psi_P(r,u)$ and $\chi(r,u)$, these functions may be locally inverted to yield the Hamiltonian as a function of the *poloidal* flux $\chi = \chi(\psi_P, u)$ or, vice versa, $\psi_P = \psi_P(\chi, u)$. The Action ψ_{P2} is nothing but the curvilinear integral of the flux $\psi_P(\chi, u)$: inverting the relation $\psi_{P2}(\chi)$ in the function $\chi(\psi_{P2})$, the flux $\psi_P(\chi, u)$ can be written as a function of (ψ_{P2}, u), useful to provide the angle $u_{\vartheta h}$ conjugate to the Action through the definition of the generating function $F_2(\psi_{P2}, u)$[15]. The result is:

$$\psi_{P2}(\chi) = \frac{1}{2\pi} \oint_{\Sigma(\chi)} \psi_P(\chi, u')\, du' \tag{4.32}$$
$$F_2(\psi_{P2}, u) = \int_{u_0}^{u} \psi_P(\psi_{P2}, u')\, du' + f(\psi_{P2}) \tag{4.33}$$
$$u_{\vartheta h}(u, I) = \frac{\partial F_2}{\partial \psi_{P2}} = \int_{u_0}^{u} \frac{\partial \psi_P}{\partial \psi_{P2}}(\psi_{P2}, u')\, du' \tag{4.34}$$

where $\Sigma(\chi)$ is the magnetic surface labelled by the helical flux χ and $f(\psi_{P2})$ is set to zero, fixing the origin of the Angle $u_{\vartheta h}$ on the origin of the helical angle u. As u_h in fig.4.11, $u_{\vartheta h}$ turns its zero value turning around in the toroidal angle φ.

---

the $\chi = const$ orbits in the A–A system (χ, u_h, φ): going back to the definition (2.88) one need to remember that $\varphi \equiv t$ is the time and $\zeta \equiv u_h$ the Angle. On the helical axis $du/du_h = 0$ and drifting away $du/du_h \to 1$. The rotational transform ι_h decreases drifting away from the helical axis, but not so quickly to change the sign of n, equal to $d\vartheta/d\varphi$ on the helical axis. Therefore $\frac{d\vartheta}{d\varphi} > 0$ and this ends the proof.

[15] For the canonical transformation $(p, q) \mapsto (P, Q)$, $F_2 = F_2(q, P)$.

The canonical representation of the magnetic field associated to (χ, u, ϑ) is

$$\mathbf{B}(r,u,\vartheta) = (\nabla\psi_P(r,u) \times \nabla u - \nabla\chi(r,u) \times \nabla\vartheta)/n \tag{4.35}$$

with n toroidal mode number and $m = 1$. This form can be derived from the general one in eq.(2.138) simply substituting the toroidal angle φ and the toroidal flux $\psi_T(r,u)$ with the helical angle $u = \vartheta - n\varphi$ and the helical flux $\chi(r,u) = \psi_P - n\psi_T$ respectively. In Action–Angle coordinates $(\chi, u_{\vartheta h}, \vartheta)$ the correspondent representation can be written as

$$\mathbf{B}(\chi, u_{\vartheta h}, \vartheta) = (\nabla\psi_{P2}(\chi) \times \nabla u_{\vartheta h} - \nabla\chi \times \nabla\vartheta)/n \tag{4.36}$$

Let us see the main features of the new variables.
As it must be, the Angle $u_{\vartheta h}$ increases by 2π over one turn around any magnetic surfaces $\Sigma(\chi)$, and this introduces a good angle defined with respect to the helical axis, as discussed for the Angle u_h in the previous section.
The Action $\psi_{P2}(\chi)$ turns out to be *a poloidal* flux in Action–Angle coordinates. It is the poloidal flux related to the *old* poloidal angle, ϑ, that is defined with respect to the axisymmetric axis of the system and not with respect to the helical axis (the *time* ϑ does not change in the canonical transformation to Action–Angle coordinates). In a more formal way, one can understand this proving that the flux $\psi_{P2}(\chi)$ is indeed the flux at $\vartheta = const$[16]:

$$\begin{aligned}
\psi_{P2}(\chi) &= \frac{1}{2\pi} \oint_{\Sigma(\chi)} \psi_P(r,u')\, du' && (4.37)\\
&= \frac{1}{2\pi} \iint_{\Sigma(\chi)} dr\, du' \, \frac{\partial\psi_P(r,u')}{\partial r} && (4.38)\\
&= \frac{1}{2\pi} \iint_{\Sigma(\chi)} dr\, du' \, \sqrt{g}\, B^{\vartheta} && (4.39)\\
&= \frac{1}{2\pi} \iint_{\Sigma(\chi)} dr\, du' \, \sqrt{g}\, \mathbf{B}\cdot\nabla\vartheta && (4.40)\\
&= \frac{1}{2\pi} \iint_{\Sigma(\chi)} \mathbf{B}\cdot d\boldsymbol{\Sigma}(\vartheta) && (4.41)
\end{aligned}$$

The last equation is the definition of the poloidal flux, and in the previous steps one simply needs to remember the definition $\Sigma(\vartheta) = \sqrt{g}\nabla\vartheta dr du$ of the constant–ϑ surfaces in the (r,u,ϑ) coordinate system, and eq.(2.145)

$$B^{\vartheta} = -\frac{1}{\sqrt{g}} \frac{\partial A_u}{\partial r} \tag{4.42}$$

where $x^1 = r$, $x^3 = \vartheta$ and $A_2 = A_u = \psi_P(r,u)$ from eq.(4.30).
In fig.4.8(a) we draw the physical flux $\psi_{P2}(\chi)$ associated to ϑ, and one can

[16] As it must be, being the Action of the $(\chi, u_{\vartheta h}, \vartheta)$ coordinate system.

compare it to the poloidal flux defined with respect to the magnetic axis in fig.4.8(b) and in fig.2.2.
Further discussion on this can be found in section 4.4. And the difference with another poloidal flux there introduced is the reason because we use the symbol 2 to mark the poloidal flux in this section.

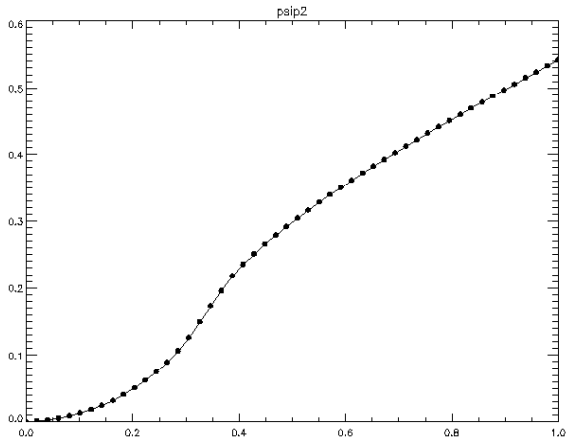

Figure 4.6: The poloidal flux $\psi_{P2}(\chi)$.

Again, as in section 4.2.2, from an operative point of view[17] we just need to begin with eq.(4.5)–(4.6) to compute the helical flux (as in eq.(9.2)) and the poloidal flux $\psi_P(r,u)$ in order to be able to compute all the mathematical expressions above.

4.2.4 The Hamiltonian time v: (χ, u, v) and (χ, u_η, v)

In sections 4.2.2 we show that in RFP machines the choice of the toroidal angle φ as the canonical time is not always good because of the reversal of the toroidal magnetic field at the edge, that can be seen also as the change in sign of the toroidal angle, and therefore of the time. And in section 4.2.3 we tell in advance[18] that during SHAx states also the choice of the poloidal angle ϑ as canonical time is not good enough: the poloidal angle ϑ is defined with respect to the cylindrical magnetic axis, hence it does not satisfy our fundamental request of angles defined with respect to the helical axis. The non monotonic toroidal flux $\psi_h(\chi)$ and the poloidal flux $\psi_{P2}(\chi)$ are in figg. 4.5-4.6.
In this section, we look for a different choice for the canonical time: using a

[17] SHEq's implementation
[18] Exhaustive analysis in section 4.4

linear combination of the poloidal and toroidal angles, we define a toroidal–like angle v that can be thought as defined on the helical axis and that do not reverse. The corresponding flux η is defined with the analogously linear combination of the poloidal and toroidal fluxes, $\psi_P(r,u)$ and $\psi_T(r,u)$. There are infinite possible choices for v angles, every one with the limitation of being linked with a flux η that is not of easy physical interpretation.
As in the previous sections, we look for Action–Angle coordinates for the system (χ,u,v), reaching the straight–field–line system (χ,u_η,v) where the Angle u_η and the conjugated Action η_h are defined with respect to the helical axis. In A–A coordinates the $\eta_h(\chi)$ fluxes are monotonic and defined with respect to the helical axis. This can help for example for the study the RFP edge.

We have already defined the helical angle $u = m\vartheta - n\varphi$ as a linear combination of the poloidal and toroidal angles, and the helical flux $\chi = m\psi_P - n\psi_T$ as the same linear combination of the poloidal and toroidal fluxes. In the same way we can define an angle v and a magnetic flux η with a general linear combination of the poloidal and toroidal angles and fluxes:

$$v = a\,\vartheta + b\,n\,\varphi \tag{4.43}$$
$$\eta = a\,\psi_P + b\,n\,\psi_T \tag{4.44}$$

with a and b general parameters and n the toroidal mode number, $m = 1$ the poloidal mode number[19]. In helical symmetry the fluxes are written in eq.(4.5)–(4.6) and

$$\eta(r,u) = a\,\psi_P(r,u) + b\,n\,\psi_T(r,u) \tag{4.45}$$
$$= [a\,\psi_{P,0} + b\,n\,\psi_{T,0}](r) + [a\,\psi_P^{m,n} + b\,n\,\psi_T^{m,n}](r)\,e^{iu} + c.c. \tag{4.46}$$
$$= \eta_0(r) + \eta^{m,n}(r)\;e^{iu} + c.c. \tag{4.47}$$

Substituting in eq.(2.138) the functions $\psi_P,\psi_T,\vartheta,\varphi$ with the functions χ,η,u,v, another equivalent form of $\mathbf{B}$ is obtained:

$$\mathbf{B} = \frac{1}{n(a+b)}(\nabla\eta\times\nabla u - \nabla\chi\times\nabla v)\;. \tag{4.48}$$

With the condition

$$\frac{1}{n(a+b)} = 1 \tag{4.49}$$

one can recognize the usual canonical form of the magnetic field, written for (χ,u,v) coordinates, and can therefore look for Action–Angle coordinates on the $\chi = const$ flux surfaces in a similar way as done in all the previous

[19] One can remember that we are dealing with a SH states in the $m = 1$ spectrum during SHAx states in RFX–mod.

sections, once the canonical variables are identified. An infinite number of combinations can solve the constraint (4.49), even remembering that we are dealing with n fixed and equal to 7 in RFX–mod SHAx states. For instance in section 4.2.2 we used the choice $a = 0, b = 1/n$, and equation (4.35) in section 4.2.3 is linked to the choice of $a = 1/n, b = 0$. In this section we am going to analyze the choice $a = 1/2n, b = 1/2n$, that correspond to the definitions

$$v = \frac{1}{2n}\vartheta + \frac{1}{2}\varphi \tag{4.50}$$

$$\eta(r,u) = \frac{1}{2n}\psi_P(r,u) + \frac{1}{2}\psi_T(r,u) \tag{4.51}$$

In (χ, u, v) coordinates, where $v = x^3$ is the ignorable coordinate, by definition, from (4.48)–(4.49) and using the relations between fluxes and covariant components of the vector potential:

$$\mathbf{B} = \nabla\eta(r,u) \times \nabla u - \nabla\chi(r,u) \times \nabla v \tag{4.52}$$

$$= \nabla A_u(r,u) \times \nabla u + \nabla A_v(r,u) \times \nabla v \tag{4.53}$$

$$= \nabla A_2(x^1,x^2) \times \nabla u + \nabla A_3(x^1,x^2) \times \nabla v \tag{4.54}$$

Using this equivalence it is easy to use the canonical identification of the magnetic variables found in eq.(2.91)–(2.94) for general (x^1, x^2, x^3) coordinates with x^3 as ignorable coordinate and the gauge $A_1 = 0$:

$$t = v \tag{4.55}$$

$$q = u \tag{4.56}$$

$$p = A_u(r,u) = \eta(r,u) \tag{4.57}$$

$$H = -A_v(r,u) = \chi(r,u) \tag{4.58}$$

It is now possible to compute Action–Angle variables, applying formulas (2.95)–(2.97) for the Action η_h, the generating function F_2 and the Angle u_η respectively, taking for granted the necessary function inversions. One just need to pay attention to the right canonical identifications:

$$\eta_h(\chi) = \frac{1}{2\pi}\int \eta(\chi,u)du = \tag{4.59}$$

$$= \frac{1}{2\pi}\int \psi_T(\chi,u)du + \frac{1}{2\pi}\int \psi_P(\chi,u)du \tag{4.60}$$

$$F_2(\eta_h,u) = \int_0^u \eta(\eta_h,u)du \tag{4.61}$$

$$u_\eta = \frac{\partial S}{\partial \eta_h} = \int_0^u \frac{\partial \eta(\eta_h,u)}{\partial \eta_h}du \tag{4.62}$$

In the definition (4.60) of the Action $\eta_h(\chi)$, the first integral is exactly the toroidal flux ψ_h across $\Sigma(\chi)$ found in (4.19) and the second integral the

$\psi_{P2}(\chi)$ flux in eq.(4.32) (that is the poloidal flux defined with respect to the cylindrical axis).
The Action is a function of the Hamiltonian only, as it must be, and we end up with a new helical Action–Angle coordinate system: (χ, u_η, v). The contravariant representation of the magnetic field in these coordinates is

$$\mathbf{B}(\chi, u_\eta, v) = \nabla\eta_h(\chi) \times \nabla u_\eta - \nabla\chi \times \nabla v \tag{4.63}$$

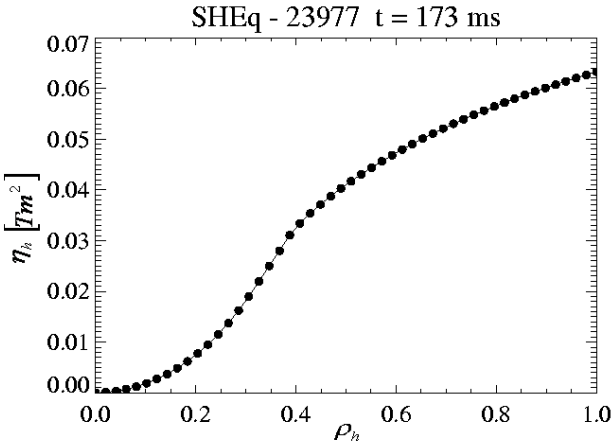

Figure 4.7: The flux $\eta_h\chi$).

As said, the toroidal flux $\psi_h(\chi)$ is not a monotonic function. We choose a different toroidal–like angle, the angle v, that does not change its sign at the reversal surface: in fig.4.7 we can indeed see that the $\eta_h(\chi)$ flux, linked to the angle v, is monotonic. But, how can we easily describe the $v = const$ surface, linked to the $\eta_h(\chi)$ flux (that is by definition the flux trough the flux surfaces $\chi = const$ at $v = const$)? The difficulty in the visualization of this flux is its only problem!

4.3 Change of radial coordinates

One wants to choose the radial variable, called here ρ, to label the magnetic flux surfaces. This is linked with the research of a frame of reference that makes evident the symmetry of the system. From the Hamiltonian point of view one can always choose the Hamiltonian as the radial variable, that is always constant on flux surfaces due to Noether theorem (see section 2.5). From the magnetic point of view this means looking for some function ρ for which

$$\mathbf{B} \cdot \nabla\rho = 0 \quad .$$

Not just one function can label the magnetic flux surfaces: the equation above is satisfied by every function of ρ only, $f(\rho)$. For instance, in SH not just the Hamiltonian $\chi = \psi_P - n\psi_T$ is a good flux function, but also the $\psi_P(\chi), \psi_T(\chi), ...$ (the fluxes found in helical Action–Angle coordinates).
In eq.(4.2) another flux function has been introduced: the adimensional and normalized square root of the helical flux ρ_h, that ranges between zero on the helical axis, and one. It is possible to introduce infinite other choices for the radial variable. Here another common choice:

$$\rho_A = N\,\rho_h \tag{4.64}$$

$$= N\sqrt{\frac{\chi - \chi_{min}}{\chi_{max} - \chi_{min}}} \tag{4.65}$$

where N can be any dimensional constant. Choosing for N the minor radius of the vacuum chamber, ρ_A ranges between zero on the helical axis, and $0.459\,m$ at the edge for RFX–mod machine.

In this short section we just want to describe some of the possibilities for the radial variable, starting from the Hamiltonian of the system. The metric tensor elements and the Jacobian of the coordinate systems change in a very simple way according to the change in the radial variable. All the metrics in the Appendixes are calculated using $\rho = \chi$, but in sections 9.2.2–9.2.3 one can find the derivatives that link the different choices and some dimensional analysis.

4.4 Discussion on the Hamiltonian time ϑ

In section 4.2.3 we end up with the definition (4.32) of a poloidal flux $\psi_{P2}(\chi)$ defined with respect to the axisymmetric axis, where the poloidal angle ϑ is defined.
One can extend the definition (4.4) of the helical flux $\chi(r,u)$ to define the same[20] helical flux $\chi(\rho)$ in any Action–Angle coordinate system:

$$\chi = m\psi_P(\rho) - n\psi_h(\rho) \tag{4.66}$$

where $\psi_h(\chi)$ is the toroidal flux through magnetic flux surfaces, just now defined in (4.19). From the definition of the helical flux in A–A coordinates, it is possible to derive another definition of the poloidal flux trough magnetic flux surfaces: $\psi_P(\chi)$. And that's why we label the first one in equation (4.32) with a 2.

[20] The helical flux $\chi(r,u)$ is already a flux function, constant on flux surfaces.

Let us compare the two definitions of the poloidal fluxes:

$$\psi_{P2}(\chi) = \frac{1}{2\pi}\oint_{\Sigma(\chi)} \psi_P(\chi, u')\, du' \tag{4.67}$$

$$\psi_P(\chi) = \chi + n\psi_h(\chi) \tag{4.68}$$

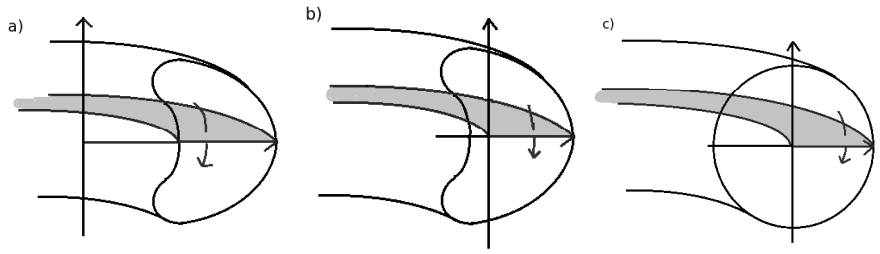

Figure 4.8: Poloidal fluxes. a) The $\psi_{P2}(\chi)$ poloidal flux through internal flux surfaces (at $\vartheta = 0$), that do not contain the cylindrical axis. b) The $\psi_P(\chi)$ poloidal flux through internal flux surfaces (at $\theta^* = 0$), that contain the helical axis. c) Both the $\psi_{P2}(\chi)$ and $\psi_P(\chi)$ poloidal fluxes, through the external flux surfaces (at $\theta = 0 = \theta^*$) that contain both the cylindrical and the helical angles. The θ^* poloidal angle is defined in the text.

The two poloidal fluxes do not coincide in the whole plasma volume. This is due to the main difference in their definition: $\psi_{P2}(\chi)$ is defined with respect to the cylindrical axis, whereas $\psi_P(\chi)$ is defined with respect to the helical axis of the system, and they can coincide only on those surfaces that contain both axes. In fig.4.8 the physical difference between equations (4.67) and (4.68) are shown. The flux $\psi_{P2}(\chi)$ through the *internal* flux surfaces is drawn as the flux of the B^ϑ component of the magnetic field through the surface identified by the segment between the two intersections with the magnetic flux surface $\Sigma(\chi)$ of a line from the axis of the vacuum chamber to a magnetic line on $\Sigma(\chi)$. The same flux through the *external* flux surfaces is the flux through the surface identified by the segment from the axis of the vacuum chamber to the magnetic surface $\chi = const.$ To understand this, one can go back to the demonstration in eq.(4.37), or remember that $\psi_{P2}(\chi)$ is the Action of the $(\chi, u_{\vartheta h}, \vartheta)$ coordinate system[21]. On the other side, the flux ψ_h is defined in the (χ, u_h, φ) coordinate system, where all the angles are defined with respect to the helical axis.

More in details, the difference between the two fluxes is plotted against the normalized helical flux in fig.4.9: the two poloidal fluxes differ through the inner flux surfaces that do not contain the cylindrical axis of the system, and coincide through the outer flux surfaces that contain both the helical

[21] A_3 = (helical) flux across $\Sigma(\rho)$ at $u_{\vartheta h} = x^2 = const.$ A_2 = (poloidal) flux across $\Sigma(\rho)$ at $\vartheta = x^3 = const.$

and cylindrical axis. One can obtain the quantitative difference simply integrating eq.(4.4)

$$\chi(r,u) = \psi_P(r,u) - n\psi_T(r,u) \tag{4.69}$$

over the angle u:

$$\frac{1}{2\pi}\oint_{\Sigma(\chi)} \chi\, du = \frac{1}{2\pi}\oint_{\Sigma(\chi)} \psi_P(r,u)\, du - n\frac{1}{2\pi}\oint_{\Sigma(\chi)} \psi_T(r,u)\, du \tag{4.70}$$

$$= \psi_{P2}(\chi) - n\psi_h(\chi) \tag{4.71}$$

Because the circulation of any flux function χ or $f(\chi)$ over the helical angle u is zero on the flux surfaces that do not contain the cylindrical axis where u is defined, one finds that

On *internal* flux surfaces:

$$\psi_{P2}(\chi) = n\psi_h(\chi) \tag{4.72}$$

$$\Longrightarrow \psi_{P2}(\chi) - \psi_P(\chi) = -\chi \tag{4.73}$$

On the other hand the same circulation is equal to $2\pi\chi$ on all the other flux surfaces, therefore:

On *external* flux surfaces:

$$\psi_{P2}(\chi) = n\psi_h(\chi) + \chi \tag{4.74}$$

$$\Longrightarrow \psi_{P2}(\chi) - \psi_P(\chi) = 0 \tag{4.75}$$

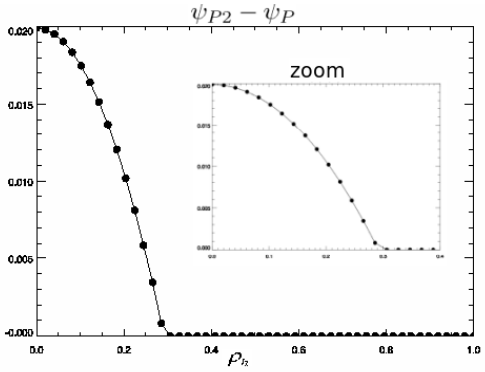

Figure 4.9: $\psi_{P2}(\chi) - \psi_P(\chi)$

The plot of the two functions $\psi_{P2}(\chi)$ and $\psi_P(\chi)$, that coincide only on the external flux surfaces that contain both axes of the system, can be seen in fig.4.10 (right). Wherease the plot of the two fluxes, $\psi_{P2}(\chi)$ and $n\psi_h(\chi)$, can be seen in fig.4.10 (left).

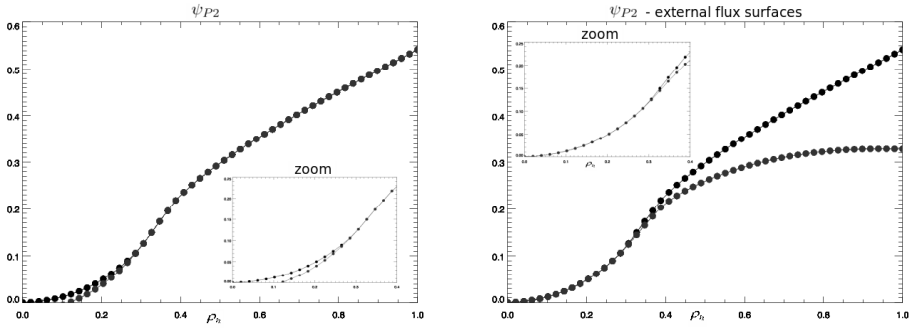

Figure 4.10: Left: black: $\psi_{P2}(\chi)$ and gray: $n\psi_h(\chi) + \chi = \psi_P(\chi)$. Right: black: $\psi_{P2}(\chi)$ and gray: $n\psi_h(\chi)$.

4.4.1 The angle θ^*

As the poloidal flux $\psi_{P2}(\chi)$ is the flux through the magnetic flux surfaces at the poloidal angle $\vartheta = const$, the poloidal flux $\psi_P(\chi)$ is associated to another poloidal angle, defined with respect to the helical axis (differently from ϑ). We briefly introduce this *new* angle, calling it θ^*, that can be derived using the two angles φ and u_h[22], that are both defined on the helical axis. To show this we start from the canonical form of the magnetic field in the (χ, u_h, φ) A–A coordinates, to obtain the equivalent form in the *new* $(\chi, \theta^*, \varphi)$ A–A system (all the angles are considered as divided by 2π):

$$\begin{aligned}
\mathbf{B}(\chi, u_h, \varphi) &= \nabla\psi_h \times \nabla u_h - \nabla\chi \times \nabla\varphi && (4.76)\\
&= \nabla\psi_h \times \nabla u_h - \nabla\psi_P \times \nabla\varphi + n\nabla\psi_h \times \nabla\varphi && (4.77)\\
&= \nabla\psi_h \times \nabla[u_h + n\varphi] - \nabla\psi_P \times \nabla\varphi && (4.78)\\
\mathbf{B}(\chi, \theta^*, \varphi) &= \nabla\psi_h \times \nabla\theta^* - \nabla\psi_P \times \nabla\varphi && (4.79)
\end{aligned}$$

simply using the definition (4.66) for the helical flux, and

$$\theta^* = u_h + n\varphi \quad . \tag{4.80}$$

In fig.4.11 one can see the difference between the poloidal and helical angles defined in this chapter: $\vartheta, \theta^*, u, u_h$. The general poloidal angle ϑ is the angle defined on the cylindrical axis that has the zero always on the horizontal plane. This is not true for the helical angle u, that is obviously not always zero when $\vartheta = 0$, but it turns also with φ. The same can be said for the poloidal and helical angles defined on the helical axis, θ^* and u_h, that go back to ϑ and u in the cylindrical limit (when the helical perturbation vanishes).

[22] Defined in section 4.2.2 for the system (χ, u_h, φ) in which also the flux ψ_h is defined.

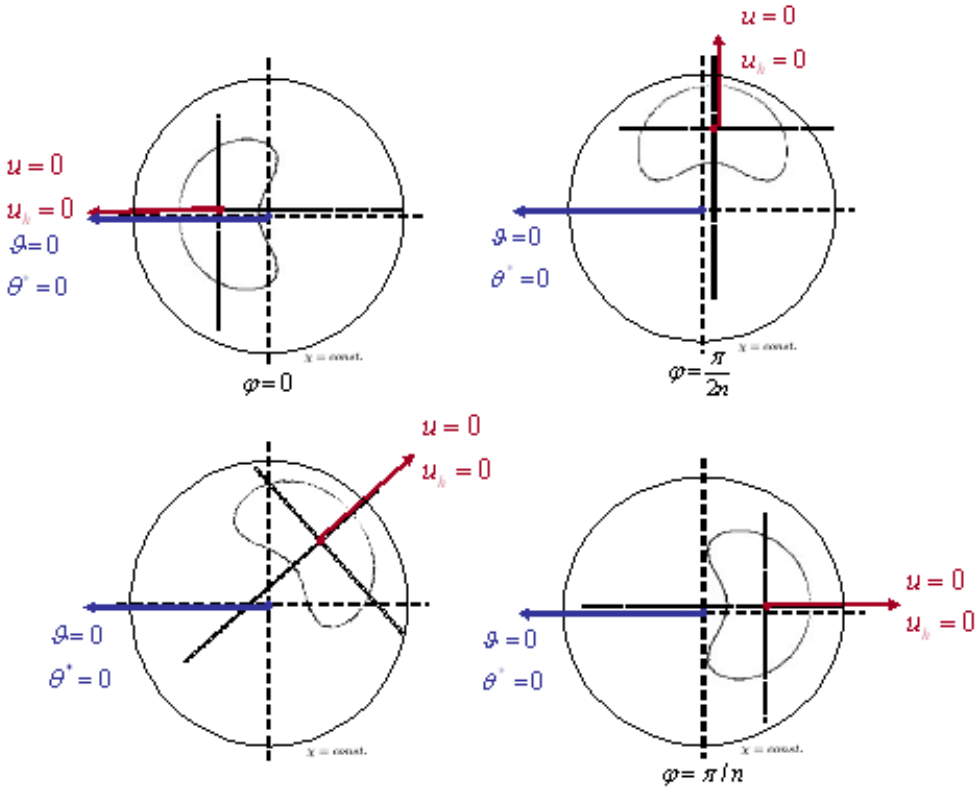

Figure 4.11: Zero of the poloidal and helical angles defined in the text. In a case of null phase of the helical perturbation, $\phi_\chi = 0$. For $\phi_\chi \neq 0$ the helical angles do not point on the convex part of the bean, but they have a fixed phase with the bean anyway because they rotate together with the bean.

We proved that $\psi_{P2}(\chi)$ is a poloidal flux already in section 4.2.3, but from now on we will use only the poloidal flux $\psi_P(\chi)$ defined in this section, related to the poloidal angle θ^*. This choice is in agreement with the request of angles defined with respect to the helical axis, and is more useful in defining helical quantities (as e.g. the helical safety factor profile, as one can see in section 6.3). The whole metrics and the Jacobian of the $(\chi, \theta^*, \varphi)$ system can be found in the detailed calculations in section 9.2.

Let us note that in the $(\chi, \theta^*, \varphi)$ coordinate system, the fluxes depend on the radial coordinate only (as it must be in every Action–Angle coordinate system). Both the poloidal and toroidal angle can be therefore used as the canonical time, with a result similar to that obtained for the (r, ϑ, φ)

coordinate system for the axisymmetric equilibrium $\mathbf{B_0}$ in section 2.10:

$$\mathbf{B}(\chi, \theta^*, \varphi) = \nabla\psi_h(\chi) \times \nabla\theta^* - \nabla\psi_P(\chi) \times \nabla\varphi \tag{4.81}$$

and the associated canonical variables can be

$$\begin{aligned} t &= \varphi && (4.82)\\ H &= -A_\varphi = \psi_P(\chi) && (4.83)\\ q &= \theta^* && (4.84)\\ p &= A_{\theta^*} = \psi_h(\chi) && (4.85) \end{aligned}$$

or

$$\begin{aligned} t &= \theta^* && (4.86)\\ H &= -A_{\theta^*} = \psi_h(\chi) && (4.87)\\ q &= \varphi && (4.88)\\ p &= A_\varphi = \psi_P(\chi) && (4.89) \end{aligned}$$

The canonical time θ^* is always increasing in 0the whole plasma volume and is linked with a poloidal flux that is well defined on the helical axis and monotonic. As the poloidal angle ϑ is a better choice for the canonical time in axisymmetric RFP equilibrium (instead of the toroidal angle that changes its sign at the reversal), in the same way θ^* is a good choice for the canonical time in RFP SHAx helical states.
The problem of a non monotonic Hamiltonian ψ_h related to the time θ^* is not really a problem, because one can use any other flux function as radial coordinate, for example the poloidal flux $\psi_P(\chi)$.
This confirms the choice of the poloidal flux $\psi_P(\chi)$ instead of $\psi_{P2}(\chi)$ from now on.

Chapter 5

Covariant and contravariant magnetic field components

In the previous chapter we find a set of helical coordinate systems, which are all characterized by curvilinear metrics due to the toroidicity of the helical systems. The toroidicity of the system has two main consequences: first, covariant and contravariant indexes of any vector field must be distinguished, and the curvilinear metrics theory (summarized in appendix B) must be used; second, a toroidal coupling between the harmonics of the fluxes and of the Jacobian arises, therefore e.g. a SH in the fluxes does not correspond to SH in the magnetic field components.
In this chapter we emphasize both this aspects. In section 5.1 we derive the formula for the contravariant magnetic field components starting from the magnetic flux eigenfunctions, both for MH and SH states. In section 5.2 and 5.3 we use the curvilinear metrics theory to derive the covariant magnetic field components from the contravariant ones and to derive the components of a field in any coordinate system if the relation between the coordinates is known. In section 5.4 we derive the measurable covariant component of the magnetic field to be compared with measures; in section 5.5 we end with some practical example useful for the applications with SHEq in the next chapter.

5.1 SH in the fluxes does not correspond to SH in the magnetic field components

SH in the fluxes does not correspond to SH in the magnetic field components, which are not constant on the magnetic flux surfaces. In order to study the helical symmetry of SHAx states we impose a SH in the system under study, neglecting the contribution of secondary modes in the $m = 1$ spectra of the fluxes. Noether theorem associates a conserved quantity to a symmetry in

the covariant components of the vector potential, that are nothing but the magnetic fluxes. The conserved quantity labels magnetic flux surfaces, and this justifies the choice of a SH in the fluxes (instead of a quantity not constant on flux surfaces, as the magnetic field).
Due to harmonics of the Jacobian, not constant on flux surfaces in a curvilinear metric, any non–flux quantity does not preserve the helical symmetry. In this section we show how the toroidal coupling between harmonics with same n toroidal number and $\Delta m = 1$ in the poloidal mode number generates other harmonics on the magnetic field components, starting from SH in the fluxes.
Using eq.(2.146)–(2.148) we end with the up magnetic field components in a toroidal symmetry, both in the general case and in the case of helical and axisymmetric symmetries. Down components and components in other frame of reference are listed in the next sections.

Let us start with the definition of any component of the the magnetic field.

$$\begin{aligned} B(r,\vartheta,\varphi) &= B_0 + \sum_{m,n} b_{m,n}(r,\vartheta,\varphi) && (5.1)\\ &= B_0 + \sum_{m,n} b_{m,n}(r)\, e^{i(m\vartheta - n\varphi)} && (5.2)\\ &= B_0 + \sum_{\substack{m\\ n>0}} b_{m,n}(r)\, e^{i(m\vartheta - n\varphi)} + c.c. && (5.3)\\ &= B_0 + \sum_{\substack{m\\ n>0}} 2\,|b_{m,n}|\, cos(\phi_{b_{mn}} + m\vartheta - n\varphi) && (5.4) \end{aligned}$$

The whole perturbation to the magnetic field must be a real value, whereas the harmonics $b_{m,n}(r,\vartheta,\varphi)$ of the Fourier decomposed perturbation in eq.(5.1) are complex numbers[1]. Using (C.12) and the polar form for the complex harmonics of the perturbation

$$b_{m,n}(r) = |b_{m,n}|(r)\, e^{i\,\phi_{b_{mn}}(r)} \qquad (5.5)$$

one gets to (5.4), where both the amplitude $|b_{m,n}|(r)$ and the phase $\phi_{b_{mn}}(r)$ are real numbers. This is true for each component of the magnetic field, and we can use formulas (2.143)–(2.145) to relate the contravariant components B^i to the derivative of the fluxes (or the covariant components of the vector potential) in the gauge $A_1 = 0$. In the same gauge, using the toroidal coordinate system (r,ϑ,φ), formulas (2.143)–(2.145) are equivalent

[1] See appendix C.1 for a discussion on this.

to (2.146)–(2.148). We begin defining the angular components B^ϑ and B^φ:

$$B^i(r,\vartheta,\varphi) = \frac{1}{\sqrt{g}}\left[\psi_0'(r) + \sum_{m,n}\psi'_{m,n}(r)\, e^{i(m\vartheta - n\varphi)}\right] \tag{5.6}$$

$$= \frac{1}{\sqrt{g}}\left[\psi_0'(r) + \sum_{\substack{m\\ n>0}}\psi'_{m,n}(r)\, e^{i(m\vartheta - n\varphi)}\right] + c.c. \tag{5.7}$$

where $B^i = B^\vartheta$ or $B^i = B^\varphi$ depending on $\psi = \psi_P, \psi_T$. For the radial component of the magnetic field the discussion is the same, but due to its different dependence on the fluxes (eq.(2.143)) explicit formulas are at the end of the section.

The (r,ϑ,φ) can be any general toroidal coordinate system. We choose here the (r,ϑ,φ) coordinate system defined in chapter 3, because it is the coordinate system in which the fluxes and their harmonics are computed solving the Newcomb–like equations (3.36)–(3.37). The metrics elements and the Jacobian must be consistent with the choice of the coordinates, and are therefore the ones in appendix B.2.3.
This is always the choice of SHEq's computations, and one can find in section 5.3 the links between these components of magnetic field in the (r,ϑ,φ) coordinates and the components in other coordinate systems (as e.g. the helical coordinates found in chapter 4).

For the magnetic coordinates (r,ϑ,φ) of the axisymmetric equilibrium field $\mathbf{B_0}$ defined in chapter 3, the Jacobian is not constant on the magnetic flux surfaces, and can be written as a sum of harmonics:

$$\frac{1}{\sqrt{g}}(r,\vartheta) = \left(\frac{1}{\sqrt{g}}\right)^{0,0} + \left(\frac{1}{\sqrt{g}}\right)^{\pm 1,0} \tag{5.8}$$

$$= \frac{1}{\sqrt{g_0}}(r) + \frac{1}{\sqrt{g_1}}(r)\left[e^{i\,\vartheta} + e^{-i\,\vartheta}\right] \tag{5.9}$$

The first term is constant on the $r = const$ flux surfaces, whereas the second term is an harmonic proportional to $\cos\vartheta$. We neglect higher order terms. The amplitudes $(1/\sqrt{g_0})$ and $(1/\sqrt{g_1})$ can be found in appendix B.2.3. As already said in chapter 3, the metrics couples modes with the same[2] toroidal mode number n but different poloidal mode number m. This is due to the toroidicity of the system, related to a non diagonal metric tensor[3]. Neglecting higher order terms in the harmonic expansion (5.8), the coupling is between the (m,n) and $(m\pm 1,n)$ harmonics.

[2]The Jacobian does not depend on the toroidal angle φ.
[3]See appendix B.2.3 for the metrics of the (r,ϑ,φ) coordinates

Going back to (5.7), due to the presence of the Jacobian, each harmonic $b_{m,n}(r,\vartheta,\varphi)$ of the perturbation to the magnetic field (with fixed (m,n)) is the sum of the three (m,n) and $(m\pm1,n)$ harmonics of the fluxes:

$$b^i_{m,n}(r,\vartheta,\varphi) = b^i_{m,n}(r)\, e^{i(m\vartheta-n\varphi)} + c.c. \tag{5.10}$$

$$= \frac{1}{\sqrt{g}} \sum_{\substack{m-1\\ n}}^{m+1} \psi'_{m,n}(r)\, e^{i(m\vartheta-n\varphi)} + c.c. \tag{5.11}$$

for each value of n. Again, b^i is the perturbation to the poloidal or toroidal magnetic field component, depending on $\psi = \psi_P, \psi_T$.
Let us write explicitly the $(m,n) = (-1,n),(0,n),(1,n),(2,n)$ following (5.11) and keeping in mind the expansion (5.9):

$$b^i_{1,n}(r)\, e^{i(\vartheta-n\varphi)} + c.c. = \frac{1}{\sqrt{g_0}}\, \psi'_{1,n}(r)\, e^{i(\vartheta-n\varphi)} + \tag{5.12}$$

$$+ \frac{1}{\sqrt{g_1}}\, e^{i(\vartheta)}\, \psi'_{0,n}(r)\, e^{i(-n\varphi)} + \tag{5.13}$$

$$+ \frac{1}{\sqrt{g_1}}\, e^{-i(\vartheta)}\, \psi'_{2,n}(r)\, e^{i(2\vartheta-n\varphi)} \tag{5.14}$$

$$+ \; c.c.$$

Multiplying the exponential in the sum (that come from the harmonics of the Jacobian and of the fluxes), one can see that every term has the right periodicity ($e^{i(\vartheta-n\varphi)}$ for $(m,n)=(1,n)$). In the same way:

$$b^i_{0,n}(r)\, e^{i(-n\varphi)} + c.c = \frac{1}{\sqrt{g_0}}\, \psi'_{0,n}(r)\, e^{i(-n\varphi)} + \tag{5.15}$$

$$+ \frac{1}{\sqrt{g_1}}\, e^{-i(\vartheta)}\, \psi'_{1,n}(r)\, e^{i(\vartheta-n\varphi)} + \tag{5.16}$$

$$+ \frac{1}{\sqrt{g_1}}\, e^{i(\vartheta)}\, \psi'_{-1,n}(r)\, e^{i(-\vartheta-n\varphi)} \tag{5.17}$$

$$+ \; c.c.$$

$$b^i_{2,n}(r)\, e^{i(2\vartheta-n\varphi)} + c.c. = \frac{1}{\sqrt{g_0}}\, \psi'_{2,n}(r)\, e^{i(2\vartheta-n\varphi)} + \tag{5.18}$$

$$+ \frac{1}{\sqrt{g_1}}\, e^{i(\vartheta)}\, \psi'_{1,n}(r)\, e^{i(\vartheta-n\varphi)} + \tag{5.19}$$

$$+ \frac{1}{\sqrt{g_1}}\, e^{-i(\vartheta)}\, \psi'_{3,n}(r)\, e^{i(3\vartheta-n\varphi)} + \tag{5.20}$$

$$+ \; c.c.$$

$$
\begin{aligned}
b^i_{-1,n}(r)\, e^{i(-\vartheta-n\varphi)} + c.c. &= \frac{1}{\sqrt{g_0}}\, \psi'_{-1,n}(r)\, e^{i(-\vartheta-n\varphi)} + && (5.21)\\
&+ \frac{1}{\sqrt{g_1}}\, e^{-i(\vartheta)}\, \psi'_{0,n}(r)\, e^{i(-n\varphi)} + && (5.22)\\
&+ \frac{1}{\sqrt{g_1}}\, e^{i(\vartheta)}\, \psi'_{-2,n}(r)\, e^{i(-2\vartheta-n\varphi)} && (5.23)\\
&+ c.c.
\end{aligned}
$$

The term in eq.(5.20) is neglected in RFX–mod, due to the fact that is related to the $m = 3$ spectrum that can not be detected because only four magnetic coils are present on the poloidal angle.
Note that to each term in (5.12)–(5.23) one need to add the complex conjugated to go back to real value of the perturbation, eq.(5.10).

Let us analyze the magnetic field component on the flux surfaces related to some symmetry of the system.
As said, the magnetic field is not a flux function, i.e. it is not constant on flux surfaces. Even the axi–symmetric part $\mathbf{B_0} = (0, B_0^\vartheta, B_0^\varphi)$ of the magnetic field[4], related to circular flux surfaces, is not constant on them:

$$
\begin{aligned}
B^i_0(r,\vartheta) &= \frac{1}{\sqrt{g}}\, \psi'_0(r) && (5.24)\\
&= \left(\frac{1}{\sqrt{g_0}} + \frac{2}{\sqrt{g_1}}\cos\vartheta\right) \psi'_0(r) && (5.25)
\end{aligned}
$$

where it is evident the dependence on the cosine[5], typical for magnetic field on flux surfaces in a torus (and usually called High or Low Field Side in Tokamaks).
Let us analyze the helical symmetry, that we impose on the fluxes (and therefore to the magnetic flux surfaces) since the beginning of chapter 4 to describe SHAx states:

$$
\psi(r,u) = \psi_0(r) + \psi_{m,n}(r)\, e^{i(m\vartheta-n\varphi)} + c.c. \qquad (5.26)
$$

with fixed (m,n) (and therefore $u = m\vartheta - n\varphi$).
In equations (5.12)–(5.23) we write the harmonics (with fixed (m,n)) of the perturbation to the magnetic field, that are the sum of the three (m,n) and $(m \pm 1, n)$ harmonics of the fluxes. On the other hand we now look to the harmonics of the magnetic field that arises from a single harmonic (fixed

[4] $B^r = \mathbf{B}\cdot\nabla r = 0$ by definition.

[5] Note that the poloidal angle ϑ has been defined with the origin on the internal equatorial plane (that corresponds to $\vartheta_m = \pi$ for the more usual machine poloidal angle). This means that $\cos\vartheta$ is maximum on the internal equator and minimum on the external equator.

(m,n)) in the fluxes: choosing $(m,n)=(1,n)$ for the flux[6], from eq.(5.12)–(5.23), one can see that the flux $\psi_{1,n}$ contributes to the three harmonics $(b^i_{-1,n}, b^i_{0,n}, b^i_{1,n})$ of the magnetic field[7]:

$$B^i_{SH}(r,\vartheta,\varphi) \;=\; \frac{1}{\sqrt{g}}\left[\psi'_0(r) + \sum_{\substack{m-1\\ n}}^{m+1} \psi'_{m,n}(r)\, e^{i(m\vartheta - n\varphi)}\right] + c.c. \quad (5.27)$$

for a fixed (m,n) and $\psi_{m,n}$. With the subscript SH we just want to remind that (5.27) is the way to write the poloidal or toroidal component of the magnetic field that arises from a single harmonic in the flux. From (5.27) for $(m,n)=(1,n)$ and $\psi_{m,n}=\psi_{1,n}$, or choosing explicitly $\psi_{1,n}$ in eq.(5.12)–(5.23), for the magnetic field components related to a SH in the fluxes, one reads:

$$\begin{aligned}
B^i_{SH}(r,\vartheta,\varphi) &= B^i_0(r,\vartheta) + & (5.28)\\
&+ \frac{1}{\sqrt{g_0}}\,\psi'_{1,n}\, e^{i(\vartheta - n\varphi)} + & (5.29)\\
&+ \frac{1}{\sqrt{g_1}}\, e^{-i(\vartheta)}\, \psi'_{1,n}\, e^{i(\vartheta - n\varphi)} + & (5.30)\\
&+ \frac{1}{\sqrt{g_1}}\, e^{i(\vartheta)}\, \psi'_{1,n}\, e^{i(\vartheta - n\varphi)} + & (5.31)\\
&+ c.c. \\
&= \left(\frac{1}{\sqrt{g_0}} + \frac{2}{\sqrt{g_1}}\cos\vartheta\right)\psi'_0(r) + & (5.32)\\
&+ \frac{1}{\sqrt{g_0}}(r)\,\psi'_{1,n}(r)\, e^{i(\vartheta - n\varphi)} + & (5.33)\\
&+ \frac{1}{\sqrt{g_1}}(r)\,\psi'_{1,n}(r)\, e^{i(-n\varphi)} + & (5.34)\\
&+ \frac{1}{\sqrt{g_1}}(r)\,\psi'_{1,n}(r)\, e^{i(-2\vartheta - n\varphi)} + & (5.35)\\
&+ c.c.
\end{aligned}$$

SHEq uses another form for $B^i_{SH}(r,\vartheta,\varphi)$, related to the form in equation (5.4). Calling, in the harmonics of the magnetic field in eq.(5.12)–(5.23), the

[6] $n=7$ in RFX–mod.

[7] In general we consider just $(m\pm 1, n)$, neglecting the coupling between modes with higher Δm.

(complex) terms that depend only on $\psi_{1,n}$

$$b^{i,SH}_{1,n}(r,\vartheta,\varphi) = \frac{1}{\sqrt{g_0}}(r)\,\psi'_{1,n}(r)\,e^{i(\vartheta-n\varphi)} \tag{5.36}$$

$$b^{i,SH}_{0,n}(r,\vartheta,\varphi) = \frac{1}{\sqrt{g_1}}(r)\,\psi'_{1,n}(r)\,e^{i(-n\varphi)} \tag{5.37}$$

$$b^{i,SH}_{2,n}(r,\vartheta,\varphi) = \frac{1}{\sqrt{g_1}}(r)\,\psi'_{1,n}(r)\,e^{i(-2\vartheta-n\varphi)} \tag{5.38}$$

one can write, instead of (5.27) but in a complete equivalent way,

$$B^i_{SH}(r,\vartheta,\varphi) = B^i_0(r,\vartheta) + \sum_{\substack{m-1\\ n}}^{m+1} b^{i,SH}_{m,n}(r)\,e^{i(m\vartheta-n\varphi)} + c.c. \tag{5.39}$$

$$= B^i_0(r,\vartheta) + \sum_{\substack{m-1\\ n}}^{m+1} 2\,|b^{i,SH}_{m,n}|(r)\,cos(\phi_{b^{SH}_{mn}} + m\vartheta - n\varphi) \tag{5.40}$$

where

$$b^{i,SH}_{m,n}(r) = |b^{i,SH}_{m,n}|(r)\,e^{\,i\,\phi_{b^{SH}_{mn}}(r)} \quad . \tag{5.41}$$

SHEq uses formula (5.40).

One can stress again that, related to the SH of the fluxes (and to the helical symmetry of magnetic flux surfaces), other harmonics arise for non–flux quantities (such as the magnetic field components B^i). This is due to the toroidal geometry that couples different metrics elements and to the harmonics of the Jacobian.

Let us write explicitly also the radial component of the magnetic field, always in the (r,ϑ,φ) coordinate system.
Following what done for the poloidal and toroidal components B^i, using the SH in the fluxes $\psi^{1,n}_T$ and $\psi^{1,n}_P$, from (2.146):

$$B^r_{SH}(r,\vartheta,\varphi) = \sum_{\substack{m-1\\ n}}^{m+1} b^{r,SH}_{m,n}(r)\,e^{i(m\vartheta-n\varphi)} + c.c. \tag{5.42}$$

with

$$b^{r,SH}_{1,n}(r) = \frac{1}{\sqrt{g_0}}(r)\Big[\,i\,n\,\psi^{1,n}_T(r) - i\,m\,\psi^{1,n}_P(r)\,\Big] \tag{5.43}$$

$$b^{r,SH}_{0,n}(r) = \frac{1}{\sqrt{g_1}}(r)\Big[\,i\,n\,\psi^{1,n}_T(r) - i\,m\,\psi^{1,n}_P(r)\,\Big] \tag{5.44}$$

$$b^{r,SH}_{-1,n}(r) = \frac{1}{\sqrt{g_1}}(r)\Big[\,i\,n\,\psi^{1,n}_T(r) - i\,m\,\psi^{1,n}_P(r)\,\Big] \tag{5.45}$$

The derivatives of the fluxes (5.26) with respect to the angular variables have been used:

$$\frac{\partial \psi}{\partial \varphi} = -i\, n\, \psi_{m,n}(r)\, e^{i\,(m\vartheta - n\varphi)} + c.c. \tag{5.46}$$

$$\frac{\partial \psi}{\partial \vartheta} = i\, m\, \psi_{m,n}(r)\, e^{i\,(m\vartheta - n\varphi)} + c.c. \tag{5.47}$$

for $(m,n) = (1,n)$ and $\psi \equiv \psi_P, \psi_T$.

The radial derivatives of the fluxes, necessary to compute B^ϑ or B^φ, are explained in section 9.1.

5.2 *Down* components of the magnetic field in the (r,ϑ,φ) coordinate system

In section 5.1 we write the contravariant (*up*) components of the magnetic field in the (r,ϑ,φ) coordinate system of appendix B.2.3, using for them the harmonics of the fluxes that have been computed in the whole plasma volume (chapter 3) for this coordinate system. In order to write the covariant magnetic field components B_i in the same coordinate system, one only needs to use the general rules for curvilinear metrics:

$$B_i = g_{ij}\, B^j \tag{5.48}$$

where B^i are the contravariant components and g_{ij} the metric tensor elements, for $i = r,\vartheta,\varphi$. The elements g_{ij} are in appendix B.2.3 for the (r,ϑ,φ) coordinate system, while $B^i(r,\vartheta,\varphi)$ is written both for the general MH case and for the helical symmetry case, in section 5.1 (formulas for B^ϑ or B^φ: (5.7),(5.12)–(5.23) for the MH general case; (5.25) for $\mathbf{B_0}$; (5.27)–(5.35) or (5.36)–(5.41) for the SH case. Formulas for B^r: (5.42)–(5.45) only for the SH case).
Using the Einstein convention to sum on repeated index, eq.(5.48) means:

$$B_r = g_{rr}\, B^r + g_{r\vartheta}\, B^\vartheta \tag{5.49}$$

$$B_\vartheta = g_{\vartheta r}\, B^r + g_{\vartheta\vartheta}\, B^\vartheta \tag{5.50}$$

$$B_\varphi = g_{\varphi\varphi}\, B^\varphi \tag{5.51}$$

$$\tag{5.52}$$

because in this metric the terms $g_{r\varphi}$ and $g_{\vartheta\varphi}$ are null.

By definition the covariant components of any vector

$$B_i = \mathbf{B} \cdot \mathbf{e}_i \tag{5.53}$$

are the component of the vector along the coordinate line (whereas the contravariant components are the components along the gradient direction). Covariant components are therefore linked to the measurable fields, but one must pay attention to dimension and length of the basis in a curvilinear metrics (section 5.4).

5.3 *Up* and *Down* components of the magnetic field in various coordinate systems

Once the link between coordinates is known, it is possible to write the covariant or contravariant components of any vector in every coordinate system. In section 5.1 we write the contravariant (*up*) components of the magnetic field in the (r, ϑ, φ) coordinate system (appendix B.2.3), taking advantage of the flux harmonics already computed in the whole plasma volume in this coordinate system (chapter 3). And in section 5.2 we write the covariant (*down*) components of the magnetic field in the same coordinate system.
In order to write the *up* and *down* magnetic field components in other coordinate systems, one only needs to follow the rules of the general tensor calculus:

$$A^{i'} = A^j \frac{\partial u^{i'}}{\partial u^j} \ , \ A^j = A^{i'} \frac{\partial u^j}{\partial u^{i'}} \tag{5.54}$$

$$A_{i'} = A_j \frac{\partial u^j}{\partial u^{i'}} \ , \ A_j = A_{i'} \frac{\partial u^{i'}}{\partial u^j} \tag{5.55}$$

being $u^j = (u^1, u^2, u^3)$ and $u^{i'} = (u^{1'}, u^{2'}, u^{3'})$ two different coordinate systems (with the only limitation that their Jacobians are non zero).

5.4 Measurable components of the magnetic field

In curvilinear metrics the basis vectors are in general not adimensional and do not have unitary length. To compare reconstructed magnetic field components with measurements, we need to go back to field components that have the right dimension of the measured field and the whole length (without sharing it with the basis vector). It is enough to divide the basis vectors by their norm, but we need to pay attention to the fact that this can be done just at the end of all the calculations, because tensor calculus is based on the hypothesis of non–adimensional and non–unitary length basis vectors. For

example, writing a $\wedge$ symbol on top of measurable components[8]:

$$\mathbf{B} = B^i \nabla x^i = \widehat{B}^i \widehat{\nabla} x^i = \widehat{B}^i \frac{\nabla x^i}{||\nabla x^i||} \tag{5.60}$$

$$= B_i \mathbf{e}_i = \widehat{B}_i \widehat{\mathbf{e}}_i = \widehat{B}_i \frac{\mathbf{e}_i}{||\mathbf{e}_i||} \tag{5.61}$$

with components

$$B^i = \mathbf{B} \cdot \nabla x^i \tag{5.62}$$

$$\widehat{B}^i \neq \mathbf{B} \cdot \widehat{\nabla} x^i = \mathbf{B} \cdot \frac{\nabla x^i}{||\nabla x^i||} \tag{5.63}$$

$$B_i = \mathbf{B} \cdot \mathbf{e}_i \tag{5.64}$$

$$\widehat{B}_i \neq \mathbf{B} \cdot \widehat{\mathbf{e}}_i = \mathbf{B} \cdot \frac{\mathbf{e}_i}{||\mathbf{e}_i||} \tag{5.65}$$

An equal sign in eq.(5.63) and (5.65) can be used only for diagonal metrics. For curvilinear metrics (where the diagonal metric elements g_{ii} and g^{ii} are not one the inverse of the other) one can only use

$$\widehat{B}^i \equiv \left(\mathbf{B} \cdot \nabla x^i\right) \sqrt{g_{ii}} = B^i \sqrt{g_{ii}} \tag{5.66}$$

$$\widehat{B}_i \equiv \left(\mathbf{B} \cdot \mathbf{e}_i\right) \sqrt{g^{ii}} = B_i \sqrt{g^{ii}} \tag{5.67}$$

[8] with the definition for the normalized basis vectors:

$$\widehat{\nabla} x^i = \frac{\nabla x^i}{||\nabla x^i||} = \frac{\nabla x^i}{\sqrt{g^{ii}}} \Rightarrow \nabla x^i = ||\nabla x^i|| \, \widehat{\nabla} x^i \tag{5.56}$$

$$\widehat{\mathbf{e}}_i = \frac{\mathbf{e}_i}{||\mathbf{e}_i||} \widehat{\mathbf{e}}_i = \frac{\mathbf{e}_i}{\sqrt{g_{ii}}} \Rightarrow \mathbf{e}_i = ||\mathbf{e}_i|| \, \widehat{\mathbf{e}}_i \tag{5.57}$$

and

$$||\nabla x^i|| = \sqrt{\nabla x^i \cdot \nabla x^i} = \sqrt{g^{ii}} \tag{5.58}$$

$$||\mathbf{e}_i|| = \sqrt{\mathbf{e}_i \cdot \mathbf{e}_i} = \sqrt{g_{ii}} \tag{5.59}$$

that arise from (5.60)–(5.61).[9] [10] [11] [12]
Hatted components have the dimension of the whole field, whereas the non–hatted components have dimension that depend on the dimension of the basis vectors, and therefore on the chosen coordinates. In section 9.2.3 some dimensional analysis can be found.

Usually measurements are taken just outside the toroidal vacuum vessel, for which usually are used the machine-toroidal-coordinates (r_m, θ_m, φ) that are linked to cylindrical (R, Z, φ) and Cartesian (x, y, z) coordinates by the relations:

$$x = R\cos\varphi = (R_0 + r_m \cos\theta_m)\cos\varphi \tag{5.77}$$
$$y = R\sin\varphi = (R_0 + r_m \cos\theta_m)\sin\varphi \tag{5.78}$$
$$z = Z = r_m \sin\theta_m \tag{5.79}$$

With respect to the toroidal coordinates in appendix B.2.3 and chapter 3 one can see that the poloidal angle θ_m has the origin on the external equator and that the shift term is not present in eq.(5.77). The vanishing of the differ-

[9] And the inverse

$$B^i = \frac{\widehat{B}^i}{\sqrt{g^{ii}}} \quad B_i = \frac{\widehat{B}_i}{\sqrt{g_{ii}}} \tag{5.68}$$

[10] Using contravariant components to write the covariant ones,

$$\widehat{B}_i = (g_{ij}\, B^j)\sqrt{g^{ii}} \tag{5.69}$$
$$\widehat{B}_r = (g_{rr}\, B^r + g_{r\theta}\, B^\theta + g_{r\varphi}\, B^\varphi)\sqrt{g^{rr}} \tag{5.70}$$
$$\widehat{B}_\theta = (g_{\theta r}\, B^r + g_{\theta\theta}\, B^\theta + g_{\theta\varphi}\, B^\varphi)\sqrt{g^{\theta\theta}} \tag{5.71}$$
$$\widehat{B}_\varphi = (g_{\varphi r}\, B^r + g_{\varphi\theta}\, B^\theta + g_{\varphi\varphi}\, B^\varphi)\sqrt{g^{\varphi\varphi}} \tag{5.72}$$

for a general toroidal coordinate system. In the one of chapter 3 the terms $g_{r\varphi}$ and $g_{\vartheta\varphi}$ are null.

[11] In diagonal metrics, for which $g^{diag}_{ij} = 0$ for $i \neq j$ and $g^{diag}_{ii} = 1/(g^{ii}_{diag})$, again using contravariant components to write the covariant ones

$$\widehat{B}^i_{diag} = B^i\sqrt{g_{ii}} = B^i\frac{1}{\sqrt{g^{ii}}} = g^{ii}\, B_i\frac{1}{\sqrt{g^{ii}}} = \sqrt{g^{ii}}\, B_i \tag{5.73}$$
$$\widehat{B}^{diag}_i = B_i\sqrt{g^{ii}} = B_i\frac{1}{\sqrt{g_{ii}}} = g_{ii}\, B^i\frac{1}{\sqrt{g_{ii}}} = \sqrt{g_{ii}}\, B^i \tag{5.74}$$

[12] Just in diagonal metrics $g^{diag}_{ii} = 1/(g^{ii}_{diag})$. Therefore

$$\widehat{B}^i_{diag} = B^i\sqrt{g_{ii}} = B^i\frac{1}{\sqrt{g^{ii}}} = \mathbf{B}\cdot\nabla x^i\frac{1}{\sqrt{g^{ii}}} = \mathbf{B}\cdot\widehat{\nabla}x^i \tag{5.75}$$
$$\widehat{B}^{diag}_i = B_i\sqrt{g^{ii}} = B_i\frac{1}{\sqrt{g_{ii}}} = \mathbf{B}\cdot\mathbf{e}_i\frac{1}{\sqrt{g_{ii}}} = \mathbf{B}\cdot\widehat{\mathbf{e}}_i \tag{5.76}$$

using (5.56)–(5.57).

ential shift leads to a diagonal metric[13] for the machine-toroidal-coordinates (r_m, θ_m, φ).
To find the magnetic components $B^{r_m}, B^{\theta_m}, B^{\varphi}$ in this new coordinate system, beginning from the known ones in the (r, ϑ, φ) coordinates, one needs to use eq.(5.54) for the contravariant components and eq.(5.55) for the covariant ones. To find the (hatted) measurable components we can apply the normalization in (5.66)–(5.67).
To apply equation (5.54) one needs first to compute all the derivatives between the coordinates of the two systems. That is why it can be easy just on paper, and not in the real world, both from the analytical and numerical point of view. In order to make thing easier, we try to minimize the derivatives to be computed: in this case we can just find the magnetic field components in the cylindrical (R, Z, φ) coordinates[14], and project these on the machine coordinates. In particular, using (5.76) for the diagonal machine coordinates,

$$\widehat{B}_{r_m} = \mathbf{B} \cdot \widehat{\mathbf{e}}_{r_m} \tag{5.80}$$
$$\widehat{B}_{\theta_m} = \mathbf{B} \cdot \widehat{\mathbf{e}}_{\theta_m} \tag{5.81}$$

We can choose any coordinate system to write the magnetic field vector $\mathbf{B}$: we use the contravariant components in cylindrical coordinates that can be written in terms of the known contravariant components of the magnetic field in the toroidal system (r, ϑ, φ)[15] in a relatively easy way:

$$\mathbf{B} = B^R \, \mathbf{e}_R + B^Z \, \mathbf{e}_Z + B^{\varphi} \, \mathbf{e}_{\varphi} \tag{5.82}$$

with

$$B^R = \frac{\partial R}{\partial r} B^r + \frac{\partial R}{\partial \vartheta} B^{\vartheta} \tag{5.83}$$
$$B^Z = \frac{\partial Z}{\partial r} B^r + \frac{\partial Z}{\partial \vartheta} B^{\vartheta} \tag{5.84}$$
$$B^{\varphi} = B^{\varphi} \tag{5.85}$$

From (5.80)–(5.81) we need to do the scalar products between the covariant

[13] The metrics elements for the machine-toroidal-coordinates (r_m, θ_m, φ) can be derived from the tensor metrics elements of the geometrical coordinates $u^i = (r, \theta_g, \varphi)$ in appendix B.2 simply vanishing the shift $\Delta(r)$.
[14] Derivatives between the toroidal system (r, ϑ, φ) and the cylindrical one have already been calculated, equations (9.56)–(9.61).
[15] section 5.1

basis of the two coordinate systems[16]:

$$\widehat{B}_{r_m} = B^R\,\mathbf{e}_R\cdot\widehat{\mathbf{e}}_{r_m} + B^Z\,\mathbf{e}_Z\cdot\widehat{\mathbf{e}}_{r_m} + B^\varphi\,\mathbf{e}_\varphi\cdot\widehat{\mathbf{e}}_{r_m} \tag{5.92}$$

$$= B^R\cos\theta_m + B^Z\sin\theta_m \tag{5.93}$$

$$\widehat{B}_{\theta_m} = B^R\,\mathbf{e}_R\cdot\widehat{\mathbf{e}}_{\theta_m} + B^Z\,\mathbf{e}_Z\cdot\widehat{\mathbf{e}}_{\theta_m} + B^\varphi\,\mathbf{e}_\varphi\cdot\widehat{\mathbf{e}}_{\theta_m} \tag{5.94}$$

$$= -B^R\sin\theta_m + B^Z\cos\theta_m \tag{5.95}$$

These are the components to be compared with measures.
Note that, because $\sqrt{g_{RR}} = 1 = \sqrt{g_{ZZ}}$, from eq.(5.75) $B^R = \widehat{B}^R$ and $B^Z = \widehat{B}^Z$.

5.5 Some examples

Some example for the magnetic field B

Writing

$$\mathbf{B} = \underbrace{B^r\,\mathbf{e_r} + B^\vartheta\,\mathbf{e}_\vartheta}_{\mathbf{B}_{pol}} + \underbrace{B^\varphi\,\mathbf{e}_\varphi}_{\mathbf{B}_{tor}}\,, \tag{5.96}$$

in the toroidal coordinates (r,ϑ,φ) of chapter 3, the module of poloidal and toroidal magnetic field are:

$$B_{tor} = B_\varphi = \sqrt{g_{\varphi\varphi}}B^\varphi \tag{5.97}$$

$$B_{pol} = \sqrt{g_{rr}^2(B^r)^2 + 2g_{r\vartheta}B^rB^\vartheta + g_{\vartheta\vartheta}^2(B^\vartheta)^2}. \tag{5.98}$$

B_{tor} can also be identified with the measured covariant components B_φ on the normalized basis vectors $\mathbf{e}_\varphi$.

[16]

$$\mathbf{e}_R = \frac{1}{\sqrt{g_{RR}}}\frac{\partial\mathbf{x}}{\partial R} = \Big(\cos\varphi\,,\,\sin\varphi\,,\,0\Big) \tag{5.86}$$

$$\mathbf{e}_Z = \frac{1}{\sqrt{g_{ZZ}}}\frac{\partial\mathbf{x}}{\partial Z} = \Big(0\,,\,0\,,\,1\Big) \tag{5.87}$$

$$\mathbf{e}_\varphi = \frac{1}{\sqrt{g_{\varphi\varphi}}}\frac{\partial\mathbf{x}}{\partial\varphi} = \Big(-R\sin\varphi\,,\,R\cos\varphi\,,\,0\Big) \tag{5.88}$$

$$\widehat{\mathbf{e}}_{r_m} = \frac{1}{\sqrt{g_{r_mr_m}}}\frac{\partial\mathbf{x}}{\partial r_m} = \Big(\cos\theta_m\,\cos\varphi\,,\,\cos\theta_m\,\sin\varphi\,,\,\sin\theta_m\Big) \tag{5.89}$$

$$\widehat{\mathbf{e}}_{\theta_m} = \frac{1}{\sqrt{g_{\theta_m\theta_m}}}\frac{\partial\mathbf{x}}{\partial\theta_m} = \Big(-\sin\theta_m\,\cos\varphi\,,\,-\sin\theta_m\,\sin\varphi\,,\,\cos\theta_m\Big) \tag{5.90}$$

$$\widehat{\mathbf{e}}_\varphi = \frac{1}{\sqrt{g_{\varphi\varphi}}}\frac{\partial\mathbf{x}}{\partial\varphi} = \Big(-\sin\varphi\,,\,\cos\varphi\,,\,0\Big) \tag{5.91}$$

We can write also the modulus of the total magnetic field

$$\mathbf{B} = \mathbf{B}_{pol} + \mathbf{B}_{tor} \tag{5.99}$$

$$B = \sqrt{B_{pol}^2 + B_{tor}^2} \tag{5.100}$$

Some example for the current density J

For a force free equilibrium in Action–Angle coordinates (section 3.1.2) the axi–symmetric current density is proportional to the magnetic field through a coefficient ($\sigma(r)$) which is a function of r only[17], that is

$$\mu_0 \mathbf{J}_0 = \sigma(r)\mathbf{B}_0. \tag{5.103}$$

We use the straight field line coordinates (r, ϑ, φ) built for the axisymmetric equilibrium. From here,

$$J_0^r = 0 \tag{5.104}$$

$$J_0^\vartheta = \frac{\sigma(r)}{\mu_0} B^\vartheta \tag{5.105}$$

$$J_0^\varphi = \frac{\sigma(r)}{\mu_0} B^\varphi \tag{5.106}$$

The first order correction to the axisymmetric equilibrium, computing the total current density components from Ampère's law and plugging it into the first-order force balance equation[18], where $u^i = (r, \vartheta, \varphi)$, is

$$\mathbf{j} \times \mathbf{B}_0 + \mathbf{J}_0 \times \mathbf{b} = \frac{1}{\sqrt{g}} \epsilon^{ijk} (\hat{j}^i \hat{B}_0^j + \hat{J}_0^i \hat{b}^j) \nabla u^k = 0 \tag{5.107}$$

from which one obtains

$$j_{mn}^r = \frac{\sigma(r)}{\mu_0} b_{mn}^r \tag{5.108}$$

$$j_{mn}^\vartheta = \frac{\sigma(r)}{\mu_0} b_{mn}^\vartheta + \frac{i}{m - n\,q} \frac{\sigma'(r)}{\mu_0} b_{mn}^r \tag{5.109}$$

$$j_{mn}^\varphi = \frac{\sigma(r)}{\mu_0} b_{mn}^\varphi + \frac{i}{m - n\,q} \frac{\sigma'(r)}{\mu_0} q(r)\, b_{mn}^r \tag{5.110}$$

[17] The proportionality coefficient is given by

$$\sigma(r) = -\frac{1}{\Psi'_{P,0}} \frac{d}{dr} [K(r) \psi'_{T,0}] \tag{5.101}$$

with

$$K(r) = \frac{R_0}{r} \left(1 + \frac{\Delta}{R_0} + \frac{r}{2R_0} \Delta' - \frac{r^2}{2R_0^2} + o(\epsilon^3) \right). \tag{5.102}$$

.

[18] Axisymmetric equilibrium quantities are written with capital letters to distinguish them from the perturbative quantities.

The proportionality between perturbed radial current and perturbed radial magnetic field is similar to (5.103). Both B_0^i and the perturbative components b_{mn}^i are computed in section 5.1.
As in eq.(5.39) for the magnetic field, due to the geometric toroidal coupling

$$J^i \equiv J^i_{SH}(r,\vartheta,\varphi) \quad = \quad J^i_0(r,\vartheta,\varphi) + \sum_{\substack{m+1\\ m-1\\ n}} j^{i,SH}_{m,n}(r)\; e^{i(m\vartheta - n\varphi)} + c.c. \tag{5.111}$$

for $i = r, \vartheta, \varphi$.
Writing

$$\mathbf{J} = J^i\,\mathbf{e_i} \tag{5.112}$$

$$= \underbrace{J^r\,\mathbf{e_r} + J^\vartheta\,\mathbf{e}_\vartheta}_{\mathbf{J}_{pol}} + \underbrace{B^\varphi\,\mathbf{e}_\varphi}_{\mathbf{J}_{tor}} \tag{5.113}$$

in the toroidal coordinates (r,ϑ,φ) of section 3.1.1, the modulus of current density can be written as

$$J = \sqrt{g_{rr}^2 (B^r)^2 + 2 g_{r\vartheta} B^r B^\vartheta + g_{\vartheta\vartheta}^2 (B^\vartheta)^2 + g_{\varphi\varphi}^2 (B^\varphi)^2} \tag{5.114}$$

because the elements $g_{\vartheta\varphi} = 0$.

In chapter 6 we will compute the average of these quantities on flux surfaces.

Chapter 6

Applications

The goal of this chapter is to show some possible application of the more formal and theoretical part of the thesis till here presented.
SHEq is the code that computes all the results, solving the formulas and mathematical expressions of the previous chapters for any of the defined coordinate systems. The starting point in SHEq are the fluxes and their harmonics, reconstructed in the (r, ϑ, φ) coordinate system by some codes written to solve the Newcomb–like equation in [53][1].
In this chapter one can find magnetic flux reconstructions (section 6.1), the definition of the flux surface averages of any plasma quantity, like the poloidal or toroidal magnetic field or current density (section 6.2), and the helical safety factor profile (section 6.3).
For the flux surface reconstruction it is enough to know and compute a flux function, e.g. the helical flux in SHAx states, from equations collected in section 9.1.1. For the flux surface averages one needs to know a complete helical coordinate system, and to compute any plasma function on these coordinates. The formula for flux surface averages of plasma quantities in toroidal systems reduces to the integrals on the two angular coordinates, that must be well defined on the helical axis of the system. It does not matter to have them defined as straight–field–line (or Action–Angle) coordinates, and one can choose between any of the defined helical coordinates [2], even the geometrical one (χ, β, φ) in section 4.2.1. For the helical safety factor we use the simple formula as the ratio between the differential of the two angles, that is equivalent to the more general definition of the ratio between the differential of the two fluxes only for Action–Angle coordinates. This can be proved using the Hamiltonian mechanics, and in particular we choose the (χ, u_h, φ) or $(\chi, \theta^*, \varphi)$ coordinate systems, where the physical meaning of the fluxes is clear (see sections 4.2.2 and 4.4.1).

[1] Equations (3.36)–(3.37) in chapter 3

[2] Helical coordinates are defined in chapter 4 and their metrics are collected in the detailed calculations in section 9.2

Other examples of applications can be listed, and some of them are planned to be matter of future work. In particular, starting from the helical equilibria completely defined in chapters 4 and 9 (coordinates, Jacobian, metric tensor elements, q–profile, fluxes, fields, ...), one can think to perturb it with a helical perturbation, in a way similar to that of chapter 3 and [53], where the axisymmetric equilibrium B_0 was perturbed. In this way one can reconstruct the spectra and the profiles of the harmonics of the helical perturbation. This can be useful for example to consider the dominant mode in the $m = 0$ spectra (the $m = 0, n = 7$), neglected in SHAx states for now, but toroidally coupled with the $m = 1$ dominant mode, and essential to edge studies in RFP machines.
Some other example of work in progress for the equilibrium evolution is presented in chapter 7, where the problem of the Ohmic constraint is taken into account.

6.1 Flux surface reconstruction: DAx and SHAx

Magnetic flux surfaces in SH states are defined by the constancy of the helical flux: $\chi = const$ with χ from (9.2). In fig.4.3 we have already shown the χ contour plot, which gives the magnetic flux surfaces on the poloidal plane. With the SH, in this work, we model SHAx states. In the Introduction (chapter 1) we distinguish between SHAx and DAx states, both flavors of the more general QSH condition. In fig.6.2 one can see both the DAx and SHAx (of the $m = 1$ spectrum) magnetic topology on the poloidal plane. The magnetic island can be clearly seen during DAx states, with its typical X–point and O–point. Increasing the plasma current the amplitude of the resonant mode grows, and therefore the amplitude of the corresponding island. Beyond a threshold value of the amplitude of the dominant mode, the X–point collapses onto the original axisymmetric axis O', ending with the SHAx states topology.
With a not so bigger error (see fig.6.1), we model also DAx states as SH states, in order to analyze them with the same model built for SHAx states in this thesis. For example, fig.6.2 is built using the SHEq code, i.e. using the SH hypothesis. The SHEq code can distinguish between SHAx ad DAx states as follows.
Looking at eq.(9.4)

$$\chi = \chi_0(r) + 2|\chi^{m,n}|(r)\ \cos(u + \phi_\chi(r)) \tag{6.1}$$

We can fix the helical angle u for which

$$\cos(u + \phi_\chi) = \pm 1 \tag{6.2}$$

$$i.e.\ (u + \phi_\chi) = 0, \pi \tag{6.3}$$

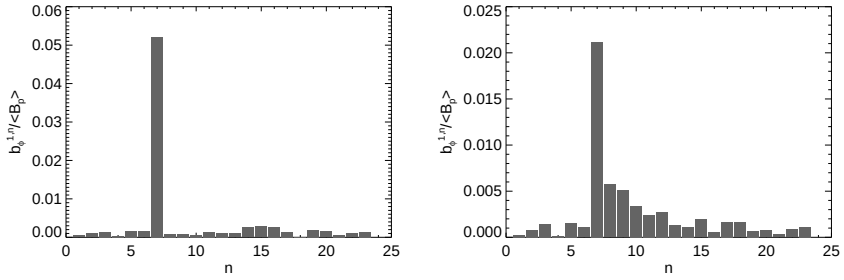

Figure 6.1: Left: Spectrum of the $m = 1$ mode during a SHAx state (shot 23977 at $t = 173.9$ ms). Right: Spectrum of the $m = 1$ mode during a DAx state (shot 23977 at $t = 197$ ms).

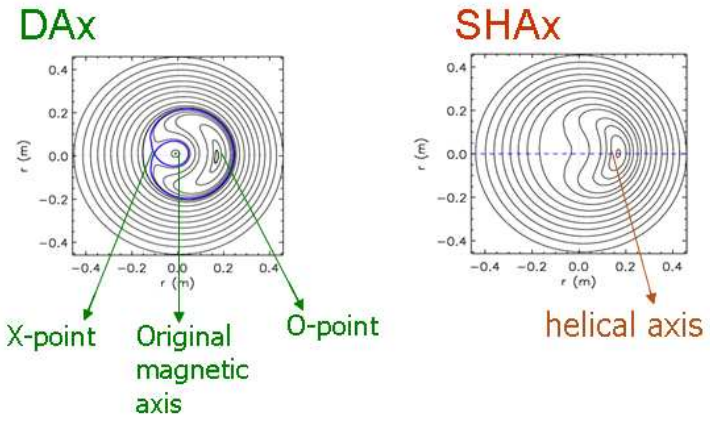

Figure 6.2: SHAx and DAx reconstructions in the poloidal plane.

In this way we obtain the $\bar{\chi}$–curve

$$\bar{\chi} = \chi_0(r) \pm 2|\chi^{m,n}|(r) \tag{6.4}$$

on the diameter passing through the points $X - O' - O$.

In fig.6.3 one can see the function (6.4) along the diameter. As one can see during DAx states the helical flux has three extremal points for which $d\chi/dr = 0$: two minima in the X-point and O–point of the island, and one maximum in the original magnetic axis of the system, the O'–point. During SHAx states only the original O–point of the island is a special point, where $d\chi/dr = 0$ defines a minimum. This correspond to the new helical axis of the system.

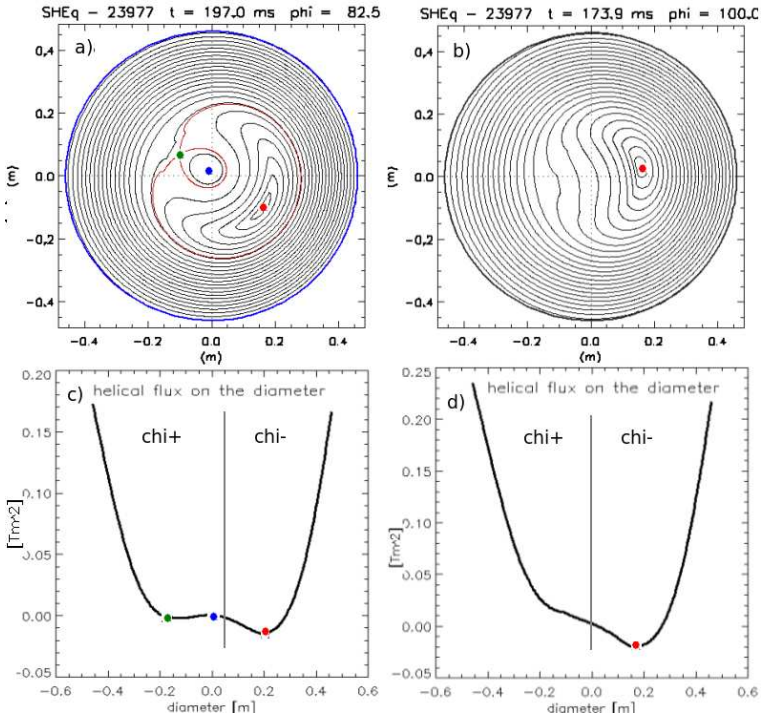

Figure 6.3: SHAx and DAx along the diameter

It is possible to think at two parts of the curve:

$$\chi_+ = \chi_0(r) + 2|\chi^{m,n}|(r) \Leftrightarrow \cos(u + \phi_\chi) = 1 \tag{6.5}$$

$$\chi_- = \chi_0(r) - 2|\chi^{m,n}|(r) \Leftrightarrow \cos(u + \phi_\chi) = -1 \tag{6.6}$$

where χ_- correspond to the convex part of the bean, whereas χ_+ correspond to the other side, where one can find the X–point and the O'–point. Notice that it is enough to study the derivative of the function χ_+ to distinguish between SHAx and DAx states: if $d\chi_+/dr > 0$ in each point, the system is in a SHAx state; if $d\chi_+/dr = 0$ in some point, the system is in a DAx state. As one can see in fig.6.4, in the same way one can also distinguish between different kinds of surfaces. For example, where

$$\frac{d\chi_+}{dr} = \frac{d\chi_0}{dr} + 2\frac{d|\chi^{m,n}|}{dr} > 0 \tag{6.7}$$

we are choosing the flux surfaces between the X–point and the O'–point of a DAx state (light yellow in fig.6.4).

To conclude let us say that the shape of the helical flux on the diameter depends on the helical flux eigenfunction, and in particular on the shape of

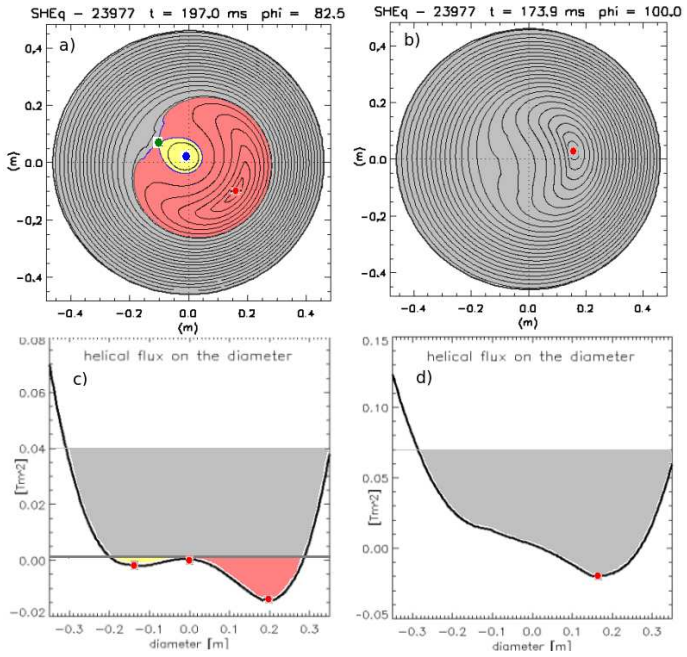

Figure 6.4: SHAx and DAx along the diameter, surfaces

the perturbation eigenfunction $\chi^{m,n}(r)$. In fig.6.5a) one can see a *good* eigenfunction profile, for which an increase of the amplitude brings from DAx to SHAx. During the porting of the SHEq code to the MST device in Madison, Wisconsin, we discovered that the shape in fig.6.5b) is not *good*: increasing the amplitude of the dominant mode it is not possible to reach SHAx states. Fig.6.5b) was the result of an initial mistake in the eigenfunction reconstructions in MST, but brings to the awareness that the eigenfunction must have a special profile, similar to fig.6.5a).

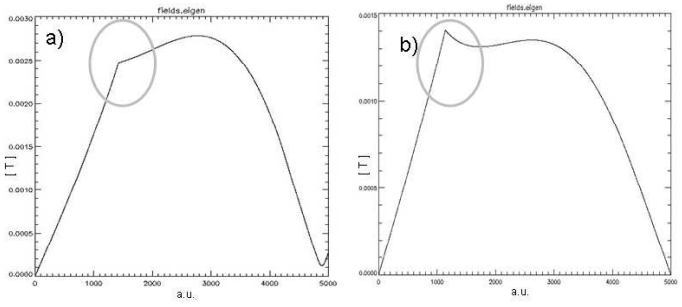

Figure 6.5: SHAx and DAx along the diameter, surfaces

6.2 Flux surface averaging

The flux surface average of a function $f(\mathbf{x})$ is defined as the volume average over an infinitesimally small shell with volume ΔV, where ΔV lies between two neighboring flux surfaces with volumes V and $V + \Delta V$. It is denoted by $\langle f \rangle$, and it is equal to [51]:

$$\langle f(\mathbf{x}) \rangle \equiv \lim_{\Delta V \to 0} \frac{\iiint f(\mathbf{x}) d^3\mathbf{x}}{\iiint d^3\mathbf{x}}$$

Following [51], it is possible to prove that the flux surface average of a generic quantity $f(\chi, \theta, \varphi)$ in a toroidal system is given by

$$\langle f \rangle = \frac{\iint d\theta d\varphi \sqrt{g} f}{\iint d\theta d\varphi \sqrt{g}} \tag{6.8}$$

where the integrals are over the poloidal–like and toroidal–like angles. The Jacobian must be consistent with the chosen coordinate system. We can choose any coordinate system defined on the helical flux surfaces: to obtain (6.8) the only requirement is to work with a radial coordinate that is label of the magnetic flux surfaces.

As an example of the application of this formula, we show in the next sections the flux surface averages of some quantities defined in section 5.5, such as the toroidal and poloidal magnetic field or the correspondent current density components. Of these quantities we compute the average on flux surfaces, in order to compute radial profiles.
The flux surface average of the power balance equation in section 6.2.2 brings to an estimation of the thermal conductivity.

6.2.1 Magnetic field and current density components

The graphs of fig.6.6 are computed using formulas of section 5.5 for the magnetic field and current density components. They show that the flux surface average of the toroidal field component is monotonically decreasing, as for the standard cylindrical models of the RFP fields, with a maximum (of 1.1 T in this 1.5 MA discharge) which is now located on the helical axis ($\nabla \rho_h = 0$), a slow decrease in the central part of the plasma, a knee around $\rho_h = 0.25$, and a reversal in the outer part of the plasma. The poloidal component is also rather flat on the inner surfaces, where it has an almost uniform value around 0.5 T. The same features are displayed by the current density components, not surprisingly since both the axisymmetric and the helical equilibria are force-free. The maximum toroidal current density, on the helical axis, is around 6 MA/m^2, while in the inner part of the plasma the poloidal component takes values a little larger than 2.5 MA/m^2. It can be also remarked that for $\rho_h > 0.8$ the toroidal current density is negligible.

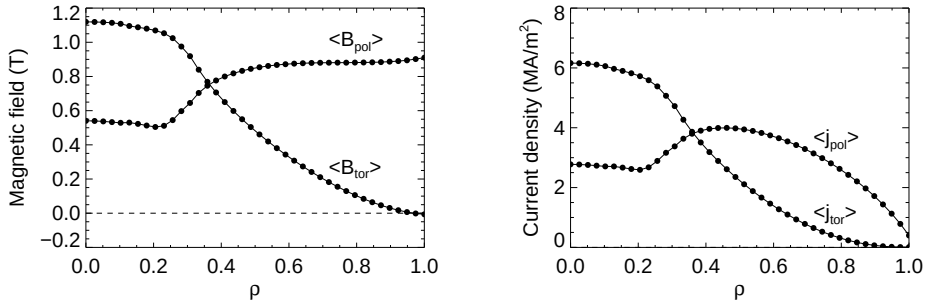

Figure 6.6: Left: Flux surface averages of the toroidal and poloidal magnetic field components. Right: Flux surface averages of the toroidal and poloidal current density components. The data refer to shot 24598, at $t = 174$ ms.

6.2.2 Thermal conductivity

The thermal conductivity κ[3] can be computed averaging the simplified power balance equation, in its form valid for stationary fluids at rest[4]:

$$\langle \nabla \cdot \mathbf{q} \rangle = \langle \eta \, J^2 \rangle \tag{6.12}$$

under the hypothesis

$$\mathbf{q} = -\kappa \, n \, \nabla T_e \tag{6.13}$$

[3] I call the thermal conductivity with the symbol κ, to distinguish it from the helical flux χ.

[4] The more general power balance equation is written [58]

$$\underbrace{\frac{D}{Dt}\left(\frac{3p}{2}\right)}_{a} + \underbrace{\frac{3p}{2}\nabla\cdot\mathbf{u}}_{b} + \underbrace{\nabla\cdot\mathbf{q}}_{c} + \underbrace{\left(\mathbf{P}\cdot\nabla\right)\cdot\mathbf{u}}_{d} = \underbrace{\mathbf{J}\cdot\mathbf{E} + \mathbf{J}\cdot\left(\mathbf{u}\times\mathbf{B}\right) - \rho\,\mathbf{u}\cdot\mathbf{E}}_{e} \tag{6.9}$$

p is the scalar pression, P the tensor of pressure forces, $\mathbf{u}$ the main plasma velocity, $\mathbf{q}$ the heat flux vector, $\mathbf{J}$ the current density vector, $\mathbf{E}$ the electric field, $\mathbf{B}$ the magnetic field, and ρ the charge density (null for neutral plasmas).
One can find in [58] the physical meaning of all the terms in the equation: the first term a in the left–hand side of the equation represents the time rate of change of the total thermal energy density of the plasma ($3p/2$) in a frame of reference moving with the global mean velocity $\mathbf{u}$. The second, b, term contributes to this rate of change through the thermal energy transferred to the volume element due to particle motion. The term c represents the heat flux and d the work done on the volume elements by all the pressure forces. Term e on the left–hand side is the work done on the volume element by the electric field in the frame of reference moving with the mean plasma velocity, $\mathbf{E}' = \mathbf{E} + \mathbf{u} \times \mathbf{B}$.
It is easy to see that for stationary ($d/dt = 0$) fluids at rest ($\mathbf{u} = 0$),

$$\nabla \cdot \mathbf{q} = \mathbf{J} \cdot \mathbf{E} \tag{6.10}$$

$$= \eta J^2 \tag{6.11}$$

if $\mathbf{E} = \eta \mathbf{J} + \mathbf{u} \times \mathbf{B}$, but $\mathbf{u} = 0$, from Ohm's law. Eq.(6.12) is the flux surface average of (6.11).

for the heat flux $\mathbf{q}$. η is the plasma resistivity and J the current density.

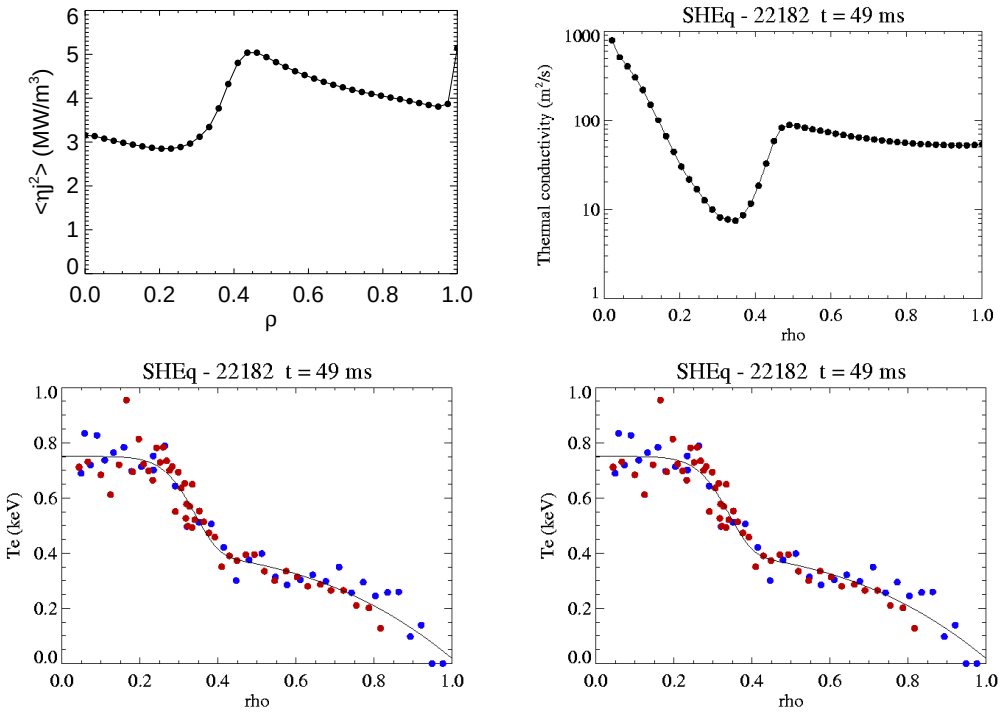

Figure 6.7: Left: The electron temperature profile Thomson scattering data. Center: Flux surface average of dissipated ohmic power. Right: Thermal conductivity profile computed from the surface-averaged power balance. The data refer to shot 22182, at $t = 49$ ms.

In fig.6.7 (center) we plot the average ohmic power $\langle \eta\, J^2 \rangle$. In doing this the Spitzer-Härm resistivity formula has been used[5], with the electron temperature profile measured by the Thomson scattering system, and plotted in fig.6.7 (left). Furthermore, we have assumed a flat effective charge profile with a value adjusted so as to match the total input power, $P = VI$, assuming stationary conditions. For this case, the correction factor turned out to be equal to 1.75, which appears a rather reasonable value[6]. It should be emphasized that the average ohmic power profile crucially depends on the profile

[5] Spitzer-Härm resistivity is proportional to the effective charge Z of the plasma and to $T_e^{-3/2}$ for the electron temperature, [11].

[6] The total input power

$$P = V(0)\, I_P \tag{6.14}$$

where $V(0)$ and I_P are the loop voltage on the axis and the plasma current, must be equal

chosen for $\sigma(r)$, as one can understand from the formulas for J in section 5.5.

The thermal conductivity profile is computed from the formula

$$\kappa = -\frac{\int \langle \eta J^2 \rangle \, V' \, d\rho}{n \, V \, \frac{dT_e}{d\rho} \, \langle \nabla\rho \cdot \nabla\rho \rangle} \tag{6.19}$$

where $V' = dV/d\rho$ is the specific volume, $\langle \nabla\rho \cdot \nabla\rho \rangle \equiv \langle g^{11} \rangle$ the first metric tensor element for the chosen helical coordinate system, $dT_e/d\rho$ the gradient of the electron temperature profile in fig.6.7 (left) and n the electron density that we consider with a uniform profile. The thermal conductivity profile is shown in fig.6.7 (right). It can be seen that the thermal conductivity displays a minimum, at a value around 8 m^2/s, corresponding to the strong gradient in the temperature profile. This is an order of magnitude lower than values obtained in MH conditions [59]. This is a typical situation during SHAx states, where the strong temperature gradint is associated to the Internal Transport Barrier (ITB), [60].
At the end of section 6.3 we compare the κ–profile with the safety factor profile at the same time instant. The magnetic equilibrium reconstruction shows that ITBs are related to a peak in the non–monotonic q–profile.

To conclude let us write the steps leading from (6.12) to (6.19): we need to use the formula for flux surface averages of a divergence

$$\langle \nabla \cdot \mathbf{q} \rangle = \frac{d\rho}{dV} \, \frac{d}{d\rho} \Big[\frac{dV}{d\rho} \langle \mathbf{q} \cdot \nabla\rho \rangle \Big] \tag{6.20}$$

where $V' = dV/d\rho$ is the specific volume and ρ the chosen radial coordinate that labels the magnetic flux surfaces. Using (6.13) and $\nabla T_e = (dT_e/d\rho)\, \nabla\rho$

---

to

$$P = \int \eta \, J^2 \, dV \tag{6.15}$$

We can write the resistivity η as

$$\eta = f(Z) \, \eta_{Z=1} \tag{6.16}$$

where Z is the effective charge of the plasma. Computing $\eta_{Z=1}$ from Spitzer, and assuming a flat charge profile, we can adjust its value, through $f(Z)$, so as to match the total input power:

$$P = f(Z) \int \eta_{Z=1} \, J^2 \, dV = V(0) \, I_P \tag{6.17}$$

therefore

$$f(Z) = \frac{V(0) \, I_P}{\int \eta_{Z=1} \, J^2 \, dV} \tag{6.18}$$

considering $T_e \equiv T_e(\rho)$:

$$\langle \nabla \cdot \mathbf{q} \rangle = \frac{1}{V'} \frac{d}{d\rho} \Big[- V' n \kappa \frac{dT_e}{d\rho} \langle \nabla\rho \cdot \nabla\rho \rangle \Big] = \langle \eta J^2 \rangle \tag{6.21}$$

Integrating the two sides of the equation in $d\rho$ [7]

$$\int d\Big[- V' n \kappa \frac{dT_e}{d\rho} \langle \nabla\rho \cdot \nabla\rho \rangle \Big] = \int \langle \eta J^2 \rangle V' \, d\rho \tag{6.22}$$

$$- V' n \kappa \frac{dT_e}{d\rho} \langle \nabla\rho \cdot \nabla\rho \rangle = \int \langle \eta J^2 \rangle V' \, d\rho \tag{6.23}$$

$$\kappa = - \frac{\int \langle \eta J^2 \rangle V' \, d\rho}{n V \frac{dT_e}{d\rho} \langle \nabla\rho \cdot \nabla\rho \rangle} \tag{6.24}$$

that is exactly (6.19).

6.2.3 ASTRA

The computation of flux surface averages of different quantities is also an essential step for building transport equations depending on one coordinate only (the flux surface label).
An example for this is the transport ASTRA code [61], built for Tokamak community and then modified both for Stellarators and RFPs.
We do not go into ASTRA details, because transport studies with this code in RFX are just now started and will be matter of future work. We mention it here because the SHEq code is at the moment the only code in RFX that can compute the helical equilibria of SHAx states and compute averages on its magnetic flux surfaces.

The main difference between ASTRA for Tokamaks and for non–axisymmetric machines is the equilibrium reconstruction. For Tokamak discharges ASTRA computes the equilibrium solving the Grad–Shafranov equation. For non–axisymmetric equilibria the Grad–Shafranov equation is not valid anymore, and ASTRA asks for the equilibrium parameters as an input.
One can find the whole set of equilibrium parameters that ASTRA needs to evolve all its transport equation in the manual. Here we cite just some example:

$$V' = \frac{dV}{d\rho_A}, \quad g^{11} = \langle \nabla\rho_A \cdot \nabla\rho_A \rangle, \quad \ldots \tag{6.25}$$

where we choose $\rho = \rho_A$ from (4.64) in order to work with a radial variable in meters[8].

[7] All the function are null on the helical axis.
[8] One can see section 9.2.2 for some example on how the metrics elements changes changing the radial variable

In section 7.3 one can find the first example of transport studies during helical states performed in RFX in collaboration with the Theory Group of TJ-II, Ciemat, Madrid: the evolution of the helical rotational transform, that is the inverse of the helical safety factor defined in section 6.3.

6.3 Helical safety factor profile

It is possible to use different equivalent definitions of the q–profile, or of its inverse, the rotational transform ι [9]. In particular one can use the basic definition of the rotational transform as the number of turns of a magnetic line around the magnetic axis that, in axi–symmetric configurations, we can usually think as the center of the vacuum vessel. In SHAx states the magnetic axis is instead the helical axis, but the number of turns around the latter has a simple relation with the number of turns around the center of the vacuum vessel: we must simply add the $n = 7$ turns of the helical axis around the center of the vacuum vessel to the turns of the magnetic line around the helical axis[10]. We will prove this using two Action–Angle coordinate systems introduced in chapter 4: (χ, u_h, φ) and $(\chi, \theta^*, \varphi)$. To confirm my results we will compare them with the results obtained in [60], where the number of turns around the center of the vacuum vessel are counted out using the ORBIT field line tracing code [63].

In chapter 4 we find good Action–Angle coordinate systems valid in SHAx states, and we can therefore use the definition of the rotational transform valid in straight field line coordinates to compute the helical safety factor. Using the (χ, u_h, φ) coordinates defined in section 4.2.2,

$$\iota_h = \frac{du_h}{d\varphi} = \frac{d\chi}{d\psi_h} \tag{6.26}$$

where the second equivalence derives from the definition of the equations of motion for Action–Angle coordinates in Hamiltonian context[11]: remembering the identification of the helical coordinates (χ, u_h, φ) with the canonical variables that we saw in section 4.2.2, this definition of the rotational transform has the expected form of the canonical equation of motion ($\dot{q}_i = \partial H/\partial p_i$) once φ has been chosen to be the canonical time. As expected, the Action $\psi_h(\chi)$ is a constant of the motion.
If we write the number ι of turns around the center of the vacuum vessel

[9] As said in the introduction, we use the symbol ι (which rigorously is the average poloidal angle described by a field line per toroidal turn) instead of $\imath = \iota/2\pi$.

[10] References for that can be found for example in old Stellarator papers, as [62]

[11] When using Action–Angle coordinates the safety factor can be define either with the ratio between fluxes or between coordinates. This arises immediately from canonical equation.

in the equivalent way as the ratio between the differential of the poloidal and the toroidal flux enclosed by the helical flux surfaces $\Sigma(\chi)$, ι can be also written as

$$\iota = \frac{d\theta^*}{d\varphi} = \frac{d\psi_P}{d\psi_h}\,, \tag{6.27}$$

remembering the result of section 4.2.2, where ψ_h turned out to be the toroidal flux. Again, the equivalence with the ratio between the coordinates is due to Hamiltonian mechanics and it is true just for Action–Angle coordinates.
As we have already said, we can also write[12]

$$\iota = \iota_h + n\,. \tag{6.30}$$

The ι_h rotational transform is computed by the SHEq code using the canonical definition (6.26) and the Action–Angle coordinates (χ, u_h, φ). The more common definition of the rotational transform ι as the ratio (6.27) is easily computed using (6.30), and the resulting safety factor profile $q = 1/\iota$ can be seen in the top frame of fig.6.8 *up*.

In fig.6.9 one can see the good agreement in the q–profiles computed by the SHEq code from formula (6.30) (red) and by the ORBIT code (blue), i.e. as the number of turns around the center of the vacuum vessel.

Fig.6.8 *top* and fig.6.9 show a typical q–profile for SHAx states, reversed, symmetric with respect to the helical axis and almost flat in the inner bean–shaped flux surfaces region. If we compare the electron temperature profile from Thomson scattering data (fig.6.8 *bottom*) with the safety factor profile, we can identify a maximum of the q in correspondence of the steep temperature gradient. The steep gradient is related to very low value of the thermal conductivity (remembering the results in section 6.2.2) and we can therefore say that the q–profile has a maximum in correspondence of the Internal Transport Barrier (ITB) that delimits the hot bean–shaped core of SHAx states [60]. The maximum in the q–profile is found to be related to the original rational surface of the dominant mode $(m, n) = (1, 7)$ (which disappeared in the transition from DAx to SHAx state) and ITBs are always

[12] We can prove this relation in this way:

$$\iota_h = \frac{d\chi}{d\psi_h} = \frac{d\psi_P - n d\psi_h}{d\psi_h} = \frac{d\psi_P}{d\psi_h} - n \equiv \iota - n \tag{6.28}$$

using eq.(4.66), $\chi = m\psi_P - n\psi_T$ for $m = 1$.
Or we can write the same using the ratio between the angular coordinates:

$$\iota_h = \frac{du_h}{d\varphi} = \frac{d\theta^* - n d\varphi}{d\varphi} = \frac{d\theta^*}{d\varphi} - n \equiv \iota - n \tag{6.29}$$

obtaining the same result because both the (χ, u_h, φ) and $(\chi, \theta^*, \varphi)$ are straight field line coordinate systems. We used here eq.(4.80) for the poloidal angle θ^*.

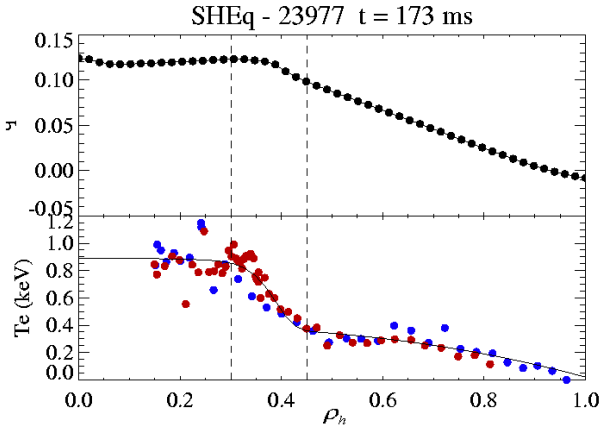

Figure 6.8: *Up*: helical q–profile computed by SHEq from the inverse of equation (6.30). *Down*: Electron temperature profile from Thomson scattering data. Reconstruction for shot 23977, time 173 ms at the toroidal position ($\varphi = 82.5°$) of the Thomson Scattering measurements. The abscissa ρ_h is the square root of the normalized helical flux (4.2).

found in this position during SHAx states.

Let us go back to the physical interpretation of the angles u_h and θ^* (section 4.4) and therefore of the rotational transform ι and ι_h defined in eq.(6.26)–(6.27): u_h is turning around with a fixed phase with respect to the bean (let us say always on the convex part of the bean, for $\phi_\chi = 0$), whereas θ^* is fixed on the horizontal plane (and can be associated to the laboratory frame of reference). Because of this one can think at ι as the number of turns of a magnetic field line counted by the laboratory frame, that will also see $n = 7$ turns of the bean for each toroidal turn. On the other side, ι_h can be thought as the number of turns of a magnetic field line counted by the local frame of reference of the bean, that will of course not see the $n = 7$ turns around the helical axis.
The rotational transform is a physical quantity whose profile does not depend on the chosen coordinates. Relation (6.30) shows that the profiles are just displaced by a constant when we change the coordinate system, and it is nothing but the relation between the definition of ι in two different frames of reference.

To conclude we want to stress that ι_h is one of the Stellarator choice for the rotational transform: $\iota_h = 0$ corresponds to a magnetic field line that after one toroidal turn goes back exactly in the same poloidal and toroidal position. Therefore what Stellarator comunity call poloidal angle is what we am calling helical angle in this thesis.
An interesting collaboration is going to start with TJ-II Theory Group, be-

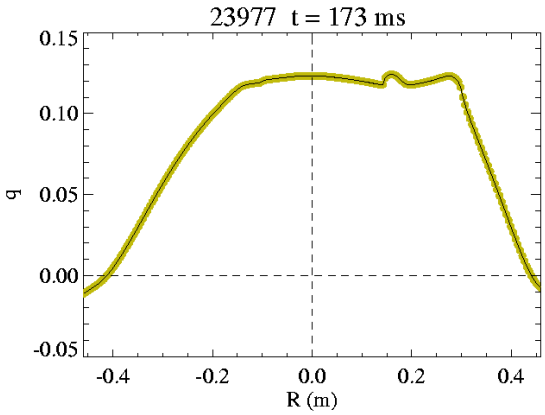

Figure 6.9: q–profiles on the horizontal diameter of the vacuum vessel. *Black*: q–profile computed by the ORBIT code; *green*: q–profile computed by the SHEq code from the inverse of equation (6.30). Shot 23977, time 173 ms, toroidal angle=255.8°. A vertical line marks the radius of the center of the vacuum vessel and a horizontal one the $q = 0$ line where the toroidal magnetic field reverses.

cause of the similarities between their rotational transform profile and our, inside the bean–shaped magnetic flux surfaces. In particular, the almost flat rotational transform profile and absolute values between zero and two. The difference that can be studied are the sign of the derivative of both the rotational transform and of the averaged magnetic well.

Chapter 7

Equilibrium evolution: the Ohmic constraint

7.1 The Ohmic problem in RFPs

As seen in the introduction (sec.1.2.4), a dynamo is acting in RFP plasmas, in order to provide the reversal and maintain the configuration for times longer than the resistive ones.
No dynamo can sustain (and therefore no reversal can be sustained by) an axi–symmetric magnetic field. This is known in astrophysics as the Cowling's theorem and by extension one can speak of a Cowling's theorem for the RFP: at least one mode of a perturbation to the axi–symmetric configuration must be present to sustain the reversal, through a dynamo ($\mathbf{v} \times \mathbf{B}$) term in the parallel Ohm's law:

$$\langle \mathbf{E}_{\parallel} \rangle + \underbrace{\langle \mathbf{v} \times \mathbf{B} \rangle_{\parallel}}_{\text{dynamo}} = \langle \eta \mathbf{j}_{\parallel} \rangle \tag{7.1}$$

with an electrostatic[1] field $\mathbf{E}$

$$\mathbf{E} = -\nabla\phi + \mathbf{E}_0 \tag{7.2}$$

where ϕ is the electrostatic potential related to a charge distribution and $\mathbf{E}_0$ the induction electric field related to the axial loop potential. $\langle ... \rangle$ means the average on magnetic flux surfaces.
The dynamo process is usually associated to the effect of perturbations in the quadratic ($\mathbf{v} \times \mathbf{B}$) term, but without an explanation of the origin of the velocity field. In the laminar SH case (where just one mode of the perturbation is present) the plasma flow $\mathbf{v}$ can be thought as a mere electrostatic drift, due to the helical distortion of the plasma[2]. This picture of the dynamo has

[1] Imagining a steady state ohmic equilibrium.
[2] One may think for the SH case at the perturbed magnetic flux surfaces of SHAx states.

been extended also to the MH case (where many MHD modes are present in the perturbation) [64]. In fig.7.1 is shown that both the electrostatic and the standard picture of the dynamo are equivalent, but the former has the merit of giving a first explanation of the origin of the velocity field.
The problem of an ohmic reversal has been studied since the beginning of the RFP history, and the emergence of the SH picture is the first step beyond Taylor's theory (sec. 1.2.5), the backbone of RFPs till the late 90's. We will describe the present status of the theory of helical RFP equilibrium just in a qualitative way (for more details see for example [65]).

J. Finn, R. Nebel and C. Bathke [10] prove the impossibility of an ohmic reversal of the toroidal field in a pure poloidal or toroidal symmetry[3]. This is done in an analytical way, using the parallel averaged Ohm's law and the force free force balance equation[4]. In the same paper, an equation (but first written by V. D. Pustovitov [66, 67])[5] for the axial magnetic field profile B_z is also given in the case of helical symmetry, in a periodic cylinder[6].
Without going into the analytical steps, we just write the V.D. Pustovitov's and J. Finn's equation[7], the so–called Pinch–Stellarator equation, where the Stellarator term $S(\rho)$ is the term that may provide the reversal of $\langle B_z \rangle$:

$$\frac{d}{d\rho}\langle B_z \rangle = \frac{E_0}{\langle \eta B^2 \rangle}\langle B_z \rangle + S(\rho) \tag{7.3}$$

ρ is a label of the helical magnetic flux surfaces and E_0 the electric field component related to the toroidal loop voltage V_t. Equation (7.3) is a first order differential equation for $\langle B_z \rangle$, which is obtained by combining the helical Grad–Shafranov equation[8] and the averaged parallel Ohm's law (in force free conditions).
The Stellarator term $S(\rho)$ is a term dominated by geometry, and vanishes for a pinch with axial symmetry. In a Stellarator (since $E_0 = 0$) it is the only term providing the variation of $\langle B_z \rangle$. When $S = 0$ due to axi–symmetry, $\langle B_z \rangle$ cannot reverse, which is a way to recover Cowling's theorem. Equation (7.3) can be formally integrated, and only[9] a positive $S(\rho)$ may *a priori* provide the reversal of $\langle B_z \rangle$.
The Pinch–Stellarator equation (7.3) is the first indication of the modern view of the helical (SH) RFP, where the configuration is linked with a helical deformation of the plasma column, and the reversal is a consequence

[3] Before them other investigated the problem of Ohmic reversal for magnetic fields symmetric by an axis, see chapter 5 in [56] and references therein.
[4] See comments to equation (A.39) in appendix A.2
[5] See also P. N. Vabishchevich et al (1983), [68, 69].
[6] B_z corresponds to the toroidal magnetic field profile in a torus.
[7] Equation (10) in Pustovitov's paper, [66, 67]; equation (35) in Finn's paper, [10]
[8] The Grad–Shafranov equation is derived using the force balance equation and Ampère's law, for the case of null pressure and velocities. For the helical Grad–Shafranov equation on a cylinder see for example [70].
[9] At least in a finite edge radial domain in ρ.

of a loss of axi–symmetry of the cylindrical pinch. This picture enables the description of the RFP through the simple wire model, which exhibits a self–organized magnetic system with field reversal where the loss of cylindrical symmetry is essential and due to a kink instability[10] (section 1.2.5).

The analytical description of the RFP is not complete, e.g. there is not a necessary *and* sufficient criterion for $S(\rho)$ to have the right sign to provide the reversal of the axial magnetic field.
Nevertheless a necessary criterion has been found. Analytically, the SH ohmic states are frequently ([70, 71]) described as a small helical perturbation of an axi–symmetric ohmic pinch (with small edge conductivity and small edge axial magnetic field), called *ultimate pinch*. Taking the ultimate pinch as the zeroth order equilibrium, and applying a second order perturbative theory to the Pinch–Stellarator equation (with the amplitude of the helical perturbation as a small parameter), D. Bonfiglio et al. in [71] derive a necessary criterion for the reversal of $\langle B_z \rangle$.

If the analytical description is not complete, from the numerical point of view the existence of an ohmic reversal for a cylindrical pinch with helically deformed magnetic flux surfaces has been proved by [8, 9], using a visco–resistive compressible non–linear MHD model in the constant–pressure and constant–density approximation.
Numerical simulations show that the necessary criterion works also for large values of the perturbations to the pinch, so the criterion is more general than suggested by the perturbative approach used for its derivation [71]. Numerical simulations reveals also that, in the presence of a helical perturbation, the reversal is easier when a finite edge radial magnetic field (that usually is vanishing with a perfect conducting shell) is applied. Experimental results agree with numerical simulation, and the necessary criterion is found to be satisfied in RFX–mod experiment during SHAx states, with a non zero edge radial magnetic field imposed by the active control [71].

The present understanding of the RFPs gives also some explanation of the dynamo process. Let us briefly see some of these considerations, [72].
In the standard invocation the dynamo electric field results from the effect of the perturbations in the quadratic $(\mathbf{v} \times \mathbf{B})$ term. On the other hand, in the laminar SH case the plasma flow can be thought as a mere electrostatic drift, due to the helical deformation of the magnetic flux surfaces: in the SH picture, when a RFP configuration appears, the gradual loss of the axial–symmetry of the magnetic field produces a current density modulation $\mathbf{j}_{\|}$ along the magnetic field lines. A current density modulation requires a modulated ohmic electric field (along these lines), which drives a charge

[10] $(m, n) = (1, n)$, kink instability due to $q < 1$.

separation to balance it: the distribution of the charge separation (ρ_c) is continuous and helically symmetric. It is related to an electrostatic potential ϕ, and can be computed through Laplace's equation[11]. The corresponding electrostatic field $\mathbf{E} = -\nabla\phi$ is the required electric field necessary to provide the helical modulation of the parallel current density $\mathbf{j}_\parallel$.
It is possible to prove [73] that the standard and the electrostatic picture of the dynamo are equivalent.
The contribution of the electrostatic field to the dynamo can be quantified using the spatial mean (over the poloidal angle and the axial coordinate z and indicated with the symbol $\langle ... \rangle_s$)[12] of the parallel Ohm's law: with the electric field from eq.(7.2), the Ohm's law ($\mathbf{E} = \eta\mathbf{J} - \mathbf{v} \times \mathbf{B}$) can be written as:

$$\mathbf{E}_0 - \nabla\phi = \eta\mathbf{J} - \mathbf{v} \times \mathbf{B} \tag{7.4}$$

Projecting now the two sides of the Ohm's law on the total (helical) magnetic field, the term $\mathbf{v} \times \mathbf{B}$ vanishes and :

$$E_0 \langle B_z \rangle_s - \langle \nabla\phi \cdot \mathbf{B} \rangle_s = \langle \eta\mathbf{J} \cdot \mathbf{B} \rangle_s \tag{7.5}$$

because $\mathbf{E}_0 \parallel \mathbf{e}_z$.
Looking at the radial profiles of this equation in fig. 7.1 a) and comparing the spatial mean of this equation with the averaged Ohm's law in eq.(7.1), one can see that the difference between the induction electromotive force term, proportional to E_0, and the mean parallel current density is balanced by the electrostatic term $\langle \nabla\phi \cdot \mathbf{B} \rangle_s$. Therefore this is the term that provides what are often named the *anti–dynamo* term in the core and the *direct–dynamo* at the edge.
The standard view, where the dynamo term has the form $\mathbf{v} \times \mathbf{B}$, is recovered projecting the two sides of the Ohm's law (eq.(7.4)) on the axi–symmetric component $\mathbf{B}_0$ of the magnetic field:

$$E_0 \langle \mathbf{e}_z \cdot \mathbf{B}_0 \rangle_s - \langle (\mathbf{v} \times \mathbf{B}) \cdot \mathbf{B}_0 \rangle_s = \langle \eta\mathbf{J} \cdot \mathbf{B}_0 \rangle_s \tag{7.6}$$

The term due to the electrostatic potential vanishes since $\nabla\phi$ has no axi–symmetric components, and the dynamo/anti–dynamo term is provided by the usual $\langle (\mathbf{v} \times \mathbf{B}) \cdot \mathbf{B}_0 \rangle_s$ term. This can be seen in fig. 7.1 b).
Therefore both the electrostatic and the standard picture of the dynamo are equivalent. However the latter is unable to explain the origin of the velocity field, while the former does: the helical modulated electrostatic potential brings a component of the electric field ($\mathbf{E} = -\nabla\phi$) perpendicular to the magnetic field $\mathbf{B}$. This component drives a $\mathbf{v} = \mathbf{E} \times \mathbf{B}$ motion, whose non axi–symmetric part is exactly the dynamo velocity field.

[11] From the divergence of the electrostatic electric field $\mathbf{E} = -\nabla\phi$, the laplacian of ϕ yields the charge density due to the ambipolarity constraint ($\nabla^2\phi = \rho_c$).
[12] It coincides with the flux surface averages on the circular flux surfaces of the axi–symmetric magnetic field $\mathbf{B}_0$.

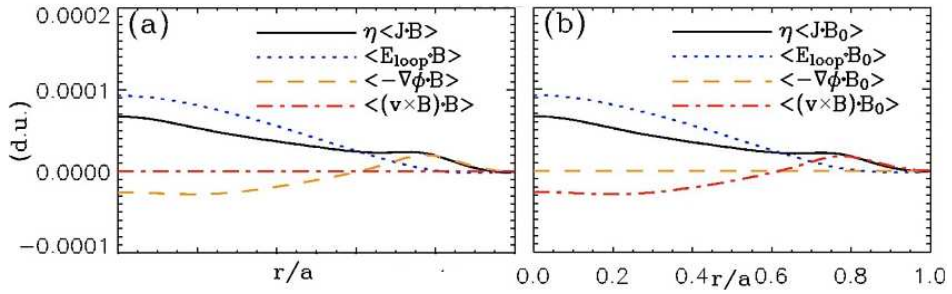

Figure 7.1: Reproduced from S. Cappello et al., [21]. *Radial profiles of mean parallel Ohm's law components, in the Single Helicity steady state. a) Ohm's parallel to the total magnetic field. b) Ohm's law parallel to the mean magnetic field.*

7.2 The Ohmic constraint in SHEq

As seen in the previous section 7.1, one would require Ohm's law to be valid for the helical equilibria.
The main work of this thesis looks for the description of the helical SHAx state RFP equilibria, now computed by SHEq code. The equilibrium system of equations that is solved for SHEq does not account for Ohm's law (chapter 3): a natural question which arises when a SHEq equilibrium has been computed is therefore whether the large current flowing in the plasma is consistent with Ohm's law.
Let us go back to the Ohmic constraint in equation (A.36), written for a stationary equilibrium:

$$\frac{V_t}{2\pi}\langle B^\varphi\rangle = \eta\langle \mathbf{j}\cdot\mathbf{B}\rangle\,. \tag{7.7}$$

In equation (7.7) V_t the toroidal loop voltage, and we can check *a posteriori* if it is verified by SHEq's equilibria.

The two sides of the Ohmic constraint (7.7) can be computed by SHEq. The magnetic field $\mathbf{B}$, its toroidal contravariant component B^φ and the current density $\mathbf{J}$ are computed as explained in section 5.5. As for the power balance described in section 6.2.2, a flat Z_{eff} profile has been assumed, and the toroidal loop voltage V_t is an experimental constant value (see appendix A).
The two sides of the Ohmic constraint are plotted in Fig. 7.2 for a typical 1.5 MA SHAx state. A remarkable discrepancy can be seen, with the first term being larger than the second one in the inner portion of the plasma, and smaller in the outer one. Such discrepancy could be partially resolved assuming a profile of effective charge with a peak in the center of the plasma, instead of the flat profile which has been assumed here. Even if this is the

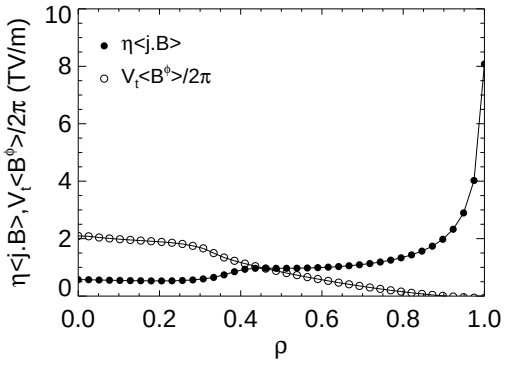

Figure 7.2: Left hand side (open circles) and right hand side (solid circles) of equation (7.7), plotted as a function of the effective radius ρ. The data refer to shot 22182, at $t = 49$ ms.

case, the $\alpha - \Theta_0$ model assumed for the zeroth-order parallel current density appears anyway to be not appropriate, since in the outer part of the plasma the profile of $\langle B^\varphi \rangle$ changes sign, whereas the other one does not. This requires either to assume a profile of σ[13] changing sign in this region, or a residual dynamo contribution of the secondary modes. Moreover, the Ohmic constraint, that SHEq's equilibria do not satisfy, has been calculated for stationary equilibria: we can consider them non steady state equilibria.

These considerations point to the need of performing equilibrium calculations which take into account the Ohmic constraint.
In section A.5 we introduce an equation for the time evolution of a non steady state equilibrium, that accounts for the Ohm's law in its formulation (the Ohm's law with non static electric field). The evolution of non steady state SHEq's equilibria is an ongoing work in collaboration with the Theory Group of TJ-II, Ciemat (Madrid) (section 7.3.2).
Moreover, in the Theory program for 2012 for RFX–mod we would also like to write a code for computing the dominant mode eigenfunction with a generic current density profile, based on the algorithm now used to compute the eigenfunction of poloidal and toroidal fluxes using NewcombâĂŹs equation (see chapter 3). The code will be integrated with the SHEq code for computing helical equilibria in QSH states, thus increasing its flexibility and allowing it to explore the effect of the current profile on the helical equilibria and in particular of an ohmic axi–symmetric current density $\mathbf{J}_0$ satisfying Ohm's law.

[13] The proportionality between the magnetic field and the plasma current density, in force free conditions: $\mathbf{j} = \sigma \mathbf{B}$.

7.3 The equilibrium evolution

In the appendix regarding the MHD equations, a section (sec. A.5) is devoted to the derivation [74] of an equation for the time evolution of the rotational transform (for its inverse, the safety factor profile, see section 9.3.1), compatible with Ohm's law and suitable for inclusion in numerical simulations.

A collaboration with the Theory Group of the TJ-II Stellarator device (Ciemat, Madrid) started with the objective of evolving eq.(A.62) for the rotational transform (or equation (9.141) for the safety factor profile), in order to reach a steady state ohmic equilibrium, both for TJ-II and for the helical SHAx states in RFX–mod. This is of course of interest for RFX–mod because (section 7.2) it has been shown that the helical equilibria computed by SHEq code do not satisfy the Ohmic constraint (eq. (7.7)), and are therefore not steady state equilibria. The interest for TJ-II is in order to analyze the discharges with non null plasma current: with some ohmic current flowing in the plasma, even their equilibria evolve in time accordingly to eq.(A.62), [75] [14].

Both the evolution of the rotational transform for TJ-II and of the helical safety factor profile in RFX–mod are done using the ASTRA transport code: some ASTRA subroutines have been written in order to evolve the equation (that is not an equation already inside ASTRA) in an iterative way.
The work done for TJ-II discharges is presented in section 7.3.1, the one for RFX–mod in section 7.3.2.

For a complete specification of the evolution problem, we need to specify the boundary condition for the rotational transform ι (or the safety factor profile q), and to choose a radial variable ρ to label the magnetic flux surfaces[15].
For consistency, however, to obtain a good description of the plasma evolution, the geometry (and therefore the radial variable ρ and the S_{ij} elements) must be frequently recalculated, to account for the changes due to evolving of the equilibrium and therefore of the magnetic field configuration. This will be done by the VMEC equilibrium code.
In RFX–mod, due to the presence of the reversal surface at the edge, the safety factor profile is evolved instead of the rotational transform, and the

[14] The configuration is not the vacuum steady state equilibrium defined by

$$\iota = -\frac{S_{12}}{S_{11}} \tag{7.8}$$

[15] Of course all the equilibrium quantities, as for example the susceptance matrix elements, must be calculated with the same choice of the radial variable ρ (see section 9.2.2).

monotonic poloidal flux is chosen as radial variable instead of the non monotonic toroidal one (remember fig.4.5). The toroidal flux is a good choice for the radial variable in TJ-II.

7.3.1 The time evolution of ι for TJ-II (Ciemat, Madrid)

The evolution equation

The equation for the Ohmic time evolution of the rotational transform is:

$$\frac{\partial \iota}{\partial t} = \frac{\partial \iota}{\partial \psi_t}\frac{\partial \psi_t}{\partial t} + \frac{\partial}{\partial \psi_t}\Big[\langle \mathbf{E}\cdot\mathbf{B}\,\frac{\partial V}{\partial \psi_t}\Big] \tag{7.9}$$

$$= \frac{\partial \iota}{\partial \psi_t}\frac{\partial \psi_t}{\partial t} + \frac{\partial}{\partial \psi_t}\Big[\frac{\eta_{\|}}{\mu_0}\psi_t'\,(S_{21}\iota + S_{22})^2\,\frac{\partial}{\partial \rho}\Big(\frac{S_{11}\iota + S_{12}}{S_{21}\iota + S_{22}}\Big)\Big] +$$
$$- \frac{\partial}{\partial \psi_t}\Big[\eta_{\|}\langle \mathbf{J_s}\cdot\mathbf{B}\rangle\frac{\partial V}{\partial \psi_t}\Big] \tag{7.10}$$

V is the volume enclosed inside the $\rho = const$ flux surfaces, ψ_t and ψ_p the toroidal and poloidal flux respectively, $\eta_{\|}$ the parallel resistivity. J_s is the contribution of the Bootstrap current, that we write here for completeness, but that we neglect from now on.
Equation (7.10) has been derived in appendix A.5 (see equation (A.62)) using the averaged Ohm's law and Faraday's law, together with the susceptance matrix elements S_{ij} which relates the currents and the radial derivative of the fluxes (Ampère's law). The susceptance matrix has been better defined in appendix A.3.

Equation (7.10) takes different forms depending on the choice of the radial variable ρ (used to label magnetic flux surfaces and therefore to compute all the equilibrium quantities). For TJ-II it has been chosen:

$$\rho = \sqrt{\frac{\psi_t}{\psi_{t,max}}}\,\rho_N = \sqrt{\frac{\psi_t}{B\pi a^2}}\,\rho_N \tag{7.11}$$

which means

$$\psi_t = \frac{B\pi a^2}{\rho_N^2}\,\rho^2 \tag{7.12}$$

$$\psi_t' = \frac{B\pi a^2}{\rho_N^2}\,2\rho \tag{7.13}$$

$$\frac{\partial}{\partial \psi_t} = \frac{\rho_N^2}{\pi B a^2}\frac{1}{2\rho}\frac{\partial}{\partial \rho} \tag{7.14}$$

In these equations B is the magnitude of the axial toroidal field and ρ_N is a constant with the dimensions of a lenght, for which one can choose $\rho_N = a$, where a is the minor radius of the vacuum chamber. This is a useful choice for the radial variable in ASTRA, that usually has the dimension of a lenght ([m]), [61]. With this choice of ρ, eq.(7.10) becomes:

$$\begin{aligned}\frac{\partial \iota}{\partial t} &= \frac{\partial \iota}{\partial \rho}\frac{\partial \rho}{\partial t} + \frac{1}{\rho}\frac{\partial}{\partial \rho}\Big[\frac{\eta_\parallel}{\mu_0}\rho\,(S_{21}\iota + S_{22})^2\,\frac{\partial}{\partial \rho}\Big(\frac{S_{11}\iota + S_{12}}{S_{21}\iota + S_{22}}\Big)\Big] + \\ &- \frac{1}{\rho}\frac{\partial}{\partial \rho}\Big[\eta_\parallel \langle \mathbf{J_s}\cdot\mathbf{B}\rangle \frac{\rho_N^4}{4\pi B^2 a^4}\frac{\partial V}{\partial \rho}\Big] \end{aligned} \tag{7.15}$$

The first term of this equation is proportional to the time derivative of the toroidal flux (and therefore of the radial variable). We do not consider this term, confident that it has only a weak influence on the evolution [74] and that it is anyway considered when recalculating the geometry (and therefore magnetic fields and fluxes) after some step of the equilibrium evolution. The last term of equation (7.15) is related to the Boostrap current, and we neglect it. With ASTRA just an approximate expression is therefore evolved:

$$\frac{\partial \iota}{\partial t} \approx \frac{1}{\rho}\frac{\partial}{\partial \rho}\Big[\frac{\eta_\parallel}{\mu_0}\rho\,(S_{21}\iota + S_{22})^2\,\frac{\partial}{\partial \rho}\Big(\frac{S_{11}\iota + S_{12}}{S_{21}\iota + S_{22}}\Big)\Big] \tag{7.16}$$

To evolve this equation we need to fix also the boundary condition for the rotational transform: $\iota(\rho = a)$. Using for ι the equation (A.50) in the appendix[16]

$$\iota = \frac{\mu_0 I}{S_{11}\psi_t'} - \frac{S_{12}}{S_{11}} \tag{7.18}$$

and remembering the choice for ρ, the boundary condition can be:

$$\iota(\rho = a) = \frac{1}{S_{11}}\Big(\frac{\mu_0}{2}\frac{I_P\,\rho_N^2}{B\pi a^3} - S_{12}\Big) \tag{7.19}$$

or, for the choice $\rho_N = a$

$$\iota(\rho = a \wedge \rho_N = a) = \frac{1}{S_{11}}\Big(\frac{\mu_0}{2}\frac{I_P}{B\pi a} - S_{12}\Big) \tag{7.20}$$

where, for the toroidal current I, $I(\rho = a) = I_P$ with I_P the plasma current (experimental value).

The iterative model in ASTRA

[16] Equivalent to eq.(8) in [74].
Due to some numerical error, future work will try different boundary condition for the rotational transform. For example, eq.(7.18) can also be written as ([74])

$$\iota = \frac{S_{22}I - S_{12}F}{S_{11}F - S_{21}I} \tag{7.17}$$

where I and F are the toroidal and poloidal current of eq. (A.43). Using $I(\rho = a) = I_P$ and the computed values of $F(\rho = a)$ and of $S_{ij}(\rho = a)$ (out of VMEC), one can use this formula for the boundary condition.

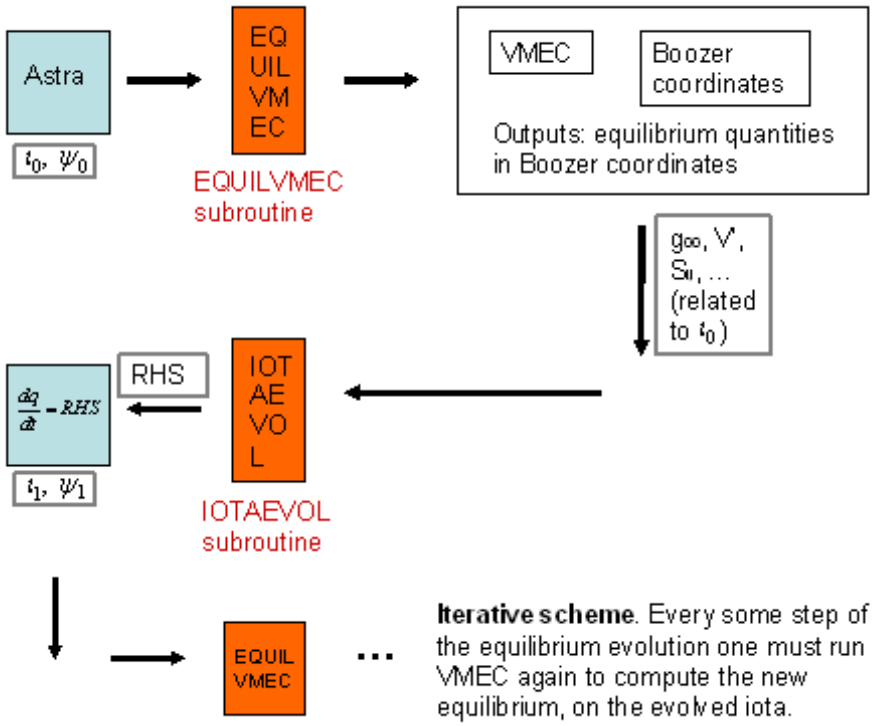

Figure 7.3: The iterative model scheme for the solution of the equilibrium time evolution with ASTRA and its subroutines: EQUILVMEC runs VMEC and computes the equilibrium quantities in Boozer coordinates; IOTAEVOL writes the RHS and the boundary condition for the equation that ASTRA must evolve. The consistent problem implies updating the metrics to be read by IOTAEVOL after several steps in the evolution with a fixed metrics.

As said in section 6.2.3, the ASTRA transport code was initially written for the analysis of Tokamaks' discharges, and only afterwards modified to work also with non axi–symmetric geometries, like Stellarators' ones (or the helical geometry of a SHAx state in RFPs). When ASTRA runs for non axi-symmetric configurations, it can not compute the equilibrium by itself, but it needs a list of equilibrium quantities as an input [61].

ASTRA runs reading an *input file* with experimental data and equilibrium quantities, and a *model file* where all the instruction for the transport analysis are listed.
The right hand side (RHS) of equation (7.16) is described to the ASTRA

evolution solver as a source term, with zero diffusivity[17] [61]. This is written in the model file, that also calls two different subroutines (EQUILVMEC and IOTAEVOL) in the iterative scheme of fig. 7.3. The first one runs the VMEC equilibrium code and writes a text file with all the useful equilibrium profiles. The second one writes the RHS of equation (7.16) for ASTRA evolution.

EQUILVMEC: It is the subroutine written to couple the transport code ASTRA with the equilibrium code VMEC.
EQUILVMEC first writes the input file for VMEC, reading ASTRA's output: the toroidal flux and the rotational transform profiles, together with the plasma current and the total value of the toroidal flux at the edge. Then, it executes the VMEC code and the code to convert the equilibrium quantities to Boozer's straight coordinates. A modified version of this code writes in a text file (named *metrics-average*) a set of radial profiles[18]: useful to evolve equation (7.16) are the S_{ij} susceptance matrix elements, the rotational transform and the poloidal and toroidal currents (F and I respectively).
The output of EQUILVMEC are read by the second subroutine, IOTAEVOL.

IOTAEVOL: It is the subroutine that writes the RHS of the evolution equation (7.16) and the boundary condition, reading the text file (*metrics-average* out of EQUILVMEC) where all the useful radial profiles are written in Boozer coordinates.
Its output is therefore the RHS equation that ASTRA must evolve and the boundary condition for the evolution.

Reading IOTAEVOL's outputs, ASTRA can evolve the rotational transform accordingly to equation (7.16) and to the boundary condition (7.19). Going back to the iterative scheme of fig.7.3, the evolution must be frequently[19] stopped, VMEC must be run again to compute the new equilibrium profiles from the evolved rotational transform, and a new RHS (together with its boundary condition) must be updated.
The codes are prepared for this kind of self consistent evolution of the rotational transform that implies updating the metrics to be read by IOTAEVOL after several steps in the evolution (with a fixed metrics). It is worth noting

[17] The diffusion equation employed in the ASTRA code is:

$$\frac{\partial A}{\partial t} = \langle \nabla \cdot (D \, \nabla A) \rangle + S(\rho) \tag{7.21}$$

for any quantity $A(\rho)$. The first term is the diffusive one (that could also account for convective transport with an *effective* diffusion coefficient D_{eff}) and $S(\rho)$ the source term. We could not separate equation (7.16) in this form, choosing therefore to write the RHS all in the source term S, with zero diffusivity.

[18] All the radial profiles are computed using the chosen radial variable ρ, eq.(7.11)

[19] Future work must find a quantitative value for this *frequently*.

that during the evolution with a fixed metrics the evolution of the RHS is only due to the evolution of the rotational transform (because their explicitly dependence in the form of equation (7.16)) while the S_{ij} elements are fixed.

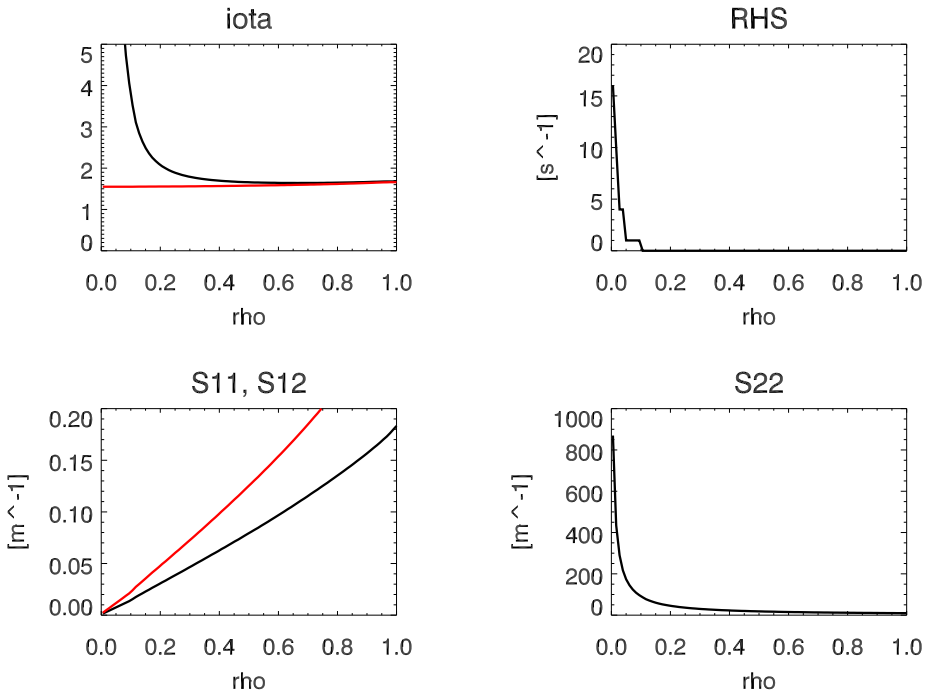

Figure 7.4: Equilibrium profiles related to the rotational transform profile obtained for plasma current $I_P = 500$ A (top–left in black) and useful to evolve equation (7.16): the RHS; the susceptance matrix elements S_{11}, S_{12} and S_{22}. All the profiles are written in Boozer coordinates for the chosen radial variable in the text file *metrics_ average* and represent the equilibrium during the "initial step" of the evolution. In top–left figure, the red rotational transform profile is related to the vacuum one for comparison. In top.–right figure, the RHS values are residual, this is why it looks steep.

The model and the subroutines have been written during my stay in Madrid.
Just some checks have been done at this time for the mentioned evolution steps. In fig 7.4 one can see the plot of some important quantities, as the RHS and the susceptance matrix elements for the initial rotational transform profile (obtained for plasma current $I_P = 500$ A).

Some preliminary result

Stellarators' discharges can be current–free, which means that $I = 0$, and

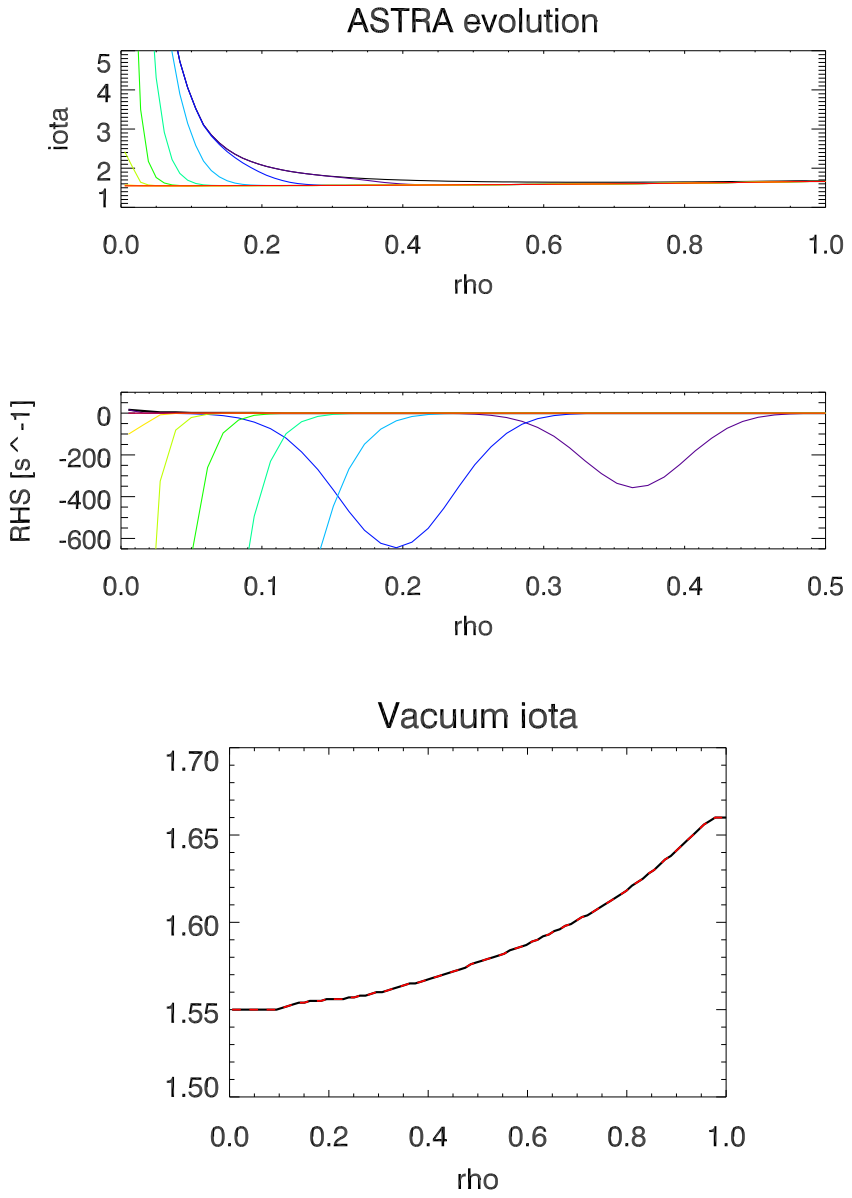

Figure 7.5: *Top:* some intermediate moment of the ASTRA time evolution of the rotational transform and the RHS from some equilibrium with $I_p \neq 0$ to the steady state equilibrium with $I_p = 0$. The initial equilibrium state is the one obtained for $I_P = 500$ A and showed in fig.7.4. In black the initial equilibrium profiles, in red the final steady state ones, colors for nine intermediate profiles. *Bottom:* the evolved rotational transform profile (black line) and the vacuum one (red points) that perfectly overlap.

therefore (see equation (A.50))

$$\iota = -\frac{S_{12}}{S_{11}} \tag{7.22}$$

It is called the *vacuum rotational transform*, and the related equilibrium must be steady state.

From the analytical point of view it is easy to prove that using eq.(7.22),

$$\left(\frac{S_{11}\iota + S_{12}}{S_{21}\iota + S_{22}}\right) \mapsto \left(\frac{S_{11}(-\frac{S_{12}}{S_{11}}) + S_{12}}{S_{21}(-\frac{S_{12}}{S_{11}}) + S_{22}}\right) = 0 \tag{7.23}$$

and therefore all the RHS in the evolution equation (7.16) vanishes, proving that the Stellarator vacuum equilibrium is already steady state.

From the operative point of view this can be a first check of the ASTRA evolution.
In ASTRA it is possible to change some discharge parameter (like the plasma current) during the run. Setting $I_P = 0$ (and therefore $I = 0$) to look for the stationary vacuum equilibrium, the system immediately relaxes to the vacuum rotational transform. In fig.7.5 (top) one can see the ASTRA evolution when $I_P = 0$ is set, both for the rotational transform profile and for the RHS of equation (7.16). It is worth noting that during this evolution the metrics elements have not been updated, therefore the evolution of the RHS in fig.7.5 is only due to the evolution of the rotational transform and not to the S_{ij} elements that represent the metrics during the "initial step". This is therefore just an example with a long time step before updating the geometry, the complete MHD problem being fulfilled just by updating the S_{ij} more often. In fig.7.5 (bottom) one can see the evolved rotational transform profile (black line) and the vacuum one (red points)[20]: as one can see, they perfectly overlap.

We are therefore confident that ASTRA is working correctly with the written subroutines for the time evolution of ι. More validation and subsequent analysis will be matter of future work.

7.3.2 The time evolution of q for RFX–mod

In section 7.3.1 is presented the work done with the Theory Group of Ciemat (Madrid) for the evolution of the rotational transform in TJ-II (non null plasma current) Stellarator discharges.

[20]The vacuum rotational transform profile comes from tj2 codes (based on Biot-Savart law) that uses the currents in the external coils as input.

The work done for RFX–mod is very similar to the one for TJ-II, but some differences arise due to the reversal region only present in RFX–mod: the safety factor profile ($q = 1/\iota$) is evolved instead of the rotational transform (that diverges at the reversal surfaces, whereas q simply vanishes) and a function of the monotonic poloidal flux must be chosen for the radial variable (instead of a function of the toroidal flux that is non monotonic in a reversed configuration).
This implies some modifications of the ASTRA model and subroutines (EQUILVMEC and IOTAEVOL) in order to evolve the equation for the safety factor and to use the right radial variable and boundary conditions.

The equilibrium evolution is an important point for RFX–mod discharges, due to the fact that the helical equilibria computed by SHEq (for SHAx states) are not ohmic equilibria (see section 7.2).

The evolution equation

Following the same steps necessary to derive $\partial\iota/\partial t$ using Ampère's, Faraday's and the parallel Ohm's laws (see appendix A.5 and Strand's and Houlberg's paper [74]), in section 9.3.1 we derived the equation for the time evolution of the safety factor profile ($\partial q/\partial t$).
The equation for (dq/dt) is[21]:

$$\begin{aligned}\frac{\partial q}{\partial t} &= \frac{\partial q}{\partial \psi_p}\Big(\frac{\partial \psi_p}{\partial t} + V_t(0)\Big) - \frac{\partial}{\partial \psi_p}\Big[\frac{\eta_\parallel}{\mu_0}\psi_p'\,(S_{21} + S_{22}\,q)^2\,\frac{\partial}{\partial \rho}\Big(\frac{S_{11} + S_{12}\,q}{S_{21} + S_{22}\,q}\Big)\Big] + \\ &- \frac{\partial}{\partial \psi_p}\Big[\eta_\parallel \langle \mathbf{J_s}\cdot\mathbf{B}\rangle \frac{\partial V}{\partial \psi_p}\Big] \qquad (7.24)\end{aligned}$$

where ψ_p is the poloidal flux through the helical flux surfaces $\rho = const$, S_{ij} the susceptance matrix elements, V the volume enclosed inside $\rho = const$, $V_t(0)$ the toroidal loop voltage on the axis.
As done for the evolution of the rotational transform, we neglect both the term involving the Boostrap current J_s and the first term of the equation that involves the change in the geometry and the loop voltage on the axis. However, the term proportional to $V_t(0)$ (not present in the evolution of ι) should probably be taken into account and the term involving the the non–inductive current J_s could be used to account for some residual dynamo currents (but we will account for them role just in future work). We therefore evolve with ASTRA just an approximate expression (similar to eq.(7.16)):

$$\frac{\partial q}{\partial t} \approx -\frac{\partial}{\partial \psi_p}\Big[\frac{\eta_\parallel}{\mu_0}\psi_p'\,(S_{21} + S_{22}\,q)^2\,\frac{\partial}{\partial \rho}\Big(\frac{S_{11} + S_{12}\,q}{S_{21} + S_{22}\,q}\Big)\Big] \qquad (7.25)$$

[21] See equation (9.141).

Equation (7.25) takes different forms depending on the choice of the radial variable ρ. For RFX–mod the choice is[22]

$$\rho = \sqrt{\frac{\psi_p}{\psi_{p,max}}}\,\rho_N \tag{7.26}$$

which means

$$\psi_p = \frac{\psi_{p,max}}{\rho_N^2}\,\rho^2 \tag{7.27}$$

$$\psi_p' = \frac{\psi_{p,max}}{\rho_N^2}\,2\rho \tag{7.28}$$

$$\frac{\partial}{\partial\psi_p} = \frac{\rho_N^2}{\psi_{p,max}}\frac{1}{2\rho}\frac{\partial}{\partial\rho} \tag{7.29}$$

ρ_N is a constant with the dimensions of a length, and one can choose $\rho_N = a$, where $a = 0.459m$ is the minor radius of RFX–mod vacuum chamber. This is a useful choice of the radial variable for ASTRA, that usually has the dimension of a lenght ([m]). With this choice of ρ, eq.(7.25) becomes:

$$\frac{\partial q}{\partial t} \approx -\frac{1}{\rho}\frac{\partial}{\partial\rho}\Big[\frac{\eta_\parallel}{\mu_0}\rho\,(S_{21} + S_{22}\,q)^2\,\frac{\partial}{\partial\rho}\Big(\frac{S_{11} + S_{12}\,q}{S_{21} + S_{22}\,q}\Big)\Big] \tag{7.30}$$

To evolve this equation we need to fix also the boundary condition: $q(\rho = a)$. Using for q the inverse of equation (A.50) in the appendix:

$$q = \frac{S_{11}F - S_{21}I}{S_{22}I - S_{12}F} \tag{7.31}$$

where I and F are the toroidal and poloidal current, eq.(A.42)–(A.43). The boundary condition for the safety factor can be found using the edge values of all the quantities: $I(\rho = a) = I_P$ and the computed values of $F(\rho = a)$ and of $S_{ij}(\rho = a)$ (output of VMEC).

It is worth noting that the aim of this work is to evolve the helical equilibria computed by SHEq: the magnetic flux surfaces labelled by ρ are the $\Sigma(\chi)$ magnetic flux surfaces defined in section 6.1, where χ is the helical flux; the poloidal flux is the poloidal flux $\psi_p(\chi)$ defined in section 4.4 as the flux through the helical flux surfaces $\Sigma(\chi)$ at the poloidal–like angle $\theta^* = const$, defined on the helical axis of the system (section 4.4.1). This angle is related to the helical q–profile in equation (6.27):

$$q = \frac{d\varphi}{d\theta^*} = \frac{d\psi_h}{d\psi_p}(\chi) \tag{7.32}$$

[22]Consider $\psi_{p,max} = \pi\,R\,a\,B_P = \frac{R}{2}\,\mu_0 I_P$. The second equivalence is derived using this relation for the total magnetic poloidal field: $B_P(a) = \mu_0\,I/(2\pi a)$, with a minor radius and R major radius.

where $\psi_h(\chi)$ is the non monotonic toroidal flux defined in equation (4.19) and plotted in fig.4.5, and $\psi_p(\chi)$ the (monotonic) poloidal flux defined in equation (4.19).
The VMEC code converges very near to this value of q, computed by SHEq, and this is the helical safety factor that is evolved by ASTRA.
The angle θ^* is topologically equivalent ([76]) to the Boozer poloidal angle used by the VMEC equilibrium code to compute the equilibrium profiles.

Some preliminary results

The same subroutines used for TJ-II, modified for the evolution of the safety factor and its boundary condition, are used.
The VMEC equilibrium code was initially written for Stellarator machines, and then modified to work for reversed configurations too: this must be taken into account in EQUILVMEC to write the correct input file for VMEC[23].

In fig. 7.6 are plotted some important equilibrium quantities: the initially q–profile (output of VMEC), the susceptance matrix elements, and the RHS of equation (7.30).

It is not easy to devise a simple check for ASTRA evolution, as done for TJ-II with the vacuum steady state equilibrium. Does a sort of vacuum equilibrium exist for RFPs? Of course it is not the $I = 0$ case, because zero plasma current does not induce any helical SHAx state.
The work for RFX–mod is ongoing, as the collaboration with Ciemat.

7.4 The paramagnetic pinch

The paramagnetic pinch is a cylindrical magnetic configuration, with an axial electric field, $\mathbf{E} \equiv E_z$. Magnetic field lines are helix that lie on circular magnetic flux surfaces: $\mathbf{B} \equiv (0, B_\theta, B_z)$ and $\mathbf{J} \equiv (0, J_\theta, J_z)$.
We use the paramagnetic pinch as a simple example to show (section 7.1) that the axial magnetic field can not reverse in an axi–symmetric configuration, if the ohmic constraint is taken into account. An example of axi–symmetry is the cylindrical magnetic field components of the paramagnetic pinch, that depend only on the radius r of the circular (and nested) flux surfaces.

Let me write the equation system for the paramagnetic pinch equilibrium[24].

[23] In RFX–mod it is used the version 8.47 III with fixed boundary [?].

[24] Let me derive the equilibrium system from the usual MHD equations, written for a cylindrical geometry (any variable depends only on the radius r of the circular magnetic

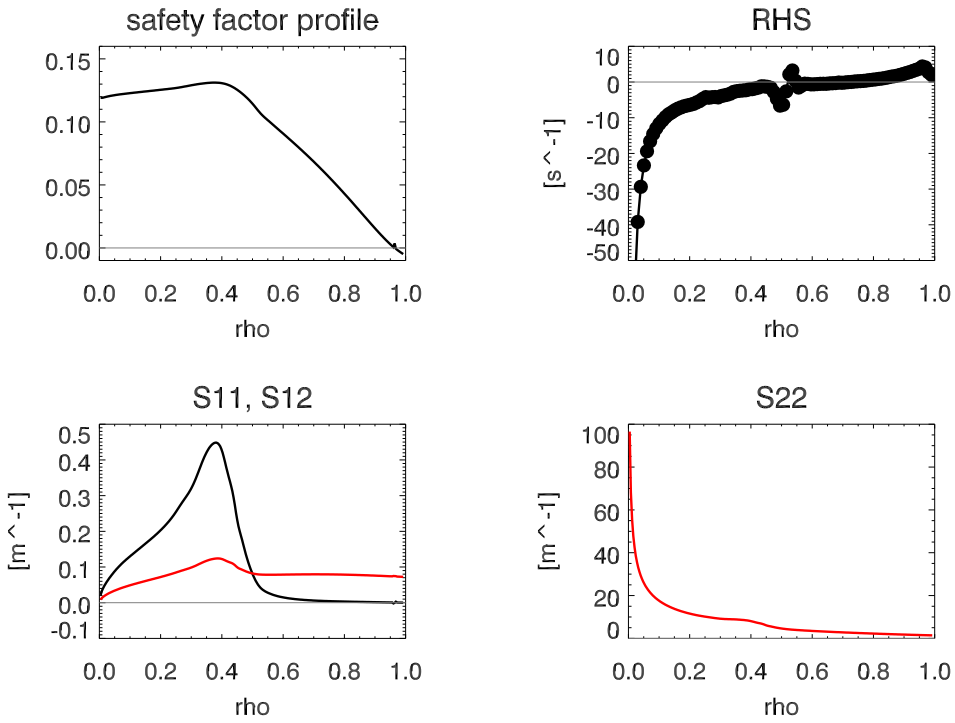

Figure 7.6: Equilibrium profiles related to the safety factor profile (top–left) and useful to evolve equation (7.30): the RHS and the susceptance matrix elements S_{11},S_{12} and S_{22}. All the profiles are written in Boozer coordinates for the chosen radial variable in the text file *metrics_average*.

flux surfaces):

$$\nabla \times \mathbf{B} = \mu_0 \mathbf{j} \mapsto \begin{cases} \frac{1}{r}\frac{d}{dr}(r\, B_\theta) = \mu_0\, j_z \\ \frac{dB_z}{dr} = -\mu_0\, j_\theta \end{cases} \tag{7.33}$$

$$\mathbf{E}_\parallel = \eta_\parallel j_\parallel \mapsto \begin{cases} j_z = \frac{E_\parallel}{\eta_\parallel}\frac{B_z}{B} = \frac{E_0}{\eta_\parallel}\frac{B_z^2}{B^2} \\ j_\theta = \frac{E_\parallel}{\eta_\parallel}\frac{B_\theta}{B} = \frac{E_0}{\eta_\parallel}\frac{B_z B_\theta}{B^2} \end{cases} \tag{7.34}$$

$$\mathbf{J} \times \mathbf{B} = 0 \mapsto \begin{cases} \mathbf{j} \equiv j_\parallel = (0, j_\theta, j_z) \\ j_\perp = 0 \end{cases} \tag{7.35}$$

From the (parallel) Ohm's law one can compute $j_\parallel = (0, j_\theta, j_z)$.
Because $\mathbf{E} = (0, 0, E_z)$ by hypothesis, $E_\parallel = E_0\,(B_z/B)$, where B_z/B is the projection operator on B_z (as B_θ/B is the projection operator on B_θ).
Using the definition

$$U = \frac{E_0\, \mu_0\, a}{\eta_\parallel B_0} \tag{7.36}$$

Using, just for simplicity of notation, the definition

$$U = \frac{E_0\,\mu_0\,a}{\eta_{\|} B_0} \tag{7.38}$$

where E_0 and B_0 are the axial electric and magnetic field, a the radius of the last closed flux surface and $\eta_{\|}$ the plasma resistivity parallel to magnetic field lines, the equations for the normalized components of the magnetic field are:

$$\begin{cases} \frac{1}{r}\frac{d}{dr}(r\,B_\theta) = U\,\frac{B_z^2}{B^2} \\ \\ \frac{dB_z}{dr} = -U\,\frac{B_z\,B_\theta}{B^2} \end{cases} \tag{7.39}$$

From the parallel Ohm's law, once the system (7.39) has been solved for the magnetic field components B_θ and B_z, one can compute the components of the parallel current density[25]:

$$\begin{cases} j_\theta = \frac{E_0}{\eta}\,\frac{B_z\,B_\theta}{B^2} \\ \\ j_z = \frac{E_0}{\eta}\,\frac{B_z^2}{B^2} \end{cases} \tag{7.40}$$

In fig. 7.7 one can see the solution of the systems (7.39) for the magnetic field components (dashed lines), whose integration is done with the boundary condition on the axis: $B_z(0) = B_0$ and $B_\theta(0) = 0$. The colored lines are the solution for some (increasing from blue to green) value of the parameter U, directly proportional to the axial electric field E_0 and therefore related to the plasma current. As one can see, no reversal is found for B_z.

Let us conclude the chapter with some analytical considerations. In section 9.3.2 the equilibrium system (A.52) of MHD equations is rearranged in a different form, and a system of two equations for the radial derivative of the poloidal F and toroidal I currents is obtained, (9.151)–(9.152). The solution is an ohmic steady state equilibrium, that has been solved for the paramagnetic pinch with the boundary condition on the magnetic axis $I(0) =$ ... and $F(0) =$ .... The solutions for I and F are shown in fig. 7.7 (continuous lines); using the system (7.46) one can compute the (measurable) magnetic

just for simplicity of notation, and the normalized variables $B_z \mapsto (B_z/B)$, $B_\theta \mapsto (B_\theta/B)$, $r \mapsto r/a$, the ohmic equilibrium system to be solved for a paramagnetic pinch is

$$\begin{cases} \frac{1}{r}\frac{d}{dr}(r\,B_\theta) = U\,\frac{B_z^2}{B^2} \\ \\ \frac{dB_z}{dr} = -U\,\frac{B_z\,B_\theta}{B^2} \end{cases} \tag{7.37}$$

.

We will prove later that it is exactly the system (A.52) for a force free ohmic equilibria in a cylindrical geometry

[25] The current density has only the parallel component, the perpendicular component being zero because of the force free hypothesis

field components from I and F: the solutions perfectly overlap to the dashed lines in fig. 7.7 that came from the solution of the paramagnetic pinch system (7.39).

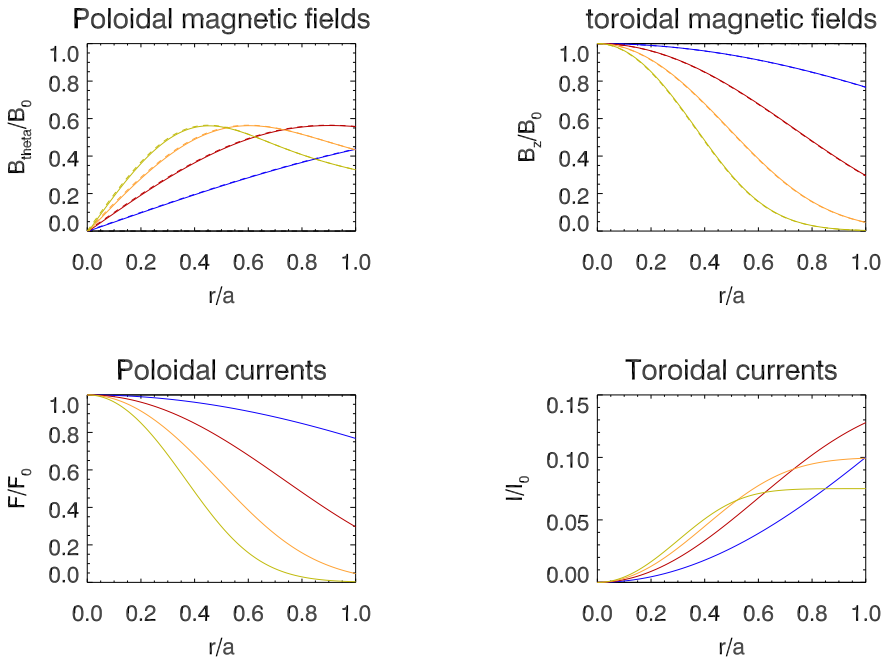

Figure 7.7: The poloidal and toroidal magnetic field components (*up*) and the correspondent currents (*down*). The colored lines are the solution for some (increasing from blue to green) value of the parameter U from equation (7.38), directly proportional to the axial electric field E_0 and therefore to the plasma current. Comments: 1. The magnetic field components are found from the solution of two equivalent equilibrium systems, eq.(7.39)–(7.46), for which are used dashed or continuous lines that perfectly overlap. From eq.(7.46), one obtains the relations: $B_\theta \sim IR/r$ and $B_z \sim F$, where R is the major radius of the torus and r the minor one. 2. Because the paramagnetic pinch is an axi–symmetric system, the toroidal field can not reverse.

7.4.1 The paramagnetic pinch in the S&H formalism

The equivalence of the two equation systems ((7.39) and (9.151)–(9.152) or (7.46)) can also be proved in an analytical way in the simple cylindrical geometry of the paramagnetic pinch.
Summarizing, we want to compare eq.(9.151) for F' (where the diagonal term of the susceptance matrix are null due to cylindrical geometry) with

the equation for B'_z:

$$F' = -\frac{\widehat{U}\,(L_{11}I)(L_{22}F)}{(L_{11}I^2 + L_{22}F^2)} \longleftrightarrow \frac{dB_z}{dr} = -U\,\frac{B_z\,B_\theta}{B^2} \tag{7.41}$$

and the same for eq.(9.152) for I' and the equation for B'_θ

$$I' = -\frac{\widehat{U}\,(L_{11}I)(L_{22}F)}{(L_{11}I^2 + L_{22}F^2)}\,\frac{I}{F} + \widehat{U}\,L_{22} \longleftrightarrow \frac{1}{r}\frac{d}{dr}(r\,B_\theta) = U\,\frac{B_z^2}{B^2} \tag{7.42}$$

In eq.(7.41)–(7.42) the radial derivative of the currents I and F are written for the easy case of a cylinder. Let us consider a cylinder of lenght L and periodicity $2\pi R$ in the axial z coordinate to write explicitly the susceptance matrix elements (and its inverse, the L_{ij} elements). Then we write the poloidal current F and the toroidal current I in terms of the magnetic field components, in order to be able to compare the relations in eq.(7.41)–(7.42).

Going back to the cylindrical metric in appendix B.2.1 and to the definitions (A.46)–(A.48) of the susceptance matrix elements (for diagonal metrics) one finds:

$$\mu_0 \begin{pmatrix} I \\ F \end{pmatrix} = \underbrace{\begin{pmatrix} \frac{Lr}{2\pi R} & 0 \\ 0 & \frac{L}{2\pi r} \end{pmatrix}}_{[S_{ij}]} \begin{pmatrix} \psi'_p \\ \psi'_t \end{pmatrix} \tag{7.43}$$

$$\begin{pmatrix} \psi'_p \\ \psi'_t \end{pmatrix} = \mu_0 \underbrace{\begin{pmatrix} \frac{2\pi R^2}{rL} & 0 \\ 0 & \frac{2\pi r}{L} \end{pmatrix}}_{[L_{ij}]=[S_{ij}]^{-1}} \begin{pmatrix} I \\ F \end{pmatrix} \tag{7.44}$$

and this solves the first step, of writing explicitly the L_{ij} elements. (No confusion will arise between the same symbol L for the cylinder lenght and the inverse of the susceptance matrix, for which just the elements L_{ij} will be used).

Let me now show how to link the currents I and F to the magnetic field components.
Using the general canonical form for the magnetic field $\mathbf{B}$ (or, in an equivalent way, equations (2.147)–(2.148)):

$$\begin{cases} B^\theta = \frac{1}{2\pi\sqrt{g}}\,\psi'_p = \frac{1}{2\pi r R}\,\psi'_p \\ \\ B^z = \frac{1}{2\pi\sqrt{g}}\,\psi'_t = \frac{1}{2\pi r R}\,\psi'_t \end{cases} \tag{7.45}$$

remembering the Jacobian $\sqrt{g} = rR$ of the cylindrical coordinates from appendix B.2.1. These are by definition the contravariant components B^i on the (non adimensional and non normalized) $\mathbf{e}_i$ basis vectors (see chapter 5).

We need to work with the (covariant) measurable components ($\widehat{B}_i$), that are easy to derive from formulas (5.66)–(5.67) in a diagonal geometry. Using for the derivative of the fluxes the susceptance matrix definition, one obtains:

$$\begin{cases} \widehat{B}_\theta = \frac{\mu_0 R}{Lr}\, I = \frac{\mu_0}{2\pi R}\, L_{11}\, I \\ \\ \widehat{B}_z = \frac{\mu_0 F}{L} = \frac{\mu_0\, L_{22}}{2\pi r}\, F \end{cases} \tag{7.46}$$

Inverting these relations one can write the equation for the current components in terms of the measurable magnetic field components:

$$\begin{cases} I = \frac{2\pi R}{\mu_0}\, \frac{1}{L_{11}}\, \widehat{B}_\theta \\ \\ F = \frac{\mu_0 F}{L} = \frac{2\pi r}{\mu_0}\, \frac{1}{L_{22}}\, \widehat{B}_z \end{cases} \tag{7.47}$$

And also the useful term

$$B^2 = (\widehat{B}_\theta)^2 + (\widehat{B}_z)^2 = \frac{\mu_0^2}{2\pi r L}\, (L_{11} I^2 + L_{22} F^2) \tag{7.48}$$

Using the equations (7.47) for I and F, some other relations must be find in order to make the comparison in eq.(7.41)–(7.42):

$$I^2 = \frac{4\pi^2 R^2}{\mu_0^2} \frac{1}{L_{11}^2}\, \widehat{B}_\theta^2 \tag{7.49}$$

$$F^2 = \frac{4\pi^2 r^2}{\mu_0^2} \frac{1}{L_{22}^2}\, \widehat{B}_z^2 \tag{7.50}$$

$$I' = \frac{2\pi R}{\mu_0} \frac{1}{L_{11}} \frac{d\widehat{B}_\theta}{dr} + \frac{L}{\mu_0 R} \widehat{B}_\theta \tag{7.51}$$

$$F' = \frac{2\pi}{\mu_0} \frac{1}{L_{22}} \widehat{B}_z - \frac{L}{\mu_0 r} \widehat{B}_z + \frac{2\pi r}{\mu_0} \frac{1}{L_{22}} \frac{d\widehat{B}_z}{dr} \tag{7.52}$$

Therefore, using these equations and the explicit geometrical values of L_{ij}, the equation for F' in (7.41) can be written as:

$$\begin{aligned} &\frac{2\pi}{\mu_0} \frac{1}{L_{22}} \widehat{B}_z - \frac{L}{\mu_0 r} \widehat{B}_z + \frac{2\pi r}{\mu_0} \frac{1}{L_{22}} \frac{d\widehat{B}_z}{dr} = \\ &= -\,\widehat{U}\, \frac{\left[\left(\frac{2\pi R^2}{rL}\right)\left(\frac{2\pi R}{\mu_0}\, \frac{1}{L_{11}}\, \widehat{B}_\theta\right)\right]\left[\left(\frac{2\pi r}{L}\right)\left(\frac{2\pi r}{\mu_0}\, \frac{1}{L_{22}}\, \widehat{B}_z\right)\right]}{\left(\frac{2\pi R^2}{rL}\right)\left(\frac{4\pi^2 R^2}{\mu_0^2}\, \frac{1}{L_{11}^2}\, \widehat{B}_\theta^2\right) + \left(\frac{2\pi r}{L}\right)\left(\frac{4\pi^2 r^2}{\mu_0^2}\, \frac{1}{L_{22}^2}\, \widehat{B}_z^2\right)} \end{aligned} \tag{7.53}$$

and (only with algebric steps) it reduces to

$$\frac{dB_z}{dr} = -U\, \frac{B_z\, B_\theta}{B^2} \tag{7.54}$$

if and only if

$$\widehat{U} = \frac{L^2}{\mu_0 2\pi R} U \tag{7.55}$$

This relation is dimensionally correct. Eq.(7.55) is the same result that arises comparing the two equations in (7.42).

This can be considered an analytical proof that solving the differential system for the currents I and F is equivalent of solving the usual static MHD equation system.
From the numerical point of view, the solutions from the integration of I' and F' perfectly overlap in the plots of fig.7.7.

Chapter 8

Plasma boundary in SHAx states

As seen in the introduction, the $m = 1$ mode spectrum during SHAx states, obtained in RFX-mod at the 1.5 MA plasma current level, displays a dominant mode (the $n = 7$ one) and a strong reduction of the secondary modes [77]. In fig. 8.1, where the average spectra of both $m = 0$ and $m = 1$ modes in SHAx states are shown, one can see that also the $m = 0$ mode spectrum is strongly peaked on the $n = 7$ mode in SHAx states. This is a direct consequence of the toroidal coupling between the two modes [54], that can be seen also in fig.8.2: increasing the plasma current the $m = 0$ spectrum displays the same behavior of the $m = 1$ one, i.e. the dominant $n = 7$ mode increases its relative amplitude while the secondary mode amplitude is reduced (one can compare fig.8.2 and fig.1.9).
Thus, it is possible to conclude that the RFP evolves, as plasma current is increased, towards a SHAx state characterized by the presence of a dominant $m = 1$ mode and a dominant $m = 0$ mode, both having the same n number.

During SHAx states the confinement properties of the configuration are enhanced, due to the development of an internal transport barrier [54]. Moreover a better distribution of the plasma–wall interaction can be observed with respect to the MH case, [78] operating at shallow reversal[1].
The $m = 0$ modes play a crucial role in determining the plasma–wall interaction, being resonant on the reversal surface, near the first wall. Nevertheless they have been neglected in the equilibrium reconstruction of the helical SHAx states computed by the SHEq code and discussed in the previous chapter (chapters 4 to 7). An idea for future work is to consider the dominant $m = 0$ mode as a perturbation to SHEq's equilibria (in the same way as the axi–symmetric equilibrium $\mathbf{B}_0$ has been perturbed by the dominant

[1] Shallow reversal means a small (absolute) value of the reversal parameter F introduced in equation (1.12) as a measure of the distance between the first wall and the reversal surface.

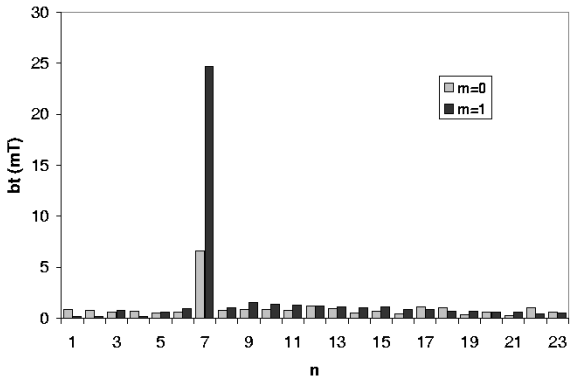

Figure 8.1: Average spectra of m=0 and m=1 modes in 1.5 MA SHAx states. The mode amplitudes are evaluated on B_ϕ measurements performed outside the plasma.

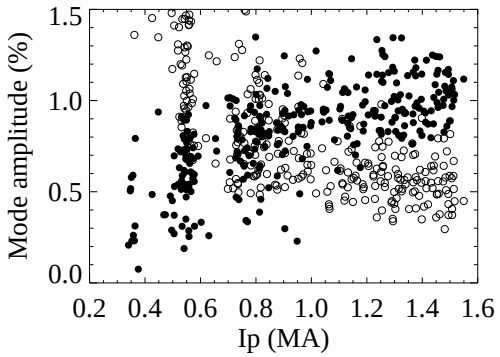

Figure 8.2: Amplitude of the $m = 0/n = 7$ mode (full circles) and of the other $m = 0$ modes up to $n = 15$ (empty circles) in QSH conditions plotted as a function of plasma current. The mode amplitudes are normalized to the average poloidal field at the wall. One should compare this figure with fig.1.9 left.

$m = 1/n = 7$ mode to compute the helical SHEq's equilibria). In this chapter we study the $m = 0$ modes role in a more experimental way.

In this sections 8.1–8.2 we perform a detailed examination of the intrinsic edge magnetic topology in SHAx states obtained in the RFX-mod device, relating it also to edge measurements. The results allow an ambitious conclusion, which is that intrinsic properties of the magnetic configuration could be exploited to develop a divertor concept, similar to the island divertor of stellarators [79] (whereas up to now in RFX–mod the graphite first wall is used as a limiter).
While further theoretical studies need to be done, and a practical implementation has to be demonstrated, the proposed approach is anyway conditioned to a good control of the radial magnetic field at the edge, which in RFX-mod is obtained through a sophisticated system of 192 feedback-controlled saddle coils [43, 80]. In section 8.3 the result of controlling the edge features by applying non–zero boundary conditions to the dominant $m = 1$ and $m = 0$ modes is presented.

The work in sections 8.1–8.2 is also published in E. Martines, R. Lorenzini, B. Momo et al., [3].
*The results of section 8.3 are related to discharges done during the 2011 RFX–mod experimental campaign, and have been already presented during APS 2011 conference (G. De Masi, B. Momo: oral section [**?**]).*

8.1 Topology of edge region in SHAx states

The $m = 0$ modes are all resonant in the RFP around the reversal surface. The distance of this surface from the first wall can be externally imposed by changing the current flowing in the toroidal field coil system. The distance from the wall is indirectly quantified by the reversal parameter F, defined in the introduction (chapter 1). A crucial observation made in RFX–mod is that shallow F, which corresponds to a small distance of the reversal surface from the wall, turns out to be a better condition at high plasma current than deeper F, as far as plasma–wall interaction is concerned. Why plasma-wall interaction in RFX-mod high current operation appears to be lower at shallow reversal is a question to which we give an answer in this section, introducing the RFP divertor idea.

In order to understand the magnetic topology of the edge region in SHAx states, and in particular the position and shape of the LCFS[2], we have used a

[2]The Last Closed Flux Surface (LCFS), that is the outermost magnetic surface not intersecting any solid object.

field-line tracing code named FLiT [81] to trace the magnetic topology in the plasma edge. FLiT uses the output of an algorithm for the reconstruction of the tearing mode eigenfunctions over the whole plasma volume based on Newcomb's equation, supplemented with edge magnetic measurements [53] (see chapter 3)[3].

Fig. 8.3 displays two Poincaré plots of the magnetic field lines in the r-φ plane on the outer equator (where the main magnetic field is almost poloidal). The first one is obtained during a 1.5 MA SHAx state at shallow reversal ($F = -0.017$), while the second depicts a similar condition obtained at deep reversal ($F = -0.181$). Thick lines are superposed on the plots, depicting the position of the LCFS, computed from FLiT outputs by looking at where, for each toroidal and poloidal position, the most internal open field line is found.
The new and striking result is that in the SHAx condition obtained at shallow reversal the LCFS is well separated from the wall by the $m = 0$ islands (and that their X-points act so as to form a *divertor–like* configuration, see fig.8.10). It is important to remark that the LCFS does not touch the wall anywhere, not only in the plane displayed in the figure.
On the contrary, at deep reversal the LCFS is located beyond the $m = 0$ island chain and a *limiter–like* condition is obtained.
In the two plots the reversal surface of the toroidal field is located at the position where the O-points of the $m = 0$ islands are found, which means at $r = 0.45$ m for the shallow F case and at $r = 0.41$ m for the deep F one.

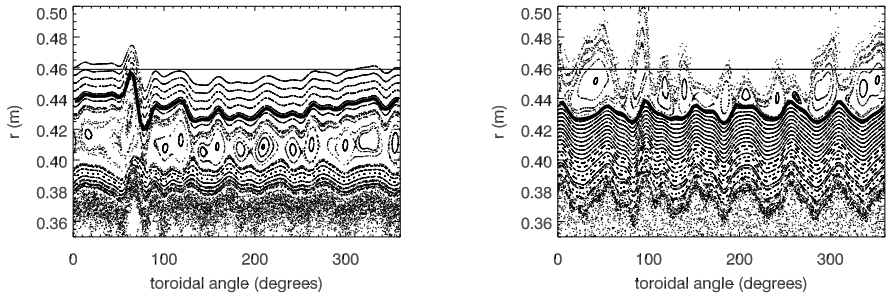

Figure 8.3: Poincaré plot of the magnetic field lines on the outer equator for a SHAx state at 1.5 MA and shallow reversal (right) and for a similar condition at deep reversal (left). The thick line marks the position of the LCFS. while the horizontal line at $r = 0.459$ m indicates the first wall position.

The relationship between the occurrence of a divertor–like configuration

[3]FLiT uses the same eigenfunctions of the perturbation to the axi–symmetric magnetic field that are used by SHEq code.

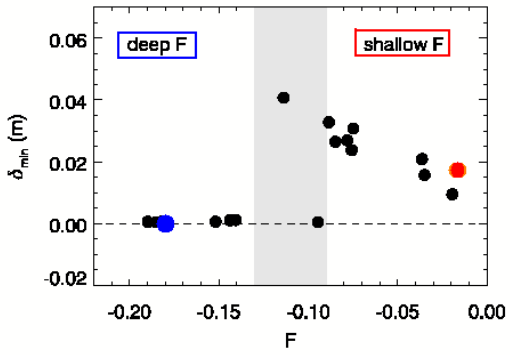

Figure 8.4: Minimum distance of the LCFS from the first wall plotted as a function of the reversal parameter F. The shaded region marks the F range where transition from a *limiter–like* geometry to a *divertor–like* one occurs. The blue point is related to the limiter–like configuration represented in the left Poincaré in fig. 8.3; the red point is related to the divertor–like configuration represented in the right Poincaré in fig. 8.3.

and the reversal parameter value has been investigated more systematically by computing the minimum distance δ_{min} of the LCFS from the wall for a set of SHAx states obtained at different F values.
Fig. 8.4 displays a plot of δ_{min} as a function of F. It is clearly seen that as F goes from zero towards more negative values, that is from shallow reversal to deep reversal, the LCFS distance from the wall is increased, up to values of F between -0.10 and -0.13, where the $m = 0$ islands do not intersect the wall any more and the limiter-like situation ($\delta_{min} = 0$) is obtained. This result has been confirmed by the single band reflectometer [82] monitoring the distance from the wall of a plasma layer with fixed density [83].
This can be considered an explanation for the empirical evidence of a reduced plasma-wall interaction in shallow F discharges, which constitute the preferred mode of operation for RFX–mod at high current.

8.2 Plasma wall interaction

In order to better understand the structure of the Scrape–Off Layer (SOL) formed beyond the LCFS in the shallow F case (shown in the left frame of Fig. 8.3), a colour scale plot of the connection lengths of field lines passing through a grid of points in the r–φ plane has been constructed. This has been done integrating the field line equations from the starting point, both forwards and backwards, until the first wall is reached. The connection length is then defined as the sum of the two lengths covered in the two directions.

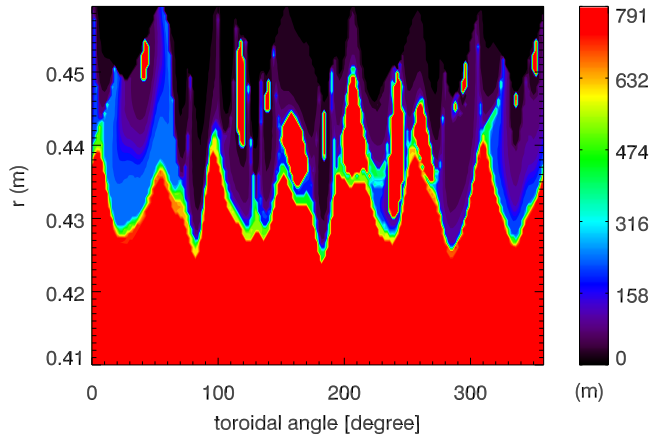

Figure 8.5: Map of the connection lengths on the r-φ plane located at $\theta = 0$ (external equatorial plane).

The result of the procedure is shown in Fig. 8.5, for the plane at $\theta = 0°$ (the external equatorial plane). The maximum value of the connection length, for which the red colour has been used, also marks the closed field lines. The confined plasma, enclosed by the LCFS modulated by the $n = 7$ pattern, can be clearly identified. Furthermore, other red regions, corresponding to $m = 0$ islands that do not touch the first wall, can be observed. Beyond the LCFS a SOL is created.
In particular, in the last cm near the first wall relatively short connection lengths are found, with only occasional regions of longer connection lengths reaching the wall.

The connection length of the field lines touching different points of the first wall is closely related to the local distance between the LCFS and the wall. This is shown in Fig. 8.6, where the connection length of points of the first wall located on the outer equator is shown as a function of the toroidal angle, for the same condition of the left frame of Fig. 8.3.
It is possible to observe that the connection length displays a $n = 7$ periodic structure, with rounded maxima which are anyway lower than the length of one poloidal turn ($\sim$ 3 m). Superimposed to this, limited regions of much larger connection lengths are found, indicating field lines which manage to perform many poloidal turns before touching again the wall. The origin of these long field lines are positioned on the maxima of the $n = 7$ pattern (and therefore on the X–points of the $m = 0$ island chain).
In the same figure is also plotted the distance between the LCFS and the first wall, again plotted as a function of the toroidal angle for points along

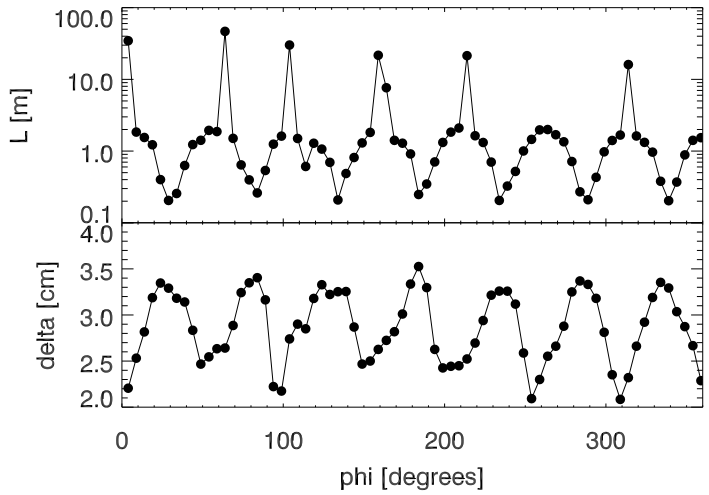

Figure 8.6: Connection lengths of field lines originating from different points of the first wall ($r = 0.459$ m) on the outboard equatorial plane ($\theta = 0°$) and distance between the LCFS and the wall on the same plane, both plotted as a function of the toroidal angle.

the outer equator. The $n = 7$ periodicity can also be clearly seen.

The comparison of the two curves allows to conclude that in the positions where long connection lengths exist, the LCFS–wall distance is shorter; while in regions of short connection length the LCFS–wall distance is larger. The consequence that can be drawn from this fact, when thinking to the plasma–wall interaction, is that in the first situation a stronger interaction is expected: both because of parallel flows, since a longer flux tube collects a larger amount of energy; and because of perpendicular fluxes, which originate from the LCFS which is less distant.

The hypothesis that regions of the first wall with larger connection length have a stronger plasma–wall interaction has been validated using experimental data, from ISIS and a fast CMOS camera.

ISIS

ISIS (the **I**ntegrated **S**ystem of **I**nternal **S**ensors) is composed by two subsystems of electrostatic and magnetic probes located inside the RFX-mod vacuum vessel (5 mm behind the graphite tiles), [84, 85]. In this work we used only the electrostatic arrays (72 probes distributed on the external equatorial plane and 7 on the poloidal plane at a specific toroidal angle) able to collect floating potential V_f data [11]. This system, thus, enables us to create a toroidal and poloidal map of the floating potential (linked to the

dynamics of the electron traveling at the edge) during the RFX-mod high plasma current operations. The result for a typical SHAx state is shown in fig.8.7 (top) and is plotted in terms of fluctuation δV_f with respect to a mean value.
The idea is to compare the floating potential behavior at the edge with the aforementioned connection lenght evaluated using FLiT code.
As previously measured by insertable probes in low plasma current discharges [86, 87], in RFX-mod the floating potential is found to be close to zero or slightly positive near the first wall, whereas it turns markedly negative in the more internal plasma layers.
Looking at the toroidal and poloidal map shown in fig.8.7 (bottom) one can reasonably interpret the regions with a $\delta V_f < 0$ (displaying a $n = 7$ periodicity) as caused by the more internal plasma layers approaching the probe (located at $r/a = 1$) and thus as a track of a localized plasma wall interaction.
This allows a direct comparison of the ISIS data with the connection lenght maps in the toroidal and the equatorial plane (also shown in fig.8.7) and would confirm the hypothesis already discussed that the regions featuring long connection lenght are those ones characterized by a larger plasma wall interaction.

Fast CMOS camera

A further confirmation comes from the fast CMOS camera that looks at H_α line emission, originating from neutral hydrogen atoms coming out from the wall[4].
Fig. 8.8a shows the emission pattern detected by the camera in a 1.5 MA discharge, during a SHAx phase. The actual image has been remapped to a regular grid in the the toroidal and poloidal angles. The figure displays an almost vertical emission pattern, with a discretization which corresponds to the tiles which compose the first wall[5].
In Fig. 8.8b the connection lengths for the same region of the first wall, in the same discharge and at the same time instant are plotted. It is clearly seen that the connection length pattern is similar to the emission pattern of the camera. The two patterns are displaced one with respect to the other by a few degrees in the toroidal direction. This discrepancy appears in all cases, and is attributed to a systematic error.

[4]Since in RFX–mod the density profile displays a strong gradient in the first few cm of the plasma, it is possible to associate the emission to the heat load of the nearby portion of the first wall, under the assumption that a stronger plasma-wall interaction heats locally the wall and causes a stronger hydrogen release. The camera used in RFX-mod was operated with a frame rate of 10,000 frames per second, and a shutter time of 1/10,000 s.

[5]This discretization is due to the tile shape, which causes an increased interaction in the central part of the tile. A darker region in the middle of the bright pattern (around $\theta = 0°$) is due to the presence of a port, as it is the dark oval region more on the left (around $\phi = 142°$), [88].

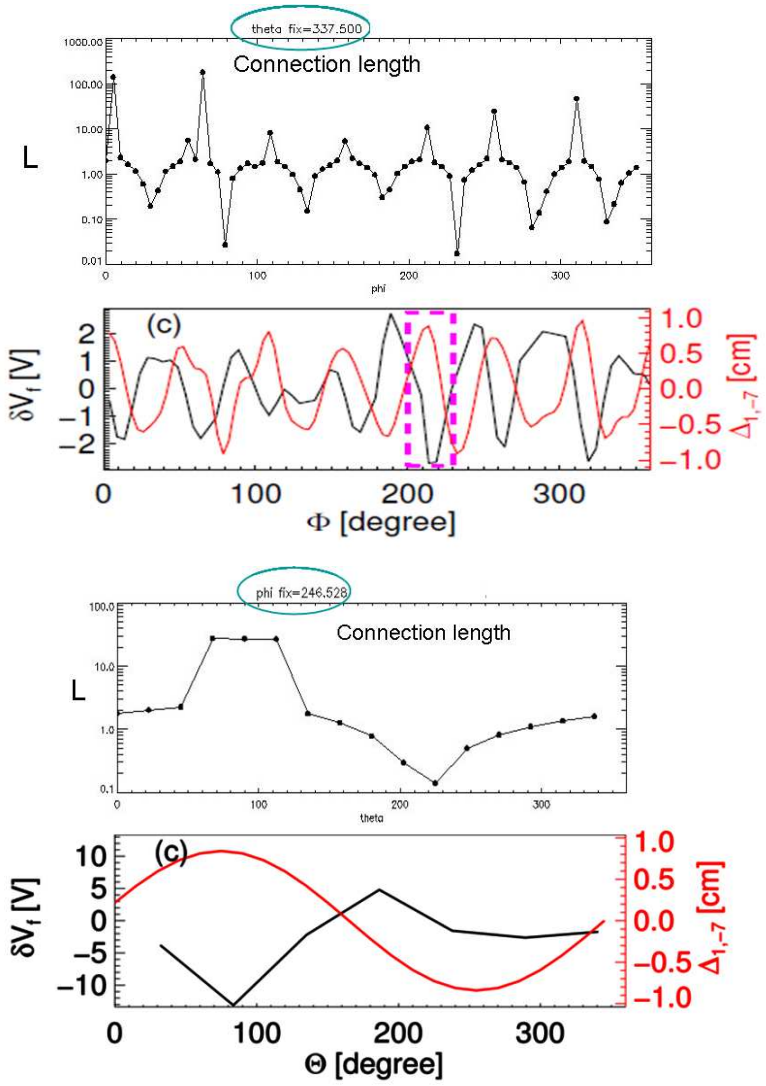

Figure 8.7: The connection lengths (L) are compared with the shift of the LCFS (that one can think as the distance of the LCFS and the first wall, already plotted in fig.8.6) in red, and with the ISIS measurements of the floating potential in black. *Top:* the comparison is between magnetic field lines length originating from different points of the first wall ($r = 0.459$ m) almost on the outboard equatorial plane ($\theta = 340.7°$) and measurements on the same plane, both plotted as a function of the toroidal angle. *Bottom:* the comparison is between magnetic field lines length originating from different points of the first wall ($r = 0.459$ m) on the poloidal plane (at $\varphi = 246.5°$) and measurements on the same plane, both plotted as a function of the toroidal angle.

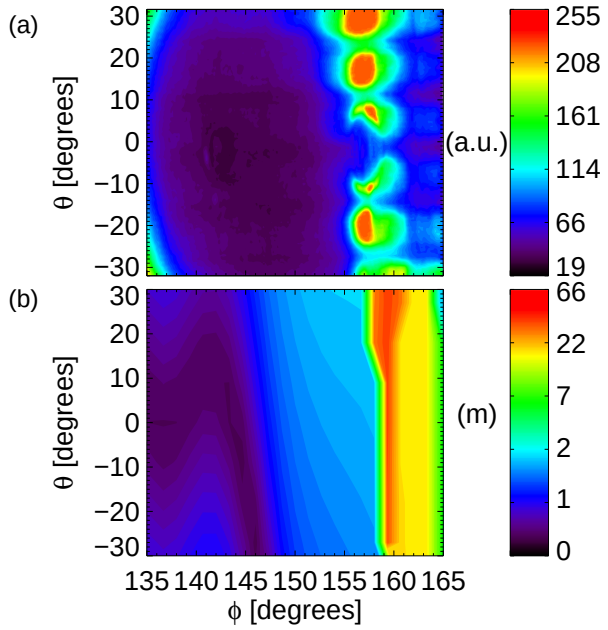

Figure 8.8: Pattern of H_α emission recorded by a fast camera and mapped onto a portion of the poloidal-toroidal plane (a). Map of the connection lengths of the field lines originating from the first wall for the same discharge and time instant (b).

Having established that the magnitude of the plasma–wall interaction in different regions of the first wall can, to a first approximation, be quantified by looking at the connection length of field lines leaving them, it is possible to build a map of this interaction by following field lines starting from a grid covering the first wall. Moreover, from the connection length one can therefore obtain complementary information with respect to the ones from the diagnostics: experimental data usually refer only to a fixed position, whereas the connection length can be computed for the whole plasma volume. On the other side, diagnostics can give information in time, whereas the connection length are computed for a fixed time (requiring long time for the field line integration, connection length is not suitable for time evolution analysis).

The left frame of Fig. 8.9 shows the interaction map on the chamber surface reconstructed using the connection length, represented as a colour scale. It can be seen that regions of higher connection lenght concentrate in the 90°-180° band, that is in the region comprised between the torus top and the inner equator. This is a non–trivial consequence of the phase relationship

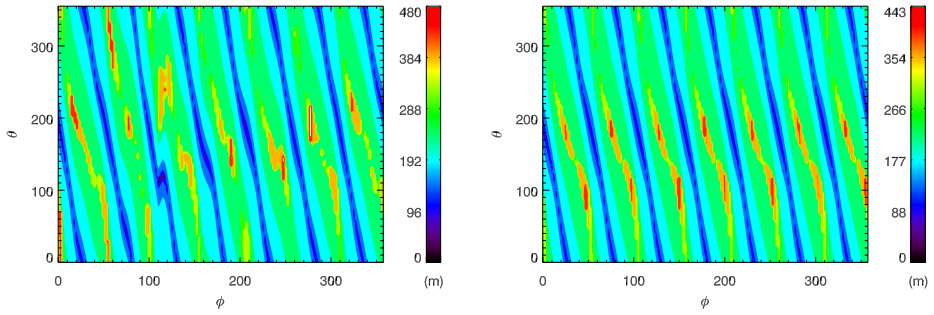

Figure 8.9: Map of the connection lengths of magnetic field lines touching the first wall for a typical 1.5 MA SHAx state (left) and same map obtained using only the amplitudes of the dominant $m = 1/n = 7$ and $m = 0/n = 7$ modes, indicating the ideal situation for a pure single helicity condition (right).

between the $m = 0$ and $m = 1$ modes depicted in fig.8.20 (see section 8.3.3). The localization is not perfect, due to the polluting effects of the secondary modes.

In order to understand what is the tendency for higher current plasmas, where the secondary modes will be lower according to present scaling, we have performed the same calculation including only the $m = 1/n = 7$ and $m = 0/n = 7$ modes in the FLiT input, that is simulating a pure single helicity condition. The result is shown in the right frame of Fig. 8.9. It can be seen that the long connection length region is now limited to two rows of inclined regions having an $n = 7$ periodicity, the first located at $\theta \simeq 90°$ and the second at $\theta \simeq 180°$.

The results described in this section give a new vision of the plasma boundary in the high performance SHAx states. Due to the toroidal coupling between the dominant $m = 1/n = 7$ mode, responsible for the achievement of a helical equilibrium, and its $m = 0$ counterpart, a set of $m = 0$ magnetic islands with a dominant $n = 7$ periodicity is formed on the reversal surface. Provided that the absolute value of the reversal parameter is small enough, that is the machine is operated with a shallow reversal, these islands intercept the first wall. Due to the regularity of the SHAx condition[6], the outcome is that the LCFS is not any more touching the first wall. On the contrary, the X-points formed between the $m = 0$ islands act as the X-point of a Tokamak divertor (a zoom of the divertor–like plasma–wall interaction already plotted

[6]During SHAx states no strong localized distortion of the plasma column due to mode locking [89] is found. And the regular $n = 7$ pattern, due to both the $m = 1$ shift and $m = 0$ islands, is evident in the right panel of fig.8.3.

in fig.8.3 can be seen in fig.8.10).
This condition is reminiscent of the island divertor concept which is being

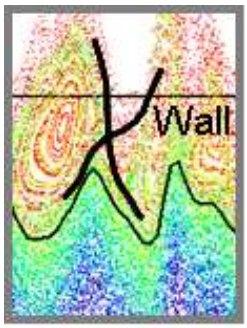

Figure 8.10: Zoom of the right Poincaré in fig.8.3, to underline the divertor idea and the role of the $m = 0$ islands and their X–points.

explored as a means of controlling plasma-wall interaction in stellarators. One is therefore led to infer that the special features of the plasma boundary in high current SHAx RFP plasmas could be exploited for building a divertor, similar in concept to the island divertor used in some stellarators. This could be achieved by locating divertor plates with appropriate pumping in the regions of strong interaction, which have been found to become more and more regular as the amplitude of the secondary modes is reduced, which is the trend experimentally observed as plasma current is increased.
Such an approach to plasma-wall interaction would require that the dominant $m = 0$ mode is stationary in time, and that one could control its island amplitude and phase. In section 8.3 the experiments done in order to use the feedback controlled saddle coils to control (or at least to interact with) the dominant $m = 1$ and $m = 0$ modes are presented. In fig.8.11 a sketch of the RFP (island) divertor is reproduced.

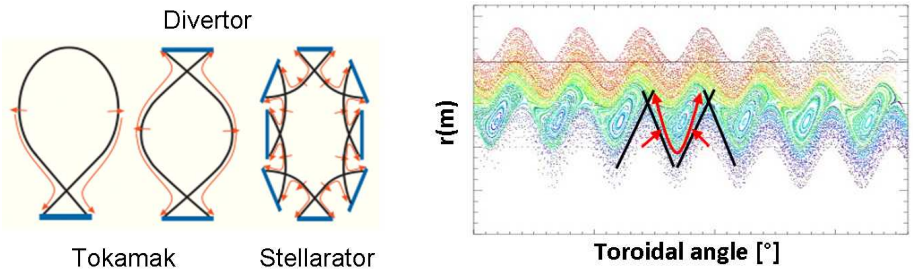

Figure 8.11: *Left:* A picture of the a divertor in Tokamak devices and of the Local Island Divertor in Stellarator devices. *Right:* The picture of the idea for a sort of island divertor in a RFP device.

8.3 External magnetic perturbations

High plasma current discharges and therefore the formation of the helical RFP SHAx states have been favored by of the improved control of the radial magnetic field at the edge, which in RFX–mod is obtained through a sophisticated system of 192 feedback–controlled saddle coils.
The feedback system is usually used to simulate a perfect conductive shell, therefore canceling the radial magnetic field of the perturbations at the wall. In the experimental campaign of 2010–2011 external magnetic perturbations have instead been used in order to control the magnetic boundary, by non–zero boundary conditions (BCs) on the radial magnetic field of the dominant $m = 1/n = 7$ and $m = 0/n = 7$ modes, [**?**, 90].
The magnetic boundary is characterized by the $m = 0/n = 7$ island chain and the plasma–wall interaction is strongly affected by its phase relation with the dominant $m = 1$ mode (responsible for the helical SHAx state deformation of the whole plasma column). The self–organized plasma properties, such as the toroidal coupling between the two modes, are the main mechanisms acting in the plasma. This must be taken into account when trying to externally interact with the plasma.

It is possible to act on the $m = 0$ island chain, if its properties are strongly correlated with the plasma self organization?
The idea of a divertor configuration for RFP boundary during helical states would require the control of the $m = 0$ island amplitudes and of their phase. Moreover, also the phase difference between the dominant $m = 0$ and $m = 1$ modes is relevant from the point of view of the plasma–wall interaction (see fig. 8.9 and section 8.2).
Experiments have therefore been performed in order to study which is the result of non–zero boundary conditions on both the $m = 0$ island amplitudes and phases. Because of the strong toroidal coupling acting in the plasma, we act both on the $m = 0/n = 7$ and on the $m = 1/n = 7$ modes.
As an example we present here two discharges: discharge 30177, where the non–zero boundary condition were only imposed on the $m = 1/n = 7$ mode; and the discharge 30200 where non–zero boundary condition were imposed also on the $m = 0/n = 7$ mode. Let us see the main features of both the discharges before analyzing more in detail the effect of the external perturbations on the mode amplitudes (section 8.3.1) and phases (section 8.3.3).

Discharge 30177.
Non–zero boundary condition on the $m = 1/n = 7$ mode

Vertical lines in fig.8.13 highlight the time instant when external non–zero boundary conditions (BCs) are applied at the boundary:

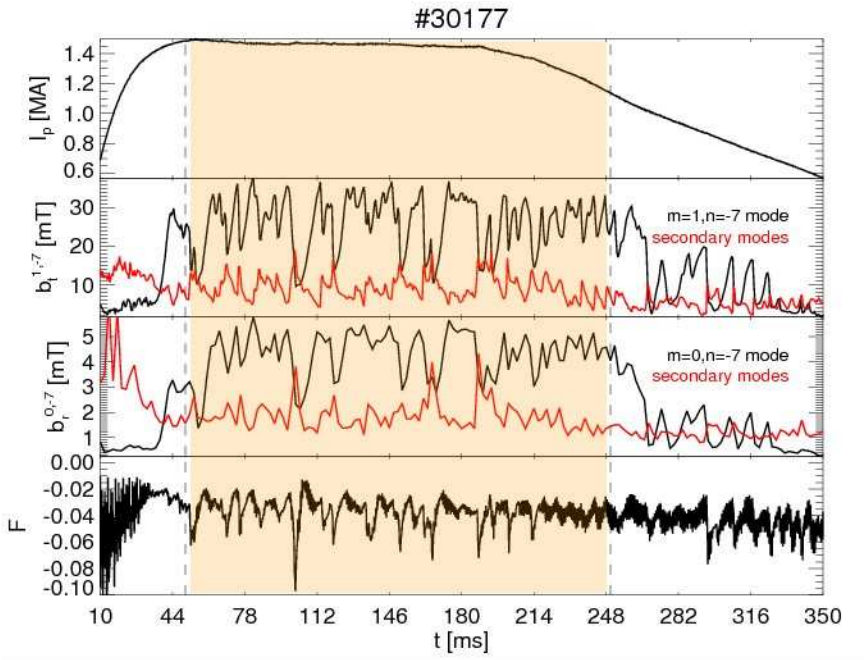

Figure 8.12: Time evolution of plasma quantities for the discharge 30177: non–zero boundary condition on the $m = 1/n = 7$ mode. Vertical lines highlight the time instants when non–zero boundary condition are applied. From top to bottom, the plotted plasma quantities are: the plasma current; the amplitude of the radial magnetic field of the dominant (black) and secondary modes (red) of the $m = 1$ and of $m = 0$ mode spectra; the time evolution of the F parameter. The radial magnetic field is the measured one outside the vaccum vessel for the $m = 1$ modes, and the reconstructed one on the resonant surface for the $m = 0$ modes.

- At time $t = 50$ ms non–zero BCs have been applied on the $m = 1/n = 7$ mode, with a reference amplitude $A_{1/7}$ =5 mT and a rotating frequency of 15 Hz.

In fig.8.12 one can see the time evolution of the plasma current, of the amplitude of the radial magnetic field of the dominant (black) and secondary modes (red) both for the $m = 1$ and $m = 0$ spectra, and the time evolution of the F parameter, always shallow, for the discharge 30177.
This experiment demonstrates how the global dynamics of the dominant $m = 1/n = 7$ mode can be modified by the external application (through the saddle coils) of a non–zero radial magnetic field $b_r^{1,7}$ as boundary condition. For example higher and longer QSH phases can be found. Good QSH phases can be found also for the $m = 0$ spectrum.

Discharge 30200.
Non–zero boundary condition on the $m = 1/n = 7$ and $m = 0/n = 7$ modes

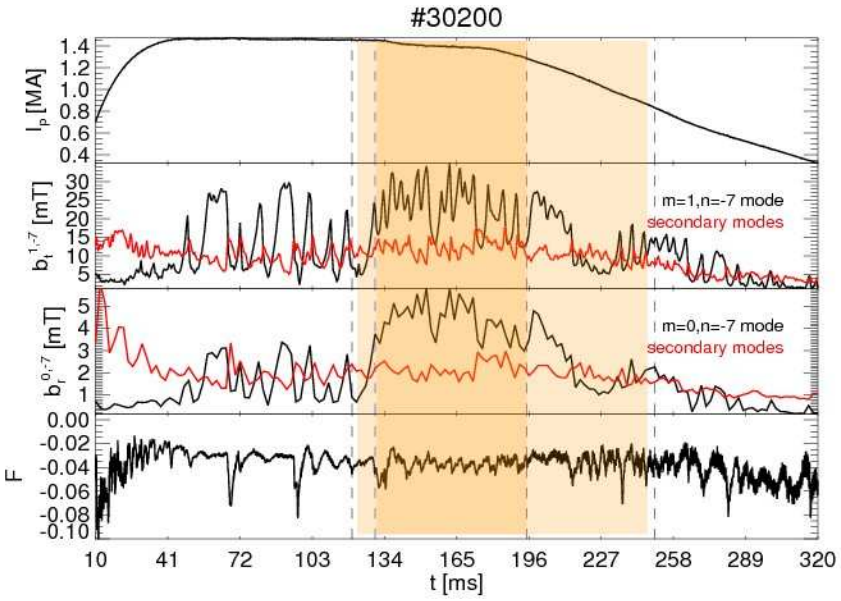

Figure 8.13: Time evolution of plasma quantities for the discharge 30200: non–zero boundary condition on the $m = 1/n = 7$ and $m = 0/n = 7$ modes. Vertical lines highlight the time instants when non–zero boundary condition are applied. From top to bottom, the plotted plasma quantities are: the plasma current; the amplitude of the radial magnetic field of the dominant (black) and secondary modes (red) of the $m = 1$ and of $m = 0$ mode spectra; the time evolution of the F parameter. The radial magnetic field is the measured one outside the vaccum vessel for the $m = 1$ modes, and the reconstructed one on the resonant surface for the $m = 0$ modes.

Vertical lines in fig.8.13 highlight the time instants when external non null references are applied at the boundary:

- In the time interval $120 < t < 250$ ms non–zero BCs have been applied on the $m = 1/n = 7$ mode, with a reference amplitude $A_{1/7}$ =5 mT and a rotating frequency of 15 Hz.

- In the time interval $130 < t < 195$ ms non–zero BCs have been applied on the $m = 0/n = 7$ mode, with a reference amplitude $A_{0/7}$ =4 mT, a phase difference $\Delta\phi = 0°$ with respect to the $m = 1/n = 7$ mode, and a rotating frequency of 15 Hz.

- In the time interval $195 < t < 250$ ms non–zero BCs have been applied on the $m = 0/n = 7$ mode, with a reference amplitude $A_{0/7}$ =4 mT, a

phase difference $\Delta\phi = -90°$ with respect to the $m = 1/n = 7$ mode, and a rotating frequency of 15 Hz.

The amplitude imposed at the boundary to the $m = 1/n = 7$ mode is chosen as to be roughly equal to the natural value that the radial magnetic field of this mode usually has at the edge. On the other side different boundary $|b_r^{0,7}| = A_{0/7}$ amplitudes of the $m = 0/n = 7$ mode have been tried.
Because of the toroidal coupling between the two dominant modes ($m = 1/n = 7$ and $m = 0/n = 7$), the ratio between their amplitudes at the edge is of the order of the aspect ratio ($\epsilon \equiv R/a \sim A_{1/7}/A_{0/7} \sim 4$ where ϵ stays for 'ratio', R is the major radius and a the minus radius of the vacuum chamber, [53]). The amplitude of the $m = 0/n = 7$ mode in the discharge 30200 has been chosen so that $A_{1/7}/A_{0/7} \sim 1.5\,\epsilon$.

In fig.8.13 one can see the time evolution of the plasma current, of the amplitude of the radial magnetic field of the dominant (black) and secondary modes (red) both for the $m = 1$ and $m = 0$ spectra, and the time evolution of the F parameter, always shallow, for the discharge 30200.
Also the $m = 0/n = 7$ mode dynamics can be modified by external application of a non–zero radial magnetic field $b_r^{0,7}$ as boundary condition.

In the next sections, the work made during the 2010–2011 experimental RFX–mod campaign in order to act both on the amplitude of the $m = 0$ magnetic islands (and therefore on the amplitude of the radial magnetic field $b_r^{0,7}$ on the reversal surface[7]) and on their phase difference with the dominant $m = 1$ mode is presented.
In particular, we want to study if and how the edge topology is modified (section 8.3.1 and 8.3.3) and how the edge plasma properties change by actively modifying the edge topology (section 8.3.2).

8.3.1 Amplitudes

Discharge 30177.
Non–zero boundary condition on the $m = 1/n = 7$ mode

To be able to increase the amplitude of the $m = 0$ islands (and therefore of the Scrape Off Layer), we need to act on the amplitude of the radial magnetic field of the $m = 0$ modes on the resonant surface (that is the reversal one). Due to the toroidal coupling with the $m = 1$ mode with the same toroidal mode number n (see chapter 5), one can increase the $m = 0/n = 7$ islands also acting on the $m = 1/n = 7$ mode.

[7] The island width is found to be proportional to the amplitude of the radial magnetic field on the resonant magnetic flux surface of the corresponding mode, [?, 13, 11].

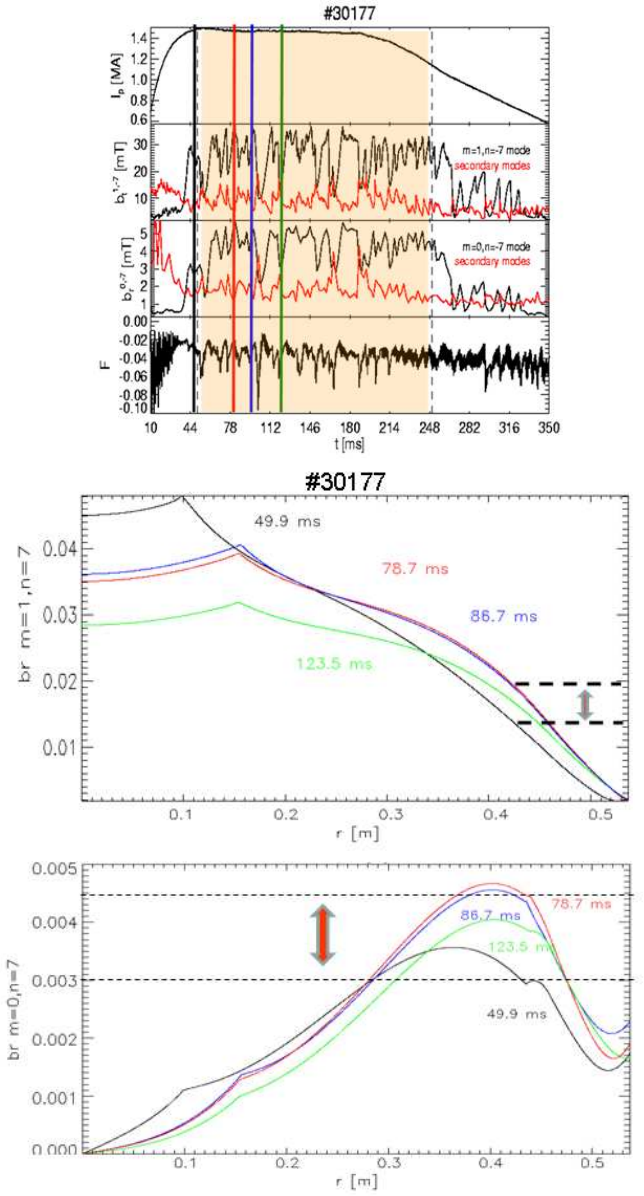

Figure 8.14: Shot 30177. *Top:* The same time evolution plots in fig.8.12 where colored lines mark the time instants of the harmonics reconstruction below. *Middle/Bottom:* The eigenfunction $b_r^{1,7}$ and $b_r^{0,7}$ of the radial magnetic field related to the $m = 1/n = 7$ (middle) and $m = 0/n = 7$ (bottom).The black curves are related to a time instant where zero boundary condition were applied to all the modes, whereas the coloured ones are related to time instants where non–zero boundary condition were applied to the $m = 1/n = 7$ mode. The first wall is at $a = 0.459$ m.

This is what is done in this discharge. The radial magnetic field eigenfunctions are plotted in fig.8.14, using the harmonics reconstruction discussed in [53] (and chapter 3). We can see that:

- An external non–zero boundary condition imposed at the edge on the $m = 1/n = 7$ mode changes the amplitude of the whole $b_r^{1,7}$ eigenfunction profile.
  In fig.8.14 (middle) the eigenfunction of the radial magnetic field related to the $m = 1/n = 7$ mode are plotted for different time instants. The black curve is the vanishing boundary condition case, as a reference time instant.

- The external non–zero boundary condition imposed at the edge on the $m = 1/n = 7$ mode increases the amplitude of the $b_r^{1,7}$ eigenfunction on the reversal surface, and this is reflected on the amplitude of the $b_r^{0,7}$ eigenfunction due to the toroidal coupling.
  In fig.8.14 (bottom) the eigenfunction of the radial magnetic field related to the $m = 0/n = 7$ mode is plotted for the same time instants of fig.8.14 (middle). The amplitude of the $b_r^{0,7}$ eigenfunction on the reversal surface is increased with respect to the vanishing boundary reference case in black.

We use the Poincaré plot reconstruction to look at the magnetic topology related to the eigenfunctions plotted in fig8.14.
In fig.8.15 we choose to compare the magnetic topology at $t = 49$ ms (zero boundary condition reference, black curve in fig.8.14) and at $t = 86.7$ ms (the blue curve in fig.8.14). The $m = 0$ island elongation due to non–zero boundary condition to the dominant $m = 1$ mode can be clearly seen in the Poincaré plot, that are shown on the same radial scale.

Discharge 30200.
Non–zero boundary condition on the $m = 1/n = 7$ and $m = 0/n = 7$ modes

Fig.8.16 is the analogue of fig.8.14, for the shot 30200 where non–zero boundary condition is imposed also to the $m = 0/n = 7$ mode. The eigenfunction profiles of the $m = 1/n = 7$ (middle) and $m = 0/n = 7$ (bottom) are plotted for different time instants (with different colours). The black curve is the vanishing boundary condition case for comparison.

From the magnetic topology side, the application of these non-zero boundary condition on both the $m = 1/n = 7$ and $m = 0/n = 7$ modes are expected to have two main effects on the $m = 0$ pattern: 1) a direct contribution to the $m = 0/n = 7$ mode amplitude by the externally applied reference on the

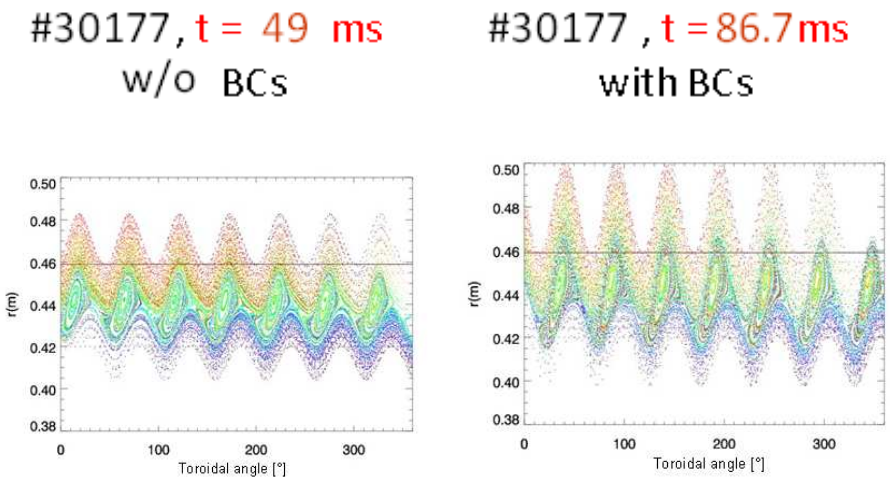

Figure 8.15: Magnetic topology reconstructions made using only the $n = 7$ harmonic for the 30177 discharge on the external equatorial plane ($\theta = 0$). *Left:* magnetic topology related to a time instant where zero boundary condition were applied to all the modes (black curve in fig.8.14). *Right:* magnetic topology related to a time instant ($t = 86.7$ ms, blue curve in fig.8.14) where non–zero boundary condition were applied to the $m = 1/n = 7$ mode.

related harmonic; 2) a further contribution coming from the toroidal coupling with the $b_r^{1,7}$ eigenfunction.
We can see this in fig.8.16 :

- The amplitude of the $b_r^{0,7}$ eigenfunction is increased on the reversal surface, as it is the $b_r^{1,7}$ eigenfunction in the same position. Comparing fig.8.14 and fig.8.16, the main contribution to this is probably due to the non–zero boundary condition on the $m = 1/n = 7$ mode.

- What is peculiar of the application of the non–zero boundary reference to the $m = 0/n = 7$ mode is the shape of the $b_r^{0,7}$ eigenfunction. It is easy to see comparing the coloured lines in fig.8.16 with the black one.

The superpositions of these two effects produces a larger radial extension of the $m = 0$ island chain with respect to discharge 30177 (compare fig.8.15 and fig.8.17).
The effect on the magnetic topology can be seen in the Poincaré plots in fig.8.17: on the right the zero boundary condition case (black curve in fig.8.16, vanishing references are applied to all the modes) is plotted; on the left a non–zero boundary condition case (at $t = 165$ ms, the blue curve in fig.8.16, with non–zero boundary condition to both the $m = 1/n = 7$ and $m = 0/n = 7$ modes) is plotted. One can see both the increased island

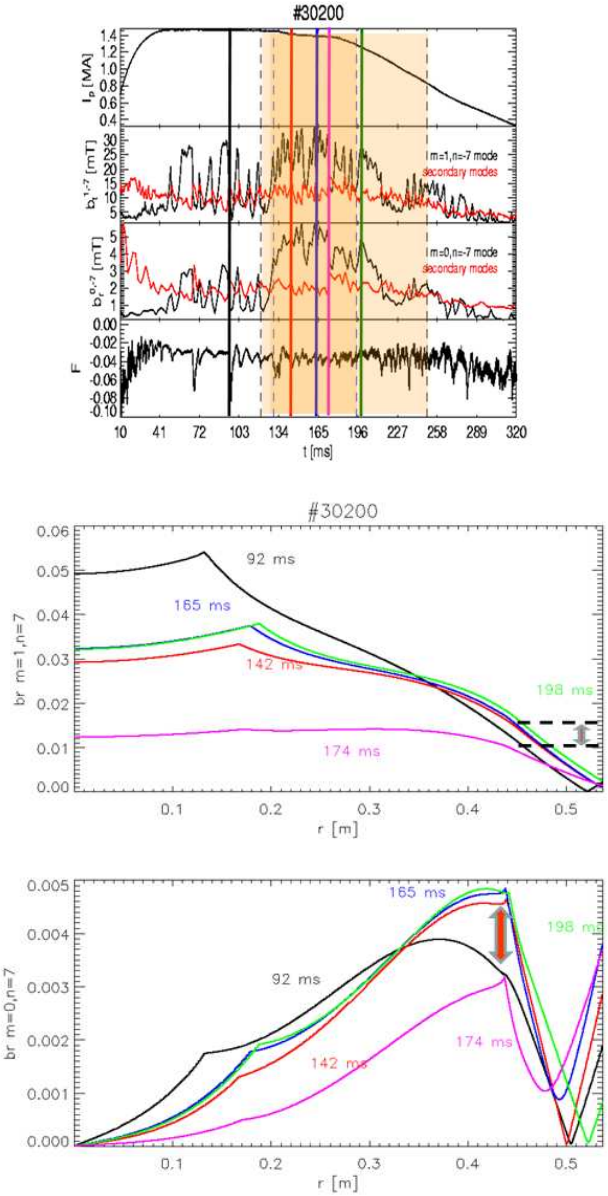

Figure 8.16: Shot 30200. *Top:* The same time evolution plots in fig.8.13 where colored lines mark the time instants of the harmonics reconstruction below. *Middle/Bottom:* The eigenfunction $b_r^{1,7}$ and $b_r^{0,7}$ of the radial magnetic field related to the $m = 1/n = 7$ (middle) and $m = 0/n = 7$ (bottom).The black curves are related to a time instant where zero boundary condition were applied to all the modes, whereas the coloured ones are related to time instants where non–zero boundary condition were applied to both the $m = 1/n = 7$ and $m = 0/n = 7$ modes. The first wall is at $a = 0.459$ m.

amplitudes and their change in shape. The Poincaré plot on the top are related to the pure SH case, whereas the ones below reproduce the effects of the secondary modes.

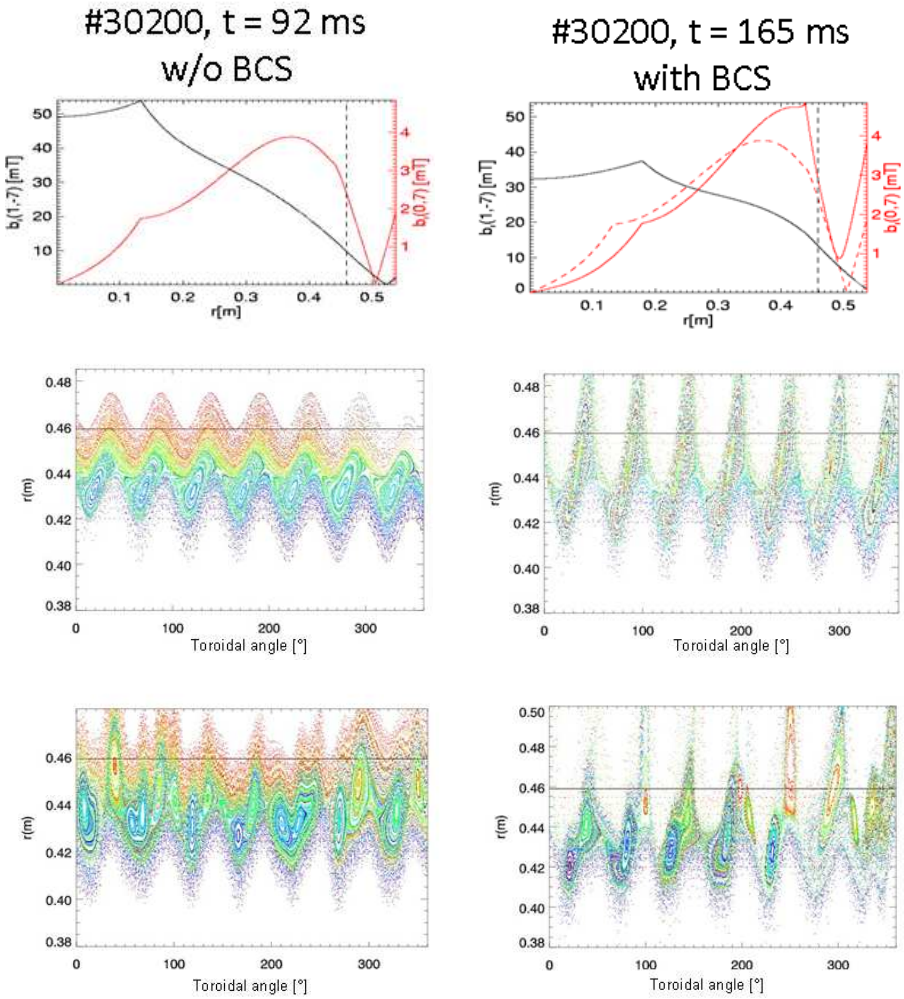

Figure 8.17: Magnetic topology reconstructions for the 30200 discharge on the external equatorial plane ($\theta = 0$). *Left:* magnetic topology related to a time instant where zero boundary condition were applied to all the modes (black curve in fig.8.16). *Right:* magnetic topology related to a time instant ($t = 92$ ms, blue curve in fig.8.16) where non–zero boundary condition were applied to both the $m = 1/n = 7$ and $m = 0/n = 7$ modes. *From top to bottom:* eigenfunction amplitudes of the dominant modes. The dashed line on the right is related to the 92ms time instant for comparison. A vertical line marks the resonant surface of the $m = 0$ modes; Poincaré reconstructions made using only the $n = 7$ harmonic; Poincaré reconstruction of the edge topology made using all the harmonics

The consequence of this different magnetic topology of the SOL is under investigation. In the next section we report some of the consequences on the edge measurements.

8.3.2 Effect of BCs application on the plasma properties

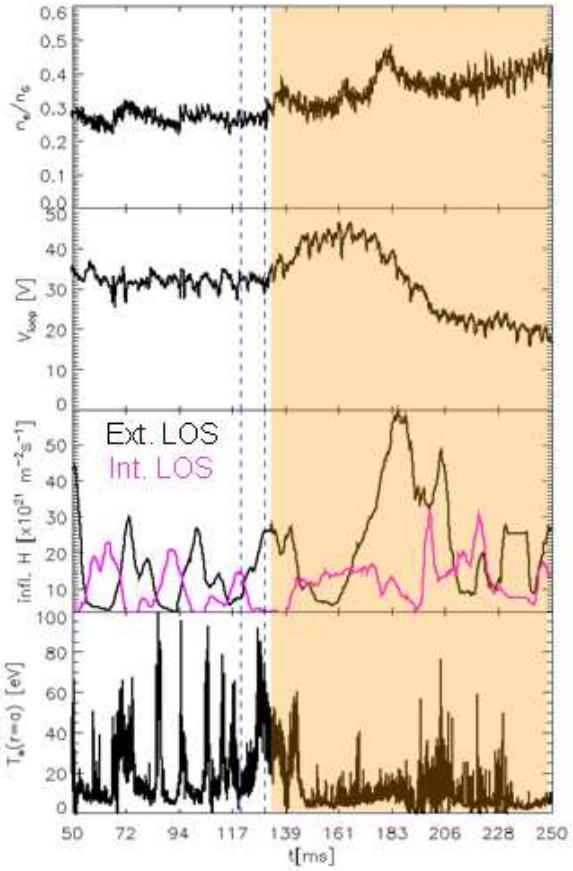

Figure 8.18: Time evolution of some experimental measurements during the discharge 30200. *From top to bottom:* The ratio n/n_G, where n is the density measured by the interferometer [91, 92] and n_G the Greenwald density, [11]; the loop voltage, as a measure of the power needed to sunstain the discharge; two H_α line emission as a measure of the plasma-wall interaction; the edge temperature measured by a fixed triple probe, [93].

The active modification of the edge magnetic topology turned out to be correlated with a turn of reproducible phenomena linked in a direct or indirect way to an increased plasma wall interaction. Nonetheless the possibility to externally impose the radial extension of the $m = 0$ magnetic islands at

the edge enable us to study the cause and effect relation of the complex edge dynamics.
For the sake of simplicity we consider again the discharge 30200 whose main features have been already presented in the previous section.
In fig.8.18 the application of the BCs can be easily associated to a rather abrupt variation of the averaged density and of the loop voltage needed to sunstain the discharge (first and second plot on the right). As already mentioned, an increased plasma-wall interaction can explain both these experimental observations since in RFX-mod the graphite first wall is a natural hydrogen repository and represents an effective fueling system [94, 95]. On the other side, it's worth noting that this technique allows to sunstain QSH states at higher n_e/n_G values (up to 0.5 in this case) with respect to the spontaneous QSH states (that usually disappear beyond $n_e/n_G \geq 0.3$).
The last two plots in fig.8.18 show the time evolution of two H_α line emission and the edge temperature (measured by a fixed triple probe, [93]). They confirm in a even more evident way the aforementioned mechanism: the BCs application causes a larger interaction with the graphite wall, the hydrogen stored is released and ionized, creating a dense and cold edge.
According to this picture, the reconstruction of the whole density profile obtained by the multichord interferometer in fig.8.19 displays a markedly hollow shape associated to the application of the BCs. Two interesting observations have to be pointed out:
1) whilst the edge density increases up to 3-4 times upon the BCs application (but a more precise estimation would need a better diagnostic coverage in that region), the central density appears almost unperturbed. A possible explanation could be that a more defined $m = 0$ pattern features better particle confinement properties (and thus the hydrogen influx from the wall would accumulate only at the edge). On the other side, also comparing the two Poincaré plots shown in fig.8.17, one can easily catch how the BCs application enlarges the extension of the more chaotic region in between the islands, probably featuring short connection lenght that could rapidly drive the particles to the wall preventing an effective core fueling;
2) the last two plots in fig.8.19 show in more detailed way the relation between the edge topology modification and the edge density profiles. In particular, comparing two time instants (before and after the BCs application) of the same discharge it is possible to highlight how a smoother density profile correspond to a smoother shape of the $m = 0, n = 7$ eigenfunction and also how in the case of BCs application the maxima of the two curves (density profile and $m = 0, n = 7$ eigenfunction) are located very close radially region.

These observations could help clarifying the role of the edge magnetic topology and, in particular, of the $m = 0$ islands in defining the plasma properties and the complex (interconnected) mechanisms regulating a crucial

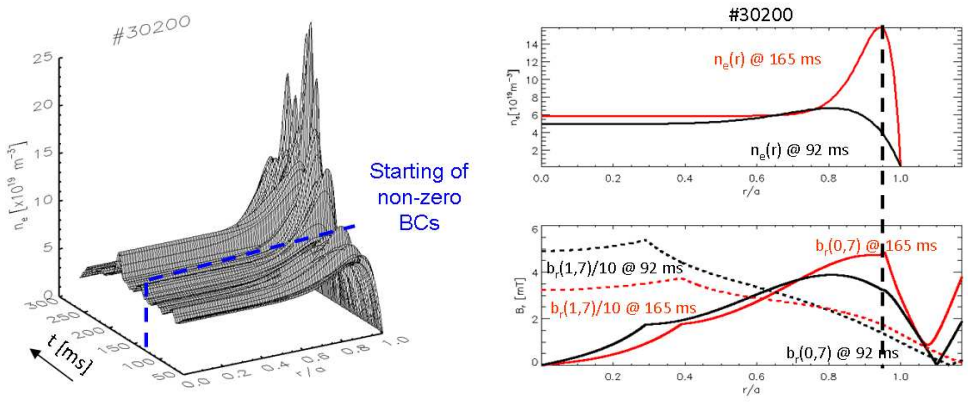

Figure 8.19: Discharge 30200. *Left:* The density profile and its time evolution obtained by the multichord interferometer, [91, 92]. *Right:* The edge density profiles and the eigenfunction of the magnetic perturbation at two time instants: 92 ms (zero boundary condition applied to all the modes) and 165 ms (with non–zero boundary condition to the $m = 0/n = 7$ and $m = 1/n = 7$ modes.)

part of the RFP physics, the edge transport and the plasma-wall interaction. An extrapolation of these results towards the development of an RFP divertor concept will be subsequent.

8.3.3 Phase relations

As already said, the idea of a divertor configuration for RFP boundary during helical states would require the control of the $m = 0$ island amplitudes and of their phase; moreover, also the phase difference between the dominant $m = 0$ and $m = 1$ modes is relevant from the point of view of the plasma–wall interaction (see fig. 8.9).
In this section we analyze the effect on the phases of the $m = 0$ and $m = 1$ modes and on their phase difference, when non–zero BCs are applied to the dominant modes.

A question arises. Which is the correct phase of the modes to be considered?
We can consider both the (m, n) harmonics of the radial magnetic field (see

equation (2.146))[8]:

$$B^r = \frac{1}{\sqrt{g}}\left(\frac{\partial \psi_T}{\partial \varphi} - \frac{\partial \psi_P}{\partial \vartheta}\right) \tag{8.1}$$

$$\Downarrow$$

$$b^r_{mn} = \left(\frac{1}{\sqrt{g}}\right)_{mn} i\,(n\psi_T^{mn} - m\psi_P^{mn}) \tag{8.2}$$

or the harmonics of the related magnetic flux which can be written as (see equation (9.21)):

$$\widehat{b}^r_{mn} = i\,(n\psi_T^{mn} - m\psi_P^{mn}) \tag{8.3}$$

$$\Downarrow$$

$$\widehat{b}^r_{1,7} = i\,(7\,\psi_T^{1,7} - \psi_P^{1,7}) \tag{8.4}$$

$$\widehat{b}^r_{0,7} = i\,7\psi_T^{0,7} \tag{8.5}$$

for the dominant modes in RFX–mode.
Due to the toroidal coupling between the harmonics of the fluxes $\widehat{b}^r_{mn}$ and of the metrics $\left(1/\sqrt{g}\right)_{mn}$, for the radial magnetic field one can write[9]:

$$b^r_{1,7} = \frac{1}{\sqrt{g_0}}\,\widehat{b}^r_{1,7} + \frac{1}{\sqrt{g_1}}\,\widehat{b}^r_{0,7} \tag{8.6}$$

$$b^r_{0,7} = \frac{1}{\sqrt{g_0}}\,\widehat{b}^r_{0,7} + \frac{1}{\sqrt{g_1}}\,\widehat{b}^r_{1,7} \tag{8.7}$$

The second term in both the equations (8.6)–(8.7) is the term due to the toroidal coupling. Remembering fig.8.2 [10] one can understand that at least during QSH states the contribution of $\widehat{b}^r_{0,7}$ to $b^r_{1,7}$ is not so big, whereas the contribution of $\widehat{b}^r_{1,7}$ to $b^r_{0,7}$ is the dominant one. A statistical study of the phase difference between the radial magnetic fields $b^r_{1,7}$ and $b^r_{0,7}$ is plotted in fig.8.20, where the importance of the toroidal coupling emerges in the constancy of the phase difference.
The contribution to the phase of the fluxes $\widehat{b}^r_{1,7}$ and $\widehat{b}^r_{0,7}$ in eq.(8.4)–(8.5) arises both from a toroidal coupling intrinsic in the toroidal Newcomb–like equation solved for the fluxes (in chapter 3) and a non–linear coupling between the dominant and the secondary modes (similar to the locking that arises also in cylindrical geometries, [89]).

Which are the phases that better describe the effect on the magnetic topology is not yet well understood. The phase difference between the dominant $m = 1$ and $m = 0$ modes related to the radial magnetic field b^r_{mn} is

[8] We consider the 2π part of the computed fluxes.

[9] The toroidal coupling has been explained in chapter 3 and 5. We neglect in these formulas the contribution that arises from the $(m, n) = (2, n)$ and $(m, n) = (-1, n)$ harmonics. The harmonics of the Jacobian are written in appendix B.2.3 for the w^i coordinates.

[10] For a more formal prof see [53].

always constant (even if it depends on the poloidal angle, as we will now explain), whereas the phase difference related to the fluxes $\widehat{b}^r_{mn}$ seems to be more easily affected by non–zero BCs. In the next sections, showing the effect of non–zero BCs, we will relate it to the Poincaré plots that we consider to well reproduce the magnetic topology.

The physical meaning of the phases

We write the Fourier decomposition of any quantity A, which can be the radial magnetic field B^r or the related radial magnetic flux $\widehat{b}$:

$$A = \sum_{mn} a_{mn}\, e^{i(m\vartheta - n\varphi + \phi_{mn})} = \sum_{mn} A_{mn}\, \cos(m\vartheta - n\varphi + \phi_{mn}) \tag{8.8}$$

This is a bi–dimensional Fourier decomposition (both on the poloidal angle ϑ and on the toroidal angle φ).
Let us explain the physical meaning of the real number ϕ_{mn}. First we write the harmonics of the two dominant mode in an explicit way:

$$a_{1,7}\cos(\vartheta - 7\varphi + \phi_{1,7}) \tag{8.9}$$
$$a_{0,7}\cos(-7\varphi + \phi_{1,0}) \tag{8.10}$$

As one can see the harmonics $a_{0,7}$ of the perturbation is uniform on the poloidal plane (does not depend on the poloidal angle).
The maximum of the perturbation must vanish the cosine function. Therefore:

- Fixing the toroidal angle ($\varphi = \varphi_{fix}$) one looks at the perturbation on the poloidal plane. The number ϕ_{mn} in this case represents the poloidal angle ϑ of the first maximum of the perturbation, which is:

$$\vartheta = 7\varphi_{fix} - \phi_{1,7} \tag{8.11}$$
$$\vartheta = 7\varphi_{fix} - \phi_{0,7} \tag{8.12}$$

  for the two dominant modes.

- Fixing the poloidal angle ($\vartheta = \vartheta_{fix}$) one looks at the perturbation in the toroidal direction. The number ϕ_{mn} in this case represents the toroidal angle φ of the first maximum of the perturbation, which is:

$$\varphi = (\vartheta_{fix} + \phi_{1,7})/7 \tag{8.13}$$
$$\varphi = (\vartheta_{fix} + \phi_{0,7})/7 \tag{8.14}$$

  for the two dominant modes.

To study the relation between the two dominant modes we can look to what we called their *phase difference* $\Delta\phi$, which is not simply $\phi_{1,7} - \phi_{0,7}$: we use the symbol $\Delta\phi$ in this section for the angle between the maxima of the two modes and therefore it depends on the angles:

- Fixing the toroidal angle ($\varphi = \varphi_{fix}$) one looks at both the perturbations on the poloidal plane. The angle $\Delta\phi$ between their maxima is:

$$\Delta\phi = \vartheta + \phi_{1,7} - \phi_{0,7} \tag{8.15}$$

- Fixing the poloidal angle ($\vartheta = \vartheta_{fix}$) one looks at both the perturbations in the toroidal direction. The angle $\Delta\phi$ between their maxima is:

$$\Delta\phi = \vartheta_{fix} + \phi_{1,7} - \phi_{0,7} \tag{8.16}$$

From an operative point of view we stress that we use the $w^i = (r, \vartheta, \varphi)$ coordinates used for the harmonics reconstruction[11]. We remind that the poloidal angle of this coordinate system is defined to have its zero value on the internal equatorial plane, which means that it differs of an angle π with respect to the machine poloidal angle that we call θ (see fig.1.4) and which has its zero value on the external equatorial plane.

The magnetic topology related to $\Delta\phi$ at different fixed poloidal angles ($\vartheta = \vartheta_{fix}$) is shown in the following of this section, both for the zero and non–zero BCs condition cases.

Zero–boundary condition.
Discharge 30200 at $t = 92$ ms.

Due to toroidal coupling, the $m = 1/n = 7$ and $m = 0/n = 7$ modes have a very clear phase relationship. This is displayed in Fig. 8.20, where the phase difference $\Delta\phi$ between the $m = 0/n = 7$ mode and the $m = 1/n = 7$ mode in RFX-mod is shown as a function of the phase of the $m = 1/n = 7$ mode for a large set of discharges, in time intervals where a strong quasi-single helicity state is observed. It can be seen that the two modes have an almost constant phase difference equal to 0. The phases concern the radial magnetic field component on the *internal* equatorial plane ($\theta_{fix} = \pi$), and have been computed at the respective resonant surfaces.

[11] see section 3.1.1 and appendix B.2.3 for the definition of the $w^i = (r, \vartheta, \varphi)$ coordinate system.

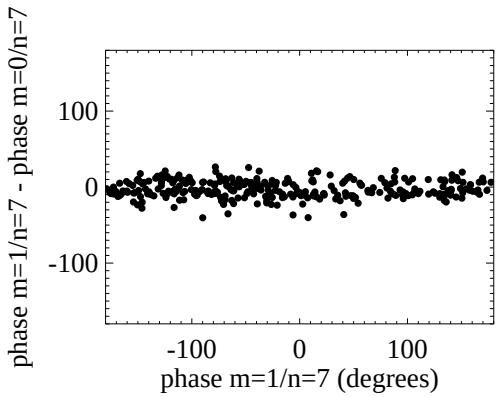

Figure 8.20: Phase difference $\Delta\phi$ on the *internal equatorial plane* ($\theta_{fix} = \pi$), between the $m = 1/n = 7$ mode and the $m = 0/n = 7$ mode plotted as a function of the phase of the $m = 1/n = 7$ mode for SHAx states obtained in 1.5 MA discharges. The phases concern the radial magnetic field component, b^r_{mn} in eq.(8.6)–(8.7).

A phase difference $\Delta\phi = 0$ means that the island O–points of the $m = 1/n = 7$ mode correspond to the O–points of the $m = 0/n = 7$ islands. A $\Delta\phi = 0$ phase difference is statistically found to be related to the internal equatorial plane. But due to the fact that the $m = 0$ modes are uniform on the poloidal plane whereas the $m = 1$ modes are not, the phase difference $\Delta\phi$ changes its value on the poloidal plane at different poloidal angles. E.g. on the *external* equatorial plane ($\theta_{fix} = 0$) the phase difference is $\Delta\phi = \pi$, which means that the $m = 0/n = 7$ island O–points are in correspondence of the $m = 1/n = 7$ island X–points. This magnetic topology corresponds to the plasma–wall interaction discussed in section 8.2.
Therefore, on the poloidal plane the phase difference $\Delta\phi$ changes with the poloidal angle, and this is reflected on the magnetic topology and on the plasma–wall interaction (as seen in fig.8.9). The magnetic topology related to the dominant $m = 0$ and $m = 1$ modes at four different poloidal angles is shown in fig.8.21, where four Poincaré plot are computed at the same time instant and at:

- $\theta_{fix} = 0$ and therefore $\Delta\phi = \pi$
- $\theta_{fix} = \frac{\pi}{2}$ and therefore $\Delta\phi = \frac{\pi}{2}$
- $\theta_{fix} = \pi$ and therefore $\Delta\phi = 0$
- $\theta_{fix} = \frac{3\pi}{2}$ and therefore $\Delta\phi = \frac{\pi}{2}$

One can see that the magnetic topology is tightly correlated to the position of the $m = 0$ island with respect to the global helical deformation due to the $m = 1$ dominant mode (with the $m = 0$ island on the top or on the bottom

of the $m = 1$ edge deformation).

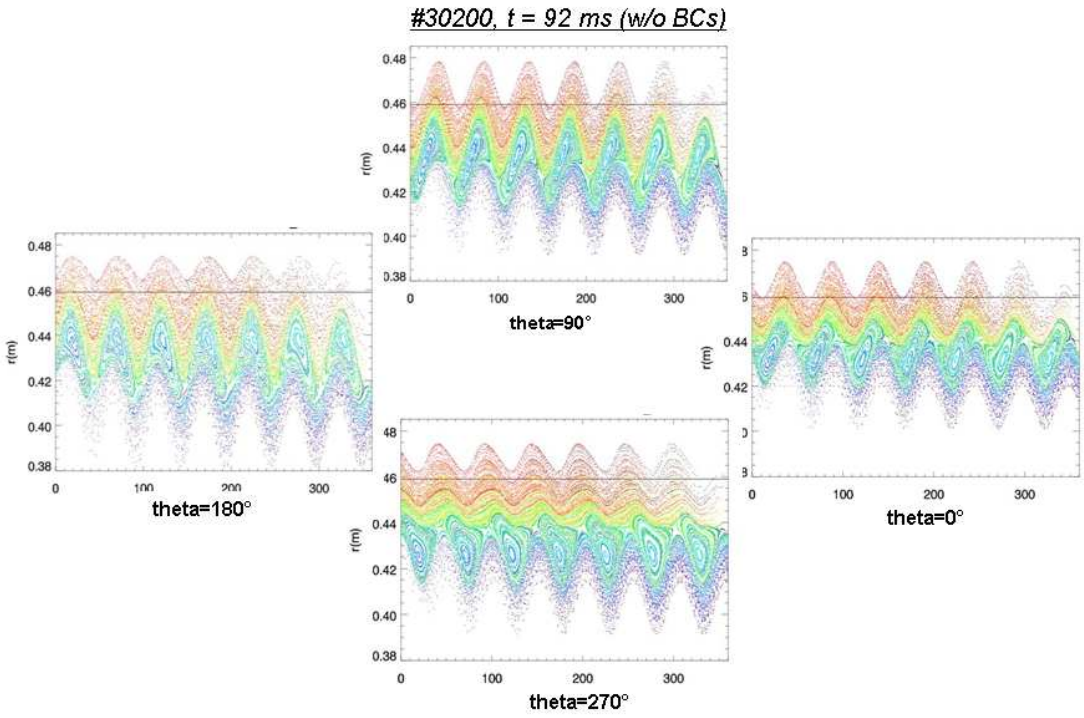

Figure 8.21: Discharge 30200 at $t = 92$ ms, therefore when zero boundary condition are imposed by the feedback control on all the modes. The magnetic topology at different poloidal angles and therefore related to different phase difference $\Delta\phi$ between the $m = 0/n = 7$ mode and the $m = 1/n = 7$ mode in RFX-mod. A phase difference $\Delta\phi = 0$ is related to the internal equatorial plane, $\theta_{fix} = \pi$.

Non–zero boundary condition.
Two examples.

The phase difference $\Delta\phi$ between the $m = 0/n = 7$ mode and the $m = 1/n = 7$ mode is therefore an important ingredient to be understood to study the plasma–wall interaction in RFX–mod.
In order to better understand the role of $\Delta\phi$ we try to change the natural phase difference, that is equal to 0 on the internal equatorial plane (fig.8.20)[12]. We do this again using the feedback controlled saddle coils to

[12] The natural $\Delta\phi$ brings a higher plasma–wall interaction between $90° < \theta < 180°$, see fig.8.20. Changing the phase relation $\Delta\phi$ between the $m = 0/n = 7$ and the $m = 1/n = 7$ modes, we could expect to change the plasma–wall interaction on the poloidal plane, and even to bring the higher interaction in front of the measurements, usually located around the external equatorial plane ($\theta = 0$).

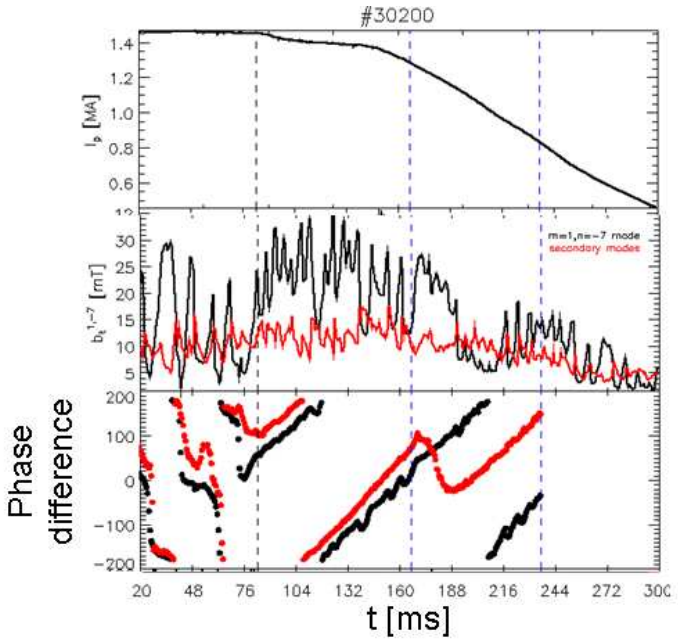

Figure 8.22: Time evolution of plasma quantities for the discharge 30200. *Top, middle:* the plasma current and the amplitude of the radial magnetic field of the dominant $m = 1$ mode that are already in fig.8.13. *Bottom:* the phases of the $\widehat{b}^r_{mn}$ flux for the $m = 1/n = 7$ (black) and $m = 0/n = 7$ (red) modes in eq.(8.4)–(8.5) computed at the resonant surface. The phase difference between the two is evident in the two time windows: $\Delta\phi = 0$ for $t < 195$ ms, while $\Delta\phi = \pi/2$ between $195ms < t < 250ms$.

impose a non–zero boundary condition to the radial magnetic field of the $m = 0/n = 7$ and the $m = 1/n = 7$ modes, with a chosen phase difference between them.
We present two examples:

- The second time window ($195ms < t < 250ms$) of the discharge 30200 (fig.8.13, right), where a phase difference $\Delta\phi = \pi/2$ was imposed between the $m = 0/n = 7$ and the $m = 1/n = 7$ modes.
  In fig.8.22 one can see that in this time window the plasma current was already decreasing, so the discharge dynamics probably makes the analysis more difficult. In any case, the applied phase difference between the modes appears clearly in fig.8.22 (bottom) for the fluxes $\widehat{b}^r_{mn}$.

- The discharge 30184. Another, more difficult, example.
  This example, defined in fig.8.23, is more difficult because the phase difference $\Delta\phi$ is continuously changing. The two modes are in fact rotating in opposite directions with respect to the toroidal angle, as

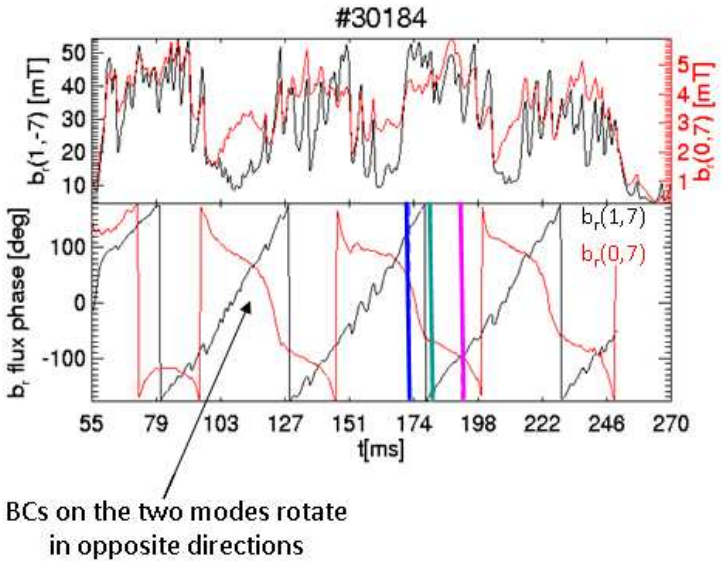

Figure 8.23: Time evolution of plasma quantities for the discharge 30184: non–zero boundary condition on the $m = 1/n = 7$ and $m = 0/n = 7$ modes. *Up:* the time evolution of the amplitude of the radial magnetic field at the edge (for the $m = 1/n = 7$ (black) and $m = 0/n = 7$ (red) modes). *Down:* the time evolution of phases of the fluxes $\widehat{b}^r_{mn}$ (for the $m = 1/n = 7$ (black) and $m = 0/n = 7$ (red) modes) computed at the resonant surface. The dynamics of the phase difference $\Delta\phi$ is related to the fact that the two modes are rotating in opposite direction in the plasma.

imposed by the feedback–controlled system.
Even if the dynamics of the applied $\Delta\phi$ is clear in fig.8.23 (bottom) for the fluxes $\widehat{b}^r_{mn}$, this can not be clearly seen on the magnetic topology which is reproduced in the Poincaré plots in fig.8.24. They are performed at different time instants (marked by colored lines in fig.8.23 bottom) when different $\Delta\phi$ should characterized the topology on the external equator plane ($\theta = 0$).

It is worth noting that a modulation is present the time evolution of the amplitude of the radial magnetic field at the edge of both the the $m = 1/n = 7$ and $m = 0/n = 7$ modes (black and red in fig.8.23 middle, respectively). This modulation is present in the whole radial domain looking at the eigenfunction reconstructions, therefore it seems that not just the $m = 1$ mode affects the $m = 0$ due to the toroidal coupling, but even the viceversa.

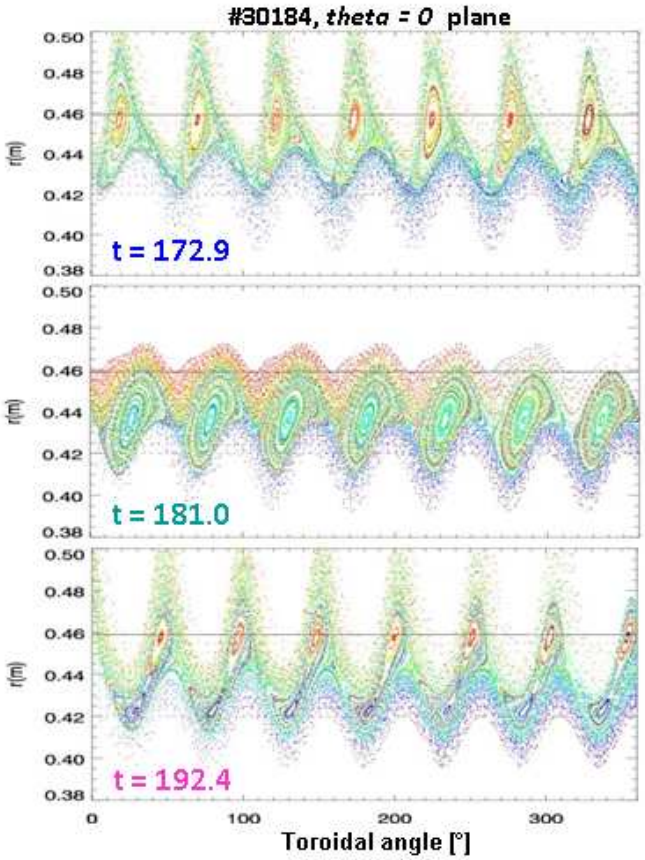

Figure 8.24

Phase modifications appear more difficult than acting on the $m = 0$ island amplitudes. Data analysis is still in progress: can we exploit this method to externally control the edge plasma dynamics?

Chapter 9

Detailed calculations on...

One can consider this chapter part of the thesis. One can find here details of calculation useful to better understand the main text of the thesis in the previous sections. Moreover detailed calculations have been useful for the implementation of formulas in SHEq–code and could be useful for future work that may want to use the details of this thesis.

9.1 On the fluxes and their derivatives

We write some common way of writing the fluxes and their complex harmonics. Especially we try to link one to the other in the following subsections.

9.1.1 On how to compute the helical flux χ

In the text (section 4.1), we write for the helical flux χ the same equations here collected in eq.(9.2)–(9.4):

$$\begin{aligned}
\chi &= m\psi_P - n\psi_T && (9.1)\\
&= [m\psi_{P,0} - n\psi_{T,0}](r) + [m\psi_P^{m,n} - n\psi_T^{m,n}](r)\, e^{iu} + c.c. && (9.2)\\
&= \chi_0(r) + \chi^{m,n}(r)\, e^{iu} + c.c. && (9.3)\\
&= \chi_0(r) + 2|\chi^{m,n}|(r)\ \cos(u + \phi_\chi) && (9.4)
\end{aligned}$$

About the complex conjugation of the fluxes one can see appendix C.1.
Here we want to show how to compute the amplitude $|\chi^{m,n}|(r)$ and the phase ϕ_χ of the perturbed helical flux $\chi^{m,n}$ (that derive from the sum of two complex numbers, $\chi_{m,n} = m\psi_P^{m,n} - n\psi_T^{m,n}$) in terms of amplitudes and phases of the harmonics of the poloidal and toroidal fluxes.
Using the results of appendix C.2 for the sum between two complex numbers,

we write [1] :

$$|\chi_{m,n}| = C \tag{9.14}$$
$$\phi_\chi = \gamma \tag{9.15}$$

and (using eq.(C.32)–(C.33) and eq.(9.12)–(9.13)): from eq.(C.32)–(C.33):

$$\begin{cases} |\chi_{m,n}| = \left[n^2|\psi_T|^2 + m^2|\psi_T|^2 - 2mn|\psi_T||\psi_P|\cos(\phi_{\psi_T} - \phi_{\psi_P})\right]^{1/2} \\ \phi_\chi = \arctan\left[\frac{m|\psi_P|\sin\phi_{\psi_P} - n|\psi_T|\sin\phi_{\psi_T}}{m|\psi_P|\cos\phi_{\psi_P} - n|\psi_T|\cos\phi_{\psi_T}}\right] \\ |\psi_T| \equiv |\psi_T^{m,n}| \equiv |\psi_T^{m,n}|(r) \qquad |\psi_P| \equiv |\psi_P^{m,n}| \equiv |\psi_P^{m,n}|(r) \end{cases} \tag{9.16}$$

where poloidal and toroidal fluxes are used with the same notation:

$$\begin{aligned} \psi_T(r,\theta,\varphi) &= \psi_{T,0}(r) + \psi_T^{m,n}(r)\, e^{i\,(m\theta - n\varphi)} \\ &= \psi_{T,0}(r) + |\psi_T^{m,n}|\, e^{i\,\phi_{\psi_T}}\, e^{i\,(m\theta - n\varphi)} \\ \psi_P(r,\theta,\varphi) &= \psi_{P,0}(r) + \psi_P^{m,n}(r)\, e^{i\,(m\theta - n\varphi)} \\ &= \psi_{P,0}(r) + |\psi_P^{m,n}|\, e^{i\,\phi_{\psi_P}}\, e^{i\,(m\theta - n\varphi)} \end{aligned} \tag{9.17}$$

The helical flux in SHEq–code

SHEq uses another form for the helical flux:

$$\chi = \chi_0 + \epsilon\,\sin(u + \psi_\epsilon) \tag{9.18}$$

[1] With respect to appendix C.2 we call:

$$z = a + ib = \rho\, e^{i\,\theta} \mapsto \psi_T^{m,n} = |\psi_T^{m,n}|\, e^{i\phi_{\psi_T}} \equiv \psi_T \tag{9.5}$$
$$t = c + id = \sigma e^{i\,\varphi} \mapsto \psi_P^{m,n} = |\psi_T^{m,n}|\, e^{i\phi_{\psi_P}} \equiv \psi_P \tag{9.6}$$
$$z - t = A + iB = C\, e^{i\gamma} \mapsto \begin{cases} \chi_{m,n} = m\psi_P^{m,n} - n\psi_T^{m,n} \equiv m\psi_P - n\psi_T \\ \chi_{m,n} = |\chi_{m,n}|\, e^{i\phi_\chi} \end{cases} \tag{9.7}$$

Therefore there are also true the following identifications:

$$a = \rho\cos\theta = |\psi_T^{m,n}|\cos\phi_{\psi_T} \tag{9.8}$$
$$b = \rho\sin\theta = |\psi_T^{m,n}|\cos\phi_{\psi_T} \tag{9.9}$$
$$c = \sigma\cos\varphi = |\psi_P^{m,n}|\cos\phi_{\psi_P} \tag{9.10}$$
$$d = \sigma\sin\varphi = |\psi_P^{m,n}|\sin\phi_{\psi_P} \tag{9.11}$$

From equations (C.30)–(C.31) one can finally write the coefficients for $\chi_{m,n}$ (A and B) in terms of the amplitudes and phases of the poloidal and toroidal fluxes (a, b, c, d):

$$A = C\cos\gamma = a - c = |\psi_T^{m,n}|\cos\phi_{\psi_T} - |\psi_P^{m,n}|\cos\phi_{\psi_P} \tag{9.12}$$
$$B = C\sin\gamma = b - d = |\psi_T^{m,n}|\cos\phi_{\psi_T} - |\psi_P^{m,n}|\sin\phi_{\psi_P} \tag{9.13}$$

The coefficient $C = |\chi_{m,n}|$ and $\gamma = \phi_\chi$ can be computed using eq.(C.32)–(C.33).

simply because it uses the eigenfunction of the perturbed fluxes from the output of another code that calculate them from Newcomb–like equations (as explained in chapter 3). In this code the helical flux perturbation ϵ is in accordance with (9.18). Let us prove that

$$2i|\chi_{mn}| = \epsilon \tag{9.19}$$
$$\phi_\chi = \psi_\epsilon \tag{9.20}$$

where $|\chi_{mn}|$ and ϕ_χ are computed from (9.16). Using the definition

$$\widehat{b}^r_{mn} = i\,(n\psi^{mn}_T - m\psi^{mn}_P) \;\Rightarrow\; (m\psi^{mn}_P - n\psi^{mn}_T) = i\,\widehat{b}^r_{mn} \tag{9.21}$$

that arises from eq.(5.43), one can write

$$\chi = [m\psi_{P,0} - n\psi_{T,0}](r) + [m\psi^{m,n}_P - n\psi^{m,n}_T](r)\,e^{iu} + c.c. \tag{9.22}$$
$$= \chi_0 + i\,\widehat{b}^r_{mn}\,e^{iu} + c.c. \tag{9.23}$$
$$= \chi_0 + i\,\widehat{b}^r_{mn}\,e^{iu} - i\widehat{b}^r_{mn}\,e^{-iu} \tag{9.24}$$
$$= \chi_0 + i\,\widehat{b}^r_{mn}\,(e^{iu} - e^{-iu}) \tag{9.25}$$
$$= \chi_0 - 2\,\widehat{b}^r_{mn}\,\sin u \tag{9.26}$$
$$= \chi_0 - 2\,|\widehat{b}^r_{mn}|\sin(u + \phi_{\widehat{b}^r_{mn}}) \tag{9.27}$$
$$\equiv \chi_0 + \epsilon\,\sin(u + \psi_\epsilon) \tag{9.28}$$
$$\equiv \chi_0 + |\chi^{m,n}|\,e^{(iu+\phi_\chi)} + c.c. \tag{9.29}$$

Comparing (9.23)–(9.28)–(9.29) one can understand the relations (9.18)–(9.19)–(9.20).

9.1.2 On the radial derivatives of complex harmonics, for the poloidal and toroidal fluxes

In this thesis the Fourier decomposition of a perturbation has been frequently used (see chapter 3–5):

$$A(r,\theta,\varphi) = A_0(r) + \sum_{m,n} a^{m,n}(r)\,e^{i(m\theta - n\varphi)} + c.c. \tag{9.30}$$

where A can be every quantity inside the plasma volume: magnetic fluxes, vector potential components, magnetic field components, ...
The harmonics of the perturbation are complex numbers: $a^{m,n}(r)\,\epsilon\,\mathbb{C}$. Therefore:

$$a^{m,n}(r) = |a^{m,n}|(r)\,e^{i\,\phi(r)} \tag{9.31}$$

where $|...|(r)$ indicates the amplitude, while $\phi(r)$ the phase of $a^{m,n}$. We remind that the amplitude and phase of a complex number are real numbers.

Perturbative analysis is done in the thesis to axisymmetric equilibrium quantities, that depend only on the radius r of the circular magnetic flux surfaces related to the axi–symmetric magnetic field $\mathbf{B_0}$. And that is why we use in this section the variable r as radial variable. But of course this still true for any perturbative analysis, for example of the SH equilibrium field that uses the helical flux $\chi(\rho)$ as radial variable.

Let us consider the radial derivative of the harmonics $\psi_{m,n}$ of the (poloidal or toroidal) magnetic fluxes[2]. This is linked to the computation of magnetic field components (eq.(2.144)–(2.145)).
Because the derivative of a complex number is still a complex number, we can write:

$$\begin{aligned} \psi'_{m,n}(r) &= a + ib & (9.32)\\ &= |\psi'_{m,n}|(r)\ e^{i\,\phi'_\psi(r)} & (9.33) \end{aligned}$$

with

$$\begin{aligned} |\psi'_{m,n}|(r) &= \sqrt{a^2+b^2} & (9.34)\\ \phi'_\psi(r) &= \tan^{-1}\frac{a}{b} & (9.35) \end{aligned}$$

The first expression in (9.32) highlights the real and the imaginary part of the complex harmonics $\psi'_{m,n}(r)$, whereas the second one writes it in the polar form.
Using the symbol $' = d/dr$, we can also write:

$$\begin{aligned} \psi_{m,n}(r) &= |\psi_{m,n}|(r)\ e^{i\,\phi_\psi(r)} & (9.36)\\ &\Downarrow & \\ \psi'_{m,n}(r) &= \frac{d}{dr}\left[|\psi_{m,n}|(r)\ e^{i\,\phi_\psi(r)}\right] & (9.37)\\ &= \left[\,|\psi_{m,n}|' + i\,|\psi_{m,n}|\phi'_\psi\,\right] e^{i\,\phi_\psi} & (9.38) \end{aligned}$$

Let us stress that the derivative of the amplitude of the function $\psi_{m,n}$ is different from the amplitude of the derivative of the same function:

$$|\psi_{m,n}|' \neq |\psi'_{m,n}| \tag{9.39}$$

The flux derivatives in SHEq–code

SHEq code uses equation (9.38) for the radial derivative of the fluxes, which must be written in the complete form of equation (9.30). Considering only

[2]Using ψ as the symbol for every flux, depending on the magnetic component that one is considering. The indexes m, n are written as down indexes just for commodity.

the perturbative part, and just one mode of the perturbation ($u = \theta - n\varphi$), we obtain:

$$\begin{aligned} \frac{\partial}{\partial r}\Big[|\psi_{m,n}|(r)\ e^{i\,\phi_\psi(r)+u} + c.c\Big] &= \Big[\,|\psi_{m,n}|' + i\,|\psi_{m,n}|\phi'_\psi\,\Big]\, e^{i\,\phi_\psi+u} + c.c. \qquad (9.40)\\ &= 2|\psi_{m,n}|'\cos(\phi_\psi+u) - 2|\psi_{m,n}|\phi'_\psi\sin(\phi_\psi+u) \end{aligned}$$

adding the complex conjugated to eq.(9.38) and considering also the angular dependence of the fluxes.
The amplitude $|\psi_{m,n}|$ and phase ϕ_ψ of the fluxes are computed solving Newcomb–like equations as explained in chapter 3. Their radial derivatives are calculated in a numerical way.

9.1.3 On the (angular and radial) derivatives of the helical flux χ

Using the form of eq.(9.4) for the helical flux χ, and then eq.(9.16), one can compute the helical flux radial and angular derivatives (which involve the radial derivatives of the fluxes, section 9.1.2):

$$\begin{aligned} \left(\ \tfrac{\partial\chi}{\partial r}\ \right) &= m\psi'_{P,0} - n\psi'_{T,0} + \qquad (9.41)\\ &\quad + 2\frac{\partial|\chi|}{\partial r}\ \cos(m\theta - n\varphi + \phi_\chi) - 2|\chi|\ \frac{\partial\phi_\chi}{\partial r}\ \sin(m\theta - n\varphi + \phi_\chi)\\ \left(\ \tfrac{\partial\chi}{\partial\theta}\ \right) &= -2\ m\ |\chi|\sin(m\theta - n\varphi + \phi_\chi) \qquad (9.42)\\ |\chi| &\equiv |\chi_{m,n}| \equiv |\chi_{m,n}|(r) \end{aligned}$$

with, making use of eq.(9.16),

$$\begin{aligned} \left(\ \tfrac{\partial|\chi|}{\partial r}\ \right) &= \frac{1}{2}\Big[2m|\psi_T||\psi_T|' + 2n^2|\psi_P||\psi_P|' - 2mn|\psi_T|'|\psi_P|\cos(\phi_{\psi_T} - \phi_{\psi_P}) +\\ &\quad - 2mn|\psi_T||\psi_P|'\cos(\phi_{\psi_T} - \phi_{\psi_P}) +\\ &\quad + 2mn|\psi_T||\psi_P|(\phi'_{\psi_T} - \phi'_{\psi_P})\sin(\phi_{\psi_T} - \phi_{\psi_P})\Big]^{-1/2} \qquad (9.43)\\ \left(\ \tfrac{\partial\phi_\chi}{\partial r}\ \right) &= \Big[1 + \Big(\frac{m|\psi_P|\sin\phi_{\psi_P} - n|\psi_T|\sin\phi_{\psi_T}}{m|\psi_P|\cos\phi_{\psi_P} - n|\psi_T|\cos\phi_{\psi_T}}\Big)^2\Big]^{-1} \times \qquad (9.44)\\ &\quad \times \quad \Big[\frac{N'D - D'N}{D^2}\Big] \end{aligned}$$

$$\begin{cases} N = m|\psi_P| \sin\phi_{\psi_P} - n|\psi_T| \sin\phi_{\psi_T} \\ D = m|\psi_P| \cos\phi_{\psi_P} - n|\psi_T| \cos\phi_{\psi_T} \\ N' = m|\psi_P|' \sin\phi_{\psi_P} + m|\psi_P|\phi'_{\psi_P} \cos\phi_{\psi_P} - n|\psi_T|' \sin\psi_{\psi_T} - n|\psi_T|\phi'_{\psi_T} \cos\phi_{\psi_T} \\ D' = m|\psi_P|' \cos\phi_{\psi_P} - m|\psi_P|\phi'_{\psi_P} \sin\phi_{\psi_P} - n|\psi_T|' \cos\psi_{\psi_T} + n|\psi_T|\phi'_{\psi_T} \sin\phi_{\psi_T} \end{cases}$$

The helical flux radial derivatives in SHEq–code

SHEq code uses a formula similar to eq.(9.40) also for the helical flux:

$$\frac{\partial\chi}{\partial r} = \frac{d\chi_0}{dr} + \frac{\partial\chi_{m,n}(r,u)}{\partial r} \tag{9.45}$$

$$= \chi_0'(r) - \epsilon'(r)\sin(u+\phi_\epsilon) - \epsilon\,\phi'_\epsilon\,\cos(u+\phi_\epsilon) \tag{9.46}$$

using definitions (9.19)–(9.20) for $\epsilon(r)$ and ϕ_ϵ, one founds that equation (9.45) is equivalent to eq.(9.41).

9.2 On helical–toroidal coordinates

Helical–toroidal coordinate systems have been defined in chapter 4 as a first step to model SHAx states (as pure SH states).
The whole metric tensors are used by the SHEq code to compute the helical plasma quantities, examples of which one can find in chapter 6.
We collect here the metrics of all the helical coordinates defined in chapter 4, in the same order for simplicity (except for the (χ, u, θ) and $(\chi, u_{\theta_h}, \theta)$ coordinate systems of section 4.2.3, for which no metrics have been calculated). It is worth noting that all the helical–toroidal metrics are all curvilinear metrics.

9.2.1 The whole metric tensor of helical coordinate systems defined in chapter 4

1. **The (χ, β, φ) coordinate system**

   This is the coordinate system defined in section 4.2.1, which is not a straight–field–line coordinate system.
   The angle β is defined with respect to the helical axis, and can be defined with respect to the cylindrical coordinates[3] in a geometric way, equation (4.11).

   Due to equations (3.14), the metric tensor and the Jacobian of this coordinate system can be derived in a relatively easy way in terms of the

[3] The tensor metric of the cylindrical coordinate system can be found in appendix B.2.1.

metrics of the zero–th order flux coordinates $w^i = (r, \vartheta, \varphi)$ defined in section 3.1.1 and appendix B.2.3. The contravariant metric tensor elements and the Jacobian can be computed using the relations between the gradients of the two coordinate systems:

$$\begin{cases} \nabla\chi = \frac{\partial\chi}{\partial r}\nabla r + \frac{\partial\chi}{\partial\vartheta}\nabla\vartheta + \frac{\partial\chi}{\partial\varphi}\nabla\varphi \\ \nabla\beta = \frac{\partial\beta}{\partial r}\nabla r + \frac{\partial\beta}{\partial\vartheta}\nabla\vartheta + \frac{\partial\beta}{\partial\varphi}\nabla\varphi \\ \nabla\varphi = \nabla\varphi \end{cases}$$

The **Jacobian** $\sqrt{g_\beta}$ of the (χ, β, φ) coordinate system is:

$$\sqrt{g_\beta} = (\nabla\chi \cdot \nabla\beta \times \nabla\varphi)^{-1} = \left(\frac{\partial\chi}{\partial r}\frac{\partial\beta}{\partial\vartheta} - \frac{\partial\chi}{\partial\vartheta}\frac{\partial\beta}{\partial r} \right)^{-1} \cdot \sqrt{g_w} \qquad (9.47)$$

where $\sqrt{g_w}$ is the Jacobian of the w^i coordinate system. The following condition must be satisfied:

$$\frac{\partial\chi}{\partial r}\frac{\partial\beta}{\partial\vartheta} > \frac{\partial\chi}{\partial\vartheta}\frac{\partial\beta}{\partial r} \qquad (9.48)$$

We write explicitly just an example, for the first **contravariant metrics element**: $g^{11} \equiv g^{\chi\chi}$:

$$\begin{aligned} g^{\chi\chi} &= \nabla\chi \cdot \nabla\chi \qquad (9.49) \\ &= \left(\frac{\partial\chi}{\partial r}\nabla r + \frac{\partial\chi}{\partial\vartheta}\nabla\vartheta + \frac{\partial\chi}{\partial\varphi}\nabla\varphi\right) \cdot \left(\frac{\partial\chi}{\partial r}\nabla r + \frac{\partial\chi}{\partial\vartheta}\nabla\vartheta + \frac{\partial\chi}{\partial\varphi}\nabla\varphi\right) = \\ &= \left(\frac{\partial\chi}{\partial r}\right)^2 g_w^{rr} + \left(\frac{\partial\chi}{\partial\vartheta}\right)^2 g_w^{\vartheta\vartheta} + \left(\frac{\partial\chi}{\partial\varphi}\right)^2 g_w^{\varphi\varphi} + \left(\frac{\partial\chi}{\partial r}\right)\left(\frac{\partial\chi}{\partial\vartheta}\right) g_w^{r\vartheta} \end{aligned}$$

The g_{ij} elements of the (inverse) **covariant matrix** can be calculated from the formulas for the inversion of a 3x3 diagonal matrix (see appendix B.3).

One needs to know the following derivatives to compute the metrics elements and the Jacobian:

$$\left(\frac{\partial\beta}{\partial r}\right), \left(\frac{\partial\beta}{\partial\vartheta}\right), \left(\frac{\partial\chi}{\partial r}\right), \left(\frac{\partial\chi}{\partial\vartheta}\right) \qquad (9.50)$$

The derivatives of the helical flux have already been discussed in section 9.1.3. We derive here the derivatives of the angle β, for which we must remember the definition of the angle β, equations (3.14) and equations

(3.12):

$$\beta = \arctan\left(\frac{Z-Z_A}{R-R_A} \right) \tag{9.51}$$

$$R = R_0 - r\cos\vartheta + \Delta(r) - r\lambda_1 \sin^2\vartheta + (\frac{3}{2} r\lambda_1^2 - 2r\lambda_2)\sin^2\vartheta\cos\vartheta$$

$$Z = r\sin\vartheta - \frac{r}{2}\lambda_1 \sin(2\vartheta) + (\frac{3}{2} r\lambda_1^2 - 2r\lambda_2)\sin\vartheta\cos^2\vartheta - \frac{r}{2}\lambda_1^2 \sin\vartheta$$

$$\lambda_1(r_f) = \frac{r_f}{R_0} - \Delta' \tag{9.52}$$

$$\lambda_2(r_f) = \frac{r_f}{4R_0}\left(\frac{r_f}{R_0} - \Delta' \right) = \frac{r_f}{4R_0}\,\lambda_1 \tag{9.53}$$

Because $d/dx(\arctan x) = (1+x^2)^{-1}$, one obtains the derivatives:

$$\left(\frac{\partial\beta}{\partial r} \right) = \left[1 + \left(\frac{Z-Z_A}{R-R_A} \right)^2 \right]^{-1} \left(\frac{1}{R-R_A}\,\frac{\partial Z}{\partial r} - \frac{Z-Z_A}{(R-R_A)^2}\,\frac{\partial R}{\partial r} \right) \tag{9.54}$$

$$= \frac{1}{(R-R_A)^2 + (Z-Z_A)^2}\left[(R-R_A)\,\frac{\partial Z}{\partial r} - (Z-Z_A)\,\frac{\partial R}{\partial r} \right]$$

$$\left(\frac{\partial\beta}{\partial\vartheta} \right) = \left[1 + \left(\frac{Z-Z_A}{R-R_A} \right)^2 \right]^{-1} \left(\frac{1}{R-R_A}\,\frac{\partial Z}{\partial\vartheta} - \frac{Z-Z_A}{(R-R_A)^2}\,\frac{\partial R}{\partial\vartheta} \right) \tag{9.55}$$

$$= \frac{1}{(R-R_A)^2 + (Z-Z_A)^2}\left[(R-R_A)\,\frac{\partial Z}{\partial\vartheta} - (Z-Z_A)\,\frac{\partial R}{\partial\vartheta} \right]$$

with

$$\left(\frac{\partial Z}{\partial r} \right) = \sin\vartheta - \frac{1}{2}\lambda_1\sin(2\vartheta) - \frac{r}{2}\sin(2\vartheta)\,\frac{\partial\lambda_1}{\partial r} + \tag{9.56}$$
$$+ \left(\tfrac{3}{2}\lambda_1^2 + 3r\lambda_1\,\tfrac{\partial\lambda_1}{\partial r} - 2\lambda_2 - 2r\,\tfrac{\partial\lambda_2}{\partial r} \right)\sin\vartheta\,\cos^2\vartheta +$$
$$- \frac{1}{2}\lambda_1^2\sin\vartheta - r\lambda_1\,\frac{\partial\lambda_1}{\partial r}\,\sin\vartheta$$

$$\left(\frac{\partial Z}{\partial\vartheta} \right) = r\cos\vartheta - r\lambda_1\cos(2\vartheta) - \frac{r}{2}\lambda_1^2\cos\vartheta + \tag{9.57}$$
$$+ \left(\tfrac{3}{2} r\lambda_1^2 - 2r\lambda_2 \right)\left(\cos^2\vartheta - 2\sin^2\vartheta \right)\cos\vartheta$$

$$\left(\frac{\partial R}{\partial r} \right) = -\cos\vartheta + \Delta' - \lambda_1\sin^2\vartheta - r\sin^2\vartheta\,\frac{\partial\lambda_1}{\partial r} + \tag{9.58}$$
$$+ \left(\tfrac{3}{2}\lambda_1^2 + 3r\lambda_1\tfrac{\partial\lambda_1}{\partial r} - 2r\tfrac{\partial\lambda_2}{\partial r} - 2\lambda_2 \right)\sin^2\vartheta\,\cos\vartheta$$

$$\left(\frac{\partial R}{\partial\vartheta} \right) = r\sin\vartheta - 2r\lambda_1\sin\vartheta\,\cos\vartheta + \tag{9.59}$$
$$+ \left(\tfrac{3}{2} r\lambda_1^2 - 2r\lambda_2 \right)\left(2\cos^2\vartheta - \sin^2\vartheta \right)\sin\vartheta$$

and

$$\left(\frac{\partial \lambda_1}{\partial r} \right) = \frac{1}{R_0} - \Delta'' \tag{9.60}$$

$$\left(\frac{\partial \lambda_2}{\partial r} \right) = \frac{r}{2R_0^2} - \frac{\Delta'}{4R_0} - \frac{r\Delta''}{4R_0}$$

$$\Delta''(r) = -\frac{1}{R_0} - \frac{\Delta'}{r}\left(1 + \frac{2r}{\hat{B_0}^{\vartheta}} \frac{d\hat{B_0}^{\vartheta}}{dr} \right) \tag{9.61}$$

2. **The (χ, u, φ) coordinate system**

This is the helical coordinate system defined in section 4.2.2, for the Hamiltonian time φ, that emphasizes the helical symmetry with respect to u on the flux surfaces $\chi = const$.
The (χ, u, φ) is not a straight–field–line coordinate system and the helical angle $u = m\vartheta - n\varphi$ is not defined with respect to the helical axis, being defined with respect to the axi–symmetric (shifted) axis of the system (as the poloidal angle ϑ).

The metric tensor and the Jacobian of this coordinate system can be derived in a relatively easy way in terms of the metrics of the zero–th order flux coordinates $w^i = (r, \vartheta, \varphi)$ defined in section 3.1.1 and appendix B.2.3.
The **Jacobian** $\sqrt{g_c}$ of the (χ, u, φ) coordinate system is:

$$\sqrt{g_c} = \left(\frac{\partial \chi}{\partial r}\right)^{-1} \left(\frac{\partial u}{\partial \vartheta}\right)^{-1} \sqrt{g_w} = \frac{1}{m}\left(\frac{\partial \chi}{\partial r}\right)^{-1} \sqrt{g_w} \tag{9.62}$$

where $\sqrt{g_w}$ is the Jacobian of the w^i coordinate system.

Also the **contravariant metric tensor elements** g_c^{ij} can be computed using the relations between the gradients of the two coordinate systems (and the easy derivation of the helical angle u with respect to

the w^i coordinates). One obtains:

$$\begin{aligned} g_c^{\chi\chi} &= \nabla\chi\cdot\nabla\chi \qquad (9.63)\\ &= \left(\frac{\partial\chi}{\partial r}\right)^2 g_w^{rr} + \left(\frac{\partial\chi}{\partial\vartheta}\right)^2 g_w^{\vartheta\vartheta} + \left(\frac{\partial\chi}{\partial\varphi}\right)^2 g_w^{\varphi\varphi} + \left(\frac{\partial\chi}{\partial r}\right)\left(\frac{\partial\chi}{\partial\vartheta}\right) g_w^{r\vartheta} \\ g_c^{\chi u} &= \nabla\chi\cdot\nabla u \\ &= m\left(\frac{\partial\chi}{\partial r}\right) g_w^{r\vartheta} + m\left(\frac{\partial\chi}{\partial\vartheta}\right) g_w^{\vartheta\vartheta} - n\left(\frac{\partial\chi}{\partial\varphi}\right) g_w^{\varphi\varphi} \qquad (9.64)\\ g_c^{\chi\varphi} &= \nabla\chi\cdot\nabla\varphi = \left(\frac{\partial\chi}{\partial\varphi}\right) g_w^{\varphi\varphi} \qquad (9.65)\\ g_c^{uu} &= \nabla u\cdot\nabla u = m^2\, g_w^{\vartheta\vartheta} + n^2\, g_w^{\varphi\varphi} \qquad (9.66)\\ g_c^{u\varphi} &= \nabla u\cdot\nabla\varphi = -n\, g_w^{\varphi\varphi} \qquad (9.67)\\ g_c^{\varphi\varphi} &= \nabla\varphi\cdot\nabla\varphi = g_w^{\varphi\varphi} \qquad (9.68) \end{aligned}$$

remembering the symmetry of the metrics elements: $g^{ij} = g^{ji}$ and $g_{ij} = g_{ji}$.

The **covariant metric tensor elements** g^c_{ij} can be calculated from the formulas for the inversion of a 3x3 diagonal matrix (see appendix B.3).

3. **The (χ, u_h, φ) coordinate system**

This is the action–angle coordinate system defined in section 4.2.2, for the Hamiltonian time φ, that emphasizes the helical symmetry with respect to u on the flux surfaces $\chi = const$.
The (χ, u, φ) is the straight–field–line coordinate system related to the helical angle u_h defined in equation (4.21).

The metric tensor of this coordinate system can be derived in a relatively easy way in terms of the metrics of the (χ, u, φ) coordinate system. One needs to know the following derivatives to compute the metrics elements and the Jacobian:

$$\begin{aligned} \frac{\partial u_h}{\partial\chi} &= \frac{\partial\chi}{\partial\psi_h}\int_0^u \frac{\partial^2\psi_T(\chi,u')}{\partial\chi^2}\,du' \qquad (9.69)\\ \frac{\partial u_h}{\partial u} &= \frac{\partial\psi_T(\chi,u)}{\partial\chi}\frac{d\chi}{d\psi_h} = \frac{1}{\iota_h}\frac{\partial\psi_T(\chi,u)}{\partial\chi} \qquad (9.70) \end{aligned}$$

remembering the definition of the helical rotational transform ι_h, eq.(6.26).

The **Jacobian** $\sqrt{g_h}$ of the (χ, u_h, φ) coordinate system is:

$$\sqrt{g_h} = \left(\frac{\partial u_h}{\partial u}\right)^{-1}\sqrt{g_c} \tag{9.71}$$

$$= \frac{1}{m}\left(\frac{\partial u_h}{\partial u}\right)^{-1}\left(\frac{\partial \chi}{\partial r}\right)^{-1}\sqrt{g_w} \tag{9.72}$$

using also equation (9.62).

The **contravariant metric tensor elements** g_h^{ij} can be computed using the relations between the gradients of the two coordinate systems (the (χ, u_h, φ) and the (χ, u, φ) coordinate systems). One obtains:

$$g_h^{\chi\chi} = \nabla\chi\cdot\nabla\chi = g_c^{\chi\chi} \tag{9.73}$$

$$g_h^{\chi u_h} = \nabla\chi\cdot\nabla u_h = \left(\frac{\partial u_h}{\partial \chi}\right) g_c^{\chi\chi} + \left(\frac{\partial u_h}{\partial u}\right) g_c^{\chi u} \tag{9.74}$$

$$g_h^{\chi\varphi} = \nabla\chi\cdot\nabla\varphi = g_c^{\chi\varphi} \tag{9.75}$$

$$g_h^{u_h u_h} = \nabla u_h\cdot\nabla u_h \tag{9.76}$$

$$= \left(\frac{\partial u_h}{\partial \chi}\right)^2 g_c^{\chi\chi} + 2\left(\frac{\partial u_h}{\partial \chi}\right)\left(\frac{\partial u_h}{\partial u}\right) g_c^{\chi u} + \left(\frac{\partial u_h}{\partial u}\right)^2 g_c^{uu}$$

$$g_h^{u_h\varphi} = \nabla u_h\cdot\nabla\varphi = \left(\frac{\partial u_h}{\partial \chi}\right) g_c^{\chi\varphi} + \left(\frac{\partial u_h}{\partial u}\right) g_c^{u\varphi} \tag{9.77}$$

$$g_h^{\varphi\varphi} = \nabla\varphi\cdot\nabla\varphi = g_c^{\varphi\varphi} \tag{9.78}$$

remembering the symmetry of the metrics elements: $g^{ij} = g^{ji}$ and $g_{ij} = g_{ji}$ and that $u_h \equiv u_h(\chi, u)$.

Again, the **covariant metric tensor elements** g_{ij}^h can be calculated from the formulas for the inversion of a 3x3 diagonal matrix (see appendix B.3).

4. **The (χ, u, v) coordinate system**

This is the helical coordinate system defined in section 4.2.4, for the Hamiltonian time $v = a\theta + bn\varphi$, that can be thought as a toroidal–like angle defined on the helical axis and that do not reverse. On the other hand, the helical angle $u = m\vartheta - n\varphi$ is not defined with respect to the helical axis and the (χ, u, v) is not a straight–field–line coordinate system.

As for the (χ, u, φ) coordinates, the metric tensor of this coordinate system can be derived in a relatively easy way in terms of the metrics of the zero–th order flux coordinates $w^i = (r, \vartheta, \varphi)$ defined in section

3.1.1 and appendix B.2.3.
The **Jacobian** $\sqrt{g_v}$ of the (χ, u, v) coordinate system is:

$$\sqrt{g_v} = \left(\frac{\partial\chi}{\partial r}\right)^{-1}\left(\frac{\partial u}{\partial\vartheta}\frac{\partial v}{\partial\varphi} - \frac{\partial u}{\partial\varphi}\frac{\partial v}{\partial\vartheta}\right)^{-1}\sqrt{g_w} \tag{9.79}$$

$$= \left(\frac{\partial\chi}{\partial r}\right)^{-1}\sqrt{g_w} \tag{9.80}$$

where $\sqrt{g_w}$ is the Jacobian of the w^i coordinate system. The simple derivations of the angles u and v with respect to ϑ and φ have been used.

Also the **contravariant metric tensor elements** g_v^{ij} can be computed using the relations between the gradients of the two coordinate systems. One obtains:

$$g_v^{\chi\chi} = \nabla\chi\cdot\nabla\chi \tag{9.81}$$

$$= \left(\frac{\partial\chi}{\partial r}\right)^2 g_w^{rr} + \left(\frac{\partial\chi}{\partial\vartheta}\right)^2 g_w^{\vartheta\vartheta} + \left(\frac{\partial\chi}{\partial\varphi}\right)^2 g_w^{\varphi\varphi} + \left(\frac{\partial\chi}{\partial r}\right)\left(\frac{\partial\chi}{\partial\vartheta}\right) g_w^{r\vartheta}$$

$$g_v^{\chi u} = \nabla\chi\cdot\nabla u$$

$$= m\left(\frac{\partial\chi}{\partial r}\right) g_w^{r\vartheta} + m\left(\frac{\partial\chi}{\partial\vartheta}\right) g_w^{\vartheta\vartheta} - n\left(\frac{\partial\chi}{\partial\varphi}\right) g_w^{\varphi\varphi} \tag{9.82}$$

$$g_v^{\chi v} = \nabla\chi\cdot\nabla v$$

$$= \frac{1}{2n}\left(\frac{\partial\chi}{\partial r}\right) g_w^{r\vartheta} + \frac{1}{2n}\left(\frac{\partial\chi}{\partial\vartheta}\right) g_w^{\vartheta\vartheta} + \frac{1}{2}\left(\frac{\partial\chi}{\partial\varphi}\right) g_w^{\varphi\varphi} \tag{9.83}$$

$$g_v^{uu} = \nabla u\cdot\nabla u = m^2\, g_w^{\vartheta\vartheta} + n^2\, g_w^{\varphi\varphi} \tag{9.84}$$

$$g_v^{uv} = \nabla u\cdot\nabla v = \frac{m}{2n} g_w^{\vartheta\vartheta} - \frac{n}{2}\, g_w^{\varphi\varphi} \tag{9.85}$$

$$g_v^{vv} = \nabla v\cdot\nabla v = \frac{1}{4n^2} g_w^{\vartheta\vartheta} + \frac{1}{4}\, g_w^{\varphi\varphi} \tag{9.86}$$

remembering the symmetry of the metrics elements: $g^{ij} = g^{ji}$ and $g_{ij} = g_{ji}$.

The **covariant metric tensor elements** g_{ij}^v can be calculated from the formulas for the inversion of a 3x3 diagonal matrix (see appendix B.3).

5. **The (χ, u_η, v) coordinate system**

This is the Action–Angle coordinate system defined in section 4.2.4, for the Hamiltonian time v. The (χ, u, φ) is therefore the straight–field–line coordinate system related to the helical Angle u_η defind in

equation (4.62) as the angle defined with respect to the helical axis..

The metric tensor of this coordinate system can be derived in a relatively easy way in terms of the metrics of the (χ, u, v) coordinate system. One needs to know the following derivatives to compute the metrics elements:

$$u_\eta(\eta_h, u) = \int_0^u \frac{\partial \eta(\eta_h, u')}{\partial \eta_h}\, du' = \frac{d\chi}{d\eta_h} \int_0^u \frac{\partial \eta(\chi, u')}{\partial \chi} \tag{9.87}$$

$$\Updownarrow$$

$$\frac{\partial u_\eta}{\partial \chi} = \iota_\eta \frac{\partial}{\partial \chi}\left(\int_0^u \frac{\partial \eta(\chi, u')}{\partial \chi}\, du'\right) + \frac{d\iota_\eta}{d\chi} \int_0^u \frac{\partial \eta(\chi, u')}{\partial \chi}\, du' \tag{9.88}$$

$$= \iota_\eta \int_0^u \left(\frac{\partial \chi}{\partial r}\right)^{-1} \left[\frac{\partial^2 \eta}{\partial r^2}\left(\frac{\partial \chi}{\partial r}\right)^{-1} - \frac{\partial \eta}{\partial r}\left(\frac{\partial \chi}{\partial r}\right)^{-2}\left(\frac{\partial^2 \chi}{\partial r^2}\right)\right] du +$$

$$+ \frac{d\iota_\eta}{d\chi}\frac{u_\eta}{\iota_\eta}$$

$$\frac{\partial u_\eta}{\partial u} = \frac{\partial \eta(\eta_h, u')}{\partial \eta_h} = \iota_\eta(\chi) \frac{\partial \eta(\chi, u')}{\partial \chi} = \iota_\eta(\chi) \frac{\partial \eta}{\partial r}\left(\frac{\partial \chi}{\partial r}\right)^{-1} \tag{9.89}$$

remembering the general definition of the helical rotational transform $\iota_\eta(\chi) = d\chi/d\eta_h$, for the Action $\eta_h(\chi)$, and with[4]:

$$\frac{\partial \eta}{\partial r} = \frac{1}{2n}\frac{\partial \psi_P}{\partial r} + \frac{1}{2}\frac{\partial \psi_t}{\partial r} \tag{9.90}$$

$$\frac{\partial^2 \eta}{\partial r^2} = \frac{1}{2n}\frac{\partial^2 \psi_P}{\partial r^2} + \frac{1}{2}\frac{\partial^2 \psi_t}{\partial r^2} \tag{9.91}$$

The **Jacobian** $\sqrt{g_\eta}$ of the (χ, u_η, v) coordinate system is:

$$\sqrt{g_\eta} = \left(\frac{\partial u_\eta}{\partial u}\right)\sqrt{g_v} \tag{9.92}$$

$$= \left(\frac{\partial u_\eta}{\partial u}\right)\left(\frac{\partial \chi}{\partial r}\right)^{-1}\sqrt{g_w} \tag{9.93}$$

using both the Jacobian of the (χ, u, v) and the $w^i = (r, \vartheta, \varphi)$ coordinate systems.

The **contravariant metric tensor elements** g_η^{ij} can be computed using the relations between the gradients of the two coordinate systems

[4]See section 9.1.2 to compute the radial derivative of the poloidal and toroidal fluxes.

(the (χ, u, v) and the $(\chi, u\eta, v)$ coordinate systems). One obtains:

$$
\begin{aligned}
g_\eta^{\chi\chi} &= \nabla\chi \cdot \nabla\chi = g_v^{\chi\chi} && (9.94)\\
g_\eta^{\chi u_\eta} &= \nabla\chi \cdot \nabla u_\eta = \left(\frac{\partial u_\eta}{\partial \chi}\right) g_v^{\chi\chi} + \left(\frac{\partial u_\eta}{\partial u}\right) g_v^{\chi u} && (9.95)\\
g_\eta^{\chi v} &= \nabla\chi \cdot \nabla v = g_v^{\chi v} && (9.96)\\
g_\eta^{u_\eta u_\eta} &= \nabla u_\eta \cdot \nabla u_\eta = \\
&= \left(\frac{\partial u_\eta}{\partial \chi}\right)^2 g_v^{\chi\chi} + 2\left(\frac{\partial u_\eta}{\partial \chi}\right)\left(\frac{\partial u_\eta}{\partial u}\right) g_v^{\chi u} + \left(\frac{\partial u_\eta}{\partial u}\right)^2 g_v^{uu} && (9.97)\\
g_\eta^{u_\eta v} &= \nabla u_\eta \cdot \nabla v = \left(\frac{\partial u_\eta}{\partial \chi}\right) g_v^{\chi v} + \left(\frac{\partial u_\eta}{\partial u}\right) g_v^{uv} && (9.98)\\
g_\eta^{vv} &= \nabla v \cdot \nabla v = g_v^{vv} && (9.99)
\end{aligned}
$$

remembering the symmetry of the metrics elements: $g^{ij} = g^{ji}$ and $g_{ij} = g_{ji}$ and that $u_\eta \equiv u_\eta(\eta_h, u) = u_\eta(\chi, u)$.

Again, the **covariant metric tensor elements** g_{ij}^{η} can be calculated from the formulas for the inversion of a 3x3 diagonal matrix (see appendix B.3).

6. **The $(\chi, \theta^*, \varphi)$ coordinate system**

This is the Action–Angle coordinate system defined in section 4.4.1, for the Hamiltonian time φ. It is a straight–field–line coordinate system related to the usual toroidal angle φ and to the poloidal angle θ^* defined with respect to the helical axis in equation (4.80):

$$\theta^* = u_h + n\varphi \quad . \tag{9.100}$$

The metric tensor of this coordinate system can be derived in a relatively easy way in terms of the metrics of the (χ, u_h, φ) coordinate system. The **Jacobian** $\sqrt{g_*}$ of the $(\chi, \theta^*, \varphi)$ coordinate system is:

$$\sqrt{g_*} = (\nabla\chi \cdot \nabla u_h \times \nabla\varphi)^{-1} = \sqrt{g_h} \tag{9.101}$$

where $\sqrt{g_h}$ is the Jacobian of the straight–field–line coordinate system (χ, u_h, φ).

The **contravariant metric tensor elements** g_*^{ij} can be computed using the relations between the gradients of the two coordinate systems

(the $(\chi, \theta^*, \varphi)$ and the (χ, u_h, φ) coordinate systems). One obtains:

$$\begin{aligned}
g_*^{\chi\chi} &= \nabla\chi \cdot \nabla\chi = g_h^{\chi\chi} && (9.102)\\
g_*^{\chi\theta^*} &= \nabla\chi \cdot \nabla\theta^* = g_h^{\chi u_h} + n g_h^{\chi\varphi} && (9.103)\\
g_*^{\chi\varphi} &= \nabla\chi \cdot \nabla\varphi = g_h^{\chi\varphi} && (9.104)\\
g_*^{\theta^*\theta^*} &= \nabla\theta^* \cdot \nabla\theta^* = g_h^{u_h u_h} + 2n g_h^{u_h\varphi} + n^2 g_h^{\varphi\varphi} && (9.105)\\
g_*^{\theta^*\varphi} &= \nabla\theta^* \cdot \nabla\varphi = g_h^{u_h\varphi} + n g_h^{\varphi\varphi} && (9.106)\\
g_*^{\varphi\varphi} &= \nabla\varphi \cdot \nabla\varphi = g_h^{\varphi\varphi} && (9.107)
\end{aligned}$$

remembering the symmetry of the metrics elements: $g^{ij} = g^{ji}$ and $g_{ij} = g_{ji}$ and computing the easy derivatives of θ^* with respect to the (u_h, φ) coordinates.

The **covariant metric tensor elements** g^*_{ij} can be calculated from the formulas for the inversion of a 3x3 diagonal matrix (see appendix B.3).

9.2.2 Radial variable choices

We note here how the Jacobian and the metrics elements vary for change of the radial variable. In section 9.2 we used the helical flux χ as radial variable, with the same choice of chapter 4. We now consider the change:

$$\chi \mapsto \rho(\chi) \tag{9.108}$$

for any coordinate system χ, θ, φ, keeping unchanged the angle variables.

The **Jacobian** $\sqrt{g_\chi}$ according to eq.(9.108) changes as follows:

$$\sqrt{g_\rho} = \left(\frac{\partial\chi}{\partial\rho}\right)\sqrt{g_\chi} \tag{9.109}$$

where $\sqrt{g_\rho}$ is the Jacobian of the ρ, θ, φ coordinate system.

The **contravariant metric tensor elements** g^{ij} changes as:

$$\begin{aligned}
g^{\rho\rho} &= \left(\frac{\partial\rho}{\partial\chi}\right)^2 g^{\chi\chi} && (9.110)\\
g^{\rho\theta} &= \left(\frac{\partial\rho}{\partial\chi}\right) g^{\chi\theta} && (9.111)\\
g^{\rho\varphi} &= \left(\frac{\partial\rho}{\partial\chi}\right) g^{\chi\varphi} && (9.112)\\
& && (9.113)
\end{aligned}$$

whereas the metric elements related to the angular coordinates only are unchanged.

The **covariant metric tensor elements** g_{ij} can be calculated from the formulas for the inversion of a 3x3 diagonal matrix in terms of the contravariant elements. Using the relations above one can find how they change under changes of the radial variable. It still true that the covariant metric elements related to the angular coordinates only are unchanged.

To conclude we note also how change some quantities important in chapter 7: the derivative of the volume V' and the diagonal susceptance matrix elements S_{ij}.

$$V'_\chi \mapsto V'_\rho = \left(\frac{\partial \chi}{\partial \rho}\right) V'_\chi \tag{9.114}$$

$$[S_{11}]_\chi \mapsto [S_{11}]_\rho = \left(\frac{\partial \rho}{\partial \chi}\right) [S_{11}]_\chi \tag{9.115}$$

$$[S_{22}]_\chi \mapsto [S_{22}]_\rho = \left(\frac{\partial \rho}{\partial \chi}\right) [S_{22}]_\chi \tag{9.116}$$

9.2.3 Dimensional analysis

We use the symbol [...] to indicate the dimension, using SI metric units.

What changes changing the radial variable is the dimension of the covariant and contravariant components of the magnetic field and vector potential. Starting from the definition of these components in every general coordinates $x^i = (x^1, x^2, x^3)$:

$$\mathbf{B} = B^i \mathbf{e}_i = B_i \nabla x^i \tag{9.117}$$

where $\mathbf{e}_i$ and ∇x^i are the covariant and contravariant basis vector, respectively. And they are one the inverse of the other (appendix B.1), ∇x^i being the gradient of the coordinate scalar function. The same relations are valid for any vector, in particular for the vector potential $\mathbf{A}$.
One starts from here for some dimensional analysis. We choose toroidal systems (ρ, θ, φ): θ and φ are two (adimensional) angles and their gradient have dimension $[m^{-1}]$, while its inverse the dimension of $[m]$. The correspondent

dimensions for the radial coordinate depend on the choice of ρ:

$$(\theta \equiv [adim]) \Rightarrow \nabla\theta \equiv [m^{-1}]\,,\ \mathbf{e}_\theta \equiv [m] \tag{9.118}$$
$$(\varphi \equiv [adim]) \Rightarrow \nabla\varphi \equiv [m^{-1}]\,,\ \mathbf{e}_\varphi \equiv [m] \tag{9.119}$$

$$(\rho = \chi \equiv [Tm^2]) \Rightarrow \nabla\rho \equiv [Tm]\,,\ \mathbf{e}_\rho \equiv [T^{-1}m^{-1}] \tag{9.120}$$
$$(\rho = \rho_h \equiv [adim]) \Rightarrow \nabla\rho \equiv [m^{-1}]\,,\ \mathbf{e}_\rho \equiv [m] \tag{9.121}$$
$$(\rho = \rho_A \equiv [m]) \Rightarrow \nabla\rho \equiv [adim]\,,\ \mathbf{e}_\rho \equiv [adim] \tag{9.122}$$

Using the definitions (B.3) and (B.1) for the contravariant and covariant metrics elements respectively, one can make from here a dimensional analysis of the tensor matrix elements.

Because the magnetic field must be Tesla $[T]$ and the vector potential $[Tm]$ (Stokes theorem), one obtains using (9.117):

$$(\rho = \chi \equiv [Tm^2]) \Rightarrow A_\rho \equiv [adim]\,,\ A_\varphi \equiv [Tm^2] \tag{9.123}$$
$$\Rightarrow B_\rho \equiv [m^{-1}]\,,\ B_\varphi \equiv [Tm] \tag{9.124}$$
$$(\rho = \rho_h \equiv [adim]) \Rightarrow A_\rho \equiv [Tm^2]\,,\ A_\varphi \equiv [Tm^2] \tag{9.125}$$
$$\Rightarrow B_\rho \equiv [Tm]\,,\ B_\varphi \equiv [Tm] \tag{9.126}$$
$$(\rho = \rho_A \equiv [m]) \Rightarrow A_\rho \equiv [Tm]\,,\ A_\varphi \equiv [Tm^2] \tag{9.127}$$
$$\Rightarrow B_\rho \equiv [T]\,,\ B_\varphi \equiv [Tm] \tag{9.128}$$

With *down* indexes:

$$(\rho = \chi \equiv [Tm^2]) \Rightarrow A^\rho \equiv [T^2m^2]\,,\ A^\varphi \equiv [T] \tag{9.129}$$
$$\Rightarrow B^\rho \equiv [T^2m]\,,\ B^\varphi \equiv [Tm^{-1}] \tag{9.130}$$
$$(\rho = \rho_h \equiv [adim]) \Rightarrow A^\rho \equiv [T]\,,\ A^\varphi \equiv [T] \tag{9.131}$$
$$\Rightarrow B^\rho \equiv [Tm^{-1}]\,,\ B^\varphi \equiv [Tm^{-1}] \tag{9.132}$$
$$(\rho = \rho_A \equiv [m]) \Rightarrow A^\rho \equiv [Tm]\,,\ A^\varphi \equiv [T] \tag{9.133}$$
$$\Rightarrow B^\rho \equiv [T]\,,\ B^\varphi \equiv [Tm^{-1}] \tag{9.134}$$

The components on the other angle, θ have the same dimensional properties.

Not all the the components of the magnetic field and of the vector potential have the dimension of the whole vector. This is obviously due to the fact that the basis vectors are not adimensional. This is at the basis of the theory for curvilinear metrics and tensorial calculations: paying attention to these rules, one can make adimensional and with unitary lenght the basis vectors $\mathbf{e}_i$ and ∇x^i dividing them for their norm. This is the way to obtain the right dimension and lenght for each component of the vectors. It is worth noting that this is necessary to compare them to experimental measurements.

9.3 On some equilibrium equations

9.3.1 The equation for dq/dt

Following the steps for the derivation of the time evolution of the rotational transform (section A.5), we derive a similar equation for the time evolution of the safety factor q.
The starting point is the same, the Faraday's law in eq.(A.54), that we now divide by ψ_p' to highlight a $q = \psi_t'/\psi_p'$ term in the equation:

$$\langle \mathbf{E} \cdot \mathbf{B} \rangle \frac{V'}{\psi_p'} = q \left[\frac{\partial \psi_p}{\partial t} + V_t(0) \right] - \left(\frac{\partial \psi_t}{\partial t} \right) \tag{9.135}$$

In order to delete the contribution from the loop voltage $V_t(0)$, let us take a radial derivative of equation (9.135). But, differently from the appendix A.5, we choose a radial derivative with respect to ψ_p:

$$\begin{aligned} \frac{\partial}{\partial \psi_p} \left[\langle \mathbf{E} \cdot \mathbf{B} \rangle \frac{V'}{\psi_p'} \right] &= \frac{\partial}{\partial \psi_p} \left(q \frac{\partial \psi_p}{\partial t} + V_t(0) \right) - \frac{\partial}{\partial \psi_p} \left(\frac{\partial \psi_t}{\partial t} \right) \\ &= \frac{\partial q}{\partial \psi_p} \frac{\partial \psi_p}{\partial t} + q \frac{\partial}{\partial \psi_p} \left(\frac{\partial \psi_p}{\partial t} \right) + \frac{\partial q}{\partial \psi_p} V_t(0) - \frac{\partial}{\partial \psi_p} \left(\frac{\partial \psi_t}{\partial t} \right) \\ &= \frac{\partial q}{\partial \psi_p} \left[\frac{\partial \psi_p}{\partial t} + V_t(0) \right] - \frac{\partial q}{\partial t} \end{aligned} \tag{9.136}$$

exchanging spatial and temporal derivatives in the second order derivatives. Highlighting the dq/dt term, one obtains:

$$\frac{\partial q}{\partial t} = \frac{\partial q}{\partial \psi_p}\left[\frac{\partial \psi_p}{\partial t} + V_t(0)\right] - \frac{\partial}{\partial \psi_p}\left[\langle \mathbf{E}\cdot\mathbf{B}\rangle \frac{V'}{\psi_p'}\right] \tag{9.137}$$

$$= \frac{\partial q}{\partial \psi_p}\left[\frac{\partial \psi_p}{\partial t} + V_t(0)\right] - \frac{\partial}{\partial \psi_p}\left[\eta_\parallel \langle (\mathbf{J}-\mathbf{J}_s)\cdot\mathbf{B}\rangle \frac{V'}{\psi_p'}\right] \tag{9.138}$$

$$= \frac{\partial q}{\partial \psi_p}\left[\frac{\partial \psi_p}{\partial t} + V_t(0)\right] + \tag{9.139}$$
$$- \frac{\partial}{\partial \psi_p}\left[\frac{\eta_\parallel \mu_0}{\psi_p'}(F\,I' - I\,F') - \eta_\parallel \langle \mathbf{J}_s\cdot\mathbf{B}\rangle \frac{V'}{\psi_p'}\right]$$

$$= \frac{\partial q}{\partial \psi_p}\left[\frac{\partial \psi_p}{\partial t} + V_t(0)\right] + \tag{9.140}$$
$$- \frac{\partial}{\partial \psi_p}\left[\frac{\eta_\parallel \mu_0}{\psi_p'} F^2 \left(\frac{I}{F}\right)'\right] + \frac{\partial}{\partial \psi_p}\left[\eta_\parallel \langle \mathbf{J}_s\cdot\mathbf{B}\rangle \frac{V'}{\psi_p'}\right]$$

$$= \frac{\partial q}{\partial \psi_p}\left[\frac{\partial \psi_p}{\partial t} + V_t(0)\right] + \frac{\partial}{\partial \psi_p}\left[\eta_\parallel \langle \mathbf{J}_s\cdot\mathbf{B}\rangle \frac{V'}{\psi_p'}\right] + \tag{9.141}$$
$$- \frac{\partial}{\partial \psi_p}\left[\frac{\eta_\parallel}{\mu_0}\psi_p'\,(S_{21}+S_{22}\,q)^2\,\frac{\partial}{\partial \rho}\Big(\frac{S_{11}+S_{12}\,q}{S_{21}+S_{22}\,q}\Big)\right]$$

These are the equations for the safety factor evolution. In section 7.3.2 one can find an example where equation (9.141) has been used.
More in detail, between eq.(9.137) and eq.(9.138) it has been used the Ohm's law in the form of eq.(A.53).
Between eq.(9.138) and eq.(9.139) (and between eq.(9.139) and eq.(9.140)) it has been used the parallel force balance equation, in the form of eq.(A.59).
Between eq.(9.140) and eq.(9.141) have been used the equations (A.60)–(A.61), where the poloidal current F and the toroidal one I are written in terms of the (radial derivative of the) poloidal and toroidal fluxes using the susceptance matrix elements. These equations are re–written to highlight the contribution of the safety factor instead of ι:

$$F^2 = \frac{(\psi_t')^2}{\mu_0^2}(S_{21}\,\iota + S_{22})^2 = (S_{21}+S_{22}\,q)^2 \tag{9.142}$$

$$\Big(\frac{I}{F}\Big)' = \frac{\partial}{\partial \rho}\Big(\frac{(S_{11}\,\iota+S_{12})}{(S_{21}\,\iota+S_{22})}\Big) = \Big(\frac{S_{11}+S_{12}\,q}{S_{21}+S_{22}\,q}\Big) \tag{9.143}$$

9.3.2 The equations for I' and F'

It is possible to write the ohmic equilibrium system (A.52) in a different way, i.e. as a system of two differential equation that can be integrated to obtain the currents I and F.
One can invert the susceptance matrix (A.44) defined in appendix A.3 to link the currents and the derivative of fluxes[5]:

$$\begin{pmatrix} \psi'_p \\ \psi'_t \end{pmatrix} = \mu_0 \begin{pmatrix} L_{11} & L_{12} \\ L_{21} & L_{22} \end{pmatrix} \begin{pmatrix} I \\ F \end{pmatrix} \tag{9.144}$$

where $[L_{ij}] = [S_{ij}]^{-1}$, and therefore

$$[L_{ij}] = \frac{1}{S_{11}\,S_{21} - S_{12}\,S_{22}} \begin{pmatrix} S_{22} & -S_{12} \\ -S_{21} & S_{11} \end{pmatrix} \tag{9.145}$$

Using the matrix L (instead of S) the ohmic equilibrium system (A.52) of section A.4 can be written in this form:

$$\begin{cases} \psi'_p = \mu_0(L_{11}\,I + L_{12}\,F) \\ \\ \psi'_t = \mu_0(L_{21}\,I + L_{22}\,F) \\ \\ V_t(0)\,\psi'_t + [V_p(0)\psi'_p] = \eta_{\|}\mu_0\,(F\,I' - I\,F') \\ \\ -p\,V' = F'\,\psi'_t + I'\,\psi'_p \end{cases} \tag{9.146}$$

Let us neglect for a first calculation the term proportional to the poloidal loop voltage on the axis, $V_p(0)$[6]. At the end of the section we will write the complete equation for I' and F' that contain also the terms proportional to the poloidal voltage.
Using the first two equations to substitute ψ'_p and ψ'_t in the other two equations, one obtains:

$$\begin{cases} (F\,I' - I\,F') = U_\varphi(L_{21}\,I + L_{22}\,F) \\ \\ -p\,V' = \mu_0\,F'\,(L_{21}\,I + L_{22}\,F) + \mu_0\,I'\,(L_{11}\,I + L_{12}\,F) \end{cases} \tag{9.147}$$

with the definition

$$U_\varphi = \frac{V_t(0)}{\eta_{\|}} \tag{9.148}$$

[5] ψ_p and ψ_t are used for the fluxes related, in a general coordinate system, to the poloidal–like and to the toroidal–like angle, respectively.

[6] If the poloidal–like angle lies on the poloidal plane, $V_P(0) = 0$ by definition. In this section we introduced the possibility of a term $V_P(0) \neq 0$ thinking to a poloidal–like angle topologically equivalent for example to a helical angle. In this case the circulation around the axis does not collapse into a point, and could be $V_P(0) \neq 0$.

From the first one it is easy to obtain an equation for I' to be substituted into the second one:

$$\begin{cases} I' = (U_\varphi\, L_{21})\,\frac{I}{F} + (U_\varphi\, L_{22})\,\frac{I}{F}\,F' \\ \\ -p\,V' = \mu_0\,F'\,(L_{21}\,I + L_{22}\,F) + \mu_0\,(L_{11}\,I + L_{12}\,F)\big[(U_\varphi\, L_{21})\,\frac{I}{F} + (U_\varphi\, L_{22})\,\frac{I}{F}\,F'\big] \end{cases} \tag{9.149}$$

From the last equation one can find an expression for F'. Using it also in the equation found for I', one finds the two equations that was looking for. The steps are simple algebra, we write only the final result.
Let me introduce the quantity d for easier notation:

$$d = \mu_0\,(L_{11}\,I^2 + L_{12}\,I\,F + L_{21}\,I\,F + L_{22}\,F^2) \tag{9.150}$$

The final equations are:

$$F' = -\frac{p'V'}{d}\,F - \frac{U_\varphi\,(L_{21}\,I + L_{22}\,F)\,(L_{11}\,I + L_{12}\,F)}{d} \tag{9.151}$$

$$\begin{aligned} I' &= -\frac{p'V'}{d}\,I - \frac{U_\varphi\,(L_{21}\,I + L_{22}\,F)\,(L_{11}\,I + L_{12}\,F)}{d}\,\frac{I}{F} + \\ &+ \frac{U_\varphi\,(L_{21}\,I + L_{22}\,F)}{F} \end{aligned} \tag{9.152}$$

To conclude, a non null poloidal loop voltage $V_p(0)$ adds some terms to the previous equations:

$$\begin{aligned} F' &= -\frac{p'V'}{d}\,F - \frac{U_\varphi\,(L_{21}\,I + L_{22}\,F)\,(L_{11}\,I + L_{12}\,F)}{d} + \\ &- \frac{U_\theta\,(L_{11}\,I + L_{12}\,F)^2}{d} \end{aligned} \tag{9.153}$$

$$\begin{aligned} I' &= -\frac{p'V'}{d}\,I - \frac{U_\varphi\,(L_{21}\,I + L_{22}\,F)\,(L_{11}\,I + L_{12}\,F)}{d}\,\frac{I}{F} + \\ &+ \frac{U_\varphi\,(L_{21}\,I + L_{22}\,F)}{F} + \\ &- \frac{U_\theta\,(L_{11}\,I + L_{12}\,F)^2}{d}\,\frac{I}{F} + \frac{U_\theta\,(L_{11}\,I + L_{12}\,F)}{F} \end{aligned} \tag{9.154}$$

with the same definition for U_θ

$$U_\theta = \frac{V_p(0)}{\eta_\parallel} \tag{9.155}$$

An example of solution of this system is given in 7.4 for the cylindrical paramagnetic pinch.

Conclusions

Summary

This thesis reports the work done to characterize the helical Reversed Field Pinch (RFP) states, named SHAx (Single Helical Axis), through the investigation of the magnetic topology in the core region and at the plasma edge. The work has been carried out in the RFX–mod experiment (Padova, Italy) and it mainly concerns the study of the 3D RFP physics which can be of interest also for the Stellarator and Tokamak comunities.

SHAx states are high plasma current states which feature the emergence of an ordered spontaneous magnetic structure in the otherwise chaotic core, and are therefore associated to improved confinement properties. The helical shape is related to the dominance of the innermost resonant mode in the MHD spectra (which is the $(m, n) = (1, 7)$ in RFX–mod device), but SHAx states are just Quasi Single Helicity (QSH) states due to the presence of secondary modes. It is worth reminding that the toroidicity of the system imposes a toroidal coupling between modes with the same toroidal mode number n and different poloidal mode number m, therefore a dominant mode arises also in the $m = 0$ mode spectrum (the $(m, n) = (0, 7)$ in RFX–mod device).
In the characterization of the plasma core, SHAx states are modeled as pure Single Helicity (SH) states (therefore neglecting the residual secondary modes). The contribution of the secondary modes and especially of the dominant $m = 0$ mode is considered in the characterization of the edge region and of the plasma–wall interaction.

A practical outcome of this thesis is the code named SHEq (Single Helical Equilibria) which is now routinely used for the computation of helical equilibria in RFX–mod. In these *Conclusions* the main results of this thesis and the possibility of future work using the SHEq code are summarized.

Characterization of the core region

For the core region, the research activity has been focused on the study of the helical SHAx configuration modeled as pure SH states.

Helical coordinates. The first step was the research of new helical coordinates that can well describe a Single Helicity state (SH) on a torus. In particular, the approach of using of the dominant tearing mode eigenfunction computed using Newcomb's equation for determining the position and shape of the helical flux surfaces has been evaluated.
As radial coordinate we use the helical flux (appropriate function of the poloidal and toroidal fluxes which labels the axi–symmetric magnetic flux surfaces), and we need then to find two angles (a poloidal-like and a toroidal-like angle) defined with respect to the helical axis of the system. Because of the toroidal dependence of the helical axis position in the poloidal plane, we define substantially a *3-dimensional coordinate system*. Moreover, no cylindrical approximation has been taken into account, looking for a curvilinear metric in order to well consider the toroidicity of the helical system (the difference between covariant and contravariant coordinates is then important). Angles have been defined both using a geometrical approach and the Hamiltonian approach to magnetic field lines. Using the more robust Hamiltonian approach it is possible to define also *helical straight-field-line coordinates*. More than one helical coordinate system has been completely defined: we calculated the Jacobian of the transformation between our helical coordinates and the Cartesian coordinates, and all the elements of the covariant and contravariant metric tensor. The complete definition of this coordinate system allows us to relate our coordinates to all the previous coordinates.
We just notice that we found a coordinate system valid in the whole plasma volume, which means both around the reversal surface and in the inner bean shaped flux surfaces (the more helically-distorted ones).

The SHEq–code and some example. The complete definition of the helical metrics is used by the SHEq-code, which is able to compute all the (helical) equilibrium plasma quantities.
First, the goodness of the *flux surface reconstruction*, labeled by the constancy of the helical flux, has been assessed by mapping the data of different diagnostics on the computed flux surfaces. Then, 3-dimensional fluxes, magnetic field and current density components can be computed, as well as their radial profile through *flux surface averaging* of these quantities.
As an example, we used the flux surface averages to calculate the thermal conductivity across the magnetic flux surfaces, averaging the energy equation in steady state for fluid at rest. Doing this we evaluated important quantities, such as the surface-averaged input power, which can be then fed into a transport code (e.g. the ASTRA transport code).

SHEq can also compute the *helical safety factor (q) profile*: during SHAx states the q-profile is not monotonic, with a maximum in correspondence of the Internal Transport Barrier that characterizes SHAx states.

SHEq has been coupled with two other codes: the VMEC equilibrium code and the ASTRA transport code.
The helical q-profile is used as input for the VMEC-code, where the helical safety factor is given as a function of the poloidal flux across the helical flux surfaces. What we found is a very good agreement with its convergence: on one hand this is a benchmark for SHEq's computations, on the other hand SHEq's helical safety factor profile is a good input for VMEC analysis.
SHEq and ASTRA have been coupled in order to perform transport analysis. ASTRA is a code most used in Tokamaks, but it can also be adapted to a 3-dimensional geometry, like the helical one in Stellarators or during SHAx states in RFPs. We used the coefficients of the metric tensor to adapt the ASTRA code to our helical geometry and some preliminary calculations of transport analysis were performed.
We are working with ASTRA also to study the evolution in time of SHEq's safety factor profiles, according to Ohm's law. This is an ongoing work in collaboration with the TJ-II (Ciemat, Madrid) team, which should allow to verify if the steady state equilibrium satisfies the Ohmic constraint given by Ohm's law, which is not an initial contraint for SHEq's computations.

Characterization of the edge region

For the plasma edge region, the research activity has been focused on the investigation of the plasma-wall interaction (PWI) during SHAx states, and in particular on the $m = 0$ magnetic islands role.
On the toroidal direction, a $n = 7$ pattern can be clearly seen in the plasma–wall interaction due to a magnetic boundary characterized by the $m = 0/n = 7$ island chain. On the poloidal plane the plasma–wall interaction is strongly affected by the phase relation between the dominant $m = 0/n = 7$ and $m = 1/n = 7$ modes, due to their toroidal coupling.
The imaginative idea of an *island divertor* to protect the RFX–mod first wall is proposed, justifying it with the regular pattern of the PWI. But the control of the edge region would require the control of the $m = 0$ island amplitudes and phases, in addition to the phase difference between the $m = 0/n = 7$ and $m = 1/n = 7$ modes. Some discharge of the 2011 RFX–mod experimental campaign were therefore dedicated to the control of these features by externally applied *non–zero boundary conditions* to both the $m = 0$ and $m = 1$ dominant modes.
To analyze the edge region during SHAx states we used field line tracing calculations and the reconstruction of the mode eigenfunction computed using Newcomb's equation, in addition to edge measurements.

Future work and collaborations

The data analysis of the 2011 RFX–mod experimental campaign discharge with non–zero boundary condition on the dominant modes is far to be complete. In particular better analysis on the phases of the modes are going on, in addition to the comparison between a larger set of edge measurements.

The activity on the use of the ASTRA code for solving time-dependent transport equations in helical equilibria according to Ohm's law will continue. This activity, which is being carried out in collaboration the Theory Group of the TJ-II Stellarator device (Ciemat, Madrid), are relevant both for RFPs in SHAx states and for Stellarators where some current is driven.

A benchmark of SHEq-code is going on with data from other experiments as well, in particular with the MST (Madison, Wisconsin) team, where the SHEq-code has recently been ported. MST is a RFP device, where SHAx states have been recently reached. We are using SHEq-code to perform their 3-dimensional magnetic reconstructions, and the mapping of 3-dimensional density and SXR (soft X–ray tomography) profiles is already a good result.

The approach of using Newcomb's equation for the reconstruction of mode eigenfunctions (used by SHEq code) uses an axi–symmetric current density profile that comes from a two–parameters fit of experimental data (the $\alpha - \Theta_0$ model), but without any constraint from the Ohm's law.
A new code for computing the dominant mode eigenfunction with a generic current density profile could be developed, base on the algorithm now used to compute the eigenfunction of poloidal and toroidal fluxes using Newcomb's equation. The code would be then integrated with the SHEq code for computing helical equilibria in QSH states, thus increasing its flexibility and allowing it to explore the effect of the current profile on the helical equilibria.

SHEq's equilibria could also be thought as the helical SH equilibria to be perturbed. One should therefore compute the eigenfunctions of the perturbation to the helical equilibria, in a way similar to the one used now to compute the eigenfunctions of the perturbation to the axi–symmetric fluxes (using Newcomb's equation). The $m = 0/n = 7$ mode could then be added to the helical equilibrium, in the same way as the dominant $m = 1/n = 7$ mode has been added to the axi–symmetric equilibrium to model SHAx states. Moreover, the MHD spectra related to the helical safety factor profile could be explored, together with its resonances. This could be interesting to better understand the magnetic topology of a SHAx state, and the possibility of

their external control.

Appendix A

MHD equations

A.1 MHD equations

MHD equations are the combination of the Maxwell equations for the (time) evolution of the electric and magnetic fields, $\mathbf{E}$ and $\mathbf{B}$; the total electric charge ρ_c conservation law; the mass, momentum and energy conservation laws; and the Ohm's law that relates the electric field to the current density $\mathbf{J}$:

$$\text{Gauss} \rightarrow \nabla \cdot \mathbf{E} = \frac{\rho_c}{\epsilon_0} \tag{A.1}$$

$$\text{magnetic solenoidity} \rightarrow \nabla \cdot \mathbf{B} = 0 \tag{A.2}$$

$$\text{Faraday} \rightarrow \nabla \times \mathbf{E} = -\frac{\partial \mathbf{B}}{\partial t} \tag{A.3}$$

$$\text{Ampère} \rightarrow \nabla \times \mathbf{B} = \mu_0 \left(\mathbf{J} + \epsilon_0 \frac{\partial \mathbf{E}}{\partial t} \right) \tag{A.4}$$

$$\text{Ohm} \rightarrow \mathbf{E} + \mathbf{v} \times \mathbf{B} = \eta \, \mathbf{J} \tag{A.5}$$

$$\text{mass conservation} \rightarrow \frac{\partial \rho_m}{\partial t} = -\nabla \cdot (\rho_m \, \mathbf{v}) \tag{A.6}$$

$$\begin{aligned} \text{Navier–Stokes} \rightarrow \; & \rho_m \frac{\partial \mathbf{v}}{\partial t} + \rho_m \left(\mathbf{v} \cdot \nabla \right) \mathbf{v} = \\ = \; & -\nabla \cdot \mathbf{P} + \mathbf{J} \times \mathbf{B} + \rho \, \mathbf{E} \end{aligned} \tag{A.7}$$

$$\text{energy conservation} \rightarrow \frac{d}{dt}\left(\frac{3p}{2} \right) + \frac{3p}{2} \nabla \cdot \mathbf{v} + \nabla \cdot \mathbf{q} + \left(\mathbf{P} \cdot \nabla \right) \cdot \mathbf{v} = \mathbf{J}' \cdot \mathbf{E}'$$

where $\mathbf{J}'$ is the current density measured in a frame of reference with velocity $\mathbf{v}$. In the same way, $\mathbf{E}'$ is the electric field measured in the frame of reference with velocity $\mathbf{v}$[1]. With respect to the electric field $\mathbf{E}$ and the current density

[1] The velocity $\mathbf{v}$ is the plasma flow, and one should also pay attention to the difference between the time derivative $(\partial/\partial t)$ in a fixed point and the derivatives on the moving flux surfaces (d/dt):

$$\frac{d}{dt} = \frac{\partial}{\partial t} + \left(\mathbf{v} \cdot \nabla \right) \tag{A.8}$$

$\mathbf{J}$ measured in a fixed point:

$$\mathbf{J}' = \mathbf{J} - \rho_c \mathbf{v} \tag{A.9}$$
$$\mathbf{E}' = \mathbf{E} + \mathbf{v} \times \mathbf{B} \tag{A.10}$$

In equations (A.1)–(A.8), ρ_m is the mass density, p the total kinetic pressure of the plasma, $\mathbf{q}$ the heat flux vector, and $\mathbf{P}$ the pressure tensor. Neglecting the viscous terms, only the diagonal terms in $\mathbf{P}$ are non null, and $\left(\nabla \cdot \mathbf{P}\right)$ reduces to ∇p in an isotropic plasma. This is the assumption used in this thesis (if not said differently).
Usually, the energy conservation law is replaced by some assumption on the system, e.g. the assumption of a given plasma pressure p.
Navier–Stokes equation is the momentum conservation law, also said the force balance equation.

Some other useful equations arise combining the equations below. Without make any proof, we write some of them: from Gauss and Ampère's laws:

$$\nabla \cdot \mathbf{J} = -\frac{\partial \rho}{\partial t} \tag{A.11}$$

From Faraday's, Ampère's and Ohm's laws:

$$\frac{\partial \mathbf{B}}{\partial t} = \nabla \times \left(\mathbf{v} \times \mathbf{B}\right) + \frac{\eta}{\mu_0} \nabla^2 \mathbf{B} \tag{A.12}$$

from Ampère's and Navier–Stokes laws:

$$\rho_m \frac{d\mathbf{v}}{dt} = \nabla p + \frac{1}{\mu_0} \underbrace{\left(\nabla \times \mathbf{B}\right) \times \mathbf{B}}_{= -\frac{\nabla B^2}{2} + \left(\mathbf{B} \cdot \nabla\right) \mathbf{B}} \tag{A.13}$$

From eq.(A.12) one can see that, for $\mathbf{v} = 0$ (equilibrium condition) and non null resistivity, the magnetic field is not frozen to the plasma, but it follows a diffusive equation where the resistivity η is the diffusion coefficient. This defines the typical diffusive time scale: $\tau_R = \mu_0 L^2/\eta$ is said the characteristic *resistive time* (L being the characteristic length). From eq.(A.13) one can see that the equilibrium condition ($\mathbf{v} = 0$) is realized by the balance between the gradient of the magnetic and kinetic pressure ($(p + B^2)/(2\mu_0)$) and the action of the parallel compression of the magnetic field ($\left(\mathbf{B} \cdot \nabla\right) \mathbf{B}/\mu_0$).

Before some simplifications, it is worth noting that the equation that fixes the solenoidity of the magnetic field is redundant. One should always pay attention to the number of variables and the number of equations in the system.

Some simplifications

First of all one usually neglects the contribution of the $\left(\partial\mathbf{E}/\partial t\right)$ current comparing to the conductive current $\mathbf{J}$ in the Ampère's law.
Neutral plasmas are considered, therefore $\rho_c = 0$.
As already said, also the viscosity of the plasma is frequently neglected, and $\left(\nabla\cdot\mathbf{P}\right)$ reduces to ∇p (Navier–Stokes equation and energy conservation law).
The energy conservation is replaced by a given plasma pressure p.

All these simplifications bring to the system:

$$\nabla \cdot \mathbf{E} = 0 \tag{A.14}$$
$$\nabla \cdot \mathbf{B} = 0 \tag{A.15}$$
$$\nabla \times \mathbf{E} = -\frac{\partial \mathbf{B}}{\partial t} \tag{A.16}$$
$$\nabla \times \mathbf{B} = \mu_0 \mathbf{J} \tag{A.17}$$
$$\mathbf{E} + \mathbf{v} \times \mathbf{B} = \eta \mathbf{J} \tag{A.18}$$
$$\frac{\partial \rho_m}{\partial t} = -\nabla \cdot (\rho_m \mathbf{v}) \tag{A.19}$$
$$\rho_m \frac{\partial \mathbf{v}}{\partial t} + \left(\mathbf{v} \cdot \nabla\right) \mathbf{v} = -\nabla p + \mathbf{J} \times \mathbf{B} \tag{A.20}$$

Another simplification is to consider just the equilibrium system of equation.

Equilibrium equations

Also called Magnetostatic, let us now write the equations for a steady state equilibrium, where $\mathbf{v} = 0$, together with the time derivative $\partial/\partial t = 0$ (and therefore also $d/dt = 0$):

$$\nabla \cdot \mathbf{E} = 0 \tag{A.21}$$
$$\nabla \cdot \mathbf{B} = 0 \tag{A.22}$$
$$\nabla \times \mathbf{E} = 0 \tag{A.23}$$
$$\nabla \times \mathbf{B} = \mu_0 \mathbf{J} \tag{A.24}$$
$$\mathbf{E} = \eta \mathbf{J} \tag{A.25}$$
$$\mathbf{J} \times \mathbf{B} = \nabla p \tag{A.26}$$

Equation (A.23) implies an electrostatic $\mathbf{E}$, that must be the divergence of some potential. This and some more considerations about the Ohm's law are in section A.2.

This is the system usually used to study the plasma equilibria. One can find another equivalent formulation in section A.4, where only the averaged Ohm's law is considered.

Force free conditions

The condition

$$\mathbf{J} \times \mathbf{B} = 0 \tag{A.27}$$

is the so–called *force free condition* of the force balance (or Navier–Stokes) equation, and it is related to the vanishing of the pressure gradient (compare eq.(A.26) and eq.(A.27).

From eq.(A.27), the current density is parallel to the magnetic field. To emphasize this, one can write

$$\mathbf{J} = \sigma \mathbf{B} \tag{A.28}$$

where σ is the proportionality profile.

The force free condition is the condition always chosen in this thesis and in particular for SHEq calculations (see chapter 3).
In the introduction a model, called $\alpha - \Theta_0$ model, to obtain the σ profile fitting experimental data is explained.

A.2 The stationary electric field and the Ohmic constraint

A current, to be sustained, must be consistent with Ohm's law and the Faraday's law.
Under stationary condition (the time variation of the magnetic field must vanish), the Faraday's law is

$$\nabla \times \mathbf{E} = 0 \tag{A.29}$$

and the static electric field must therefore be the gradient of some potential[2]:

$$\mathbf{E} = -\nabla\phi + V_t \frac{\nabla\varphi}{2\pi} \tag{A.30}$$

$$= -\nabla\phi + \mathbf{E}_0 \tag{A.31}$$

$\mathbf{E}_0$ is the uniform toroidal induction electric field, and $\mathbf{E} = -\nabla\phi$ is a fluctuating electric field produced by a charge separation[3].

[2]The loop voltages must have no spatial dependence and the gradient of the poloidal angle must be therefore zero in all the plasma volume, due to the fact that must be null on its axis. That is why there is not a term $V_p \nabla\theta/2\pi$.

[3]Even if the plasma is globally neutral, regions with net positive or negative imbalance can exist.

The electrostatic potential ϕ, the electrostatic field $\mathbf{E}_0 = -\nabla\phi$ and the charge distribution ρ_s are related by Laplace's equation:

$$\nabla \cdot \mathbf{E} = -\nabla^2\phi = \frac{\rho_s}{\epsilon_0} \tag{A.32}$$

and the charge distribution provides a current density $\mathbf{J} = \rho_s\,\mathbf{v}$.

From Ohm's law, and a stationary electric field, one can obtain the Ohmic constraint that any stationary equilibrium should satisfy.
Projecting the Ohm's law on the magnetic field direction, one obtains the so–called *parallel Ohm's law*[4]:

$$\mathbf{E} \cdot \mathbf{B} = \eta\,\mathbf{J} \cdot \mathbf{B} \tag{A.33}$$

because of the vanishing of the triple product $\big(\mathbf{v} \times \mathbf{B}\big) \cdot \mathbf{B}$. The stationary electric field must be of the form in equation (A.30), therefore the parallel Ohm's law in stationary conditions can be written as:

$$-\mathbf{B} \cdot \nabla\phi + \frac{V_t}{2\pi}\,\mathbf{B} \cdot \nabla\varphi = \eta\,\mathbf{J} \cdot \mathbf{B} \tag{A.34}$$

It is usually interesting to study the parallel Ohm's law averaged on magnetic flux surfaces, because the term related to the (usually unknown) electrostatic potential ϕ vanishes: $\langle -\mathbf{B} \cdot \nabla\phi \rangle = 0$ due to the divergence theorem. The averaged Ohm's law for an electrostatic potential is the *Ohmic constraint*, that must be valid on each magnetic flux surface[5]:

$$\frac{V_t}{2\pi}\,\langle \mathbf{B} \cdot \nabla\varphi \rangle = \langle \eta\,\mathbf{J} \cdot \mathbf{B} \rangle \tag{A.36}$$

An information can be added using the force balance equation. If force free conditions are assumed, $\mathbf{J} = \sigma\mathbf{B}$, therefore the Ohmic constraint can also assume the form[6]:

$$\frac{V_t}{2\pi}\,\langle \mathbf{B} \cdot \nabla\varphi \rangle = \sigma\,\langle \eta\,B^2 \rangle \tag{A.39}$$

[4] So, even when $\mathbf{v} \neq 0$, the parallel Ohm's law takes the form in equation (A.25): $\mathbf{E}_\parallel = \eta_\parallel\,\mathbf{J}_\parallel$.

[5] In a cylinder, with inductive electric field $\mathbf{E}_0$ parallel to the axial direction z, and $\nabla\varphi \mapsto \mathbf{e}_z$, the Ohmic constraint takes the form:

$$\mathbf{E}_0 \langle B_z \rangle = \langle \eta\,\mathbf{J} \cdot \mathbf{B} \rangle \tag{A.35}$$

[6] This is the form used by Finn (see section 7.1) to prove the impossibility of an ohmic reversal of the toroidal magnetic field in any axi–symmetric configurations and, on the other side, the possibility of the reversal in a helical symmetric configuration. Using force free conditions and Ampère's law, the proportionality σ between the magnetic field and the current density can be written as:

$$\sigma = \frac{d\langle B_{tor} \rangle}{d\rho} \tag{A.37}$$

using for ρ a label of the magnetic flux surfaces. B_{tor} is the axial B_z magnetic field in a

A.3 Susceptance matrix

Following P.I. Strand and W.A. Houlberg (S&H) [74], one can introduce the so–called *susceptance matrix*, which relates the radial derivative of the fluxes to the currents. We use the symbol ρ to label the magnetic flux surfaces, and (θ, φ) for the general poloidal–like and toroidal–like angles.

The poloidal and the toroidal fluxes (ψ_p and ψ_t respectively) can be written in terms of the contravariant components of the magnetic field (B^i):[7]

$$\psi_p(\rho) = \int_0^{2\pi} d\varphi \int_0^{\rho} \sqrt{g}\, B^\theta \, d\rho \tag{A.40}$$

$$\psi_t(\rho) = \int_0^{2\pi} d\theta \int_0^{\rho} \sqrt{g}\, B^\varphi \, d\rho \tag{A.41}$$

$\sqrt{g}$ is the Jacobian of the coordinate system.
The poloidal and toroidal currents (F and I respectively) can be written in terms of the covariant components of the magnetic field (B_i), using Amere's law:[8]

$$F(\rho) = \int_0^{2\pi} d\varphi \int_0^{\rho} \sqrt{g}\, J^\theta \, d\rho = \frac{1}{\mu_0} \int_0^{2\pi} d\varphi \, B_\varphi \tag{A.42}$$

$$I(\rho) = \int_0^{2\pi} d\theta \int_0^{\rho} \sqrt{g}\, J^\varphi \, d\rho = \frac{1}{\mu_0} \int_0^{2\pi} d\theta \, B_\theta \tag{A.43}$$

The currents are linearly related to the radial derivative of the fluxes through the so–called susceptance matrix S, with elements S_{ij}[9]

$$\mu_0 \begin{pmatrix} I \\ F \end{pmatrix} = \begin{pmatrix} S_{11} & S_{12} \\ S_{21} & S_{22} \end{pmatrix} \begin{pmatrix} \psi_p' \\ \psi_t' \end{pmatrix} \tag{A.44}$$

By using the general properties of curvilinear coordinates, the definitions (A.40)–(A.43), and the canonical form of the magnetic field

$$\mathbf{B} = \frac{1}{2\pi}(\nabla\psi_t \times \nabla\theta - \nabla\psi_p \times \nabla\varphi) \tag{A.45}$$

one can obtain equations (37)–(40) of S&H's paper, where the S_{ij} susceptance matrix elements are entirely written in terms of the metrics.

---

cylinder, o the toroidal one in a torus. Using eq.(A.39), the Ohmic constraint takes the form:

$$\frac{d\langle B_{tor}\rangle}{d\rho} = \frac{V_t}{2\pi} \frac{\langle B_{tor}\rangle}{\langle \eta\, B^2\rangle} \tag{A.38}$$

In the case of helical symmetry, it is the Pinch–Stellarator equation of section 7.1.

[7] Eq. (1)–(2) of S&H's paper, [74].
[8] Eq. (5)–(6) of S&H's paper, [74].
[9] Eq. (7) of S&H's paper, [74].

For straight field line coordinates, for which the S matrix is symmetric, the S_{ij} reduces to:

$$S_{11} = \frac{V'}{4\pi^2}\langle\frac{g_{\theta\theta}}{g}\rangle \tag{A.46}$$

$$S_{12} = \frac{V'}{4\pi^2}\langle\frac{g_{\theta\varphi}}{g}\rangle = S_{21} \tag{A.47}$$

$$S_{22} = \frac{V'}{4\pi^2}\langle\frac{g_{\varphi\varphi}}{g}\rangle \tag{A.48}$$

$V'(\rho)$ is the radial derivative of the volume[10], g_{ij} the metrics elements.
Let us notice that in axi–symmetric geometries, S is a diagonal matrix ($g_{ij} = 0$ for $i \neq 0$).
The radial dependence of the S_{ij} elements is related to the choice of the flux surface label ρ. One can see some example in section 9.2.2

To conclude, another important relation in S&H's paper[11] is the equation for the rotational transform, that can be derived inverting the susceptance matrix S:

$$\iota = \frac{\psi'_p}{\psi'_t} = \frac{S_{22}I - S_{12}F}{S_{11}F - S_{21}I} = \frac{\mu_0 I}{S_{11}\psi'_t} - \frac{S_{12}}{S_{11}} \tag{A.50}$$

In this equation for ι the last term is a current free term, called Stellarator term[12]. This term has been written first by V.D. Pustovitov [66] for a cylindrical non axi–symmetric magnetic configuration: it is the geometrical term discussed in section 7.1 that allows the reversal of the helical deformed RFP configuration.

We use equation (A.50) for the rotational transform ι to evolve it in time (section 7.3).

[10]

$$V' = \iint_0^{2\pi} \sqrt{g}\, d\theta\, d\varphi \tag{A.49}$$

[11] Eq. (8) of S&H's paper, [74].
[12] It is also said vacuum term, due to the fact that Stellarators usually runs without plasma current.

A.4 S&H's equations

The adequate system to describe a magnetostatic plasma equilibrium compatible with Ohm's law, is[13]:

$$\begin{cases} \mathbf{J} \times \mathbf{B} = \nabla p \\ \nabla \times \mathbf{B} = \mu_0 \mathbf{J} \\ \nabla \cdot \mathbf{B} = 0 \\ \langle \mathbf{E} \cdot \mathbf{B} \rangle = \eta_{\parallel} \langle \mathbf{J} \cdot \mathbf{B} \rangle \\ \nabla \times \mathbf{E} = 0 \end{cases} \tag{A.51}$$

The averaged (on magnetic flux surfaces) Ohm's law has been considered, and not yet the force free condition ($\nabla p \neq 0$).
Following P.I. Strand and W.A. Houlberg (S&H) [74] and M.D. Kruskal and R.M. Kulsrud (K&K) [76], it is possible to write this system in another form:

$$\begin{cases} \mu_0 \, I = S_{11} \psi_p' + S_{12} \psi_t' \\ \mu_0 \, F = S_{21} \psi_p' + S_{22} \psi_t' \\ V_t(0) \, \psi_t' + V_p(0) \psi_p' = \eta_{\parallel} \mu_0 \, (F \, I' - I \, F') \\ -p \, V' = F' \, \psi_t' + I' \, \psi_p' \end{cases} \tag{A.52}$$

In these equations: F is the poloidal current (A.42), I the toroidal current (A.43); ψ_p is the poloidal flux (A.40), ψ_t the toroidal flux (A.41). $V_t(0)$ is the toroidal loop voltages on the magnetic axis of the system; $V_p(0)$ is the poloidal loop voltage on the magnetic axis, which is always zero for poloidal–like angles that lie on the poloidal plane (but could be non vanishing in the case of a poloidal–like angle topologically equivalent to a helical angle). p is the total plasma kinetic pressure.
The first two equations[14] are the Ampère's law, written with the susceptance matrix formalism (appendix A.3) that relates the currents and the derivative of the fluxes in general coordinate system [15].
The third equation[16] is the parallel Ohm's law, averaged on magnetic flux

[13] In order: the force balance equation, Ampère's law, the divergence free of the magnetic field. The parallel Ohm's law averaged on flux surfaces, and Faraday's law.
[14] Eq. (7) of S&H's paper, [74].
[15] The names *poloidal* and *toroidal* are used for quantities related to the poloidal–like and to the toroidal–like angle, respectively.
[16] Eq. (11)+(19) of S&H's paper, [74] or equation (D12) of M.D. K&K's paper, [76].

surfaces, and the electric field has been eliminated in favor of the time derivative of the fluxes, using Faraday's law. It is worth noting that in this equation there is a term more than in S&H and K&K, in order to allow the use of a poloidal–like angle related to a non vanishing loop voltage $V_p(0)$ on the axis. The last equation [17] is the radial force balance equation.

Solving this system one can compute a steady state ohmic equilibrium. In section 9.3.2 this system is rearranged in two differential equations for the currents I and F. An example of solution is given in section 7.4 for the cylindrical paramagnetic pinch.

Using this system one can derive an equation for the equilibrium time evolution in appendix A.5. Two example of solution are given in sections 7.3.1 and 7.3.2, for the evolution of the rotational transform in the TJ-II Stellarator and the evolution of the safety factor profile in the RFX–mod RFP.

A.5 The equation for $d\iota/dt$

We derive here the equation for the time evolution of the rotational transform, already present in S&H's paper [74][18] (but not all the steps are present there).

The derivation of Eq. (22) of S&H's paper starts from the averaged parallel Ohm's law and from Faraday's law[19][20]. The two equations are:

$$\langle \mathbf{E}\cdot\mathbf{B}\rangle = \eta_{\parallel}\langle(\mathbf{J}-\mathbf{J}_s)\cdot\mathbf{B}\rangle \tag{A.53}$$

$$\langle \mathbf{E}\cdot\mathbf{B}\rangle V' = \left[\frac{\partial\psi_p}{\partial t}+V_t(0)\right]\psi_t' - \left(\frac{\partial\psi_t}{\partial t}\right)\psi_p' \tag{A.54}$$

In the averaged Ohm's law it has been taken into account also a non–inductive source, like the Boostrap current $\mathbf{J}_s$. This is done for completeness, and to follow exactly S&H's calculations, but this contribution is not used in the framework of this thesis.
In order to highlight the rotational transform $\iota = \psi_p'/\psi_t'$ (in which we are interested), let us first divide Faraday's equation (A.54) by ψ_t':

$$\langle \mathbf{E}\cdot\mathbf{B}\rangle \frac{V'}{\psi_t'} = \left[\frac{\partial\psi_p}{\partial t}+V_t(0)\right] - \left(\frac{\partial\psi_t}{\partial t}\right)\iota \tag{A.55}$$

[17] Eq. (12) of S&H's paper, [74] or equation (D19) of K&k's paper, [76]. First derived by KeK.
[18] Eq. (22) of S&H's paper, [74].
[19] Eq. (19) of S&H's paper, [74].
[20] in Faraday's equation $V_p(0) = 0$. We do not account for the $V_p(0) \neq 0$ case in the derivation of the rotational transform evolution (as done by Strand and Houlberg).

Getting now a radial derivative $(\partial/\partial\psi_t)$ of eq.(A.55) in order to cancel the contribution from the induced loop voltage $V_t(0)$, we write[21]

$$\frac{\partial}{\partial\psi_t}\left[\langle\mathbf{E}\cdot\mathbf{B}\rangle\,\frac{V'}{\psi_t'}\right] = \frac{\partial}{\partial\psi_t}\left(\frac{\partial\psi_p}{\partial t}\right) - \frac{\partial}{\partial\psi_t}\left(\iota\,\frac{\partial\psi_t}{\partial t}\right) \tag{A.56}$$

$$= \frac{\partial}{\partial t}\left(\frac{\partial\psi_p}{\partial\psi_t}\right) - \left(\frac{\partial\iota}{\partial\psi_t}\right)\left(\frac{\partial\psi_t}{\partial t}\right) - \iota\,\frac{\partial}{\partial t}\left(\frac{\partial\psi_t}{\partial\psi_t}\right) \tag{A.57}$$

(it is always possible to exchange spatial and temporal derivatives in a second order derivative).
Highlighting the $d\iota/dt$ term, one obtains:

$$\frac{\partial\iota}{\partial t} = \left(\frac{\partial\iota}{\partial\psi_t}\right)\left(\frac{\partial\psi_t}{\partial t}\right) + \frac{\partial}{\partial\psi_t}\left[\langle\mathbf{E}\cdot\mathbf{B}\rangle\,\frac{V'}{\psi_t'}\right] \tag{A.58}$$

The final form of this equation uses the Ohm's law, eq.(A.53) for the term $\langle\mathbf{E}\cdot\mathbf{B}\rangle$, and equation Eq. (11) of S&H's paper, [74] (see also section A.4):

$$\langle\mathbf{J}\cdot\mathbf{B}\rangle\,V' = \mu_0\,(F\,I' - I\,F') = \mu_0\,F^2\left(\frac{I}{F}\right)' \tag{A.59}$$

I and F are the toroidal and poloidal currents respectively, and one can therefore use the susceptance matrix (appendix A.3) to write also:

$$F^2 = \frac{(\psi_t')^2}{\mu_0^2}\,(S_{21}\,\iota + S_{22})^2 \tag{A.60}$$

$$\left(\frac{I}{F}\right)' = \frac{\partial}{\partial\rho}\left(\frac{(S_{11}\,\iota + S_{12})}{(S_{21}\,\iota + S_{22})}\right) \tag{A.61}$$

to obtain the right form of equation (22) in S&H's paper:

$$\frac{\partial\iota}{\partial t} = \frac{\partial\iota}{\partial\psi_t}\frac{\partial\psi_t}{\partial t} + \frac{\partial}{\partial\psi_t}\left[\frac{\eta_\parallel}{\mu_0}\psi_t'\,(S_{21}\iota + S_{22})^2\,\frac{\partial}{\partial\rho}\left(\frac{S_{11}\iota + S_{12}}{S_{21}\iota + S_{22}}\right)\right] + - \frac{\partial}{\partial\psi_t}\left[\eta_\parallel\langle\mathbf{J_s}\cdot\mathbf{B}\rangle\frac{\partial V}{\partial\psi_t}\right] \tag{A.62}$$

This equation is used in section 7.3.1 to evolve the TJ-II (Ciemat, Madrid) Stellarator rotational transform profile.

[21] $V_t(0)$ is a constant, therefore $\frac{\partial V_t(0)}{\partial\psi_t} = 0$.

Appendix B

Toroidal coordinates

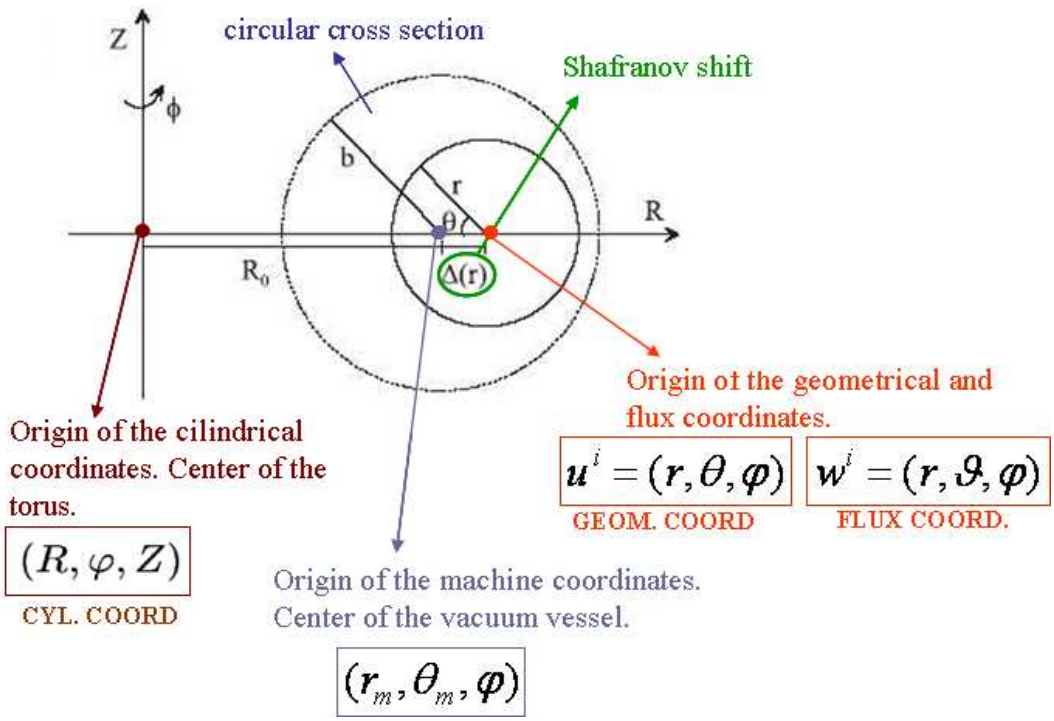

Figure B.1: Scheme of the coordinates defined on the circular–cross–section of the axi–symmetric magnetic field in RFX–mod. The coordinates and their metrics are defined in this appendix.

B.1 On curvilinear coordinates

The covariant metric tensor for a curvilinear coordinate system $u^i = (u^1, u^2, u^3)$ is defined by

$$g_{ij} = \mathbf{e}_i \cdot \mathbf{e}_j \,, \tag{B.1}$$

where

$$\mathbf{e}_i = \frac{\partial \mathbf{x}}{\partial u^i} \,, \tag{B.2}$$

while the contravariant one is defined by

$$g^{ij} = \nabla u^i \cdot \nabla u^j \tag{B.3}$$

where

$$\nabla u^i = \frac{\partial u^i}{\partial \mathbf{x}} \,. \tag{B.4}$$

The two tensors are related by $g^{ij} \cdot g_{jk} = \delta^i_k$, so g^{ij} is the inverse matrix of g_{jk}. The Jacobian of the coordinate system is

$$\sqrt{g} = \sqrt{\det[g_{ij}]} = (\nabla u^1 \cdot \nabla u^2 \times \nabla u^3)^{-1} \tag{B.5}$$

Given a vector $\mathbf{A}$, its contravariant components are defined as

$$A^i = \mathbf{A} \cdot \nabla u^i \qquad \text{or} \qquad A^i = g^{ij} A_j \tag{B.6}$$

the second one expresses the contravariant component in terms of the covariant ones. In the same way,

$$A_i = \mathbf{A} \cdot \mathbf{e}_i \qquad \text{or} \qquad A_i = g_{ij} A^j \tag{B.7}$$

It is worth noting that in curvilinear metrics the basis vectors $\mathbf{e}_i$ and ∇u^i are not adimensional (the dimension depending on the dimension of the coordinate u^i) and do not have unitary length.
To go back to field components that have the right dimension of a measured field and the whole length (without sharing it with the basis vector) it is enough to divide the basis vectors by their norm. But one needs to pay attention to the fact that this can be done just at the end of all the calculations, because tensor calculus is based on the hypothesis of non–adimensional and non–unitary length basis vectors! Some example can be find in chapter 5.

B.2 Coordinate systems on a torus

The metrics elements and the Jacobian of the cylindrical, geometrical and of the toroidal coordinate systems defined in chapter 4 are here collected.

B.2.1 Cylindrical coordinates

The cylindrical coordinate system is a diagonal metrics, that therefore do not accounts for the toroidicity of the problem. One can think to a periodic cylinder to model a torus in a simple way.

Cylindrical coordinates (R, φ, Z) are defined with respect to Cartesian coordinates $\mathbf{x} = (x, y, z)$ as follows (see fig.1.4):

$$\begin{cases} x = R\cos\varphi \\ y = R\sin\varphi \\ z = Z \end{cases} \tag{B.8}$$

Therefore, from eq.(B.2):

$$\mathbf{e}_R = \frac{\partial \mathbf{x}}{\partial R} = \begin{pmatrix} \cos\varphi \\ \sin\varphi \\ 0 \end{pmatrix}, \quad \mathbf{e}_\varphi = \frac{\partial \mathbf{x}}{\partial \varphi} = \begin{pmatrix} -R\sin\varphi \\ R\cos\varphi \\ 0 \end{pmatrix}, \quad \mathbf{e}_Z = \frac{\partial \mathbf{x}}{\partial Z} = \begin{pmatrix} 0 \\ 0 \\ 1 \end{pmatrix}$$

and, from eq.(B.1) and its inverse:

$$\mathbf{g_{ij}}^{cyl} = \begin{pmatrix} 1 & 0 & 0 \\ 0 & R^2 & 0 \\ 0 & 0 & 1 \end{pmatrix} \quad \mathbf{g^{ij}}_{cyl} = \begin{pmatrix} 1 & 0 & 0 \\ 0 & \frac{1}{R^2} & 0 \\ 0 & 0 & 1 \end{pmatrix}$$

The Jacobian, from eq.(B.5), is: $J_{cyl} = \sqrt{g}_{cyl} = R$.

B.2.2 Geometrical coordinates

The geometrical coordinate system is a non–diagonal metrics, that therefore does account for the toroidicity of the problem.
The geometrical coordinates have been defined in section 3.1.1 with the symbol $u^i = (r, \theta, \varphi)$. We refer to the figure of section 3.1.1 for a geometrical interpretation of their definition, usually related to the cylindrical system (R, φ, Z):

$$\vec{x} = (x, y, z) = (R\cos\varphi,\ R\sin\varphi,\ Z)$$

$$\begin{cases} R = R_0 - r\cos\theta + \Delta(r) \\ Z = r\sin\theta \end{cases}$$

The angle θ is called poloidal and the angle φ is called toroidal. A non–zero horizontal $\Delta(r)$ shift of the non-concentric circular magnetic flux surfaces (related to $\mathbf{B}_0$ defined in chapter 3) is a consequence of the toroidicity of the system.

Using (B.1) and (B.2) the g^u_{ij} elements, that link them to the Cartesian coordinates, can be explicitly calculated:

$$g^u_{ij} = \begin{pmatrix} 1 - 2\Delta'\cos\theta + \Delta'^2 & r\Delta'\sin\theta & 0 \\ r\Delta'\sin\theta & r^2 & 0 \\ 0 & 0 & R^2 \end{pmatrix} \tag{B.9}$$

* The g^{ij}_u elements of the inverse matrix are usually calculated from the formulas for the inversion of a block diagonal matrix ($g^u_{r\varphi} = g^u_{\varphi r} = 0$ and $g^u_{\theta\varphi} = g^u_{\varphi\theta} = 0$):

$$\mathbf{g^{ij}_u} = \frac{1}{g_u} \begin{pmatrix} g^u_{\theta\theta}\, g^u_{\varphi\varphi} & -g^u_{r\theta}\, g^u_{\varphi\varphi} & 0 \\ -g^u_{r\theta}\, g^u_{\varphi\varphi} & g^u_{rr}\, g^u_{\varphi\varphi} & 0 \\ 0 & 0 & g^u_{rr}\, g^u_{\theta\theta} - (g^u_{r\theta})^2 \end{pmatrix} \tag{B.10}$$

The Jacobian $\sqrt{g_u} = \sqrt{\det[g^u_{ij}]} = (\nabla r \cdot \nabla\theta \times \nabla\varphi)^{-1}$ of the geometric coordinates is given by

$$\sqrt{g_u} = rR(1 - \Delta'\cos\theta) \tag{B.11}$$

B.2.3 Toroidal straight coordinates

In section 3.1.1 we have defined the coordinate system $w^i = (r, \vartheta, \varphi)$, which is the *magnetic* coordinate system of the zeroth-order axisymmetric equilibrium $\mathbf{B}_0$: it is the coordinate system that one obtains deforming the poloidal angle θ of the geometrical coordinates u^i in order to achieve straight magnetic field lines:

$$\begin{cases} r = r \\ \vartheta = \theta + \lambda(r, \theta) \\ \varphi = \varphi \end{cases}$$

For $\lambda(r, \theta)$ we have obtained an explicit expression from Ampère's law, eq.(3.11).

Tensor metrics elements

We write the metrics elements for the system $w^i = (r, \vartheta, \varphi)$ relating them to the metrics elements of the geometrical coordinate system $u^i = (r, \theta, \varphi)$.
The contravariant metric tensor elements can be computed using the relations between the gradients of the two coordinate systems:

$$\nabla r = \nabla r \tag{B.12}$$

$$\nabla\vartheta = \left(1 + \frac{\partial\lambda}{\partial\theta}\right)\nabla\theta + \frac{\partial\lambda}{\partial r}\nabla r \tag{B.13}$$

$$\nabla\varphi = \nabla\varphi \tag{B.14}$$

From eq.(B.3) is therefore found:

$$g_w^{r\vartheta} = g_w^{\vartheta r} = \frac{\partial\lambda}{\partial r} g_u^{rr} + \left(\frac{\partial\lambda}{\partial\theta} + 1\right) g_u^{r\theta} \tag{B.15}$$

$$g_w^{\vartheta\vartheta} = \left(\frac{\partial\lambda}{\partial r}\right)^2 g_u^{rr} + 2\left(\frac{\partial\lambda}{\partial\theta} + 1\right)\frac{\partial\lambda}{\partial r} g_u^{r\theta} + \left(\frac{\partial\lambda}{\partial\theta} + 1\right)^2 g_u^{\theta\theta} \tag{B.16}$$

while all the other elements are equal to those of the geometric coordinates:

$$g_w^{rr} = g_u^{rr} \tag{B.17}$$

$$g_w^{\varphi\varphi} = g_u^{\varphi\varphi} \tag{B.18}$$

$$g_w^{r\varphi} = g_w^{\varphi r} = 0 \tag{B.19}$$

$$g_w^{\vartheta\varphi} = g_w^{\varphi\vartheta} = 0 \tag{B.20}$$

The g_{ij}^w elements of the inverse matrix can again be calculated from the formulas for the inversion of a block diagonal matrix (see eq.(B.35)), or can be computed by writing the relation between the w^i and the (R, φ, Z) cylindrical system.
In this second case, using equations (3.14), the covariant metric tensor elements are found to be

$$g_{rr}^w = 1 + \left(2\Delta'^2 + \frac{r^2}{2R_0^2} + \frac{r^2}{2}\Delta''^2 - \frac{r^2}{R_0}\Delta'' - \frac{2r}{R_0}\Delta' + r\Delta'\Delta''\right) - 2\Delta'\cos\vartheta + o(\epsilon^2 b^2) \tag{B.21}$$

$$g_{\vartheta\vartheta}^w = r^2\left(1 + \frac{r^2}{2R_0^2} + \frac{1}{2}\Delta'^2 - \frac{r}{R_0}\Delta'\right) - 2r^2\left(\frac{r}{R_0} - \Delta'\right)\cos\vartheta + o(\epsilon^2 b^2) \tag{B.22}$$

$$g_{r\vartheta}^w = r\left(r\Delta'' + \Delta' - \frac{r}{R_0}\right)\sin\vartheta + o(\epsilon^2 b) \tag{B.23}$$

$$g_{\varphi\varphi}^w = R^2. \tag{B.24}$$

with $g_{r\varphi}^w = g_{\varphi r}^w = g_{\vartheta\varphi}^w = g_{\varphi\vartheta}^w = 0$.
In computing these elements the approximation used in ref.[53] has been adopted of retaining the secular terms (i.e. those not dependent on ϑ) up to $o(\epsilon^2)$ and the harmonics up to $o(\epsilon)$.
One can therefore write:

$$\mathbf{g_{ij}^w} = g\begin{pmatrix} g^{\vartheta\vartheta}g^{\varphi\varphi} & -g^{r\vartheta}g^{\varphi\varphi} & 0 \\ -g^{r\vartheta}g^{\varphi\varphi} & g^{rr}g^{\varphi\varphi} & 0 \\ 0 & 0 & \underbrace{g^{rr}g^{\vartheta\vartheta} - (g^{r\vartheta})^2}_{g_{\varphi\varphi}=R^2} \end{pmatrix} = \begin{pmatrix} (B.21) & (B.23) & 0 \\ (B.23) & (B.22) & 0 \\ 0 & 0 & R^2 \end{pmatrix}$$

Jacobian

The Jacobian is

$$\frac{1}{\sqrt{g_w}} = \frac{K(r)}{R^2} \tag{B.25}$$

with $K(r)$ already written in (3.16). In order to compute the harmonics of the first order perturbation, one wishes to expand also the metric tensor elements:

$$\frac{1}{\sqrt{g_w}} = \frac{1}{\sqrt{g_{w0}}} + \frac{1}{\sqrt{g_{w1}}} e^{i\vartheta} + c.c. \tag{B.26}$$

with

$$\frac{1}{\sqrt{g_{w0}}} = \frac{1}{rR_0}\left(1 + \frac{2r^2}{R_0^2} - \frac{\Delta}{R_0} - \frac{r}{2R_0}\Delta' + o(\epsilon^3)\right) \tag{B.27}$$

$$\frac{1}{\sqrt{g_{w1}}} = \frac{1}{\sqrt{g_{w0}}}\left(\frac{r}{R_0} + o(\epsilon^3)\right), \tag{B.28}$$

being the $m = 0/n = 0$ and $m = \pm 1/n = 0$ harmonics of the Jacobian respectively.

We can also relate the Jacobian $\sqrt{g_w}$ to $\sqrt{g_u}$. Using (B.13) one obtains

$$\frac{1}{\sqrt{g_w}} = \frac{1}{\sqrt{g_u}}\left(1 + \frac{\partial \lambda}{\partial \theta}\right). \tag{B.29}$$

Some metric tensor element combination

Finally, the metric tensor element combinations appearing in equations. (3.36) and (3.37) are

$$\left(\frac{g^w_{\vartheta\vartheta}}{\sqrt{g_w}}\right)^{0,0} = \frac{r}{R_0}\left(1 + \frac{r^2}{2R_0^2} + \frac{\Delta'^2}{2} + \frac{r}{2R_0}\Delta' - \frac{\Delta}{R_0} + o(\epsilon^3)\right) \tag{B.30}$$

$$\left(\frac{g^w_{r\vartheta}}{\sqrt{g_w}}\right)^{0,0} = \frac{o(\epsilon^4 b)}{\sqrt{g_{w0}}} \tag{B.31}$$

$$\left(\frac{g^w_{rr}}{\sqrt{g_w}}\right)^{\pm 1,0} = \frac{1}{\sqrt{g_{w0}}}\left(\frac{r}{R_0} - \Delta' + o(\epsilon^3)\right) \tag{B.32}$$

$$\left(\frac{g^w_{\vartheta\vartheta}}{\sqrt{g_w}}\right)^{\pm 1,0} = \frac{1}{\sqrt{g_{w0}}}\left(r^2\Delta' + o(\epsilon^3 b^2)\right) \tag{B.33}$$

$$\left(\frac{g^w_{r\vartheta}}{\sqrt{g_w}}\right)^{\pm 1,0} = \pm\frac{r}{2i\sqrt{g_{w0}}}\left(r\Delta'' + \Delta' - \frac{r}{R_0} + o(\epsilon^3)\right). \tag{B.34}$$

B.3 The inverse of 3x3 matrix

Let us consider the 3x3 matrix the tensor matrix of some coordinate system. The covariant and contravariant metrics are one the inverse of the other:

$$\mathbf{g_{ij}} = \begin{pmatrix} g_{\chi\chi} & g_{\chi\beta} & g_{\chi\varphi} \\ g_{\beta\chi} & g_{\beta\beta} & g_{\beta\varphi} \\ g_{\varphi\chi} & g_{\varphi\beta} & g_{\varphi\varphi} \end{pmatrix} \quad \mathbf{g^{ij}} = \begin{pmatrix} g^{\chi\chi} & g^{\chi\beta} & g^{\chi\varphi} \\ g^{\beta\chi} & g^{\beta\beta} & g^{\beta\varphi} \\ g^{\varphi\chi} & g^{\varphi\beta} & g^{\varphi\varphi} \end{pmatrix}$$

If the covariant g_{ij} matrix is a block diagonal matrix, its inverse is the matrix calculated as follows:

$$\mathbf{g^{ij}} = \frac{1}{g}\begin{pmatrix} g_{\theta\theta}\, g_{\varphi\varphi} & -g_{r\theta}\, g_{\varphi\varphi} & 0 \\ -g_{r\theta}\, g_{\varphi\varphi} & g_{rr}\, g_{\varphi\varphi} & 0 \\ 0 & 0 & g_{rr}\, g_{\theta\theta} - (g_{r\theta})^2 \end{pmatrix} \tag{B.35}$$

where $\sqrt{g}$ is the Jacobian.

If the covariant g_{ij} matrix is complete 3x3 matrix (not a block diagonal matrix), its inverse is the matrix calculated as follows:

$$\mathbf{g_f^{ij}} = \frac{1}{g}\begin{pmatrix} g^{\beta\beta}g^{\varphi\varphi} - (g^{\beta\varphi})^2 & g^{\varphi\beta}g^{\chi\varphi} - g^{\chi\beta}g^{\varphi\varphi} & g^{\chi\beta}g^{\beta\varphi} - g^{\beta\beta}g^{\chi\varphi} \\ g^{\chi\varphi}g^{\beta\varphi} - g^{\beta\chi}g^{\varphi\varphi} & g^{\chi\chi}g^{\varphi\varphi} - (g^{\varphi\chi})^2 & g^{\beta\chi}g^{\chi\varphi} - g^{\chi\chi}g^{\beta\varphi} \\ g^{\beta\chi}g^{\beta\varphi} - g^{\beta\beta}g^{\varphi\chi} & g^{\varphi\chi}g^{\chi\varphi} - g^{\chi\chi}g^{\varphi\beta} & g^{\chi\chi}g^{\beta\beta} - (g^{\beta\chi})^2 \end{pmatrix}$$

It is worth stressing that all the tensor metrics are related to symmetric matrix, due to the symmetry of the metrics elements: $g^{ij} = g^{ji}$ and $g_{ij} = g_{ji}$.

Appendix C

Complex harmonics

C.1 On complex conjugation

Any perturbation $a(r,\theta,\varphi)$ can be Fourier decomposed as:

$$a(r,\theta,\varphi) = \sum_{\substack{m,n \\ \epsilon\,\mathbb{Z}}} a^{m,n}(r)\; e^{i(m\theta - n\varphi)} = \sum_{\substack{m \\ n>0}} a^{m,n}(r)\; e^{i(m\theta - n\varphi)} + c.c. \qquad \text{(C.1)}$$

Let us prove the relations in eq.(C.1). We need to remember that:

- the perturbation is a real number, $a(r,\theta,\varphi)\,\epsilon\mathbb{R}$
- the harmonics of the perturbation are complex numbers, $a^{m,n}(r)\,\epsilon\,\mathbb{C}$
- the amplitude and the phase of a complex number written in polar form ($a^{m,n}(r) = |a^{m,n}|\, e^{i\,\psi}$) are real numbers, $|a^{m,n}|\,\epsilon\mathbb{R}$ and $\psi\,\epsilon\mathbb{R}$.

Starting from the first expression in eq.(C.1) we obtain the second one as follows:

$$\begin{aligned}
a(r,\theta,\varphi) &= \sum_{\substack{m,n \\ \epsilon\,\mathbb{Z}}} a^{m,n}(r)\; e^{i(m\theta - n\varphi)} && \text{(C.2)}\\
&= \sum_{m,n>0} a^{m,n}(r)\; e^{i(m\theta - n\varphi)} + a^{-m,-n}(r)\; e^{i(-m\theta + n\varphi)} && \text{(C.3)}\\
&= \sum_{m,n>0} a^{m,n}(r)\; e^{i(m\theta - n\varphi)} + a^{-m,-n}(r)\; e^{-i(m\theta - n\varphi)} && \text{(C.4)}\\
&= \sum_{m,n>0} a^{m,n}(r)\; e^{i(m\theta - n\varphi)} + a^{*\,m,n}(r)\; e^{-i(m\theta - n\varphi)} && \text{(C.5)}\\
&= \sum_{\substack{m \\ n>0}} a^{m,n}(r)\; e^{i(m\theta - n\varphi)} + c.c. && \text{(C.6)}
\end{aligned}$$

as we wanted. In the sum over integer m,n in eq.(C.2) one have both the positive and the negative value of the mode numbers. Writing the symbol *

for the complex conjugation, we are able to go to eq.(C.5) using the important conjugation property:

$$a^{-m,-n} = a^{*\,m,n} \tag{C.7}$$

The relation (C.7) is also the condition for which one can go back to the reality of any measurable field (like $a(r,\theta,\varphi)\,\epsilon\mathbb{R}$) from the complexity of the Fourier transformed harmonics $a^{m,n}(r)\,\epsilon\,\mathbb{C}$. Let us now derive the third expression for $a(r,\theta,\varphi)\,\epsilon\mathbb{R}$ in eq.(C.1), starting from the second one and using the polar form of complex numbers:

$$\begin{aligned}
a(r,\theta,\varphi) &= \sum_{\substack{m\\ n>0}} a^{m,n}(r)\; e^{i(m\theta-n\varphi)} + c.c. && \text{(C.8)}\\
&= \sum_{\substack{m\\ n>0}} |a^{m,n}|\, e^{i\,\phi}\, e^{i(m\theta-n\varphi)} + c.c. && \text{(C.9)}\\
&= \sum_{\substack{m\\ n>0}} |a^{m,n}|\, e^{i\,\phi}\, e^{i(m\theta-n\varphi)} + |a^{m,n}|\, e^{-i\,\phi}\, e^{-i(m\theta-n\varphi)} && \text{(C.10)}\\
&= \sum_{\substack{m\\ n>0}} |a^{m,n}|\Big[\, e^{i\,\phi}\, e^{i(m\theta-n\varphi)} + e^{-i\,\phi}\, e^{-i(m\theta-n\varphi)}\,\Big] && \text{(C.11)}\\
&= \sum_{\substack{m\\ n>0}} 2\,|a^{m,n}|\, cos(\phi + m\theta - n\varphi) \quad \epsilon\mathbb{R} && \text{(C.12)}
\end{aligned}$$

It is always true that adding the complex conjugated to a complex number one delete the imaginary part:

$$\begin{aligned}
A &= a + i\,b && \text{(C.13)}\\
A^* &= a - i\,b && \text{(C.14)}\\
A + A^* &= 2a && \text{(C.15)}
\end{aligned}$$

or

$$\begin{aligned}
A &= \rho\, e^{i\phi} && \text{(C.16)}\\
A^* &= \rho\, e^{-i\phi} && \text{(C.17)}\\
A + A^* &= 2\rho\, \cos(\psi) && \text{(C.18)}
\end{aligned}$$

Therefore $(A + A^*)\,\epsilon\,\mathbb{R}$ in any case.

Going back to the magnetic fluxes perturbation, it is now clear that even choosing Single Helicity in the fluxes (that means deleting the sum over (m,n) in expression (C.1) because they are fixed[1]) one must add the complex conjugated to obtain the real perturbation to the fluxes:

$$\psi(r,u) = \psi_0(r) + \psi^{m,n}(r)\; e^{iu} + c.c. \tag{C.19}$$

as written in eq.(4.1) making use of the helical angle $u = m\theta - n\varphi$.

[1] We remind that $(m,n = 1,7)$ in RFX–mod during SHAx states.

C.2 On the sum between complex numbers

$z \epsilon \mathbb{C}$, therefore one can choose between one of these expressions to write z:

$$z = a + ib = \rho\, e^{i\,\theta} = \rho(\cos\theta + i \sin\theta) \tag{C.20}$$

where

$$\rho = \sqrt{a^2 + b^2} \tag{C.21}$$

$$\theta = \tan^{-1}\left(\frac{b}{a}\right) \tag{C.22}$$

because

$$a = \rho\cos\theta \tag{C.23}$$

$$b = \rho\sin\theta \tag{C.24}$$

Let us see how to sum two complex numbers, $z \epsilon \mathbb{C}$ and $t \epsilon \mathbb{C}$:

$$z = a + ib = \rho\, e^{i\,\theta} \mapsto \begin{cases} a = \rho\cos\theta \\ b = \rho\sin\theta \end{cases} \tag{C.25}$$

$$t = c + id = \sigma e^{i\,\varphi} \mapsto \begin{cases} c = \sigma\cos\varphi \\ d = \sigma\sin\varphi \end{cases} \tag{C.26}$$

We write the difference between two complex numbers, because it is useful for section 9.1.1. For the sum it is enough to change every minus sign with a plus sign.
The difference between two complex numbers is a complex number, therefore:

$$z - t = A + iB = C\, e^{i\gamma} \mapsto \begin{cases} A = C\cos\gamma \\ B = C\sin\gamma \end{cases} \tag{C.27}$$

We can write:

$$\begin{aligned} z - t &= (a + ib) - (c + id) = (a - c) + i(b - d) = A + iB = \sqrt{A^2 + B^2}\, e^{i\gamma} \\ &= \rho e^{i\,\theta} - \sigma e^{i\,\varphi} = \sqrt{a^2 + b^2}\, e^{i\theta} - \sqrt{c^2 + d^2}\, e^{i\varphi} \qquad \text{(C.28)} \\ &= C\, e^{i\gamma} \qquad \text{(C.29)} \end{aligned}$$

therefore

$$A = a - c \tag{C.30}$$

$$B = b - d \tag{C.31}$$

and

$$C = \sqrt{A^2 + B^2} \tag{C.32}$$

$$\gamma = \cos^{-1}\left(\frac{A}{\sqrt{A^2 + B^2}}\right) = \tan^{-1}\left(\frac{B}{A}\right) \tag{C.33}$$

Bibliography

[1] B. Momo, E. Martines, D.F. Escande, and M. Gobbin. Magnetic coordinate systems for for helical shax states in rfp plasmas. *Plasma Phys. Control. Fus.*, 53(125004):13pp, 2011.

[2] E. Martines, R. Lorenzini, and B. Momo et al. Equilibrium reconstruction for single helical axis reversed field pinch plasmas. *Plasma Phys. Control. Fusion*, 53(035015):18pp, 2011.

[3] E. Martines, R. Lorenzini, and B. Momo et al. The plasma boundary in single helical axis rfp plasmas. *Nucl. Fusion*, 50(035014):7pp, 2010.

[4] W.H. Bennet. *Physical Review*, 45:890, 1934.

[5] I. Morozov and L. S. Solovev. *Rev. Plasma Phys.*, 2:229, 1966.

[6] L.A. Artsimovitch. *Nucl. Fusion*, 20:1255, 1980.

[7] H. Ji and S.C. Prager. The α dynamo effects in laboratory plasmas. *Magnetohydrodynamics*, 38(1-2):191–210, 2002.

[8] S. Cappello and R. Paccagnella. *Proc. Workshop on Theory of Fusion Plasmas ed E. Sindoni (Bologna: Compositori)*, page 595, 1990.

[9] S. Cappello and R. Paccagnella. Nonlinear plasma evolution and sustainment in the reversed field pinch. *Phys. Fluids*, B(4):611, 1992.

[10] J. M. Finn, R. Nebel, and C. Bathke. Single and multiple helicity ohmic states in reversed-field pinches. *Phys. Fluids B*, 4(5):1262–1279, May 1992.

[11] J. Wesson. *Tokamaks*. Clarendon Press, 1987.

[12] A.H. Boozer. Physics of magnetically confined plasmas. *Review of Modern Phys.*, 76:1071–1139, October 2004.

[13] R.B. White. Resistive reconnection. *Review of Modern Physics*, 58(1):183–207, 1986.

[14] B. Chirikov. A universal instability of many-dimensional oscillator systems. *Physics Reports (Review Section of Physics Letters)*, 52:263–379, 1979.

[15] M.E. Puiatti and M. Valisa. Internal and external electron transport barriers in the rfx-mod reversed field pinch. *Nucl. Fusion*, 51(073038):9pp, 2011.

[16] M.E. Puiatti et al. Helical equilibria and magnetic structures in the reversed field pinch and analogies to the tokamak and stellarator. *Plasma Phys. Control. Fusion*, 51(124031):14pp, 2009.

[17] D.F. Escande, R. Paccagnella, S. Cappello, C. Marchetto, and F.D'Angelo. Chaos healing by separatrix disappearance and quasisingle helicity states of reversed field pinch. *Phys. Rev. Lett.*, 85(15):3169–3172, Oct 2000.

[18] D.F. Escande et al. Quasi-single-helicity reversed-field-pinch plasmas. *Phys. Rev. Lett.*, 85(8):1662, 2000.

[19] R. Lorenzini and D. Terranova et al. Single-helical-axis states in reversed-field-pinch plasmas. *Phys. Rev. Lett.*, 101(025005):4pp, 2008.

[20] S. Cappello and D.F. Escande. Bifurcation in viscoresistive mhd: The hartmann number and the reversed field pinch. *Phys. Rev. Lett.*, 85(18):3838–3841, Oct 2000.

[21] S. Cappello, D. Bonfiglio, and D. F. Escande. Magnetohydrodynamic dynamo in reversed field pinch plasmas: Electrostatic drift nature of the dynamo velocity field. *Phys. Plasmas*, 13(056102):7pp, 2006.

[22] K.A. Werley. A mean field description of reversed field pinch: equilibrium, dynamo, plasma heating and confinement. *Nuclear Fusion*, 35(4):455–466, 1995.

[23] T. G. Cowling. *Magnetohydrodynamics (New York: Interscience)*, 1957.

[24] J.B. Taylor. Relaxation of toroidal plasma and generation of reverse magnetic field. *Phys. Rev. Lett.*, 33(19):1139, Nov. 1974.

[25] S. Cappello, D. Bonfiglio, and D.F. Escande et al. The reversed field pinch toward magnetic order: a genuine self-organization. *Theory of Fusion Plasmas, Joint Varenna-Lausanne International Workshop, AIP Conf. Proc.*, 1069:27–39, 2008.

[26] H.A.B. Bodin. *IAEA Fusion Energy Conference, Lausanna*, 1:417, 1984.

[27] M.G. Rusbridge. *Plasma Phys. Control. Fus.*, 33:1381, 1991.

[28] B.B. Kadomtsev. *Tokamak plasma: a complex physical system.* Institute of Physics, Bristol, 1992.

[29] D.F. Escande and D. Benisti. *Proc. of the 7th European Fusion Theory Conference (A. Rogister, Julich: Forschungzentrum KFA)*, 1:127, 1997.

[30] D.F. Escande et al. Single helicity: a new paradigm for the reversed field pinch. *Plasma Phys. Control. Fus.*, 42:B243 – B253, 2000.

[31] P. Sonato. *Fusion Eng. Des.*, 66-68:161, 2003.

[32] G. Rostagni. *Fusion Engineering and Design*, 25:301, 1995.

[33] http://www.igi.pd.cnr.it.

[34] www.cnr.it.

[35] http://www.enea.it.

[36] http://www.unipd.it.

[37] http://www.acciaierievenete.it.

[38] http://www.infn.it.

[39] P. Zaccaria, S. Dal Bello, and D. Marcuzzi. Tests and analysis for the mechanical and thermal qualification of the new rfx first wall tiles. *Fusion Engineering and Design*, 66-68:289–293, 2003.

[40] P. Martin et al. Overview of rfx-mod results. *Nuclear Fusion*, 47:1245, 2007.

[41] A. Lucchetta et al. http://www-naweb.iaea.org/napc/phisics/fec/fec2006/html/index.htm. *Proc. 21st Int. Conf. on Fusion Energy*, 2006.

[42] S. Martini et al. Active mhd control at high currents in rfx-mod. *Nucl. Fusion*, 47(8):783, 2007.

[43] P. Zanca, L. Marrelli, G. Manduchi, and G. Marchiori. Beyond the intelligent shell concept: the clean-mode-control. *Nucl. Fusion*, 47:1425–1436, 2007.

[44] L. Marrelli, P. Zanca, M. Valisa, and G. Marchiori et al. Magnetic self organization, mhd active control and confinement in rfx-mod. *Plasma Phys. Control. Fusion*, 49(12B):359–369, 2007.

[45] P. Piovesan and M. Zuin et al. Magnetic order and confinement improvement in high-current regimes of rfx-mod with mhd feedback control. *Nucl. Fusion*, 49(085036):9pp, 2009.

[46] V.I. Arnold. *Metodi matematici della meccanica classica*, volume IV edizione. agosto 2004.

[47] T.F. Jordan. Steppingstones in hamiltonian dynamics. *Am. J. Phys.*, 72(8):1095–1099, August 2004.

[48] J. Cary and R. Littlejohn. Noncanonical hamiltonian mechanics and its application to magnetic field line flow. *Annals of Physics*, 151:1–34, 1983.

[49] E. Pina and T. Ortiz. On hamiltonian formulations of magnetic field line equations. *J. Phys. A: Math. Gen.*, 21:1293–1295, 1988.

[50] K. Elsasser. Magnetic field line flow as a hamiltonian problem. *Plasma Phys. Control. Fusion*, 28(1743):1743–1752, 1986.

[51] W.D. D'Haeseleer, W.N.G. Hitchon, J.D. Callen, and J.L. Shohet. *Flux Coordinates and magnetic Field Structure*. 1991.

[52] A.H. Boozer. What is a stellarator? *Phys. of Plasmas*, 5(5):1647–1655, May 1998.

[53] P. Zanca and P. Terranova. Reconstruction of the magnetic perturbation in a toroidal reversed field pinch. *Plasma Phys. Control Fusion*, 46(7):1115–1141, 2004.

[54] R. Lorenzini et al. Self-organized helical equilibria as a new paradigm for ohmically heated fusion plasmas. *Nature Phys.*, 5(570):5pp, 2009.

[55] A. Alfier and R. Pasqualotto. New thomson scattering diagnostic in rfx-mod. *Rev. Sci. Instrum.*, 78(013505), 2007.

[56] S. Ortolani and D.D.Schnack. *Magnetohydrodynamics of Plasma Relaxation*, volume 1. 1993.

[57] R. Paccagnella. Linear magnetohydrodynamic stability in reversed field pinch with distant and multiple resistive walls. *Nucl. Fusion*, 38(7):1067–1081, 1998.

[58] J.A. Bittencourt. *Fundamentals of Plasma Physics*, volume Third edition. 2004.

[59] R. Bartiromo et al. Improved confinement and transport studies in the reversed field experiment (rfx). *Phys. Plasmas*, 6:1830–1837, 1999.

[60] M. Gobbin, D. Bonfiglio, and et al. D.F. Escande. Vanishing magnetic shear and electron transport barriers in the rfx-mod reversed field pinch. *Phys. Rev. Lett.*, 101(025005):4pp, 2011.

[61] G. Pereverzev and P.N. Yushmanov. Astra automated system for transport analysis in a tokamak. report ipp 5/98. *Max-Planck-Institut fur Plasmaphysik*, Garching, February 2002.

[62] R.L. Dewar, D.A. Monticello, and W.N.C. Sy. Magnetic coordinates for equilibria with continuous symmetry. *Phys. Fluids*, 27, 1984.

[63] R.B. White and M.S. Chance. Hamiltonian guiding center drift orbit calculation for plasmas of arbitrary cross section. *Phys. Fluids.*, 27:2455, 1984.

[64] D. Bonfiglio, S. Cappello, and D.F. Escande. Electrostatic dynamo in reversed field pinch plasmas: simple common fundamental nature of laminar and turbulent regimes. *Theory of Fusion Plasmas, Joint Varenna-Lausanne International Workshop, AIP Conf. Proc.*, CP871:14pp, 2006.

[65] S. Cappello, D. Bonfiglio, and D.F. Escande et al. Equilibrium and transport for quasi-helical reversed field pinches. *Nucl. Fusion*, 51(103012):13pp, 2011.

[66] V.D. Pustovitov. Evolution equation of a stabilized helical pinch. *Pis'ma Zh. Eksp. teor. Fiz.*, 35(1):3–5, 1982.

[67] V.D. Pustovitov. Evolution equation of a stabilized helical pinch. *JETP Lett.*, 35(1), 1982.

[68] P N Vabishchevich et al. *Fiz. Plazmy*, 9:484, 1983.

[69] P N Vabishchevich et al. *Soviet J. Plasma Phys.*, 9:280, 1983.

[70] G. Miller, V. Faber, and A.B. White. Resistive evolution of magnetic fields in plasmas. *Journal of computational Physics*, 85:323–341, 1989.

[71] D. Bonfiglio, D.F. Escande, P. Zanca, and S. Cappello. Necessary criterion for the magnetic field reversal in the reversed-field pinch. *Nucl. Fus.*, 51(063016):1–10, 2011.

[72] D.F. Escande. Change of paradigm of the reversed field pinch. *International Symposium on Waves, Coherent Structure, and Turbolence in Plasmas*, page 12pp, 2010.

[73] D. Bonfiglio, S. Cappello, and D.F. Escande. Dominant electrostatic nature of the reversed field pinch dynamo. *Phys. Rev. Lett.*, 94(145001):1–4, 2005.

[74] P.I Strand and W.A. Houlberg. Magnatic flux evolution in highly shaped plasmas. *Physics of plasmas*, 8(6):2782–2792, June 2001.

[75] D. Lopez-Bruna et al. Tracking magnetic resonances in the effective electron heat diffusivity of ech plasmas of the tj-ii heliac. *EPL*, 82:65002, 2008.

[76] M.D. Kruskal and R.M Kulsrud. Equilibrium of a magnetically confined plasma in a toroid. *Phys. Fluids*, 1(265):213–220, 1958.

[77] R. Lorenzini et al. *Plasma Phys. Control. Fusion*, 16(056109), 2009.

[78] P. Scarin and N. Vianello et al. Topology and transport in the edge region of rfx-mod helical regimes. *Nucl. Fusion*, 51(073002):11pp, 2011.

[79] R. Konig et al. The divertor program in stellarators. *Plasma Phys. Control. Fus.*, 44:2365–2422, 2002.

[80] P. Zanca. Avoidance of tearing modes wall-locking in a reversed field pinch with active feedback coils. *Plasma Phys. Control. Fusion*, 51(015006):38pp, 2009.

[81] P. Innocente et al. Transport and confinement studiesin rfx-mod reversed filed pinch experiment. *Nucl. fus.*, 47(9):1092–1100, 2007.

[82] R. Cavazzana and M. Moresco. Robust measurement of group delay in the presence of density fluctuations by means of ultrafast swept reflectometry. *Rev. Sci. Instrum.*, 79(10F105):4pp, 2008.

[83] G. De Masi et al. Edge density characterization in the rfx-mod experiment using the ultrafast reflectometry technique. *Nuclear Fusion*, 51(053016):7pp, 2011.

[84] G. Serianni, W. Baker, and S. Dal Bello. High-spatial resolution edge electrostatic probe system for rfx. *Review of Scientific Instruments*, 74(3):1558–1562, 2003.

[85] G. Serianni et al. Development, tests, and data acquisition of the integrated sysytem of internal sensors for rfx. *Review of Scientific Instruments*, 75(10):4338–4340, 2004.

[86] D. Desideri et al. Radial electric field at the edge of rfx. *Czechoslovak Journal of Physics*, 48(12):1641–1642, 1998.

[87] N. Vianello et al. Vf in extrap t2r properties of the edge plasma in the rebuilt extrap-t2r reversed field pinch experiment. *Plasma Phys. Control. Fusion*, 44:2513âĂŞ2523, 2002.

[88] http://www.photron.com/.

[89] Zanca P., Martines E., and Bolzonella T. et al. *Plasma Phys*, 8:516, 2001.

[90] P. Piovesan et al. Influence of external 3d magnetic fields on helical equilibrium and plasma flow in rfx-mod. *Plasma Phys. Control. Fusion*, 53(8):084005, 2011.

[91] P. Innocente and S. Martini. A two color multichord infrared interferometer for rfx. *Proceedings of the 9th topical Conference on high temperature plasma diagnostics*, 63:4996–4998, 1992.

[92] P. Innocente et al. Upgrade of the rfx co2 interferometer using in-vessel optics for extended edge resolution. *Proceedings of the 11th topical Conference on high temperature plasma diagnostics*, 68:694–697, 1997.

[93] P. Vincenzi. Studio statistico dell'andamento di densita e temperatura al bordo del plasma di rfx-mod. *Master's thesis, Universita degli Studi di Padova, Italy*, 2003.

[94] S. Barison et al. Analysis of the interaction between plasmas and the graphite first wall in rfx-mod. *Journal of Nuclear Materials*, 415(Supplement):S274–S277, August 2011.

[95] A. Canton et al. Density control in rfx-mod reversed field pinch device. *Proceedings of the 35th EPS Conference of Plasma Physics*, 32D(ECA):D–1.002, 2008.